



Improving Seismic Behaviour of Steel Plate Shear Walls with and without cut-outs

By

Ahmad Maleki

A thesis submitted in partial fulfilment of the requirement for the Degree of

Doctor of Philosophy

In

Structure-Earthquake Engineering

ABSTRACT

In this work experimental and numerical investigations were conducted on seismic behaviour of steel plate shear wall systems (SPSW) with and without cut-outs. Medium-scale specimens with moment-resisting connections between beam and columns and specific edge connections for fish plates were designed and constructed. The specimens were subjected to the cyclic quasi-static load. A loading system and proper lateral bracing unit was designed and built to apply the loading history according to ATC-24 protocol.

Nonlinear finite element analysis models with dynamic formulation were developed to analyse test specimens. The results were validated with available published test results from other researchers. After validation, the model was used for estimating the maximum load required for testing of specimens. The efficiency of the method was finally proved by comparing the pushover and hysteresis analysis results with tests carried out in Kingston University's lab.

The test series comprised frame-only, steel plate shear wall with two different types of steel plate and corresponding specimens with circular cut-outs in the steel plates, GFRP-steel Sandwich Shear Walls (GSSW) with different GFRP lay-up, GSSW with cut-outs and finally the steel plate shear wall with cut-out and optimally designed steel stiffeners. The specification of boundary members and the type of connections was kept unchanged in all specimens.

The effectiveness of utilising the GFRP plies and steel stiffeners for improving the seismic performance of steel plate shear walls with and without cut-outs was explored. The effectiveness of these methods for enhancing the initial stiffness and ultimate load capacity of specimens with no noticeable requirements for increasing flexural stiffness for columns was verified.

TABLE OF CONTENTS

ABSTRACT	II
TABLE OF CONTENTS	III
LIST OF TABLES.....	VIII
LIST OF FIGURES	IX
LIST OF SYMBOLS	XXIII
DEFINITIONS AND ABBREVIATIONS.....	XXIV
DEDICATION.....	XXVII
ACKNOWLEDGMENT	XXVIII
1. INTRODUCTION.....	1
<i>1.1. General</i>	<i>1</i>
<i>1.2. Objectives.....</i>	<i>2</i>
<i>1.3. Scope</i>	<i>2</i>
<i>1.4. Outline of the thesis.....</i>	<i>3</i>
2. LITERATURE REVIEW	5
<i>2.1. Introduction</i>	<i>5</i>
<i>2.2. Chronological development of steel plate shear walls.....</i>	<i>8</i>
2.2.1. Early research on steel plate shear walls (1973-1999).....	8
2.2.2. Further developments on steel plate shear walls (2000-2009)	35

TABLE OF CONTENTS

2.2.3. Recent advances on steel plate shear Walls (from 2010 onward).....	73
2.3. Practical applications and case studies of Steel plate shear walls.....	81
2.3.1. 20-storey office building in Tokyo, Japan	81
2.3.2. 53-storey high-rise building in Tokyo	82
2.3.3. 30-storey hotel in Dallas, Texas	83
2.3.4. 6-storey hospital in Los Angeles, California	83
2.3.5. 35-storey office building in Kobe, Japan.....	84
2.3.6. 24-storey building in Seattle, Washington	85
2.3.7. 26- and 31-storey buildings in Japan.....	86
2.3.8. 56-storey L.A. Live hotel and residences building in California.....	86
2.3.9. 75-storey Jinta Tower in Tianjin, China	87
2.3.10. Airport control tower of Edmonton international airport, Canada.....	89
2.4. Summary.....	89
3. FINITE ELEMENT SIMULATION TECHNIQUE FOR SPSWS.....	91
3.1. Introduction	91
3.2. Finite Element Model.....	92
3.3. Implicit finite element method and convergence problem.....	93
3.4. Explicit finite element method.....	94
3.4.1. Dynamic explicit method – stability limitation	94
3.4.2. Evaluation of Quasi-Static Solution	95
3.5. Description of the FE model for quasi-static testing	96
3.5.1. Element selection	96
3.5.2. Geometry and initial imperfection.....	97
3.5.3. Loading and boundary conditions.....	98
3.5.4. Residual stresses.....	98
3.5.5. Material properties	99
3.5.6. Displacement control analysis	100
3.6. Validation of the FE modelling	100
3.6.1. Pushover analysis of SPSW test specimen.....	103
3.6.2. Cyclic analysis of SPSW test specimen	107
3.7. Effects of cut-outs on behaviour of SPSW systems.....	108
3.8. Restoring the behaviour of SPSW systems with cut-outs.....	111
3.8.1. Introducing the longitudinal and transverse stiffeners to steel plate	111
3.8.2. Increasing the thickness of steel plate	113

TABLE OF CONTENTS

3.9. Summary.....	115
4. EXPERIMENTAL TEST SET-UP	117
4.1. Introduction	117
4.2. Material tests.....	118
4.3. Test specimen specifications and construction procedure.....	119
4.4. Lateral supporting system.....	130
4.5. Loading system.....	130
4.6. Loading history.....	132
4.7. Instrumentation and data acquisition	133
4.8. Innovative sliding measurement system.....	138
4.9. Thermal imaging using infrared camera.....	139
4.10. Assessment of reaction frame.....	140
4.11. Testing procedures and protocol.....	140
4.12. Trial test specimen (T).....	141
4.13. Summary.....	147
5. SEISMIC BEHAVIOUR OF SPSW SYSTEMS WITHOUT CUT-OUTS EXPERIMENTAL AND NUMERICAL STUDY.	148
5.1. Introduction	148
5.2. Preliminary analysis of test specimens	149
5.3. Test results and discussion of frame-only specimen (F).....	149
5.3.1. Behaviour of frame-only specimen during the test	150
5.3.2. Load displacement behaviour of frame-only specimen	152
5.3.3. Finite Element Analysis for frame-only specimen (F).....	155
5.4. Test results and discussion of steel plate shear wall specimens.....	156
5.4.1. Test results and discussion of W1 specimen	157
5.4.1.1. Behaviour of W1 during the test	158
5.4.1.2. Load-displacement behaviour of W1 specimen	160
5.4.2. Test results and discussion of W2 specimen	161
5.4.2.1. Behaviour of W2 specimen during the test.....	162
5.4.3. Finite element analysis of W1 and W2 specimens.....	166
5.5. Testing of GFRP-Steel sandwich shear walls	170
5.5.1. Test results and discussion of W1G1 specimen	174

TABLE OF CONTENTS

5.5.1.1. Behaviour of W1G1 specimen during the test	174
5.5.2. Test results and discussion of W1G2 specimen	180
5.5.2.1. Behaviour of W1G2 specimen during the test	181
5.5.2.2. Load-displacement behaviour of W1G2 specimen	185
5.5.3. Test results and discussion of W1G3 specimen	187
5.5.3.1. Behaviour of W1G3 specimen during the test	187
5.5.3.2. Load-displacement behaviour of W1G3 specimen	191
5.5.4. Finite element analysis results for W1G1, W1G2 and W1G3 specimens	193
5.6. Summary	196
6. SEISMIC BEHAVIOUR OF SPSW SYSTEMS WITH CUT-OUTS EXPERIMENTAL AND NUMERICAL STUDY	197
6.1. Introduction	197
6.2. Test results and behaviour of W1O specimen during the test.....	198
6.3. Test results and behaviour of W2O specimen	203
6.4. Test results and behaviour of W1OG specimen.....	208
6.5. Test results and behaviour of W2OS Specimen	213
6.6. Summary.....	219
7. DISCUSSION ON EXPERIMENTAL AND NUMERICAL RESULTS	220
7.1. Introduction	220
7.2. Effect of steel plate thickness on the behaviour of SPSW specimens.....	220
7.3. Effects of cut-outs on the behaviour of test specimens	222
7.4. Improving the Seismic behaviour of SPSW system using sandwich shear panels.....	224
7.4.1 GFRP-steel sandwich shear wall specimens without the cut-outs.....	225
7.5. Improving the seismic behaviour of SPSW system with cut-outs using steel stiffeners	233
7.6. Finite element analysis of specimens.....	236
7.7. Summary.....	239
8. SUMMARY, CONCLUSIONS, AND RECOMMENDATIONS FOR FUTURE RESEARCH	240
8.1. Introduction	240
8.2. Summary.....	240
8.3. Conclusions	242
8.4. Recommendations for future research	246

TABLE OF CONTENTS

REFERENCES	247
APPENDIX A: USER DEFINED SUBROUTIN FOR LOADING SYSTEM AND DATA ACQUISITION.....	269
APPENDIX B: THE STATE OF MAXIMUM PRINCIPLE STRESSES IN TEST SPECIMENS	272
APPENDIX C: BEST IMAGE AWARD FOR ABAQUS MODELLING	279
APPENDIX D: PUBLISHED PAPERS.....	281

LIST OF TABLES

Table 2.1: Categorization of Steel plate shear walls based on performance characteristics and expectations (Kharrazi, 2005)	8
Table 2.2: Component of test specimens (Zhao, 2004)	38
Table 2.3: Summary of peak results for specimen tested by Vian et al. (2003)	46
Table 2.4: Specification of material properties for specimens tested by Gholhaki and Sabouri-Ghomi (2009)	71
Table 2.5: Evaluation of VBE shear and strength requirements (Qu and Berman, 2010b)	76
Table 3.1: Summary of material properties determined from coupon tensile testing (Kharrazi, 2005)	102
Table 4.1: Summary of material properties determined from coupon testing	119
5.1: Loading amplitudes used for quasi-static test of frame-only specimen in accordance with ATC-24 protocol	151
Table 5.2: Loading amplitudes used for quasi-static test of W1 and W2 specimens in accordance with ATC-24 protocol	157
Table 5.3: General specification of GFRP-Steel sandwich shear walls	172
Table 5.4: Loading amplitudes used for quasi-static test of W1G1, W1G2 and W1G3 specimens in accordance with ATC-24 protocol	173
Table 6.1: Loading amplitudes used for quasi-static test of W1O, W2O, W1OG and W2OS specimens in accordance with ATC-24 protocol	198

LIST OF FIGURES

Figure 2.1: Typical steel plate shear wall system.....	6
Figure 2.2: Scheme of steel plate shear wall with details depicting an un-stiffened steel plate and steel plate with multiple stiffeners (From Kharrazi, 2005)	6
Figure 2.3: A comparison between plate girder and typical steel plate shear wall (Astaneh-Asl, 2001)	7
Figure 2.4: Hysteresis behaviour of (a) An un-stiffened SPSW and (b) Heavily stiffened SPSW (Takahashi et al., 1973)	10
Figure 2.5: Monotonic load-displacement behaviour of an SPSW showing contribution by frame and steel plate (Mimura and Akiyama, 1997)	10
Figure 2.6: Hysteresis model proposed by Mimura and Akiyama (1997)	11
Figure 2.7: Strip model representation of a single storey SPSW (Thorburn et al., 1983) .	12
Figure 2.8: Equivalent Brace Model (Thorburn et al., 1983)	13
Figure 2.9: One-Storey test specimen (Timler and Kulak, 1983)	16
Figure 2.10: SPSW as tested by Tromposch and Kulak (1987)	17
Figure 2.11: Load-Displacement hysteresis model (Tromposch and Kulak, 1987)	18
Figure 2.12: 3-storey model used by Chen (1991)	19
Figure 2.13: Servo hydraulic testing machine (Sabouri-Ghomi and Roberts, 1991).....	20
Figure 2.14: Comparison between analytical model prediction and experimental results (Sabouri-Ghomi and Roberts, 1991).....	21
Figure 2.15: Effect of circular perforation on strength (left) and stiffness (right) of shear panel (Roberts and Sabouri-Ghomi, 1992a)	21
Figure 2.16: Test set-up and hysteresis behaviour of specimens (Caccese et al., 1993) ..	22
Figure 2.17: Cyclic strip model (Elgaaly et al., 1993).....	23

LIST OF FIGURES

Figure 2.18: Tri-linear stress-strain relationship for strip model (Elgaaly et al., 1993)	24
Figure 2.19: Stress-strain diagram of low-yield steel and other steel grades (Nippon Steel, 1998)	26
Figure 2.20: Scheme and elevation of test specimen with hysteresis curves for first storey (Driver et al., 1997) (photo courtesy of R. Driver).....	28
Figure 2.21: Hysteresis model proposed by Driver et al. (1997)	30
Figure 2.22: Envelope curves for one-storey and four-storey specimens (Lubell, 1997) .	31
Figure 2.23 Four-storey Shake table test specimen (Rezai, 1999).....	32
Figure 2.24: Shake table test for the SPSW specimen (Rezai, 1999)	33
Figure 2.25: Scheme of different strip models for analyzing SPSWs (a) 'Strip model' used in the Canadian Steel Design Code (CSA, 2000) and (b) 'Multi-Angle Strip Model' as proposed by Rezai (1999).....	34
Figure 2.26: Scheme for (a) location of specimens (b) Test specimen One (c) test specimen Two (Astaneh-Asl., 2000)	35
Figure 2.27: Test specimen and scheme of test set-up (Astaneh-Asl and Zhao, 2000)	36
Figure 2.28: Specimen tested by Astaneh-As and Zhao (2001a), (a) Scheme of specimen (b) Specimen Two, during the test	37
Figure 2.29: Scheme view of composite shear wall tested by Astaneh-Asl., 2000 (a) with composite shear walls placed within a moment frame (b) innovative composite wall (c) Traditional composite wall	38
Figure 2.30: Shear force-Drift behaviour of specimens (Astaneh-Asl, 2001c)	39
Figure 2.31: SPSW failure mechanism hierarchy (Astaneh-Asl, 2001b)	39
Figure 2.32: Hysteresis curves of base shear versus first storey drift for three-storey specimen (Behbahanifard, 2003b)	40
Figure 2.33: (a) Single strip model (b) Single storey collapse mechanism (Berman, 2003a)	42
Figure 2.34: Multi-storey collapse mechanism proposed by Berman and Bruneau (2003b) (a) Soft storey mechanism (b) Unified collapse mechanism	43
Figure 2.35: Scheme of typical specimen dimensions (Vian, 2003).....	44
Figure 2.36 The scheme of (a) Reduced Beam Section (RBS) and reinforced corner cut-out (b) Torsion of top beam during the test (Vian and Bruneau, 2004)	44

LIST OF FIGURES

Figure 2.37 The hysteresis behaviour of specimens and corresponding deformed shape of specimens at the certain drift level (Vian et al., 2003) with (a) Regularly perforated steel plate (b) Corner cut-out steel plate (c) Solid steel plate	45
Figure 2.38: Components of M-PFI model for the (a) shear load-displacement: frame only, plate only and combined effects in panel (b) bending load-displacement of the panel (combined web plate and frame) (c) the modified load displacement diagram for shear resistance of the SPSW (d) bending and shear interaction of an SPSW panel	47
Figure 2.39: Test set-up and lateral support framing for a) Quasi-static test (b) Shake table test (Kharrazi, 2005)	48
Figure 2.40: Comparison of M-PFI model prediction and experimental results (Kharrazi, 2004) from tests conducted at university of Alberta, (a) (Behbahanifard, 2003), (b) (Driver, 1997)	49
Figure 2.41: Typical test set-up for specimens tested (Berman and Bruneau, 2005a, 2005b).....	50
Figure 2.42: Test samples specifications and experimental hysteresis curves for specimens: (a) FP; (b) CP; (c) B1; (d) B2; (e) B3; (f) B4 (Berman, 2005-a)	51
Figure 2.43: Typical frame-joint model detail for rigid connections.....	53
Figure 2.44: Compression struts and deterioration strips in detailed model proposed by Shishkin et al. (2005)	55
Figure 2.45: Scheme of (a) Strip geometry (b) FE model of Vian et al. (2005), developed by Purba (2006)	56
Figure 2.46 FE modelling of Vian et al. (2005) specimen by Purba (2006).....	56
Figure 2.47: Steel plate strength ratio versus perforation ratio for (a) Rigid Floor mode, (b) Rigid Beam model (Purba, 2009)	57
Figure 2.48: Scheme of test specimens (Park et al., 2007).....	58
Figure 2.49: Different configurations of test specimens tested by Choi et al. (2008) for (a) Partially connected steel plate, FSPW4 specimen, (b) Coupled wall, FSPW5 specimen, (c) Bolt-connection, BSPW2 specimen, (d) CBF specimen	60
Figure 2.50: Load-top displacement relationships of test specimens for (a) FSPW2, (b) SFPW4, (c) FSPW5, (d) BSPW2, (e) CBF, (f) MRF tested by Choi et al. (2008)	61
Figure 2.51: Cumulative energy dissipation capacity for specimens (Choi et al., 2008)...	62

LIST OF FIGURES

Figure 2.52 Free body diagram for vertical boundary members (Berma and Bruneau, 2008a)	63
Figure 2.53: (a) Scheme of the SPSW (b) plastic hinge formation at the base of the boundary columns (c) soft ground storey (Ghosh et al., 2009)	65
Figure 2.54: Scheme of the four-storey steel frame structures studied by Gosh et al.(2009) based on proposed method	67
Figure 2.55: (a) Typical dimensions of specimens (b) Assumed relationship between stress and strain (Alinia et al., 2009b)	68
Figure 2.56: Load-inplane displacement analysis results for SPSW system and its components (Alinia et al., 2009b)	69
Figure 2.57: Scheme of geometrical specification of stiffened walls (a) Typical sub-plate dimensions, (b) Dimension of stiffeners (c) Various stiffener arrangements studied by Alinia and Sarraf (2009a)	69
Figure 2.58: Scheme of three-storey SPSW specimen tested by Gholhaki and Sabouri-Ghomi (2009)	72
Figure 2.59 Elastic and plastic response of structures	72
Figure 2.60: Hysteresis and multi linear behaviour of first floor for (a) SPSW-R specimen (b) SPSW-S specimen tested by Gholhaki and Sabouri-Ghomi (2009).....	73
Figure 2.61: Deformation of a cantilever plate girder under transverse load (Wagner, 1931)	74
Figure 2.62: The relationship between flexibility factor and stress uniformity ratio developed by Qu and Bruneau (2010).	75
Figure 2.63: The scheme of strip element cyclic axial load behaviour (Berman, 2011) ...	77
Figure 2.64: (a) Configuration of steel plate (b) Detail of CSPSW tested by Lanhui et al. (2011).....	79
Figure 2.65: (a) Fibre directions angle (b) FE results for of SPSW strengthened with two 0.5 mm plies for two different fibre directions (Rahai et al, 2011)	79
Figure 2.66: (a) Scheme of test specimen dimensions (b) FE modelling of specimen (Hatami et al, 2011)	80
Figure 2.67: Three different configuration of cut-out edge strengthening using FRP strip material (Alipour et al, 2011)	80

LIST OF FIGURES

Figure 2.68: Pushover analysis results for SPSW with and without cut-out and perforated wall strengthened using patterns A and B (Alipour et al, 2011).....	81
Figure 2.69: Typical floor plan of Nippon Steel Building	82
Figure 2.70: (a) Elevation view (b) Plan (c) Transverse section of 53-storey Shinjuku Nomura Building in Tokyo (Photo courtesy of P. Becker)	83
Figure 2.71: (a) Floor plan (b) elevation section (c) Photo of 35-storey Kobe building (Photo courtesy of C.E. Ventura).....	85
Figure 2.72: Coupled SPSW under construction regarding to 24-storey US Courthouse Building, Seattle, Washington.....	86
Figure 2.73: (a) Steel plate shear walls under construction (b) Elevation view of 56-storey L.A. Live hotel and residence building (Photo courtesy of AEG and Gensler).....	87
Figure 2.74: (a) The architectural impression (b) Outrigger truss of Jinta tower	88
Figure 2.75 Stiffened shear panels adopted in Jinta tower.....	88
Figure 2.76: Construction of Edmonton International Airport’s control tower with steel plate shear wall system in Canada (Courtesy of Ellis Don Inc)	89
Figure 3.1: Connection of three distinct stages in ABAQUS (Hibbitt et al.; 2007).....	92
Figure 3.2: Scheme for deformed shape of the lowest buckling mode	98
Figure 3.3: Dimensions of the single storey DSPW-1 specimen tested by Kharrazi, 2005	101
Figure 3.4: Fish plate connection detail for DSPW-1 specimen (Kharrazi, 2005)	102
Figure 3.5: FE model developed in accordance with DSPW-1 specimen	103
Figure 3.6: Scheme of smooth step amplitude function with two data points.....	104
Figure 3.7: Energy history of the pushover analysis of SPSW-0.7 model.....	104
Figure 3.8: Kinematic energy history of the pushover analysis for SPSW-0.7 model	105
Figure 3.9: Contour plot of stresses for SPSW-0.7 specimen in accordance with von Mises stress criteria at early stage of loading.....	105
Figure 3.10: Von Mises counter plate for SPSW-0.7 specimen at the final stage of loading	106
Figure 3.11: Load-displacement results obtained from finite element analysis (SPSW-0.7) and envelop of hysteresis test results for DSPW-1	107

LIST OF FIGURES

Figure 3.12: Comparison of tension field development; (a) During loading of the specimen in FE analysis for SPSW-0.7; (b) During quasi-static for DSPW-1	107
Figure 3.13: Load-displacement hysteresis loop of (a) DSPW-1 from quasi-static test (b) SPSW-0.7 from FE analysis.....	108
Figure 3.14: Scheme of FE model for SPSWC-0.7 specimen.....	109
Figure 3.15: (a) Deformed shape and; (b) hysteresis loop for SPSWC-0.7 specimen	109
Figure 3.16: Contour plot of stress distribution for SPSWC-0.7 specimen	110
Figure 3.17: Pushover analysis results for SPSWC-0.7 specimen with variation of circular cut-out diameter	110
Figure 3.18: The ultimate load capacity of SPSWC-0.7 specimen with different cut-out diameters	111
Figure 3.19: Scheme of FE model for stiffened SPSW with cut-out using.....	112
Figure 3.20: (a) Deformed shape and; (b) hysteresis behaviour for SPSWCS-0.7 specimen	112
Figure 3.21: Entire yielding of sub-plates for SPSWCS-0.7 specimen	113
Figure 3.22: Pushover analysis results for SPSW system with circular cut-outs using different thickness of steel plate	114
Figure 3.23: (a) Deformed shape and (b) Hysteresis loops for SPSWC-1 specimen	114
Figure 3.24: Comparative results for push-over analysis of specimens.....	115
Figure 4.1 Coupon tensile test procedure for steel materials.....	118
Figure 4.2: Overall geometry and dimensions for single-storey test specimens	120
Figure 4.3: Detailed view for dimensions and type of connection between steel plate and boundary elements	121
Figure 4.4: Moment-resisting connections between beam and columns.....	122
Figure 4.5: Connection of fish plate to boundary members using intermittent fillet welding on both sides of fish plate	122
Figure 4.6: Different edge connection of test specimens (measurements in mm).....	123
Figure 4.7: Details of the proposed edge connection	124
Figure 4.8: Connection of steel plates to fish plates (a) Using HSFG bolts for 0.675 mm thick steel plate and (b) Using MIG weld for 1.4 mm thick steel plates	124

LIST OF FIGURES

Figure 4.9 Different trials for welding of steel plate to fish plates and stiffeners to steel plate using MIG welding	125
Figure 4.10: Testing of welding joint by MIG welding.....	126
Figure 4.11 Connection of steel plate to boundary members via fish plate	126
Figure 4.12: Jig frame was designed and constructed to improve the efficiency of specimen's construction	127
Figure 4.13: Utilising stiffener to create sufficient connection between column and base plate	127
Figure 4.14: Specimens' connection to the reaction frame using HSFG bolts and clamped plates	129
Figure 4.15: Lateral supporting system (out-of-plane bracing) for quasi-static tests	130
Figure 4.16: Detailed design and manufactured rigid connection box (all dimensions in mm).....	131
Figure 4.17: Connection of rigid box and screw jack to reaction frame	131
Figure 4.18 Different parts of loading unit	132
Figure 4.19: Deformation history for quasi-static test of specimens according to ATC-24 protocol.....	133
Figure 4.20: Connection of Loadcell to corresponding parts of loading system using locking nuts	134
Figure 4.21: Locations of rosette strain gauges within the shear panel for test specimens (a) without cut-out (b) with cut-out.....	135
Figure 4.22: Un-axial Strain gauge locations on flanges of beam and columns	136
Figure 4.23: Locations of cable-extension displacement sensors	137
Figure 4.24: Loading plate was equipped with LVDT, CDS and dial gauge to measure the screw jack stroke	137
Figure 4.25: Innovative sliding measurement system.....	138
Figure 4.26: Manually measurement of out-of-plane buckling of steel plate.....	138
Figure 4.27: Infrared thermal camera is used for capturing delaminating and debonding of GFRP composite layers	139
Figure 4.28: The strength and stiffness assessment of reaction frame	140
Figure 4.29: Tightening the lock nuts when system is running under tensile loading....	141

LIST OF FIGURES

Figure 4.30: General configuration of test set up for trial specimen.....	142
Figure 4.31: Double check for CDS devices calibration using LVDT	142
Figure 4.32: Monitoring any slippage between test specimen and reaction frame.....	143
Figure 4.33: Occurrence of shear fracture in nut.....	143
Figure 4.34: Utilising longer nuts and clamps precluded any uplifting of base plate	144
Figure 4.35: Utilising rigid clamp plates prevent damage of welding at location of connection between loading plate and column's outer flange	144
Figure 4.36: Anti rotation hanger prevents any rotation to be applied to the test specimens	145
Figure 4.37: Premature stretching of steel plate at connections to the fish plates	146
Figure 4.38: Hysteresis behaviour of Trial specimen	146
Figure 5.1: Specifications of frame-only specimen	149
Figure 5.2: (a) Test set up and, (b) Preliminary finite element analysis results for frame-only specimen (F)	150
Figure 5.3: Fracture in the weld connection of column-to-base plate stiffeners at both columns of the frame-only specimen.....	151
Figure 5.4: Plastic hinges were noted at the bottom of both columns.....	152
Figure 5.5: Testing results for hysteresis behaviour of frame-only specimen	153
Figure 5.6: Yield point of frame-only specimen based on Load-displacement diagram.	153
Figure 5.7: Formation of plastic hinges at the bottom of columns as was estimated by FEA results.....	154
Figure 5.8: Fracture in weld of beam to column connection plate during the last cycle of testing for frame-only specimen.....	154
Figure 5.9: Pushover finite element load-displacement results and test quasi-static response for frame-only specimen	155
Figure 5.10: Load-displacement hysteresis loops for frame-only specimen from finite element (FE) analysis and quasi-static test.....	156
Figure 5.11(a) Test set up and, (b) Preliminary finite element analysis results for W1 specimen.....	158

LIST OF FIGURES

Figure 5.12: W1 (a) after the first nine cycles (b) in cycle #14 considerable elastic deformation (c) in cycle #20 distinct tension field and extensive yielding of steel plate	159
Figure 5.13: Weld fracture of connection between fish plate and right column for W1 specimen.....	159
Figure 5.14: Testing results for hysteresis behaviour of W1 specimen	160
Figure 5.15: Tension field orientation in the steel plate for W1 specimen.....	161
Figure 5.16: (a) Test set up and, (b) Preliminary finite element analysis results for W2 specimen.....	162
Figure 5.17: positioning of diagonal tension field within the steel plate for W2	162
Figure 5.18: Development of diagonal tension field and yield zone within the steel plate at storey drift of 10 mm for W2 specimen	163
Figure 5.19: Massive out-of-plane deformation of steel plate at storey drift of 20 mm for W2 specimen.....	164
Figure 5.20: Fracture of weld connection between base plate and left column stiffener at a nominal drift index of 2.5% for W2	164
Figure 5.21: Testing results for hysteresis behaviour of W2 specimen	165
Figure 5.22: Pushover finite element load-displacement results and test quasi-static response for W1 specimen	166
Figure 5.23: Pushover finite element load-displacement results and test quasi-static response for W2 specimen	166
Figure 5.24: In-plane maximum principle stresses at the mid-surface of the elements of W1 (left) and W2 (right) at the applied drift of 10 mm.....	167
Figure 5.25: Load-displacement hysteresis loops for W1 from finite element (FE) analysis and quasi-static test	168
Figure 5.26: Load-displacement hysteresis loops for W2 from finite element (FE) analysis and quasi-static test	168
Figure 5.27: Deformed shape of W1 specimen from analysis and quasi-static test at the nominal drift index of 2% cycle, (a) for loading toward (b) for neutral state including steel plate with out-of-plane deformation.....	169

LIST OF FIGURES

Figure 5.28: Deformed shape of W2 specimen from analysis and quasi-static test at the nominal drift index of 2% cycle, (a) for loading toward (b) for neutral state including steel plate with out-of-plane deformation.....	170
Figure 5.29: Preparation of composite specimens (a) Laminating the first layers of plies (b) Stacking of second layers of GFRP plies (c) Vacuum bagging of specimens (d) Specimen after curing.....	171
Figure 5.30: Scheme of (a) Curing cycle (b) Vacuum bagging inside the oven for GSSW specimens	171
Figure 5.31: Scheme of composite layers for W1G1, W1G2 and W1G3 specimens.....	172
Figure 5.32: (a) Test set up and, (b) Preliminary finite element analysis results for W1G1 specimen.....	174
Figure 5.33: Linear and non-linear behaviour of W1G1 specimen during loading and unloading stages for nominal drift index of 0.12%	175
Figure 5.34: Initiation of elastic buckling noted during cycle #13 for W1G1 specimen .	175
Figure 5.35: Scheme of sandwich panel's image captured by infrared camera at storey drift of 5mm	176
Figure 5.36: Location of debonding of GFRP ply and steel plate.....	177
Figure 5.37: Formation of plastic hinge at the bottom of the column	178
Figure 5.38: Sate of GFRP-sandwich panel W1G1 at the storey drift of 25mm	178
Figure 5.39: Sate of composite panel for W1G1 specimen during cycle #29Load-displacement behaviour of W1G1 specimen.....	179
Figure 5.40: Testing results for hysteresis behaviour of W1G1 specimen.....	179
Figure 5.41: Tearing of GFRP plies along the fibres orientation in W1G1 specimen.....	180
Figure 5.42: Tension field orientation in the sandwich panel for W1G1 specimen	180
Figure 5.43: (a) Test set up and, (b) Preliminary finite element analysis results for W1G2 specimen.....	181
Figure 5.44: Different behaviour of W1G2 specimen for positive and negative storey drift of 1.2 mm during cycle #8.....	182
Figure 5.45: Formation of diagonal tension field and elastic buckling of W1G2 specimen during cycle #14 corresponding to storey drift of (a) +2.5 mm (b) -2.5 mm.....	182

LIST OF FIGURES

Figure 5.46: Infrared thermal image of sandwich panel W1G2 specimen during cycle #18	183
Figure 5.47: Location of delamination between steel plate and GFRP plies W1G2 specimen during cycle # 23.....	183
Figure 5.48: Initiation of tearing of GFRP ply in both.....	184
Figure 5.49: Formation of plastic hinges at the end of beam.....	185
Figure 5.50: Hysteresis behaviour of W1G2 during the quasi-static test.....	185
Figure 5.51: Variation of inclination angle between (a) reinforced direction and (b) non-reinforced direction of sandwich panel for W1G2 specimen.....	186
Figure 5.52: Tearing of GFRP plies due to stretching of the steel plate in direction perpendicular to fibres for W1G2	186
Figure 5.53: (a) Test set up and, (b) Preliminary finite element analysis results for W1G3 specimen.....	187
Figure 5.54: Linear behaviour of W1G3 up to storey drift of 1.2 mm	188
Figure 5.55: The shape of sandwich panel W1G3 specimen during cycle #21 (a) storey drift of +10 mm (b) initial position (c) storey drift of -10 mm	188
Figure 5.56: Location of possible induced defect during story drift of 15 mm	189
Figure 5.57: Tearing of GFRP plies at both sides of sandwich panels during cycles #24 and #25	189
Figure 5.58: Weld fracture between stiffeners and column connections.....	190
Figure 5.59: (a) State of sandwich panel during the final loading cycle and development of plastic hinges at the end part of (b) Beam and (c) Columns	190
Figure 5.60: Testing results for hysteresis behaviour of W1G3 specimen.....	191
Figure 5.61: The orientation of inclination angles for W1G3 specimen as the load is applied in each direction	192
Figure 5.62: Tearing of GFRP plies at nominal drift index level of 2.5% for W1G3 specimen.....	192
Figure 5.63: Comparison between envelop curves for hysteresis behaviour of FE and test results for W1G1 specimen.....	193
Figure 5.64: Comparison between envelop curves for hysteresis behaviour of FE and test results for W1G2 specimen.....	194

LIST OF FIGURES

Figure 5.65: Comparison between envelop curves for hysteresis behaviour of FE and test results for W1G3 specimen.....	194
Figure 5.66: Monotonic test results for W1, W1G1, W1G2 and W1G3 specimens.....	195
Figure 6.1: (a) Test set up and, (b) Preliminary finite element analysis results for W10 specimen.....	199
Figure 6.2: (a) Deformation of steel plate, (b) FE results for von Mises stress distribution for W10 during cycle #23	200
Figure 6.3: Occurrence of local buckling in the steel plate and fish plate	200
Figure 6.4: Weld fracture between column and connection plate during storey drift of (a) 30 mm for left column, (b) 35 mm for right column.....	201
Figure 6.5: Hysteresis behaviour of W10 specimen during the quasi-static test	202
Figure 6.6: Comparison between cyclic test results and envelope of FE hysteretic analysis for W10 specimen.....	202
Figure 6.7: Test set up and preliminary FE analysis results for W20.....	203
Figure 6.8: Permanent deformation of steel plate initially started at 5 mm story drift .	204
Figure 6.9: Noticeable out-of-plane buckling deformation of steel plate during cycle #25 for W20 specimen.....	205
Figure 6.10: Deformed shape of steel plate during cycle #24 at storey drift of +20 mm (left), initial position (middle) and -20 mm (right).....	205
Figure 6.11: State of column at the end of the test for W20 specimen	206
Figure 6.12: Hysteresis behaviour of W20 specimen during the quasi-static test.....	206
Figure 6.13: Comparison between cyclic test results and envelope of FE hysteretic analysis for W20 specimen.....	207
Figure 6.14: The state of W20 specimen for storey drift of 30 mm and corresponding results for finite element simulations	207
Figure 6.15: Test set up and preliminary push over FE results for W10 specimen.....	208
Figure 6.16: (a) Alteration of buckling mode shape in sandwich panel, (b) Capturing of changing in buckling mode by FE model for W10G specimen.....	209
Figure 6.17: The area that is indication for debonding failure of GFRP plies as result of infrared monitoring	210
Figure 6.18: Extension of tears in GFRP laminates	211

LIST OF FIGURES

Figure 6.19: (a) Formation of plastic hinges at the end of beam, (b) No buckling was noted at fish plates during the last cycle.....	211
Figure 6.20: The state of W10G specimen during the last cycle of loading	212
Figure 6.21: Hysteresis behaviour of W10G specimen recorded during the quasi-static test.....	212
Figure 6.22: Comparison between cyclic test results and envelope of FE hysteretic analysis for W10G specimen	213
Figure 6.23: (a) General view and stiffener arrangements (b) Preliminary finite element analysis results for W2OS specimen.....	214
Figure 6.24: Formation of buckling deformations in sub panels (a)During cycle #16 within sub panels B, D, F, (b)During cycle #18 within sub panels B, D, F and H.....	215
Figure 6.25: Counter plot of sub panels based on von Mises criteria at nominal drift index of 1%.....	215
Figure 6.26: State of infill panel for storey drift of (a) +20 mm, (b) -20 mm for W2OS..	216
Figure 6.27: Weld fracture and formation of plastic hinges at end of the column	217
Figure 6.28: Deformed shape of infill panel for W2OS after termination of the test (overall buckling of steel plate is turned to local buckling of subpanels)	217
Figure 6.29: Hysteresis behaviour of W2OS recorded during the quasi-static test	218
Figure 6.30: Comparison between cyclic test results and envelope of FE hysteretic analysis for W2OS specimen.....	218
Figure 7.1: Load-displacement behaviour of W1 and W2 specimens	220
Figure 7.2: Comparison between envelopes of the cyclic quasi-static test results for W1 and W2 specimens	221
Figure 7.3: Hysteretic energy dissipation for W1 and W2 specimens	221
Figure 7.4: Hysteretic curves for W1 and W10 specimens recorded during the quasi-static test program	222
Figure 7.5: Comparison between envelopes of the quasi-static cyclic test results for specimens with/and without cut-outs	223
Figure 7.6: Comparison between energy dissipation capacities for specimens with/and without cut-outs.....	224

LIST OF FIGURES

Figure 7.7: Hysteretic curves for W1G1 and W1G3 specimens recorded during the quasi-static test program	225
Figure 7.8: Comparison between envelopes of the quasi-static test results for W1, W2, W1G1, W1G2 and W1G3 specimens.....	226
Figure 7.9: The effect of GFRP laminates on initial stiffness of specimens.....	227
Figure 7.10: Comparative results for capability of specimens for energy dissipation....	227
Figure 7.11: Vertical deflection measurements for mid part of the beam	228
Figure 7.12: Hysteresis behaviour of W1O and W1OG specimens during the test.....	229
Figure 7.13: Comparison between the envelopes of quasi-static test results for W1O and W1OG specimens	230
Figure 7.14: Energy dissipating capacity for W1O and W1OG specimens	230
Figure 7.15: The effect of GFRP laminates on initial stiffness of specimens.....	231
Figure 7.16: Vertical deflection measurements for mid part of the beam	232
Figure 7.17: Comparative results for initial stiffness of W1, W1O, W2O and W1OG specimens	233
Figure 7.18: The state of hysteresis curves for W2O and W2OS specimens recorded during the quasi-static test program.....	234
Figure 7.19: Comparison between the envelopes of quasi-static test results for W2O and W2OS specimens.....	234
Figure 7.20: Energy dissipating capacity for W2O and W2OS specimens.....	235
Figure 7.21: Alteration of initial stiffness for test specimen due to implementation of cut-out (W2O) and introducing the stiffeners (W2OS)	235
Figure 7.22: Vertical deflection results for the mid part of beam element	236
Figure 7.23: Initiation of minor buckling deformations within the sub-panels is captured by FE model for W2OS specimen.	238
Figure 7.24: Validation of FE results for the vertical deformation of W2OS specimen at mid part of beam element.....	238

LIST OF SYMBOLS

A_b	crosses sectional area of beam
A_c	crosses sectional area of column
b_f	flange width of I section
d_c	overall depth of I section
E	elastic modulus
H	storey height
h_s	column height
I_b	moment of inertia for the beam
I_c	moment of inertia for the column
L	frame width
R	seismic force reduction factor
t_f	flange thickness of I section
t_w	web thickness of I section
w	steel plate thickness
α	inclination angle of tension field measured from vertical
σ_{ty}	tension field stress corresponding to yield

DEFINITIONS AND ABBREVIATIONS

AISC	American Institute of Steel Construction
Analytical model	Simplified mathematical rationale for a structural system
ASD	Allowable Stress Design
ATC	Applied Technology Council
CBF	Centrally Braced Frame
CDS	Cable-Extension Displacement Sensor
CDM	Capacity Design Method
CFSS	Cold formed Steel Stud
CFT	Concrete Filled Tube
CNC	Computer Numerical Control
Critical buckling	First buckling mode of the structural system
EBF	Eccentrically Braced Frame
EDMS	Energy Dissipation Mechanism
Elastic-perfectly-plastic	Bi-linear model without hardening (elasto-plastic material)
FE	Finite Element

DEFINATIONS AND ABBREVIATIONS

FEA	Finite Element Analysis
FEMA	Federal Emergency Management Agency
FRP	Fibre Reinforced Polymer
GFRP	Glass Fibre Reinforced Polymer
GSSW	Glass-steel Sandwich Shear Wall
HSFG	High Strength Friction Grip
Initial imperfection	out-of-flatness of steel plate prior to loading
ICD	Indirect Capacity Design
ISMS	Sliding Measurement System
ITC	Infrared Thermal Camera
LDS	referred to LVDT
LRFD	Load and Resistance Factor Design
LVDT	Linear Variable Displacement Transducers
LYP	Low Yield Point
LYS	Low Yield Steel
MAC	Modal Assurance Criteria
M-PFI	Modified-plate Frame Interaction
MRF	Moment-Resisting Frame
N.A.	Neutral Axis
MIG	Metal Inert Gas

DEFINATIONS AND ABBREVIATIONS

NEHRP	National Earthquake Hazards Reduction Program
Numerical model	Numerical approach for modelling a structural system such as finite element method
Overturning-moments	moments created by the lateral loads in the upper floors
PBSD	Performance-Based Seismic Design
Post-buckling	State of the plate after critical elastic/plastic buckling occurred
POA	Push-Over Analysis
RC	Reinforced Concrete
RBS	Reduced Beam Section
SMA	Shielded Metal Arc weld
Solid Panel	usually referred to steel plate without any cut-out
Steel panel	usually referred to a single unit or storey unit of steel plate wall
SP	Steel Plate
SPSW	Steel Plate Shear Wall
SSW	Steel Shear Wall
Tension field	Post-buckling stage of the steel plate
UBC	Uniform Building Code
UD-GFRP	Unidirectional Glass Fibre Reinforced Polymer
Ultimate capacity	State of panel when it reaches its ultimate resistance capacity

DEDICATION

This thesis is dedicated to my wife, to my parents. For their continuous love, support and encouragement during my studies, without which, this research would not have been possible.

ACKNOWLEDGMENT

Firstly I would like to thank God Almighty for all his blessings without which nothing is possible.

I would like to thank my director of studies Dr. Ted Donchev for his guidance and support through the launching of this project. I am indebted to him for the vast amount of time and he has provided towards me throughout my studies at Kingston University. I would like to thank Dr Hadavinia for sharing a great deal of his knowledge and experience with me throughout this project.

I would like to thank Professor Limbachiya for his valuable contribution in this research. I would also like to express my deep gratitude to Dr. Saeed Sabouri for providing valuable guidance particularly for experimental work. I am thankful to Dr. Mohammad Adil for his help and valuable consultancy during the experimental work. I would to thank Dr. Anna Cheah for her valuable help and effort at the early stage of this research.

Many thank to Mr. Daren Chapman for his unwavering support during the preparation of experimental samples. Special thanks go to the Kingston University structure laboratory technicians for their contributions to the experimental program.

This research was supported financially in the form of scholarship by Islamic Azad University in Iran (Maragheh Branch).

1. INTRODUCTION

1.1. General

Shear walls are common lateral load resisting system. They are used to reduce in-plane force effects applied along the height of a building produced by both wind and earthquake loads. Currently, reinforced concrete is widely used to construct shear walls. However, experimental and numerical studies during last three decades have demonstrated that steel plate shear wall (SPSW) system is an effective alternative to reinforced concrete shear walls. In general, SPSW system comprises of a thin steel plate wall, two boundary columns and horizontal floor beams. Steel plate shear wall systems consist of a high initial elastic stiffness followed by yielding of steel plates under tensile stress. After developing diagonal tension fields within the steel plates, the frame develops localized plastic hinges until the ultimate strength of the system is reached. This performance of the system occurs after a gradual deterioration in strength at relatively large displacements. The inherent ductility of the system creates a large energy dissipation capacity of the SPSW system.

Use of steel plate shear walls is more cost effective than the other lateral load resisting systems (Timler and Ventura, 1999). SPSWs are much lighter than the commonly used reinforced concrete shear walls, as they reduce both the gravity loads and seismic forces (Kristeva, 2010, 56-storey L.A. Live hotel). This aspect significantly reduces the foundation cost and practical complications (Lee et al., 2010, 75-storey Jinta Tower). Despite the benefits of SPSWs they are not widely used. Many previous experimental and analytical studies have shown that the flexural stiffness demand of columns in a

SPSW are both complex and, for typical systems, extremely large. SPSWs also have a lower flexural stiffness relative to concrete walls, which makes more challenging the use of this system. Introducing relatively large cut-out into the infill plate, causes significant reduction in initial stiffness and other seismic parameters of SPSWs.

The current research conducted to investigate the effects of relatively large cut-outs on seismic behaviour of SPSW system. The preliminary research has suggested practical methods to improve the performance of SPSW with cut-outs. Test results and FEA show that contribution of beam element for anchoring diagonal tension field action has increased. This contribution of horizontal boundary element could reduce flexural stiffness demands for columns.

1.2. Objectives

The main objectives of this research work are as follows:

1. Increasing the initial stiffness and ultimate-load capacity of SPSW systems without increasing flexural stiffness for vertical boundary members.
2. Assessing the effects of cut outs on the seismic behaviour of SPSW systems.
3. Improving the seismic behaviour of SPSW systems with cut-outs.
4. Developing a finite element method for simulating and analysing the SPSW systems with and without cut-outs.

1.3. Scope

To achieve the research objectives, the following actions were taken;

First, a loading system was designed and constructed to apply the cyclic quasi-static load. Loading history was defined according to ATC-24 protocol. The quasi-static cyclic test provides detailed information on the stress flow in the steel plate and boundary members, load-displacement measurement data at critical locations, stiffness, ductility, energy dissipation capacity and strength degradation for test specimens.

FE models were developed for simulating SPSW systems and the results were initially validated by available test results from literature. The method was subsequently used for further studies. The accuracy of the models was confirmed by comparing test results with FEA results.

From the literature review it was found that increasing the strength or stiffness of steel plate and practical construction considerations leads to design of strong columns for SPSW systems. In this research, GFRP-steel sandwich shear walls were designed and manufactured not only to improve the seismic performance of steel plate but also to decrease the flexural stiffness demand of vertical boundary members.

For evaluating the contribution of a beam element for bearing the diagonal tension field action, the vertical displacement for the mid part of the beam element during the cyclic loading was monitored and recorded. For this purpose, an innovative sliding-measurement system was developed.

The effectiveness of laminating GFRP plies on steel plate for improving the performance of systems with and without the cut-outs was proved based on test and FEA results.

The final part of this research dealt with the application of optimally designed steel stiffeners for improving the seismic behaviour of SPSW systems with cut-outs where longitudinal and transversal stiffeners were welded on one side of the steel plate.

1.4. Outline of the thesis

This section provides an overview of the thesis organisation.

Chapter 2 provides a revision of numerous past research studies performed on SPSWs.

Chapter 3 describes the finite element method used to predict the behaviour of specimens during the test program. The models were validated with the results of British Columbia tests on the SPSW system. The method was then applied to analyse the specimen with cut-outs. Variety of cut-out dimensions, thickness of steel plate and application of steel stiffeners were considered in the model.

CHAPTER 1: INTRODUCTION

Chapter 4 provides detailed information about the manufacturing of test specimens, design and construction of the loading system for applying the cyclic quasi-static load to the test specimens and the design and construction of the lateral bracing system. The coupon test results, outlining of instrumentations, design of the innovative sliding measurement system, introducing the utilisation of imaging techniques via infrared thermal camera for localisation of delamination in sandwich panels are also described in this chapter. The testing of a trial specimen is the final section of this chapter. This test was used for checking the loading system, data acquisition system, instrumentations and the suitability of connections between test specimen and reaction frame.

Chapter 5 describes the quasi-static experimental program and corresponding FEA results for all specimens. Test programme includes the frame-only specimen, steel plate shear wall with two different types of steel plate and GFRP-steel sandwich shear wall specimens with different configurations of sandwich panels. Detailed discussion of the behaviour of specimens during the test program, instrumentation and data acquisition system, as well as the loading protocol and individual results for each test are presented. The application of imaging techniques for detecting the possible delamination of sandwich panels and comparison of the results obtained from experimental tests and finite element analysis are also presented in this chapter.

Chapter 6 describes the program of experimental and numerical studies on steel plate shear walls with cut-outs. The effects of cut-outs on the essential parameters of seismic performance of specimens such as initial stiffness, ultimate load capacity and energy dissipation capacity are investigated using the test results and corresponding FE analysis. Two different methods are suggested for restoring the design characteristics of specimens. The use of GFRP plies with specific attention to the results obtained in chapter 5 and the optimal design of longitudinal and reversal steel stiffeners.

Chapter 7 presents comparative studies of various tests and discusses the results, assessing the FE method for estimating the behaviour of test specimens.

Chapter 8 provides a summary of the research program, the key conclusions of the research and recommendations for future research.

2. LITERATURE REVIEW

2.1. Introduction

Over the last three decades numerous research programs have been conducted on Steel Plate Shear Walls. Experimental and theoretical studies have demonstrated that properly designed SPSWs are an effective and economical system in comparison with other steel systems, such as reinforced concrete elevator cores and shear walls (Agelidis and Mansell, 1982; Timler, 1998-b) for resisting lateral loading due to either wind or earthquake loads. Steel plate shear walls have been used in a number of buildings in North America and Japan as lateral load resisting system. In early designs, shear buckling of steel plate was prevented by utilising either appropriately thick steel plate or heavily stiffened steel plate. In recent years, however, the idea of using the post-buckling shear strength of steel plate has gained wide attention from researchers and designers.

Under cyclic loading, diagonal tension fields are formed within the steel plate which acts like diagonal action in braced frames. This kind of behaviour of SPSW completes the truss action and thus it is efficient for control of lateral drift in buildings. In other words when shear panels are designed properly, the load-resisting mechanism changes from in-plane shear to inclined tension field after buckling of the shear panel.

A conventional steel plate shear wall is comprised of boundary members including beams, columns and steel plate (Figure 2.1).

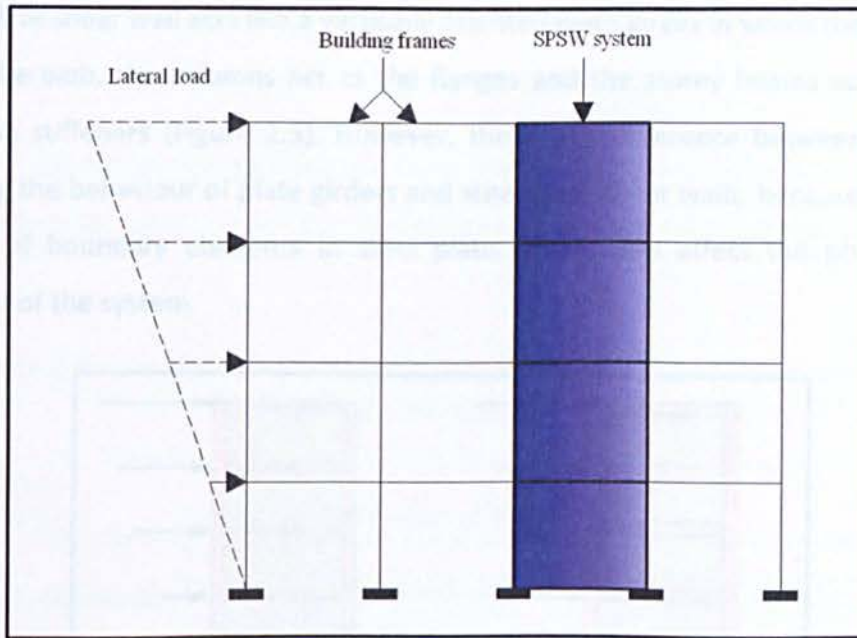


Figure 2.1: Typical steel plate shear wall system

There are various types of steel plate shear walls such as stiffened and un-stiffened steel plate, shear and rigid beam-to-column connections, perforated and non-perforated steel plates and welded and bolted steel plate to boundary members (Figure 2.2).

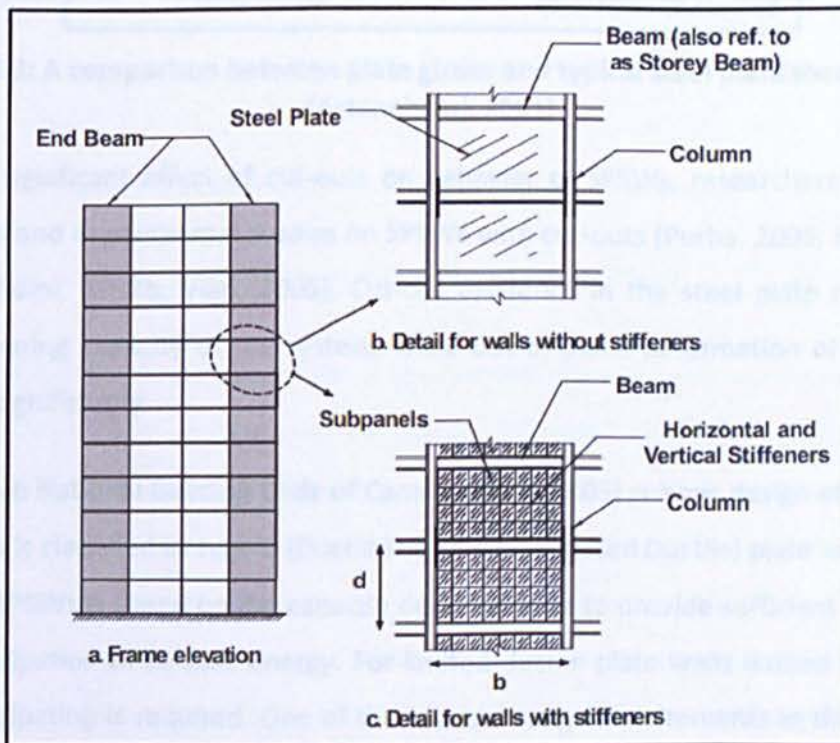


Figure 2.2: Scheme of steel plate shear wall with details depicting an un-stiffened steel plate and steel plate with multiple stiffeners (From Kharrazi, 2005)

A steel plate shear wall acts like a vertically oriented plate girder in which the steel plate acts as the web, the columns act as the flanges and the storey beams act similar to transverse stiffeners (Figure 2.3). However, there is a difference between equations governing the behaviour of plate girders and steel plate shear walls, because noticeable stiffness of boundary elements in steel plate shear walls affect the post buckling behaviour of the system.

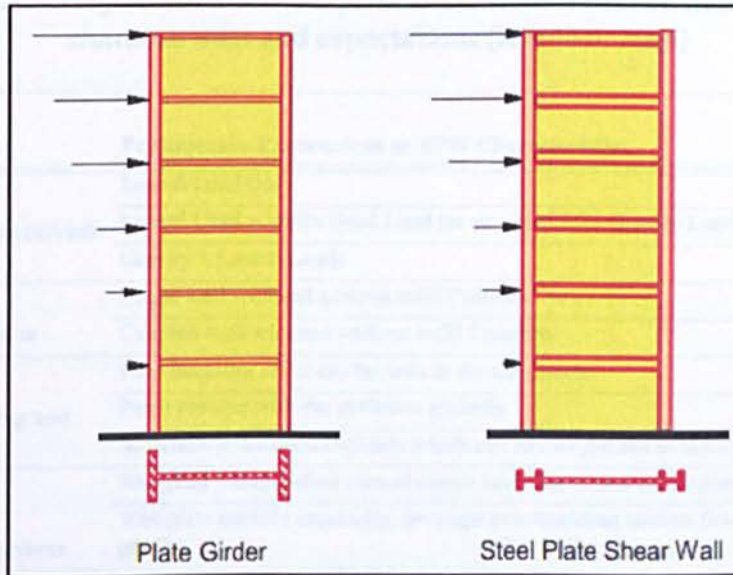


Figure 2.3: A comparison between plate girder and typical steel plate shear wall (Astaneh-Asl, 2001)

Due to a significant effect of cut-outs on behavior of SPSWs, researchers have done theoretical and experimental studies on SPSWs with cut-outs (Purba, 2006; Roberts and Sabouri-Ghomi, 1992b; Vian, 2005). Cut-out existence in the steel plate reduces the loading bearing capacity of the system, while out of plane deformation of steel plate increases significantly.

According to National Building Code of Canada (NRCC 2005) seismic design of steel plate shear walls is classified as type D (Ductile) or type LD (Limited Ductile) plate walls. Design of ductile SPSWs is based on the capacity design criteria to provide sufficient capacity of energy dissipation of seismic energy. For limited ductile plate walls limited capacity of energy dissipating is required. One of the seismic design requirements in the Canadian steel design standard CAN/CSA S16-01 (CSA 2001) and current AISC provisions (AISC 2005) is that SPSWs be designed in accordance with capacity design principles. Capacity

design for SPSWs is based on tension yielding of the steel plate prior to the columns attaining their factored capacity.

In general, SPSWs are categorized based on their performance, selection of structural and load-bearing system, and the presence of stiffeners and perforation (Kharrazi, 2005).

Table 2.1: Categorization of Steel plate shear walls based on performance characteristics and expectations (Kharrazi, 2005)

Performance Characteristic	Performance Expectations or SPW Characteristics
Type of Loading carried by SPW	Lateral Load Only
	Lateral Load + Wall's Dead Load (or so called 50% Gravity Load)
	Gravity + Lateral Loads
Structural System	Single wall with and without infill Columns
	Coupled wall with and without infill Columns
Stiffener Spacing and Size	Post-Buckling effect can be seen in the sub panels
	Panel buckles with the stiffeners globally
	Stiffeners produces sub-panels which can be categorized as thick panel
Web Plate Behaviour	Web plate yields before critical elastic buckling occurs (thick plate)
	Web plate buckles elastically, develops post-buckling tension field, then yields (thin plate)
Web Plate Perforations	With perforations
	Without perforations

2.2. Chronological development of steel plate shear walls

2.2.1. Early research on steel plate shear walls (1973-1999)

Takahashi et al. (1973) conducted the first extensive experimental work on SPSWs. The main objective of their research was to test the suitability of different configuration of stiffeners on the behaviour of stiffened steel plates. The research program comprised 12 quarter-scale one-storey specimens and two full-scale two-storey specimens, which were tested under quasi-static cyclic loading. The aspect ratio of 12 specimens was 1.33 with a width of 1200mm, a height of 900mm and a thickness of 2.3mm, 3.2mm and 4.5mm for steel plates. In order to simulate relatively pure shear behaviour in the steel plate, the specimens were loaded in diagonal direction. The connections between boundary members had an extremely stiff bolted connection. For quarter scaled

specimens the width and spacing of stiffeners on one side or both sides of the steel plate were the main parameters of focus within this research program. All specimens had vertical or vertical and horizontal welded stiffeners on one or both sides of the steel plates with the exception of the control specimen. Based on the outcome from this portion of tests three different types of behaviour were observed (Takahashi et al., 1973):

- i. Global buckling of the steel plate due to the lack of flexural stiffness of the transverse stiffeners;
- ii. Local buckling of sub-plates due to large spacing of stiffeners and sufficient stiffness of associated stiffeners;
- iii. Specimens with stiffeners mounted to both sides were more stable in comparison to specimens with stiffeners only on one side.

All specimens were stable and ductile and drift angle in some cases exceeded 0.1 radians under cyclic loading (Figure 2.4). Hysteresis curves, post buckling behaviour, effect of stiffeners, and effect of stiffness and spacing on seismic behaviour of the specimens were investigated in the first part of the test program. They recommended that the stiffeners should be designed so that buckling occurs in the sub-plates, whilst global elastic buckling of the steel plate is prevented.

In the second part of the test program, the attempt was made to construct and test two full scale single-bay 2-storey stiffened steel plate shear wall specimens as part of 32-storey building. One specimen represented the steel plate shear wall with cut-out and the other one without cut-out. The thickness of the steel plate was 4.5 mm and 6 mm, respectively. They concluded that conventional shear theory could be used to calculate strength and stiffness of stiffened steel plate shear walls. As part of this research program, a full-scale specimen was modelled analytically utilising elastic-perfectly plastic material model with von Mises criterion. The analytical result was in good agreement with test results.

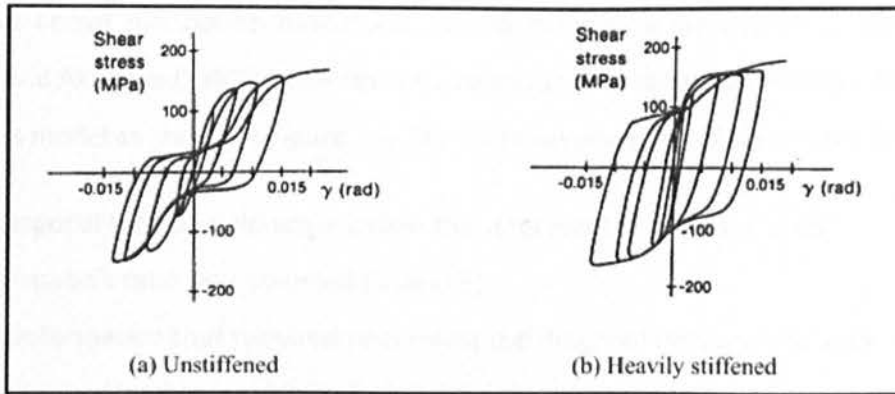


Figure 2.4: Hysteresis behaviour of (a) An un-stiffened SPSW and (b) Heavily stiffened SPSW (Takahashi et al., 1973)

Mimura and Akiyama (1997) studied the behaviour of un-stiffened steel plate shear walls. They developed an analytical method to predict monotonic and hysteretic response of SPSWs. This load-displacement model was pursued further at the University of Alberta. In the model proposed by Mimura and Akiyama (1997) the overall capacity of the system was computed based on well-established elastic buckling theory of plates with the pinned boundary assumption. They assumed that the elastic buckling of steel plate occurs prior to ultimate shear strength of steel plate and then diagonal tension field act as load resisting mechanism (Wagner, 1931). In other words, the ultimate strength of the system can be determined by considering the force required for elastic buckling of steel plate and post buckling strength of steel plate plus strength of boundary elements. Figure 2.5 illustrates the monotonic load-displacement diagram for a steel plate shear wall for elastic-perfectly plastic behaviour of the surrounding elements.

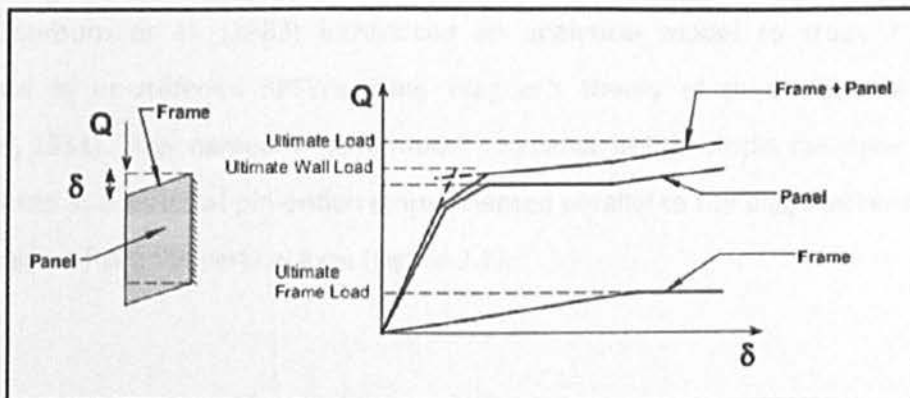


Figure 2.5: Monotonic load-displacement behaviour of an SPSW showing contribution by frame and steel plate (Mimura and Akiyama, 1997)

Based on above mentioned monotonic load-displacement behaviour of the system, Mimura and Akiyama (1997) made several assumptions in order to develop a theoretical hysteresis model as shown in Figure 2.6. The main assumptions of this model are:

- i. Diagonal tension field angle within the steel plate is constant at 45° ;
- ii. Poisson's ratio was assumed to be 0.5;
- iii. Deformation that required re-forming the diagonal tension field while reversing the applied load is equal to half of the plastic deformation from the previous cycle.

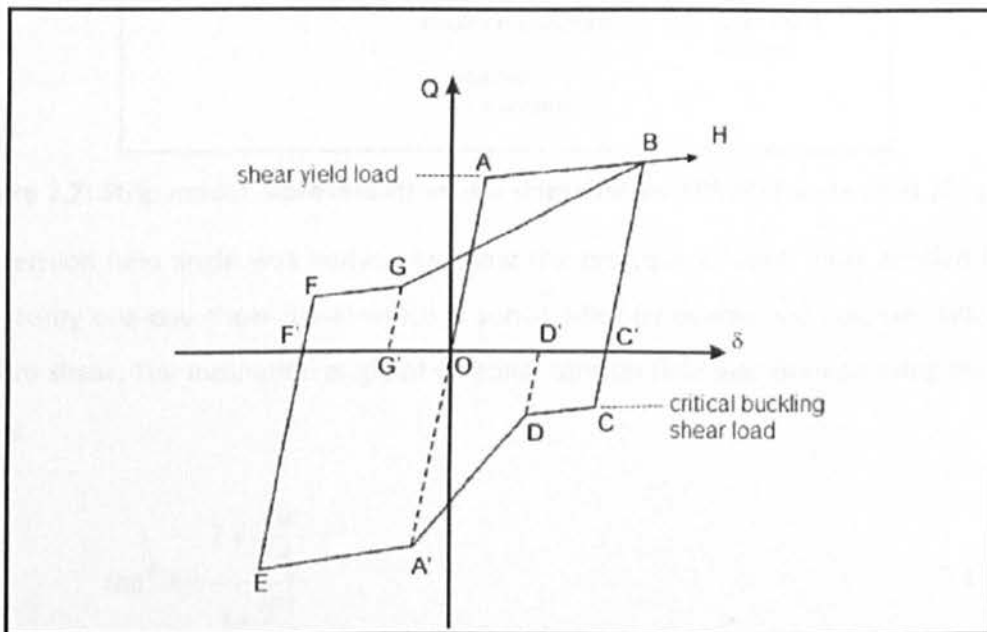


Figure 2.6: Hysteresis model proposed by Mimura and Akiyama (1997)

Thorburn et al. (1983) noted that although thin steel plate buckles in the very early stage of loading, the system can carry noticeable load due to post buckling behaviour of steel plate. Thorburn et al. (1983) introduced an analytical model to study the shear resistance of un-stiffened SPSWs using Wagner's theory of pure diagonal tension (Wagner, 1931). They named it "strip model", because in this model the shear panel is represented as a series of pin-ended strips oriented parallel to the diagonal tension field at the angle α from the vertical axes (Figure 2.7).

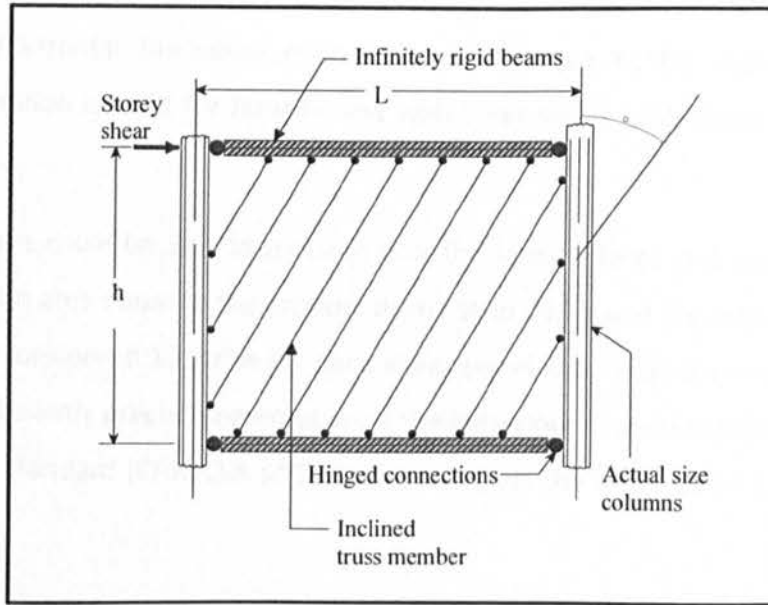


Figure 2.7: Strip model representation of a single storey SPSW (Thorburn et al., 1983)

The tension field angle was derived by using the principle of least work applied to the one-storey one-bay shear panel which is surrounded by beams and columns subjected to pure shear. The inclination angle of diagonal tension field was derived using equation below:

$$\tan^4 \alpha = \frac{1 + \frac{Lw}{2A_c}}{1 + \frac{hw}{A_b}} \quad 2.1$$

where L is the frame width; w is the steel plate thickness; h is the storey height; A_c is the cross sectional area of the column and A_b is the cross sectional area of the beam.

Some of the assumptions that researchers took into account are as follows:

- i. The proposed strip model was based on hinged connection between horizontal and vertical boundary elements;
- ii. The analysis was limited to elastic material behaviour;
- iii. Columns are assumed to be infinitely flexural stiff to ensure a uniform distributed tension field over the steel plate;
- iv. The compressive stress perpendicular to the diagonal tension field is insignificant;

- v. The horizontal boundary elements are assumed to be infinitely stiff. This assumption is valid for floor beams with steel plates both above and below the beam.

Strip members could be able to transmit only the tension force and each member was assigned to an area equal to the product of the strip width and the plate thickness. The researchers considered 10 strips for each shear panel and demonstrated that 10 strips could be sufficiently precise presentation of the behaviour of tension field. The Canadian steel design standard (CAN/CSA S16-01) recommends the strip model as a design tool for SPSWs.

In order to simplify the iterative process of designing a SPSW, Thorburn et al. (1983) described a Prat truss model, which is known as an Equivalent Brace Model (Figure 2.8). This model is used to simplify the steel plate as a single diagonal tension spanning between beam-to-column joints of the frame.

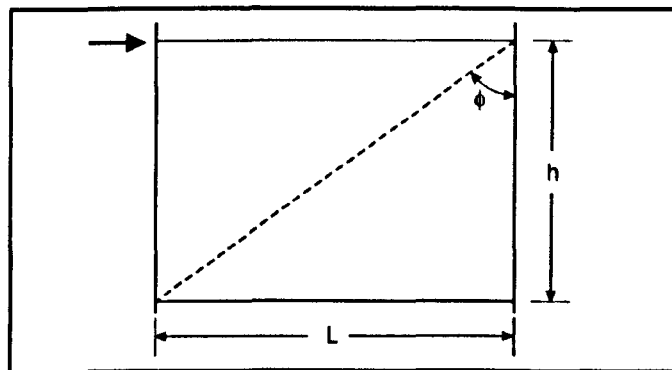


Figure 2.8: Equivalent Brace Model (Thorburn et al., 1983)

The model is based on rigid boundary elements and represents the stiffness characteristics of the tension field in the steel plate. The proposed equation for the area of the equivalent brace is shown below:

$$A = \frac{wL \sin 2\alpha}{2\sin\Phi \sin 2\Phi} \quad 2.2$$

where ϕ is the acute angle described by brace and columns.

CAN/CSA S16-01 (Clause 20.2) recommends the Equivalent Brace Model as a preliminary design tool for SPSWs.

CHAPTER 2: LITERATURE REVIEW

In order to assess the effects of steel plate thickness, storey width and height and also vertical boundary element stiffness on the behaviour of un-stiffened SPSW, Thorburn et al. (1983) conducted a series of parametric studies. They found that:

- i. There was a linear relationship between panel stiffness and the thickness of steel plate, which means an increase of steel plate thickness, causes the stiffness of the panel to increase;
- ii. There was an inversely linear relationship between storey height and panel stiffness;
- iii. For certain vertical boundary elements, by increasing the panel width the panel stiffness was decreased. This result is valid up to a certain limit of panel aspect ratio. After reaching the panel aspect ratio of 1, the increase of panel width caused an increase of panel stiffness.

Timler and Kulak (1983) tested a full-scale, single-storey and one-bay SPSW specimen with steel plate thickness of 5mm and aspect ratio of 1.5 to verify the adequacy of the strip model proposed by Thorburn et al.(1983). Due to the test set-up in this research, the columns were the horizontal boundary members while the beams were the vertical boundary members. The specimen consisted of two panels, both 3750 mm wide and 2500 mm in height. The interior beam of the specimen incorporated moment-resisting beam to column connection, while pin joints were placed at the exterior ones (Figure 2.9). The specimen was tested in two stages. During the first stage the frame was statically loaded with three complete cycles up to its maximum allowable serviceability drift limit of $h_s/400$ or 6.25 mm according to Canadian Standard Association, (CSA-S16.1-M78) 1978. In this stage the specimen remained in the elastic region and then during the second stage it was tested under monotonic loading to determine the ultimate capacity. The test set-up did not include gravity loads to the columns.

Timler and Kulak (1983) noted that the inclination angle for tension field under the service loading varied along the centre line of steel plate between 44° and 56°, but at the yield load level the overall value of inclination angle along the steel plate centre line was consistent with the analytical results. The researchers noted that the performance

of SPSWs and, subsequently, the magnitude of inclination angle along the steel plate centre line are dependent on flexural stiffness of vertical boundary members. They modified the Eq.(2.1) for, α , proposed by Thorburn et al. (1983) to take into account the flexural stiffness of columns. The modified equation is:

$$\tan^4 \alpha = \frac{1 + \frac{Lw}{2A_c}}{1 + hw \left(\frac{1}{A_b} + \frac{h^3}{360I_c L} \right)} \quad 2.3$$

I_c is the second moment of inertia for the column and all other parameters are as defined earlier in Eq. (2.1).

There was a good agreement between predicted and measured magnitudes of the steel plate stresses, load-deflection response and axial strain. The discrepancies found in the results using the Thorburn et al.(1983) equation for α were insignificant. However, it was recommended that the revised Eq. (2.3) be used in order to gain higher accuracy when computing the inclination angle for the diagonal tension field. Due to the lack of panel above the top beam which could introduce tension fields in the opposite direction in comparison to panel below, the required flexural stiffness for the top panel beam is different from interior beams. The equation for the inclination angle was interpreted for the top panel of SPSWs. Similar to the previous equation pinned connection was assumed between the beam and columns. See below:

$$\tan^4 \alpha = \frac{1 + Lw \left(\frac{1}{2A_c} + \frac{L^3}{120I_b h} \right)}{1 + hw \left(\frac{1}{2A_b} + \frac{h^3}{360I_c L} \right)} \quad 2.4$$

where I_b is the second moment of inertia of the beam about the axis orthogonal to the web of the beam.

As a result, the simplified strip model developed by Thorburn et al. (1983) predicts reasonably the overall load-deflection behaviour of specimens. The predicted elastic stiffness of specimens using this model was slightly higher than the measured value.

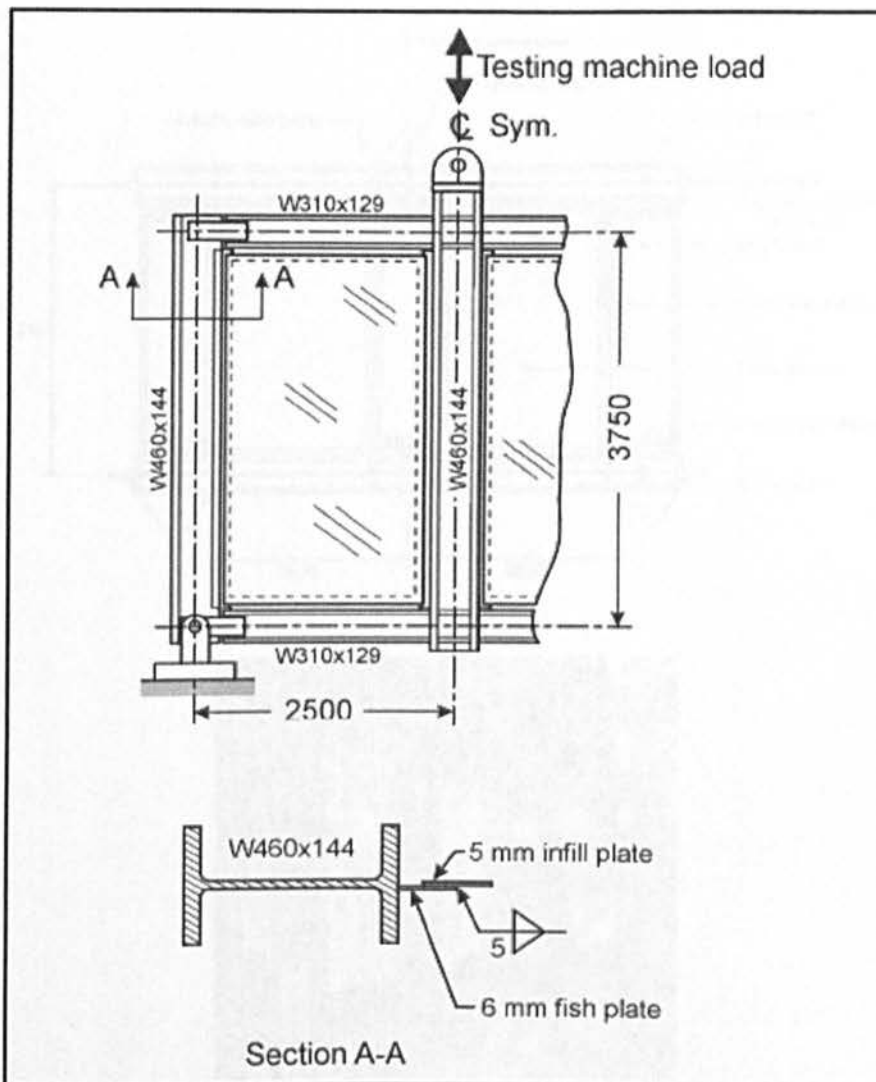


Figure 2.9: One-Storey test specimen (Timler and Kulak, 1983)

Tromposch and Kulak (1987) tested a full-scale single-storey two panel un-stiffened SPSW specimen under the quasi-static fully reversed cyclic loading (Figure 2.10). The specimen was similar to that tested by Timler and Kulak in 1983. The major differences between the two specimens are as follows:

- i. Change in the bay dimension to 2200 mm in height and 2750 mm in width;
- ii. Bolted beam-to-column connection;
- iii. Thinner hot rolled steel plate with 3.25 mm thickness;
- iv. Stiffer beams;
- v. The columns were pre-loaded prior to the loading of specimens through high strength pre-stressed rods and anchored at both ends of the columns.

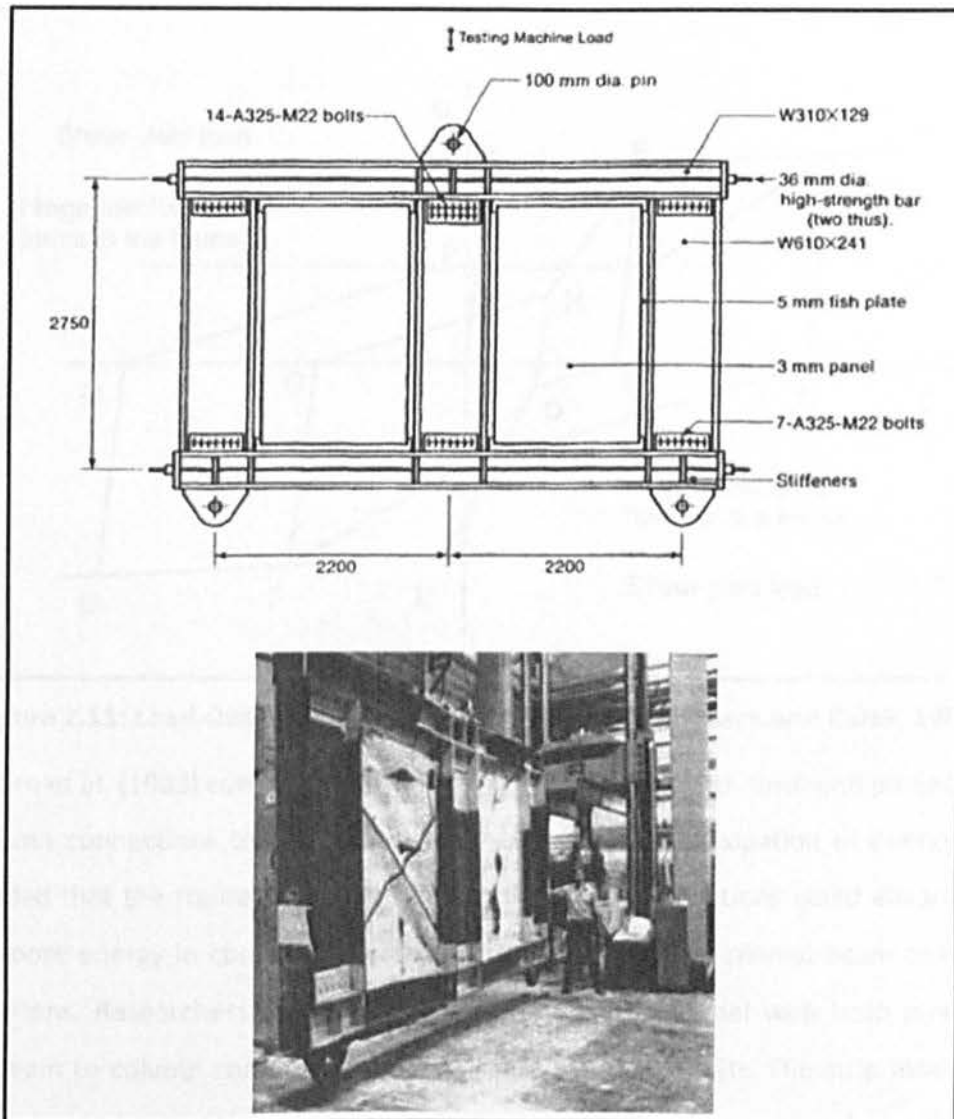


Figure 2.10: SPSW as tested by Tromposch and Kulak (1987)

Due to the restriction of the hydraulic actuator system, the specimens were loaded up to approximately 67% of their ultimate capacity cyclically in twenty eight cycles. Afterwards configuration of the loading system was modified and the pre-load of the columns was removed, then the specimen was loaded monotonically. Tearing of welds was observed in several corners of the steel plate during final loading stage (Tromposch and Kulak, 1987).

The hysteresis graph introduced by the specimen was pinched but stable. Figure 2.11 illustrates the hysteresis model proposed by Tromposch and Kulak (1987) to predict the hysteresis behaviour of an un-stiffened SPSW which was based on the previous research conducted by Mimura and Akiyama (1977).

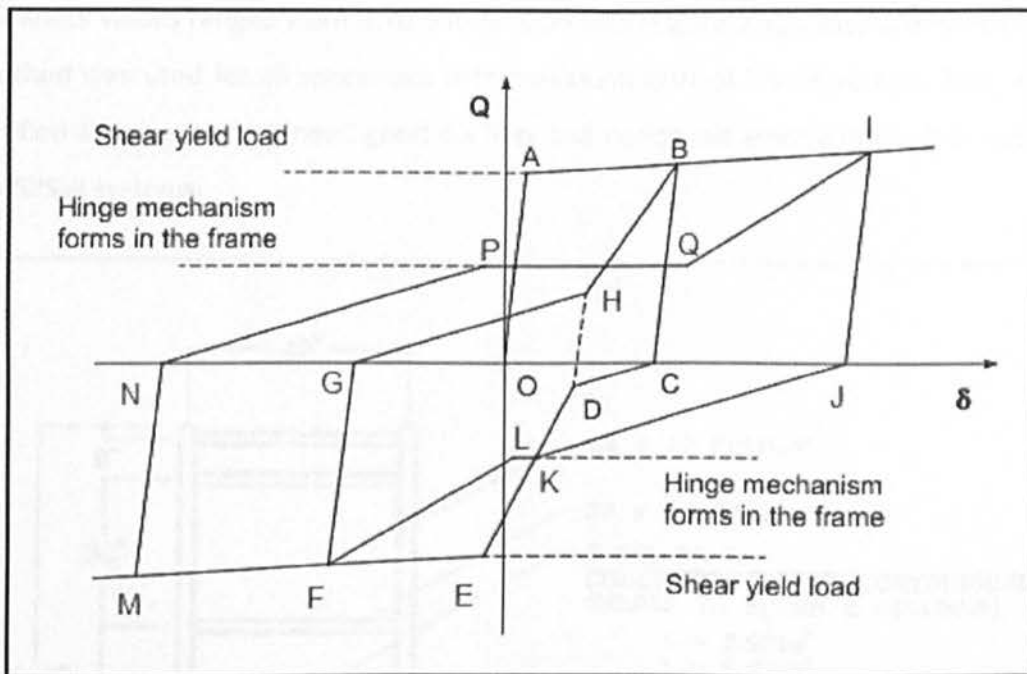


Figure 2.11: Load-Displacement hysteresis model (Tromposch and Kulak, 1987)

Thorburn et al. (1983) conducted further parametric studies with fixed and pinned beam to column connections to assess the ability of system for dissipation of energy. They concluded that the frames with fixed beam to column connections could absorb three times more energy in comparison with the frame with simple pinned beam to column connections. Researchers analysed the SPSW using strip model with both pinned and fixed beam to column connections and compared to test results. The strip model with fixed connection provided an upper bound solution and a lower bound solution with pinned beam to column connection. The test specimen result fell in between the two extremes. The strip model with pinned boundary elements underestimated the initial stiffness of the system by 40% and ultimate capacity of the system by 16%, while the model with fixed boundary element connections underestimated the initial stiffness by 17% and overestimated the ultimate capacity of the system by 11%. The researchers also concluded that the eccentricity of fish plates in respect to boundary members has no noticeable effect on the performance of SPSW.

Chen (1991) conducted a test program on ten quarter scale, 3-storey, single bay SPSWs. Specimens were subjected to cyclic loading which consisted of 24 fully reversed cycles. The beams to column connections were either simple or fixed connections. Steel plate

thickness values ranged from 0.76 mm to 2.66 mm (Figure 2.12). Displacement control method was used for all specimens with maximum drift of 2% or 50 mm. Test results verified a high initial stiffness, good ductility and noticeable energy dissipation capacity for SPSW systems.

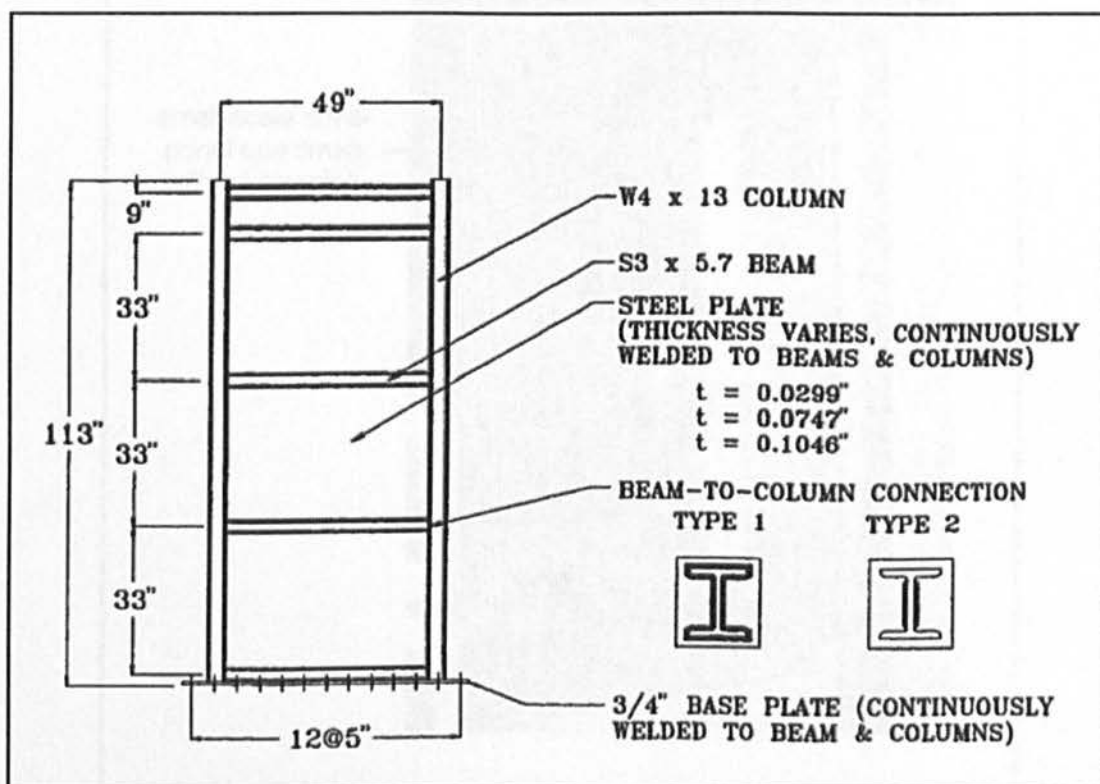


Figure 2.12: 3-storey model used by Chen (1991)

Roberts and Sabouri-Ghomi (1991) conducted a series of 16 small scale quasi-static cyclic loading test on slender un-stiffened shear panels without cut-outs and with centrally placed circular cut-outs to investigate their load-displacement characteristics. Steel plate thicknesses were 0.54 mm, 0.83 mm and 1.23 mm. The thinnest plate was made of aluminium alloy and the rest of them were made of steel. The dimensions of steel plate were 300 mm by 300 mm and 300 mm by 450 mm for square and rectangular panels respectively.

The steel plate edges were clamped to boundary members by two rows of 8 mm high tensile bolts. Boundary members were connected to the servo-hydraulic testing machine grips with two diagonally opposite pinned corners (Figure 2.13).

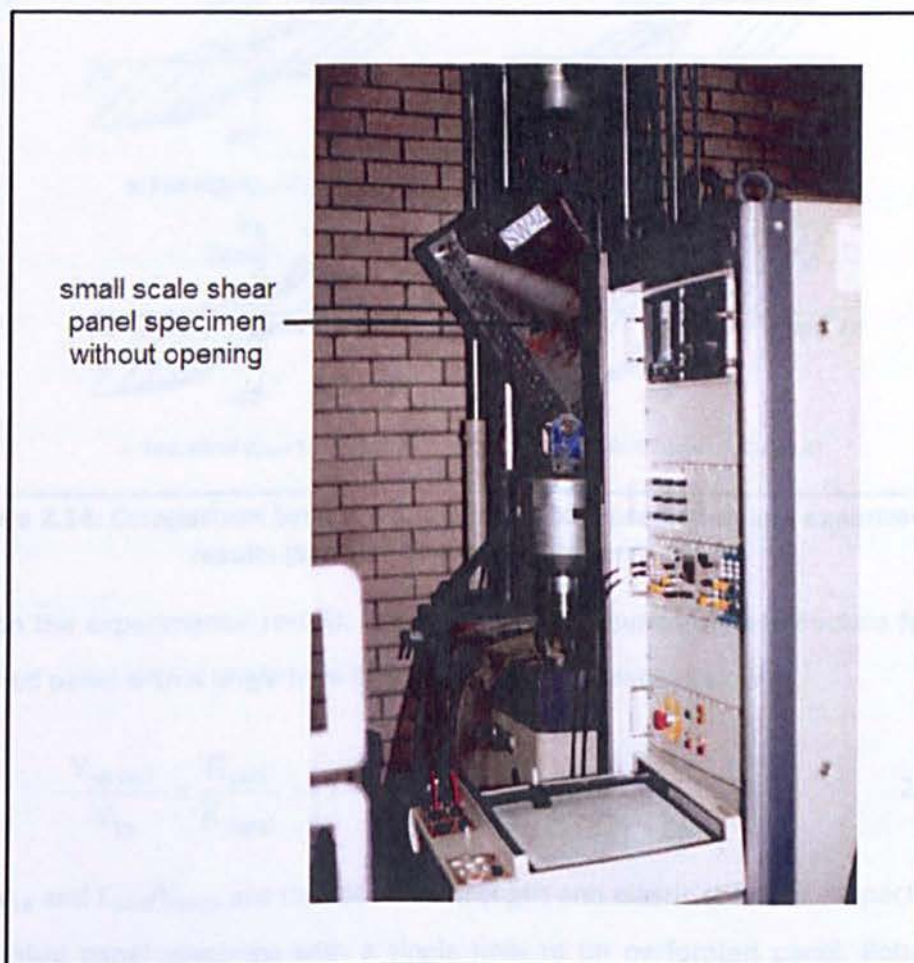


Figure 2.13: Servo hydraulic testing machine (Sabouri-Ghomi and Roberts, 1991)

Tensile load was applied diagonally to specimens until the panel experienced an elastic-perfectly plastic behaviour. After that, the specimen was subjected to the same magnitude of compressive load. This procedure was continued until gaining at least four complete cycles of load-displacement cycles by gradually increasing diagonal displacement. All panels indicated stable behaviour, but the hysteresis loops were pinched (Figure 2.14). Typical hysteresis loops presented by Roberts and Sabouri-Ghomi (1992a) indicate that the specimens show ductility of more than seven without significant decrease in strength. They investigated the effects of perforations of steel plate on the strength and stiffness of the system.

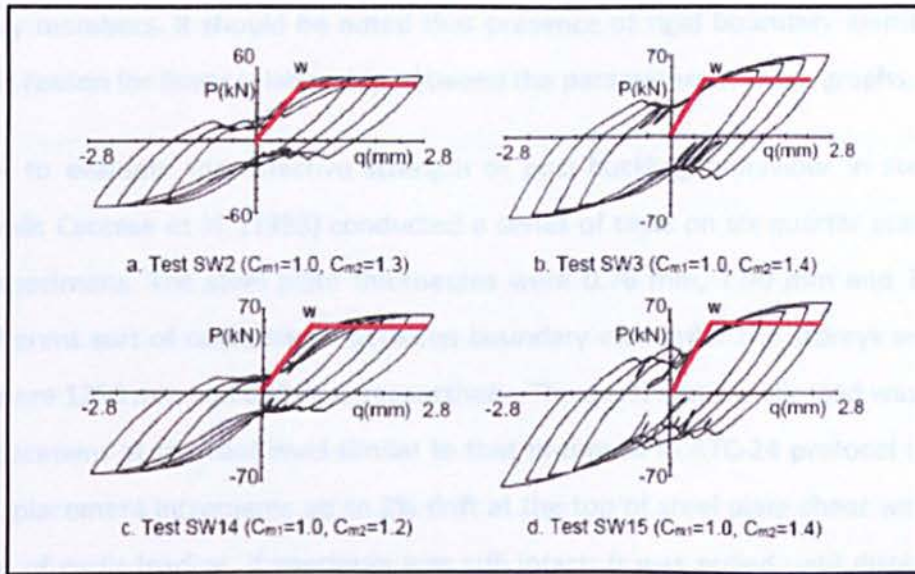


Figure 2.14: Comparison between analytical model prediction and experimental results (Sabouri-Ghomi and Roberts, 1991)

Based on the experimental results, they proposed an approximate reduction factor for perforated panel with a single hole in equation demonstrated below:

$$\frac{V_{yp,perf}}{V_{yp}} = \frac{K_{perf}}{K_{panel}} = \left[1 - \frac{D}{b} \right] \quad 2.5$$

$V_{yp,perf}/V_{yp}$ and K_{perf}/K_{panel} are the ratios of strength and elastic stiffness, respectively for a perforated panel specimen with a single hole to unperforated panel. Roberts and Sabouri-Ghomi (1992a) concluded that the strength and stiffness of wall will decrease linearly with an increase in $(1-D/b)$ as shown in Figure 2.15.

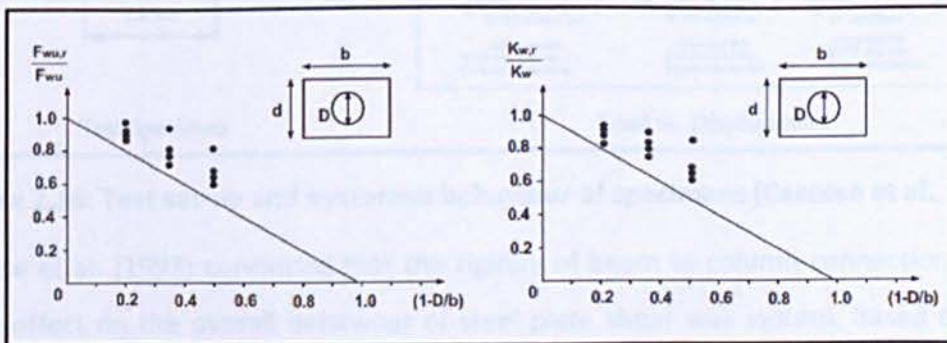


Figure 2.15: Effect of circular perforation on strength (left) and stiffness (right) of shear panel (Roberts and Sabouri-Ghomi, 1992a)

Based on test results, Roberts and Sabouri-Ghomi (1991) proposed an analytical model for predicting the hysteresis behaviour of shear panel with pinned connection to rigid

boundary members. It should be noted that presence of rigid boundary elements was the main reason for linear relationship between the parameters in these graphs.

In order to evaluate the effective strength of post-buckling behaviour in steel plate shear walls Caccese et al. (1993) conducted a series of tests on six quarter scale three-storey specimens. The steel plate thicknesses were 0.76 mm, 1.90 mm and 2.66 mm with different sort of connections between boundary elements. The storeys width and height were 1250 mm and 830 mm, respectively. The quasi-static cyclic load was applied to all specimens at the roof level similar to that proposed in ATC-24 protocol (1992) in eight displacement increments up to 2% drift at the top of steel plate shear walls. After each set of cyclic loading, if specimen was still intact; it was pulled until displacement limit of actuator. Figure 2.16 shows test set-up and hysteresis behaviour for Caccese et al. (1993) specimens.

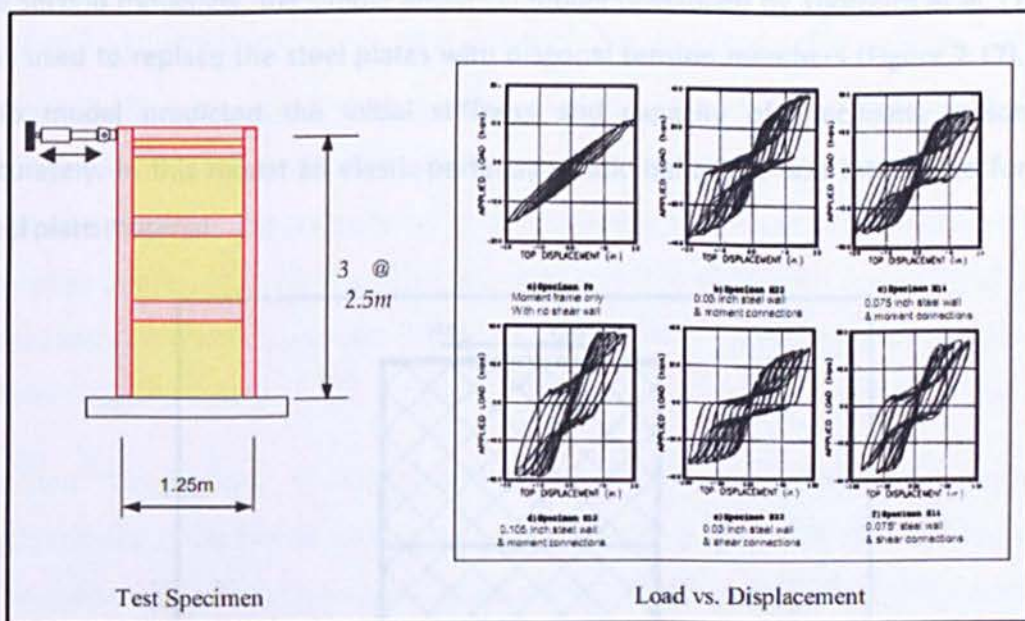


Figure 2.16: Test set-up and hysteresis behaviour of specimens (Caccese et al., 1993)

Caccese et al. (1993) concluded that the rigidity of beam to column connections has a minor effect on the overall behaviour of steel plate shear wall system. Based on their findings, this is due to continuous weld connections between steel plate, surrounding beams and columns. They also concluded that for the slender steel plates the inelastic behaviour of system is initiated by yielding of steel plate, and the ultimate strength of the system is governed by the formation of plastic hinges in the columns. When the

CHAPTER 2: LITERATURE REVIEW

thicker plate is used, the failure mode of specimen is governed by instability of columns while insignificant increase is achieved for the capacity of system. In other words, the use of thicker plates would not necessarily enhance the capacity of steel plate shear wall system.

Following the experimental study, Elgaaly et al. (1993) carried out two computer-based models to study the ultimate capacity of specimens under the monotonic loading. In the first modelling, a non-linear finite element analysis, including both material and geometric non-linearity was carried out. The steel plate and boundary members were modelled with shell and beam elements respectively. The finite element results over estimated both the initial stiffness and ultimate strength of specimens. The main reason for these discrepancies was related to initial out-of-plane deformation of steel plate and overall out-of-plane deformation of specimens that occurs during the test procedure. In the second modelling, the simple analytical model developed by Thorburn et al. (1983) was used to replace the steel plates with diagonal tension members (Figure 2.17). The strip model predicted the initial stiffness and capacity of specimens reasonably accurately. In this model an elastic-perfectly plastic behaviour was introduced for the steel plate material.

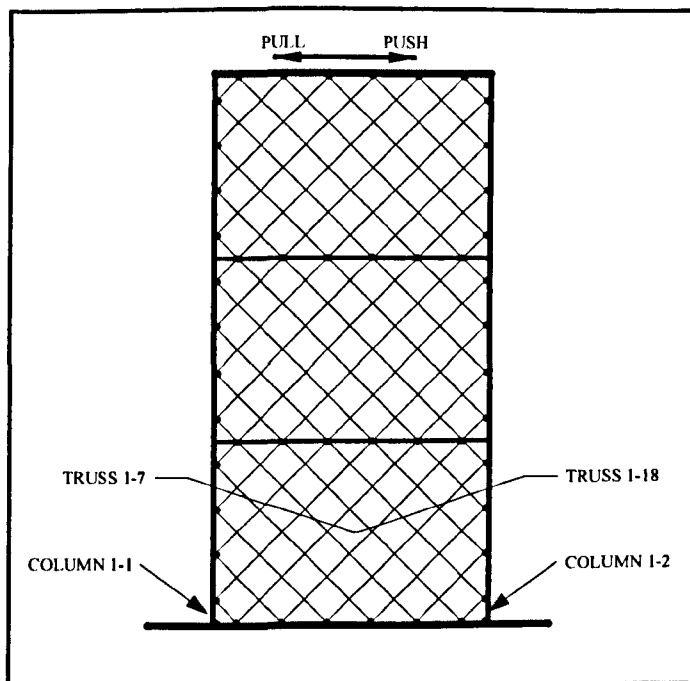


Figure 2.17: Cyclic strip model (Elgaaly et al., 1993)

CHAPTER 2: LITERATURE REVIEW

In order to gain a better prediction for monotonic behaviour of the system using Thorburn's strip model, a tri-linear, stress-strain diagram was proposed (Figure 2.18). The monotonic behaviour of specimens was predicted accurately using this model.

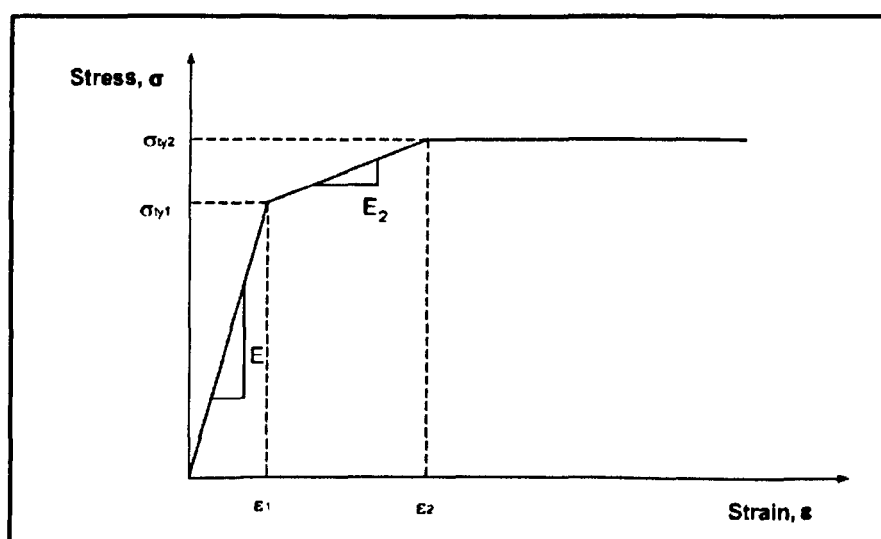


Figure 2.18: Tri-linear stress-strain relationship for strip model (Elgaaly et al., 1993)

In Figure 2.18 the slope of E_1 represents the elastic modulus for steel and E_2 is selected Young Modulus that provides a good agreement between experimental test and numerical results. In this diagram, the stress σ_{ty1} corresponds to the load at which the steel plate starts to yield. The stress σ_{ty2} represents the yield stress for steel plate. The magnitude of σ_{ty1} and E_2 was determined empirically, which is dependent on slenderness of steel plate.

Xue and Lu (1994-a, b) examined analytical studies on different connection configurations of six twelve-storey three-bay steel plate shear wall. The widths of the exterior bays and interior bay were 9144 mm and 3658 mm, respectively. The height of panels for lowest storey and for the rest of storeys was 4572 mm and 3685 mm, respectively. The beam to column connections for exterior bay were moment resisting connections while the interior bay contained the steel plate with either rigid or simple beam to column connections. Two different connections of steel plate to boundary members were considered. In the first scenario the steel plate was connected to surrounding beams and columns, while in the second scenario steel plate was only connected to floor beams and there is no connection between steel plate and columns.

CHAPTER 2: LITERATURE REVIEW

Different thicknesses were selected for shear panels. For bottom, middle and four top storeys, the thickness of steel plate was 2.8 mm, 2.4 mm and 2.2 mm respectively. The most important parameter investigated in this study was the lateral stiffness of the system at design load level because the drift control is the major design consideration. In the analysis conducted, steel plate was allowed to buckle or yield, however it was assumed that boundary members remain elastic. Boundary members were modelled using beam elements while steel plate was modelled by four-node shell elements with large deformation capacity. Lateral loads were applied monotonically at the floor levels without addition of the gravity loads.

Results obtained from analytical model for each specimen were compared to a lower and upper bound specimens. The lower bound model consisted of moment resisting exterior frames and an interior frame with simple beam to column connections without steel plate. The upper bound model consisted of moment resisting interior and exterior frame with fully welded steel plate to all boundary members of interior frame. Xue and Lu (1994a) demonstrated that presence of shear panels caused a significant increase in the lateral stiffness of the systems; nevertheless, moment resisting connections in interior frame had negligible effect on increasing lateral stiffness. It was also concluded that the systems with simple beam to column connections in the bay filled by steel plate and shear panels with no connection to vertical boundary members were the most economical systems (Xue and Lu, 1994-a). There was no experimental confirmation for this conclusion.

Later, Xue and Lu (1994-b) also conducted a numerical parametric study on a one-bay one-storey steel plate shear wall to find out the load-displacement characteristics of frame-wall system. The system consisted of simple beam to column connections with steel plate connection to the girder only. The width-to-thickness ratio of steel plate and the aspect ratio of panel were studied by finite element analysis for 20 different cases. The researchers found that the variation of width-to-thickness ratio has no significant effect on the load-displacement performance of the structure. In their study, the need for further investigation related to the effects of width-to-thickness ratio on ultimate load capacity of shear panels was emphasised (Xue and Lu, 1994-b). The aspect ratio of

the panels had noticeable effect on the performance of shear panels, because the development of diagonal tension fields mainly depends on the aspect ratio of shear panels. The effect of panel aspect ratio was found significant within the ratio of 1 to 2, in which the yield strength capacity of the system increased by as much as 30%. Conversely the increase of the panel aspect ratio from 2.0 to 2.5 had no apparent effect on enhancing the overall yield capacity of the model (Xue and Lu, 1994-b).

Nakashima et al. (1994, 1995a, b) studied the cyclic behaviour of a steel plate shear wall built with panels made of Low Yield Steel (LYS). Figure 2.19 shows the stress-strain diagram for mild steel which is similar to ASTM A36/A36M-97, the stress-strain for high strength steel which is similar to A572, Gr. 50, and the LYS developed by Nippon Steel (1998) in Japan.

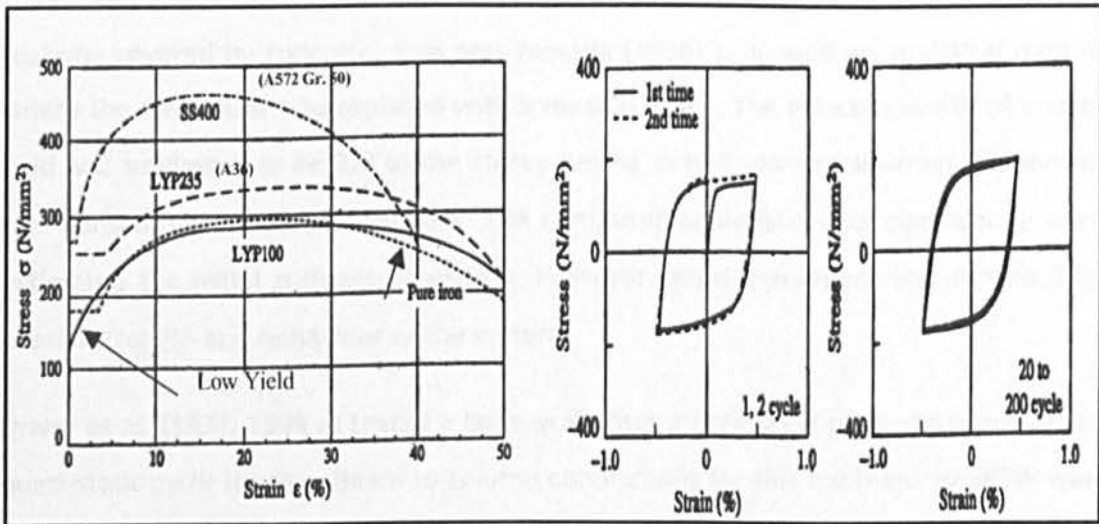


Figure 2.19: Stress-strain diagram of low-yield steel and other steel grades (Nippon Steel, 1998)

As shown in Figure 2.19, the yield point of LYS is about half that of A36 and its ultimate strain is twice that of A36 steel. These specifications cause early yielding of steel plate and relatively large energy absorption capacity. The tests conducted on the LYS under cyclic loads confirmed stable hysteresis curves and relatively large energy dissipation capability (Nakashima et al., 1994; Nakashima et al., 1995b).

The application of Low Yield Steel (LYS) walls in high-rise buildings was studied by Torii et al. (1996). In recent years more interest and effort in Japan has been given to use and

development of LYS application in high-rise buildings. These research efforts have led to design and construction of a number of buildings utilising this system (Yamaguchi et al, 1998). The research results for using this system are promising. However, more research and development need to be done in this field.

Sugi and Yamada (1996) conducted experimental test and analytical study on twenty-three one-tenth scaled specimens with a height of 300 mm with and without concrete covering. The main focus of this research was the aspect ratio of shear panel from 1:1 to 1:2, thickness of shear panel from 0.4 mm to 1.2 mm and thickness of concrete. Specimens were subjected to monotonic and cyclic loading. In this research specimens were made of two adjacent identical panel connected together with a deep beam. The specimens were subjected to loading along this deep beam. Similar setup was used by Timler and Kulak (1983). The boundary members for all tests were wide flange steel sections covered by concrete. Sugi and Yamada (1996) proposed an analytical method where the steel plate was replaced with a tension brace. The effective width of tension field was suggested to be $2/3$ of the storey height. A tri-linear stress-strain relationship was considered for brace members. The computer analysis results significantly over-estimated the initial stiffness of system. However, good agreement was achieved for overall strength and behaviour of the system.

Driver et al. (1997, 1998-a) tested a large-scale four-storey steel plate shear wall under quasi-static cyclic loading. Beam to column connections for this multi-storey SPSW were designed as full moment connection. Total height of specimen was 7.5 m with the width of 3.4 m. Thicknesses of steel plates for the first and second storey were 4.8 mm and for third and fourth storey were 3.4 mm. Welded connections were applied for connections between steel plate to fish plates and fish plates to boundary members. The system was subjected to equal cyclic lateral loads at the level of floors and two analogous gravity loads were applied at the top of columns (Figure 2.20).

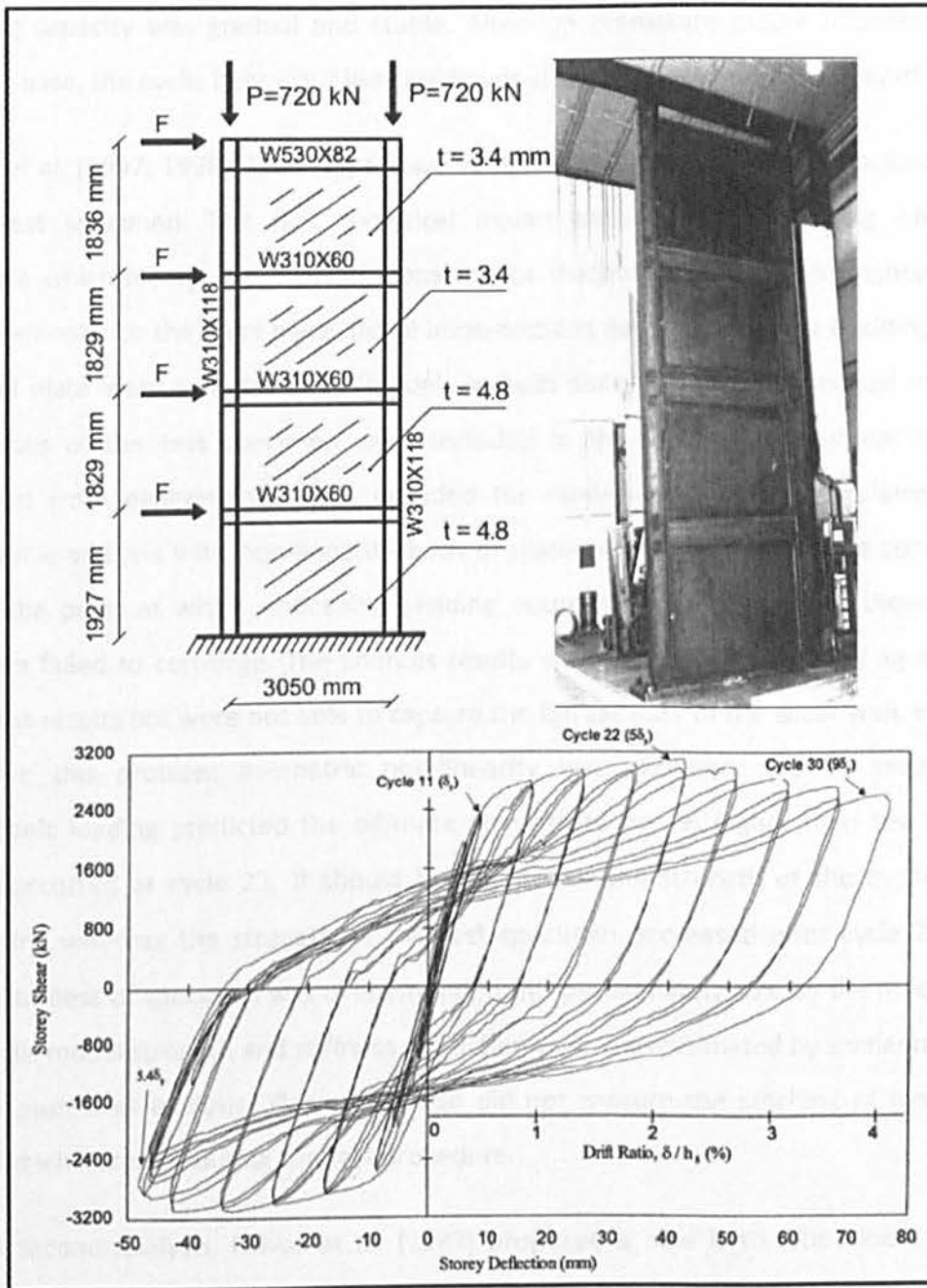


Figure 2.20: Scheme and elevation of test specimen with hysteresis curves for first storey (Driver et al., 1997) (photo courtesy of R. Driver)

In total 30 cycles were performed on the specimen where last 20 cycles were in inelastic range. The specimen behaviour was more flexible than predicted by the FE analysis model. However, it was robust and demonstrated a high initial stiffness, excellent ductility and significant energy absorption capacity. The frame reached an ultimate strength (3080 kN) at five times yield deflection where the column locally buckled at the base and fractured subsequently. Shortly thereafter the deterioration of the load-

carrying capacity was gradual and stable. Although premature failure happened at a column base, the cyclic behaviour indicated over-strength of 1.3 and a ductility of nine.

Driver et al. (1997; 1998-b) developed two analytical models to predict the behaviour of their test specimen. The first analytical model was developed utilising ABAQUS[®] software which incorporated beam elements for the beam and column members and shell elements for the steel plate. Initial imperfections based on the first buckling mode of steel plate were included in FE model. As built dimensions and measured material properties of the test specimen were included in the model. The residual stresses obtained from experiments were included for modelling of boundary elements. A monotonic analysis with non-linearity both of material and geometry were conducted up to the point at which noticeable yielding occurred in specimen, and thereafter program failed to converge. The analysis results were found to be in good agreement with test results but were not able to capture the full capacity of the shear wall. In order to solve this problem geometric non-linearity was excluded. The FE results for monotonic loading predicted the ultimate strength to be 7% higher than test results which occurred at cycle 22. It should be noted that the strength of the model kept increasing whereas the strength of the test specimen decreased after cycle 22. The initial stiffness of specimen was overestimated by approximately 15% by the model. For the cyclic model strength and stiffness prediction were overestimated by similar margins as the push-over analysis. This model also did not capture the pinching of hysteresis loops which occurred during the test procedure.

In the second analysis, Driver et al. (1987) proposed a new hysteretic model, which consisted of strip model based on the previous work of Mimura and Akiyama (1997) and Tromposch and Kulak (1987). In this model the behaviour of the steel plate shear wall was divided in two distinct components including the boundary members and steel plate (Figure 2.21).

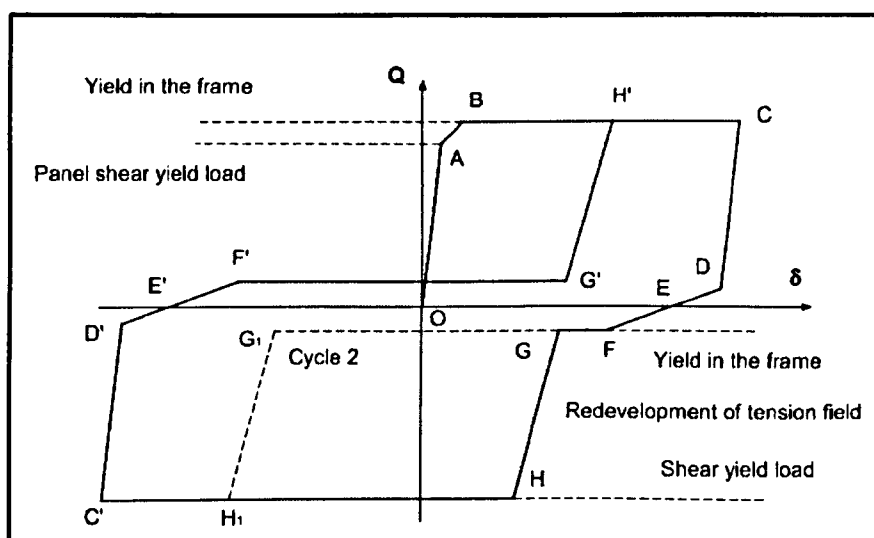


Figure 2.21: Hysteresis model proposed by Driver et al. (1997)

The strain distribution within the steel plate along a diagonal tension strip is not uniform (Elgaaly et al. 1993) and yielding of the strips commence at the boundaries and extends towards the centre of the strips. Elgaaly and Liu (1997) based on the model proposed by Thorburn et al. (1983) presented a new modelling technique as a concept of strip-gusset elements in order to simulate the non-uniform distribution of strain along the length of the tension strips. In the proposed analytical method 45° tension strips were connected to the surrounding elements by gusset plates. It was assumed that a tri-linear relationship governs the relation between stress and strain. The model was developed for both bolted and welded plate connections. Comparing these two different types of connections, researchers stated that due to slippage and local deformations at connections, a bolted shear wall may provide a lower initial stiffness and yielding but it does not make a big difference in ultimate capacity of system. Analytical models were able to predict the pushover envelope and hysteresis curves of tested specimens accurately.

Lubell et al. (1997) conducted cyclic testing on two single panel specimens, SPSW-1 and SPSW-2, respectively, and one four-storey specimen SPSW-4 at the University of British Columbia. The test specimens were designed as quarter-scale models of a one-bay steel-framed core. In all specimens the joints between beams and columns were moment-resisting connections. Each specimen was tested under a fully reversed cyclic quasi-static load based on ATC-24 (Applied Technology Council 1992) requirements.

Steel masses were placed at each storey of the SPSW-4 specimen to simulate gravity loading. The single-storey specimens were very ductile, with inelastic deformations at about $6\delta_y$ and an approximate over-strength of 1.5. However initial stiffness of specimens differed by a considerable value (Figure 2.22). This probably was because of the large initial imperfection of specimen SPSW-1 and the higher beam stiffness in specimen SPSW-2. In all specimens due to the low flexural stiffness of columns the noticeable pull-in behaviour of columns was observed.

Lubell (1997) conducted a series of analytical studies of test specimens. The results for the monotonic SPSW-1 were not completely consistent with the test results. Lubell attributed these inaccuracies to the massive amount of initial imperfections for steel plates as well as variation of α throughout the test and finally inaccurate modelling of the top beam. The cyclic analysis of specimen SPSW-1 was not pursued because of numerical inaccuracies.

The monotonic analysis for specimen SPSW-2 was in good agreement with the test results for initial stiffness, but slightly underestimated the ultimate strength of the specimen. Overall behaviour of the cyclic model matched those of the test results whereby the cyclic model captured the pinching of the hysteresis curves. The pull-in effect which was observed in Lubell's tests was discussed by Montgomery and Medhekar (2001). They reported that this issue observed in Lubell's tests was due to inadequate column stiffness and unusual geometric characteristics.

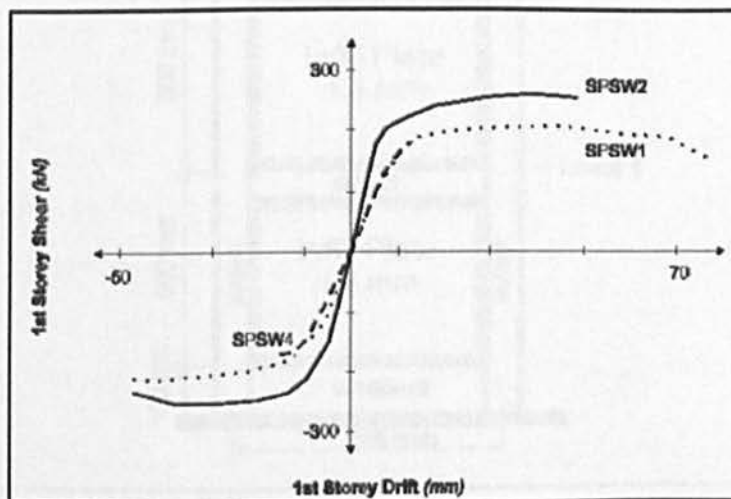


Figure 2.22: Envelope curves for one-storey and four-storey specimens (Lubell, 1997)

CHAPTER 2: LITERATURE REVIEW

Lubell et al. (2000) conducted a parametric analysis on SPSWs. Based on the experimental and numerical results of these studies, researchers stated that the current Canadian code provisions e.g. CAN/CSA-S16.2-M94 may not adequately address the design issues for multi-storey steel plate shear wall frames including the effect of large overturning moments, influence of aspect ratio, and the potential for undesirable yielding sequences of the shear wall components (Lubell, 2000).

Rezai et al. (1999) conducted a shake table test on quarter-scale, 4-storey steel plate shear wall to study the seismic performance of multi storey SPSW. The 4-storey specimen specifications are presented in Figure 2.23. The thicknesses of steel plates were 1.5 mm for all panels. An aspect ratio of 1:1 was selected for panels with full moment connection between beams and columns. At each storey additional steel plates were placed on the beams to simulate a storey mass of 1700 Kg.

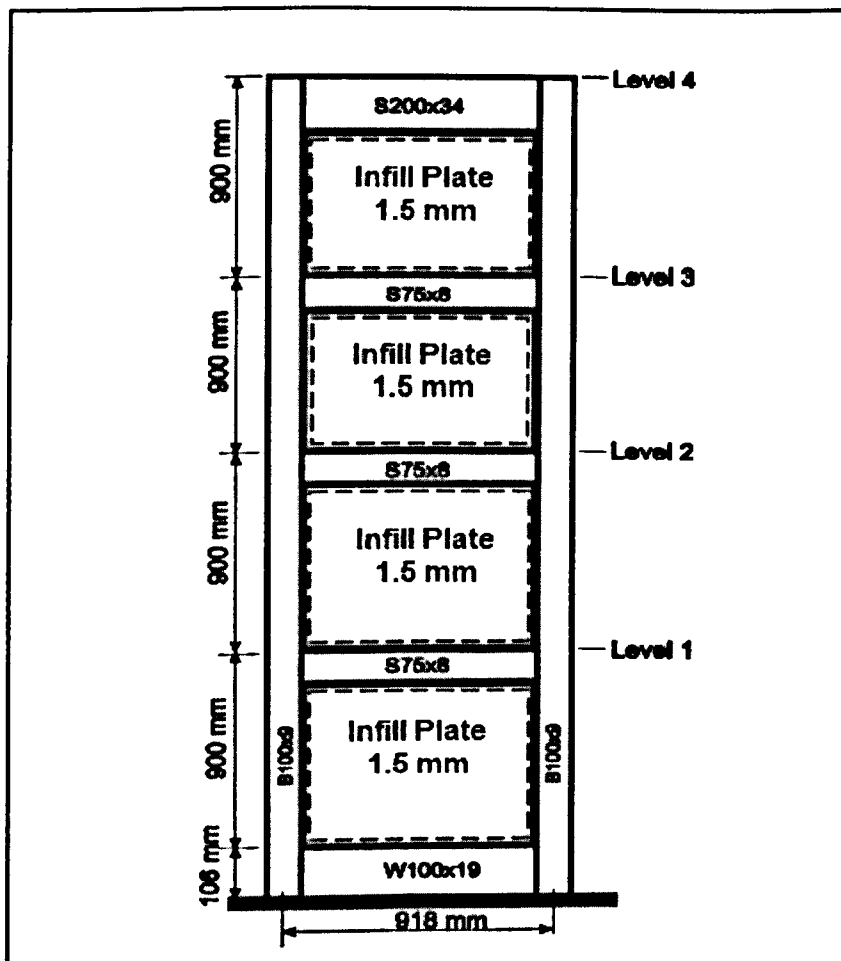


Figure 2.23 Four-storey Shake table test specimen (Rezai, 1999)

Due to limitations of the shake table facilities, the test results remained mainly elastic and the nonlinear behaviour of the specimen could not be explored in detail. Thus, the discussion and interpretation by researchers focused mainly on the response of the specimen in the elastic range.

In order to determine the frequency of 4-storey specimen, Rezai conducted low-amplitude vibration test. The fundamental frequency of the specimen was estimated to be 6.1 Hz. Figure 2.24 shows the test set up for the shake table test.

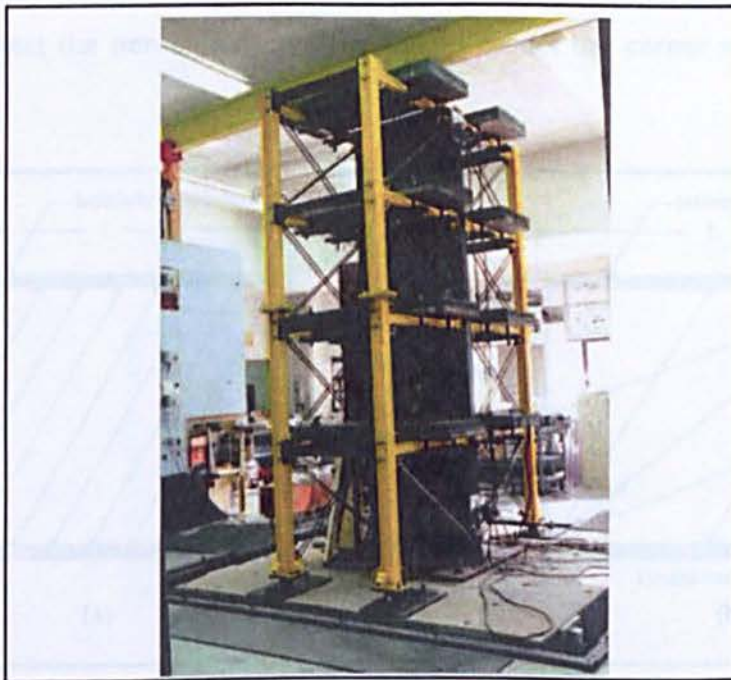


Figure 2.24: Shake table test for the SPSW specimen (Rezai, 1999)

It was found that the first mode was the primary mode of vibration with very little contribution from higher modes (Rezai, 1999). From load-displacement plots it was found that the majority of the input energy was dissipated by the first floor. The first storey was dominated mostly by shear deformation, while the top floor behaved mostly as a rigid body rotation about the first floor. For the four-storey specimen a maximum displacement ductility of 1.5 was obtained prior to a global instability failure induced by yielding of the columns. The specimen also exhibited over-strength of about 1.2.

The strip model was found to over-predict the elastic stiffness of specimens. The discrepancies between the theoretical and experimental results were more dramatic for

CHAPTER 2: LITERATURE REVIEW

the four-storey specimen in comparison with single-storey specimens. It was concluded that conducting analysis of high-rise steel plate shear walls system one panel at a time, as recommended in CAN/CSA-S16.1-94 (1994), is not a reliable method of determining storey displacements and design forces for members.

An improved analytical model was proposed by this researcher for analysis simplicity and is shown in Figure 2.25. The tension-only strips for each panel were placed diagonally between opposite corners and from the corners to the mid-span of the boundary members, for a total of five strips per panel. The strips were set up in this manner to reflect the non-uniformity of α and to reflect the corner stiffness of each panel.

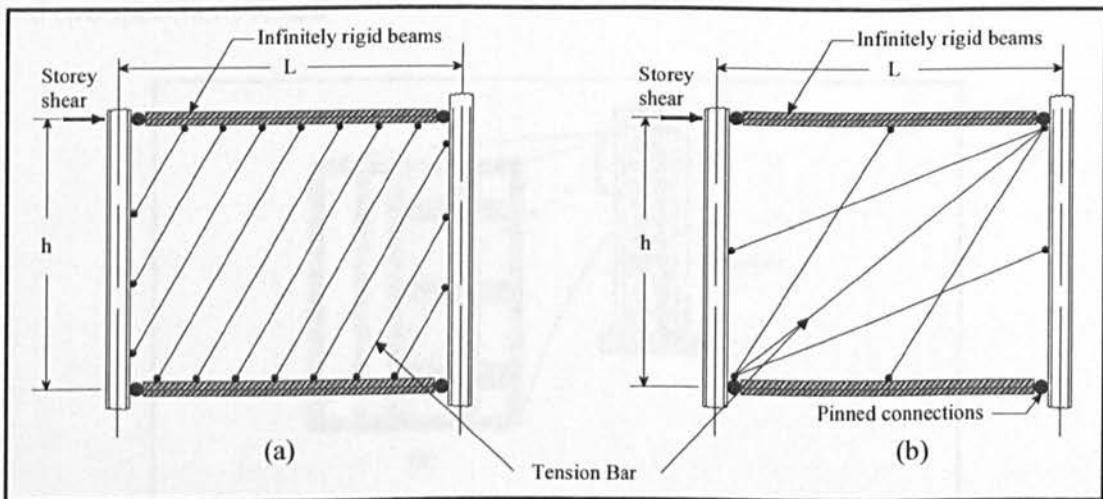


Figure 2.25: Scheme of different strip models for analyzing SPSWs
(a) 'Strip model' used in the Canadian Steel Design Code (CSA, 2000) and
(b) 'Multi-Angle Strip Model' as proposed by Rezaei (1999)

This proposed model predicted acceptable stiffness results for both pushover and dynamic time-history analysis. However, the elastic stiffness and yield strength of the specimen were over- and under-predicted by the proposed model. The need for further analytical studies using finite element formulation, including both material and geometric non-linearity, may be necessary for slender steel plate shear wall specimens. It was noted that as the overturning moment to base shear ratio increases, flexural deformations dominate the response of the system, especially at the upper floors. This transition from shear behaviour to flexural behaviour was shown to be the weakness of

the strip model as it fails to reasonably predict the load-displacement behaviour of the system.

2.2.2. Further developments on steel plate shear walls (2000-2009)

Astaneh-Asl and Zhao conducted together two parallel research projects on composite shear walls (Astaneh-Asl, 2000a; Astaneh-Asl, 2001b) and SPSWs (Astaneh-Asl, 2001c) at the department of Civil and Environmental Engineering of the University of California, Berkeley. Totally four types of specimens were tested in these researches.

The specimens for steel plate shear wall tests were two half-scale, three-storey steel plate shear wall frame. Figure 2.26 shows scheme a of the location of original specimen and two specimens tested.

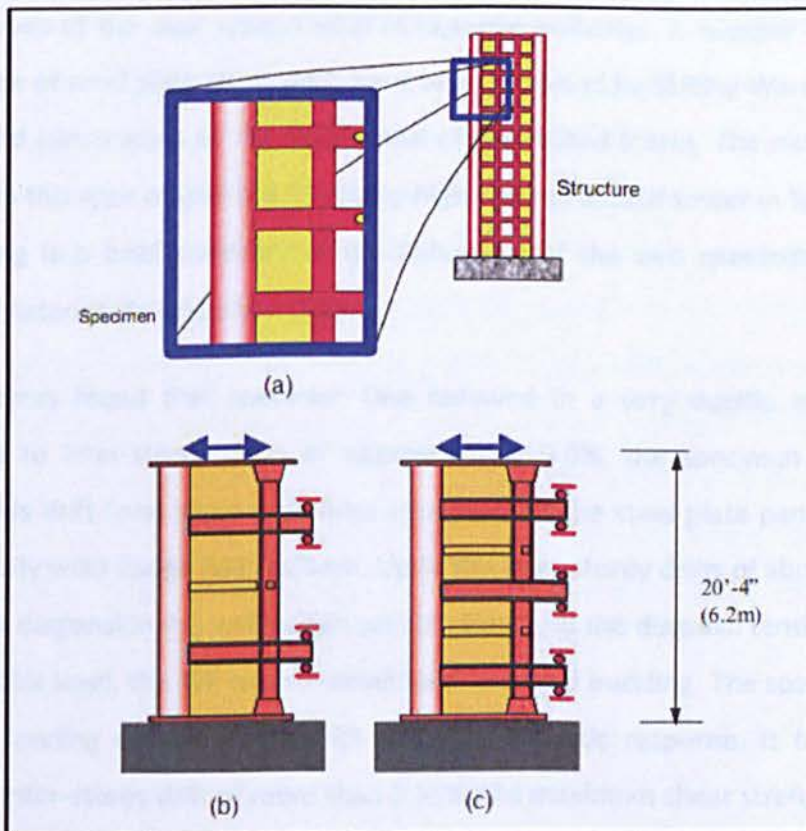


Figure 2.26: Scheme for (a) location of specimens (b) Test specimen One (c) test specimen Two (Astaneh-Asl., 2000)

The specimens were one-half of a coupled wall with concrete-filled hollow steel section as columns and had a total height of 6.2 m (Figure 2.27).

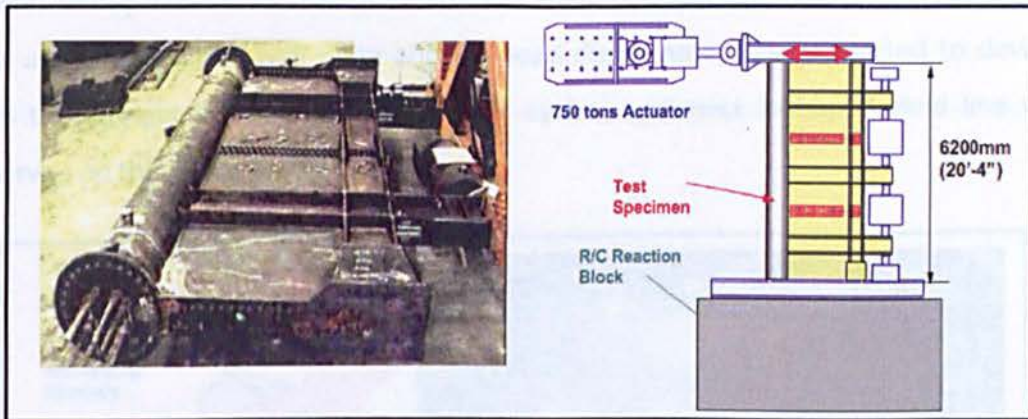


Figure 2.27: Test specimen and scheme of test set-up (Astaneh-Asl and Zhao, 2000)

The specimen One had height-to-width ratio of about 1.5 while the height-to-width ratio of the wall in specimen Two was 1.0. The specimens were half-scale realistic representatives of the dual system used in high-rise buildings. A number of structures with this type of steel plate shear walls have been designed by Skilling Ward Magnusson Barkshire and constructed on the West Coast of the United States. The most important building with this type of wall is a 51-storey high-rise residential tower in San Francisco. The following is a brief summary of the behaviour of the two specimens of SPSWs provided by Astaneh-Asl and Zhao (2000).

The researchers found that specimen One behaved in a very ductile and desirable manner. Up to inter-storey drifts of approximately 0.6%, the specimen was almost elastic. At this drift level some yield lines appeared on the steel plate panel as well as the non-gravity wide flange (WF) column. Up to the inter-storey drifts of about 2.2%, the compression diagonal in the wall panels was buckling and the diagonal tension field was yielding. At this level, the WF column developed localized buckling. The specimen could tolerate 79 loading cycles including 39 cycles of inelastic response. It failed before reaching an inter-storey drift of more than 3.35% and maximum shear strength of about 4,080 kN (917 Kips). At this level of drift, the upper floor-coupling beam was observed to fracture at the face of the column (due to low-cycle fatigue) and the shear strength of the specimen was noted to drop to about 60% of the maximum capacity of the specimen (Astaneh-Asl and Zhao, 2000, and Astaneh-Asl, 2001).

Specimen Two behaved much like specimen One in a ductile and desirable manner. Up to inter-storey about 0.7%, the specimen was almost elastic. At this drift level some yield lines appeared on the wall plate and the load-displacement curve started to deviate from the straight elastic line. During later cycles, a distinct X-shaped yield line was observed on the SPSW (Figure 2.28).

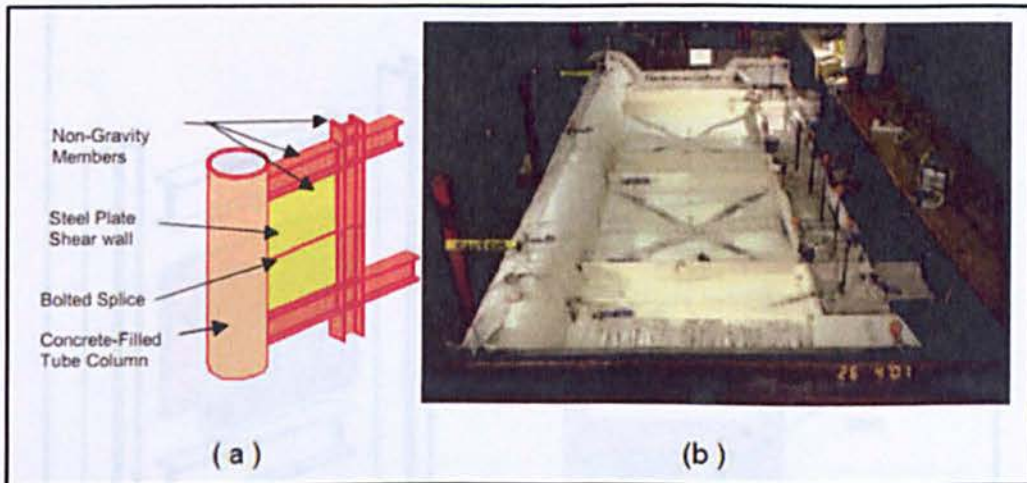


Figure 2.28: Specimen tested by Astaneh-As and Zhao (2001a), (a) Scheme of specimen (b) Specimen Two, during the test

The specimen Two tolerated 29 cycles, of which 15 cycles were inelastic. The specimen reached an inter-storey drift of more than 2.2% and maximum base-shear force of 5,450 kN (1,225 Kips). At this level of drift, the upper floor coupling beam fractured at the face of the column (due to low-cycle fatigue) and the shear strength of the specimen dropped to approximately 75% of the maximum shear force reached in previous cycles. Since the capacity of the SPSW dropped below 80% of maximum strength, the specimen was considered to have failed and the testing was terminated. More information on these tests can be found in Astaneh-Asl and Zhao (2001-a).

The main objective of composite shear wall project was to conduct cyclic testing of a traditional and innovative composite shear wall and to develop the design and modelling recommendations.

Figure 2.29 shows the basic attributes of traditional and innovative composite shear walls tested by researchers. Both innovative and traditional composite shear walls studied were “dual” system with composite shear walls placed within a moment

resisting frame. The only difference between the traditional and innovative proposed system is that in the innovative system there is a gap between the concrete wall and boundary members. This seemingly simple difference resulted in significant improvements in the performance as well as an increase in ductility and reduction in damage (Astaneh-Asl., 2000).

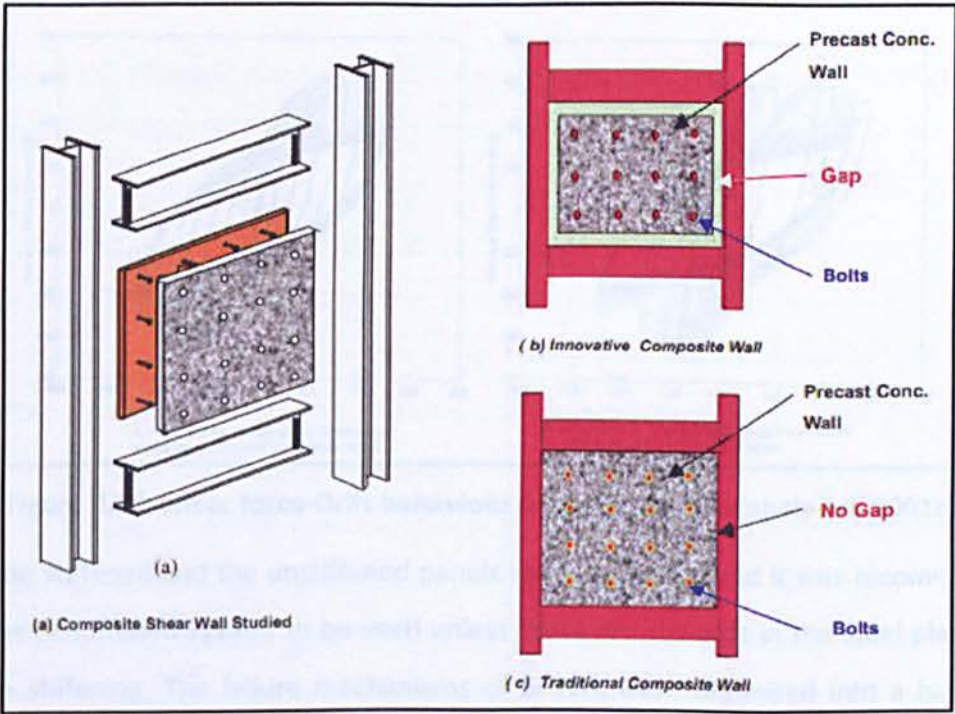


Figure 2.29: Scheme view of composite shear wall tested by Astaneh-Asl., 2000 (a) with composite shear walls placed within a moment frame (b) innovative composite wall (c) Traditional composite wall

The test specimens were half-scale, three-storey, one-bay structures. The specimens had identical properties with the exception of 30 mm gap provided between concrete wall and boundary beams and columns for innovative specimen. Table 2.2 gives the properties of the test specimens.

Table 2.2: Component of test specimens (Zhao, 2004)

Steel Wall Plate Thickness	Pre-cast R/C wall				Wall Bolts Dia.	Beam Section*	Column Section*
	Thickenss	Rebar Dia.	Rebar Spacing	Reinf. Ratio			
4.8 mm (3/16 inch)	76 mm (3 inch)	10 mm (3/8 inch)	102 mm (4 inch)	0.92%	13 mm (½ inch)	W12x26	W12x120

* Properties of cross sections refer to the AISC Manuals

CHAPTER 2: LITERATURE REVIEW

Researchers reported that in both specimens, concrete walls were able to brace the steel wall and prevent their buckling before yielding. It appears that the participation of the concrete wall did not add to the stiffness of the system significantly (Astaneh-Asl, 2001c). Both specimens were able to reach inter-storey drifts of 4% without reduction in their strength (Figure 2.30).

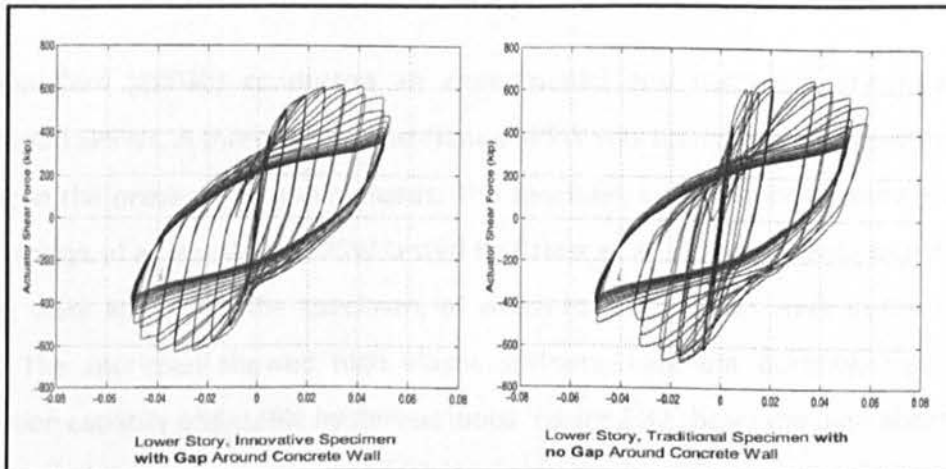


Figure 2.30: Shear force-Drift behaviour of specimens (Astaneh-Asl, 2001c)

Both the stiffened and the unstiffened panels were examined and it was recommended that the unstiffened system to be used unless there are cut-outs in the steel plate that require stiffening. The failure mechanisms of SPSWs were organised into a hierarchy system as shown in Figure 2.31.

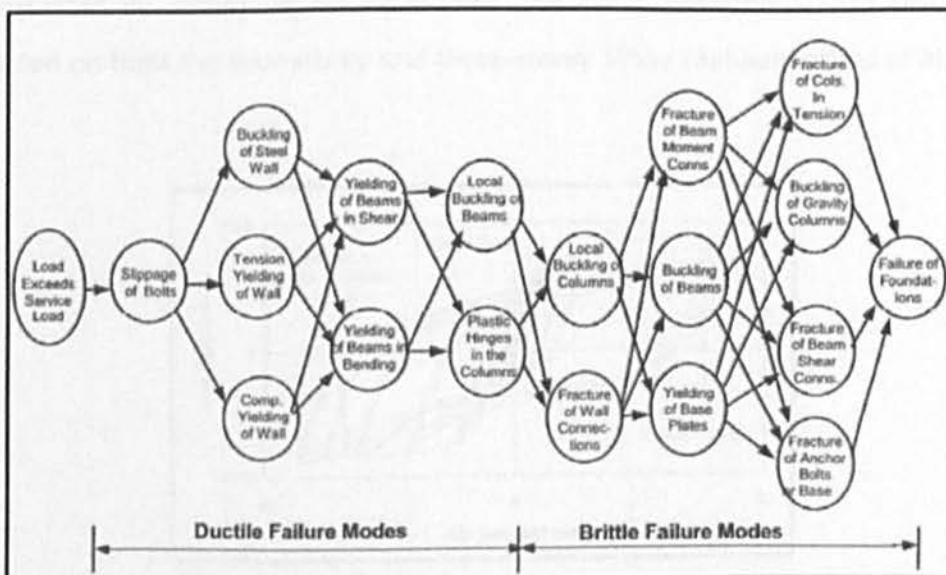


Figure 2.31: SPSW failure mechanism hierarchy (Astaneh-Asl, 2001b)

CHAPTER 2: LITERATURE REVIEW

Astaneh-Asl (2001-c) recommended that the plate girder equations described by AISC (1999) be used for the design of unstiffened SPSWs. This approach would be conservative than those based on other means of analysing steel plate shear walls (i.e., Thorburn et al. 1983). Berman and Bruneau (2004) emphasised that SPSWs are not plate girders. They discussed this point in more numerical aspects and concluded that the plate-girder analogy is inadequate for the design of SPSWs.

Behbahanifard (2003b) conducted an experimental and numerical investigation of unstiffened SPSWs. A three storey unstiffened SPSW was tested under quasi-static cyclic loading in the presence of gravity loads. The specimen consisted of undamaged upper three storeys of a four-storey SPSW tested by Driver et al. (1997). Twenty-four cycles of loading were applied to the specimen, of which fourteen cycles were in the inelastic range. The specimen showed high elastic stiffness, excellent ductility, high energy dissipation capacity and stable hysteresis loops. Figure 2.32 shows the base shear versus first storey drift of the three-storey SPSW. Behbahanifard developed a finite element model for analysis of SPSW based on a non-linear, dynamic explicit formulation using ABAQUS/Explicit platform. Material and geometric nonlinearities were included in the model. A kinematic hardening material model subroutine was implemented to simulate the Bauschinger effect and a special loading frame was developed to implement a displacement control analysis. The effectiveness and validity of the model was demonstrated by comparing its monotonic and cyclic predictions with test results conducted on both the four-storey and three-storey SPSW (Behbahanifard et al., 2003-a).

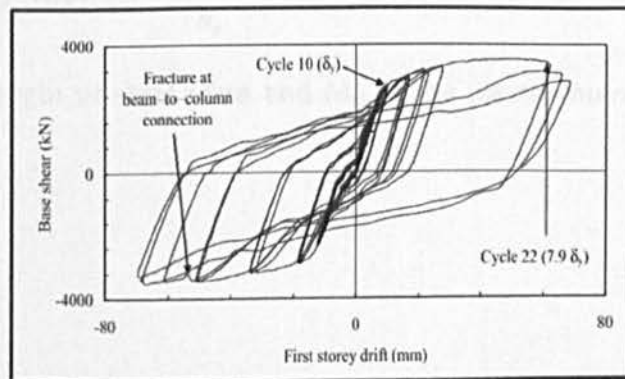


Figure 2.32: Hysteresis curves of base shear versus first storey drift for three-storey specimen (Behbahanifard, 2003b)

CHAPTER 2: LITERATURE REVIEW

The numerical model was then used for a parametric study of a single panel of steel plate shear wall with rigid floor beams. He identified a set of ten scale-independent, non-dimensional parameters that described the behaviour of an SPSW subjected to shear and gravity load. A parametric study was conducted to identify the effect of some of the main parameters on the stiffness and capacity of single panel SPSW. Based on his study, a decrease in the aspect ratio (L/h) was found to increase the capacity of the SPSW also the stiffness of SPSW would increase as the ratio of steel plate axial stiffness to the axial stiffness ($tL/2A_c$) increased. It was observed that initial imperfections of steel plate could result in a noticeable reduction in the stiffness of the system. It was suggested that the initial imperfections of steel plate is limited to 1% of \sqrt{Lh} . It was also found that increasing either the gravity load or overturning moment reduces the elastic stiffness of the system in an almost linear manner or also significantly reduces the normalised capacity and ductility (Behbahanifard, 2003a).

Berman and Bruneau (2003a) used the plastic analysis of the model to develop equations for the ultimate capacity of both single and multi-storey SPSWs with either simple or rigid beam-to-column connections. Using the assumed collapse mechanism shown in Figure 2.33, the storey shear strength capacity for a single storey SPSW with either simple or rigid beam-to-column connections are given by Eqs (2.6) and (2.7), respectively.

$$V = \frac{1}{2} F_y t L \sin 2\alpha \quad 2.6$$

$$V = \frac{1}{2} F_y t L \sin 2\alpha + \frac{4M_{pc}}{h_s} \quad 2.7$$

F_y is the yield strength of steel plate and M_{pc} is the plastic moment capacity of the column.

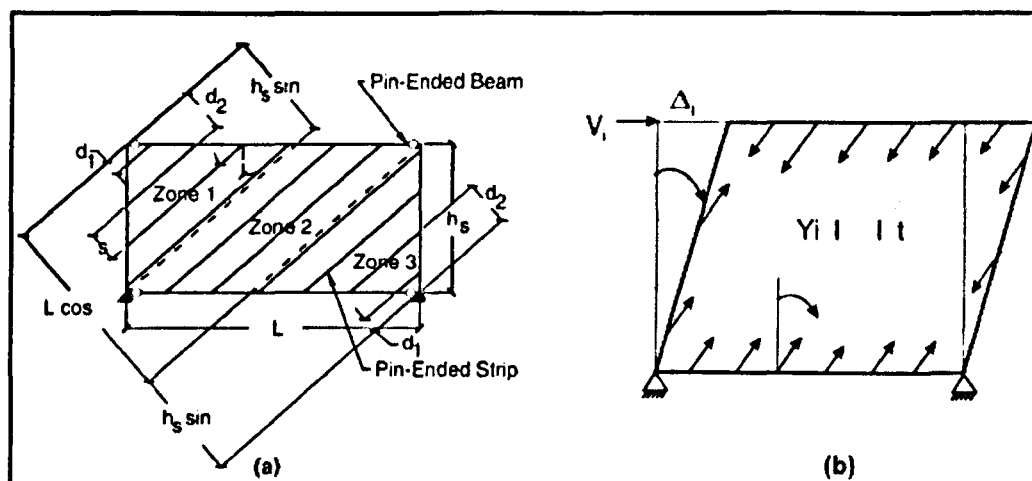


Figure 2.33: (a) Single strip model (b) Single storey collapse mechanism (Berman, 2003a)

In order to calculate the ultimate strength of multi-storey SPSWs, the two failure modes were assumed (Figure 2.34), soft storey failure and uniform yielding of steel plates over every storey simultaneously which is more desirable collapse mechanism.

Berman and Bruneau (2003b) reviewed the CAN/CSA S16-01 and recommended the procedure for the analysis and design of SPSWs which is based on the equivalent storey brace method (Thorburn, 1983) and found instances where this procedure can lead to unconservative designs with a lower than expected ultimate capacity. Using the results of plastic analyses a new procedure for the sizing of steel plates was proposed as follows:

$$t = \frac{2V_s \Omega_s}{F_y L \sin 2\alpha} \quad 2.8$$

V_s is the storey shear force and Ω_s is the system overstrength factor taken between 1.1 to 1.5. The actual system overstrength factor can be obtained from a pushover analysis, or conservatively used as 1.5.

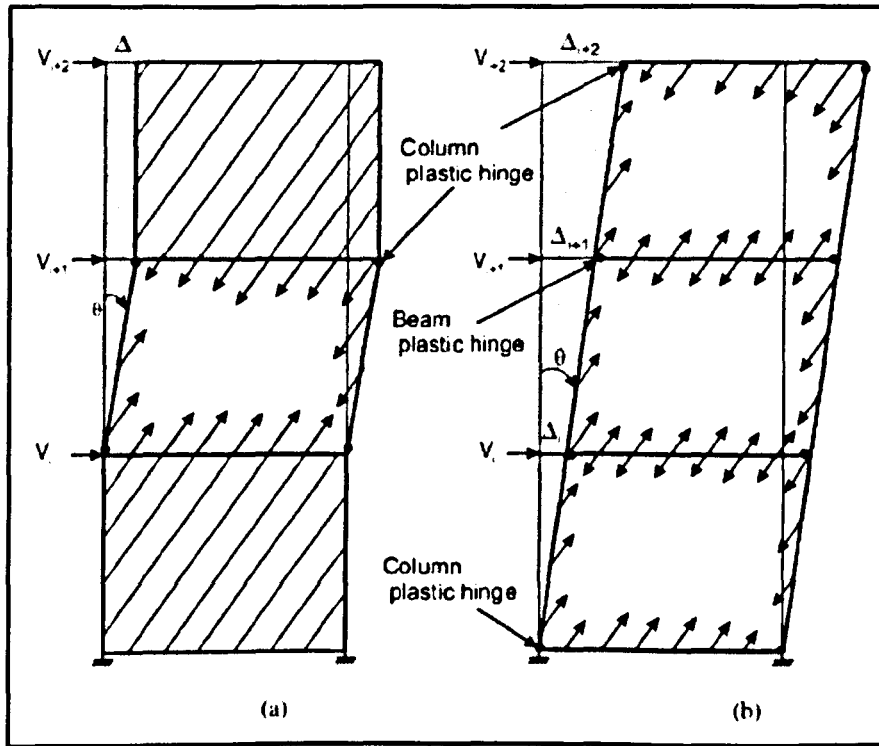


Figure 2.34: Multi-storey collapse mechanism proposed by Berman and Bruneau (2003b) (a) Soft storey mechanism (b) Unified collapse mechanism

Berma and Bruneau (2003b) provided comparisons of experimentally obtained ultimate strength of SPSWs and those predicted by plastic analysis and observed reasonable agreement.

Vian and Bruneau conducted an experimental program on four single-storey, single-bay SPSW specimens where the steel plate was Low Yield Strength (LYS) steel (Vian et al., 2003; Vian and Bruneau, 2004; Vian et al., 2009). The scheme of typical specimen dimensions is given in Figure 2.35. All specimens had Reduced Beam Section (RBS) at the beam ends. Two specimens had solid steel plate while the remaining two provide utility access through the panel by means of cut-outs. One specimen consisted of a steel plate with a total of twenty holes with the diameter of 200 mm. The second perforated specimen was designed with quarter-circle cut-outs in the panel corners where it is reinforced to transfer steel plate forces to the adjacent frame (Figure 2.36).

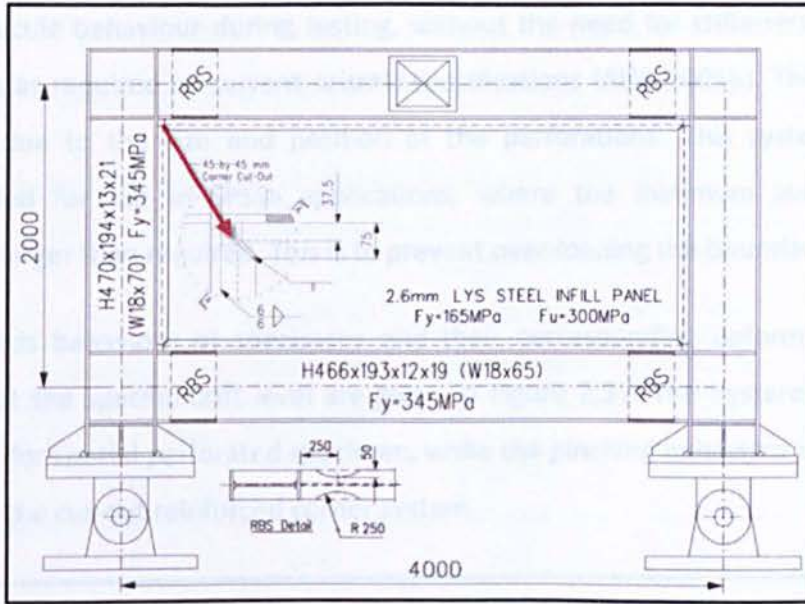


Figure 2.35: Scheme of typical specimen dimensions (Vian, 2003)

The specimens were subjected to quasi-static, displacement controlled cyclic loading, according to ATC-24 protocol requirements, up to their maximum strength and displacement capacity.

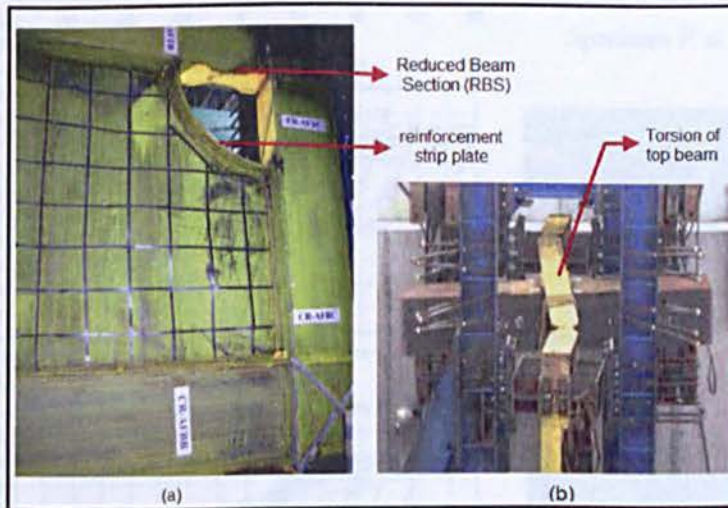


Figure 2.36 The scheme of (a) Reduced Beam Section (RBS) and reinforced corner cut-out (b) Torsion of top beam during the test (Vian and Bruneau, 2004)

Vian et al. (2009) reported that the RBS design concept ensured that the beams could continue to anchor the steel plate diagonal tension field forces, without developing a collapse mechanism with mid-span plastic hinging that could comprise the overall system strength. They also reported that the special perforated steel plate specimen

CHAPTER 2: LITERATURE REVIEW

exhibited ductile behaviour during testing, without the need for stiffeners around the perforations as required by current seismic specifications (AISC 2005b). This conclusion is possibly due to the size and position of the perforations. This system also was recommended for use in SPSW applications, where the minimum available plate thickness is larger than required. This is to prevent over-loading the boundary elements.

The hysteresis behaviour of specimens and their corresponding deformity shape of specimens at the specific drift level are given in Figure 2.37. The hysteresis loops are more stable for special perforated specimen, while the pinching behaviour is more often observed in the cut-out reinforced corner system.

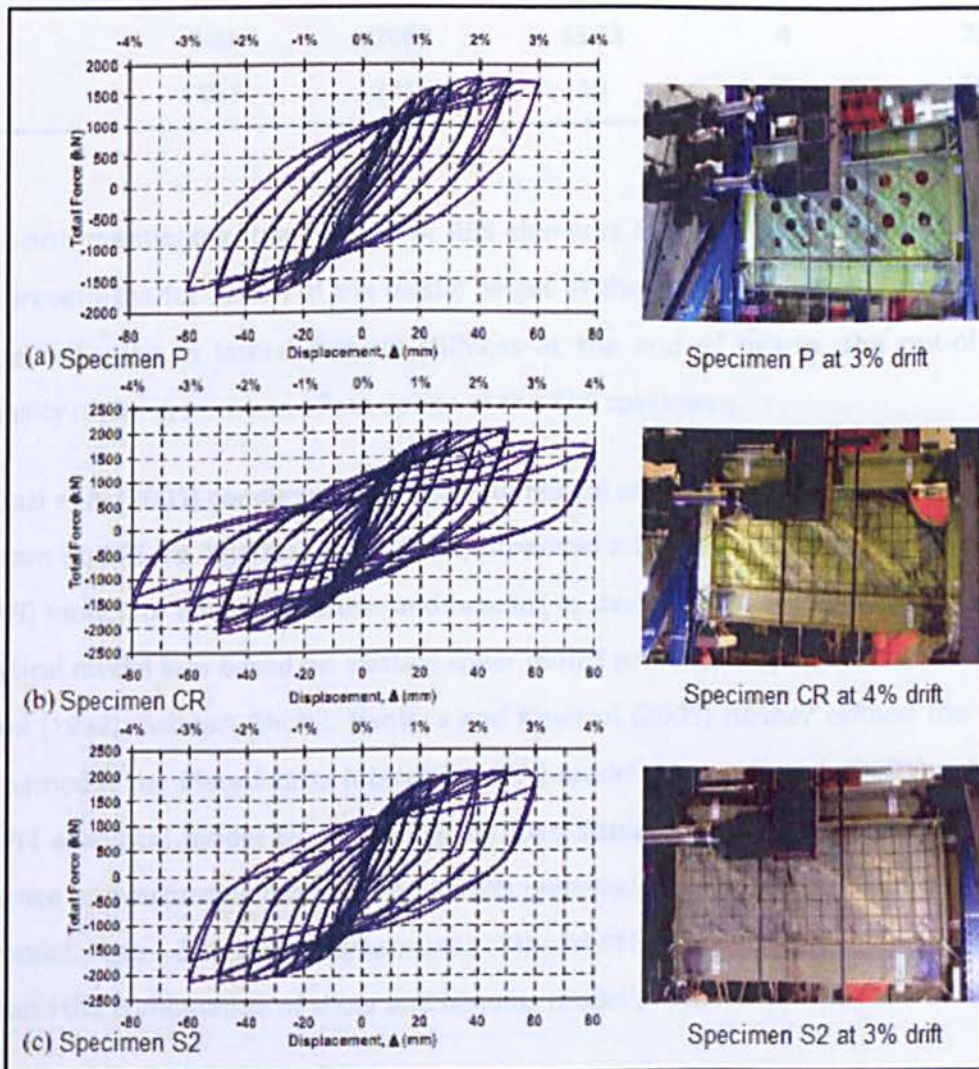


Figure 2.37 The hysteresis behaviour of specimens and corresponding deformed shape of specimens at the certain drift level (Vian et al., 2003) with (a) Regularly perforated steel plate (b) Corner cut-out steel plate (c) Solid steel plate

CHAPTER 2: LITERATURE REVIEW

The values of peak base shear strength, ductility, drift and elastic stiffness of test specimens are summarised in Table 2.3 (Vian and Bruneau, 2004).

Table 2.3: Summary of peak results for specimen tested by Vian et al. (2003)

Specimen	Elastic stiffness (kN/mm)	Maximum base shear strength (kN)	Approximate	Maximum inter-storey drift (%)	Strength
			maximum displacement ductility ($\mu=\Delta/\Delta_y$)		reduction at maximum drift (%)
P	115	1790	10	3	14.5
CR	140	2050	13.33	4	30
S2	135.5	2115	10	3	18

It is worth mentioning that the use of RBS elements in steel plate shear wall systems may prevent the formation of the plastic hinges at the ends of columns. However, due to the reduction in lateral flexural stiffness at the end of beams, the out-of-plane instability of the system can affect design of the RBS specimens.

Kharrazi et al (2005) conducted a valuable numerical analysis, parametric study and test program on SPSWs. Kharrazi et al. (2004) proposed a Modified Plate-Frame Interaction (M-PFI) model for analysis of shear and bending in steel plate shear walls. The proposed analytical model was based on existing shear model presented by Roberts and Sabouri-Ghomi (1992); Sabouri-Ghomi, Ventura and Kharrazi (2005) further refined the model and named it the Plate-Frame Interaction (PFI) model. Kharrazi et al. (2005) enhanced the PFI analytical model by modifying the load-displacement diagram to account for influence of overturning moments on SPSWs behaviour. It was therefore named the M-PFI model. Figure 2.38 shows components of the M-PFI model under shear load, bending load and the combination of shear and bending model proposed by Kharrazi et al (2005).

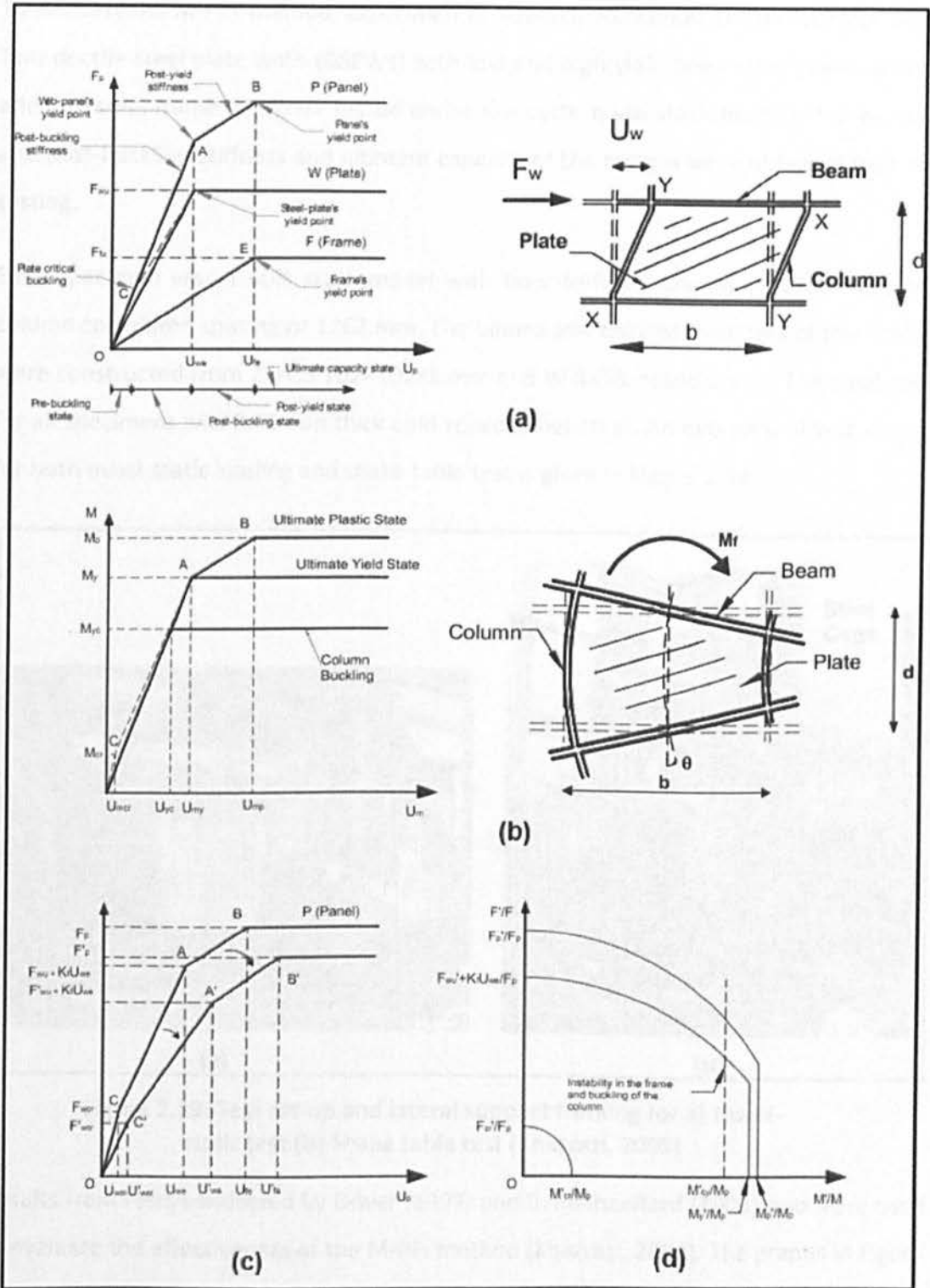


Figure 2.38: Components of M-PFI model for the (a) shear load-displacement: frame only, plate only and combined effects in panel (b) bending load-displacement of the panel (combined web plate and frame) (c) the modified load displacement diagram for shear resistance of the SPSW (d) bending and shear interaction of an SPSW panel

CHAPTER 2: LITERATURE REVIEW

To evaluate the M-PFT method, experimental research was conducted by Kharrazi, 2005. Two ductile steel plate walls (DSPWs) with low and high yield point steel plates, and an addition steel frame (SF) were tested under low cyclic quasi-static loading. Pre-buckling and post-buckling stiffness and ultimate capacity of the system were obtained from the testing.

Each specimen was a 60% scale model with floor-to-floor spacing of 1800 mm, and column-to-column spacing of 1262 mm. The beams and column members of the Frames were constructed from 2×HSS 102×102×8 mm and W 8×58, respectively. The steel plate for all specimens was 0.75 mm thick cold-rolled sheet steel. An overview of test set-ups for both quasi-static loading and shake table test is given in Figure 2.39.

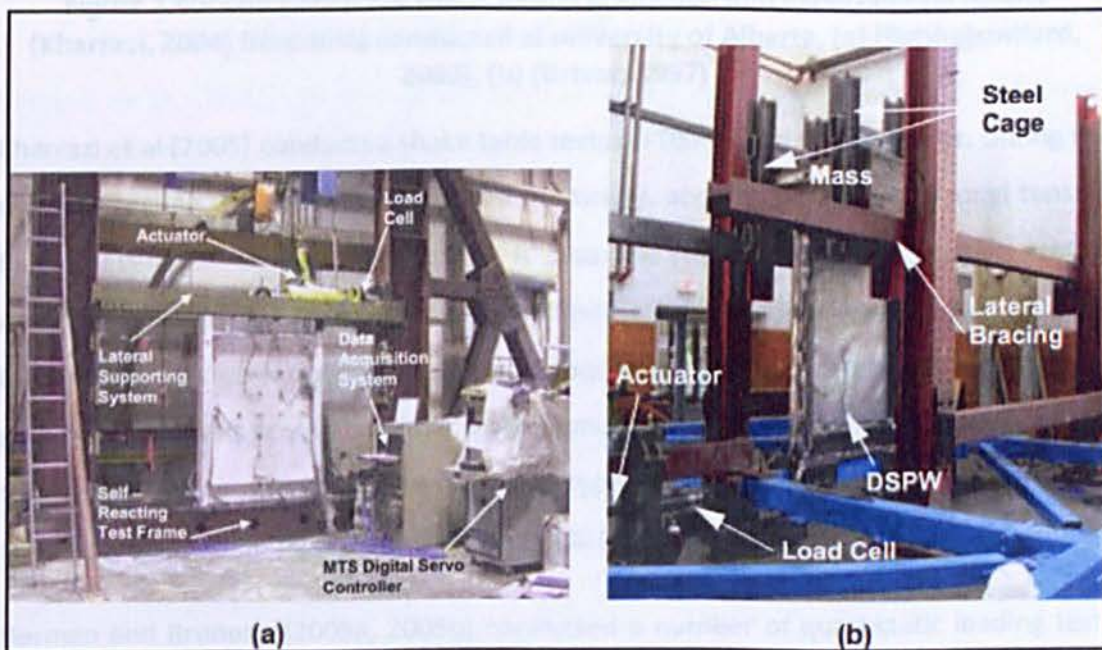


Figure 2.39: Test set-up and lateral support framing for a) Quasi-static test (b) Shake table test (Kharrazi, 2005)

Results from tests conducted by Driver (1997) and Behbahanifard (2003) also were used to evaluate the effectiveness of the M-PFI method (Kharrazi, 2004). The graphs in Figure 2.40 indicate comparison of M-PFI model prediction and experimental results from tests conducted at the University of Alberta (Behbahanifard, 2003; Driver, 1997). For both specimens, an assumed tension field of 45° was used in the model. The proposed model does not provide ductility and a failure mechanism for the specimens.

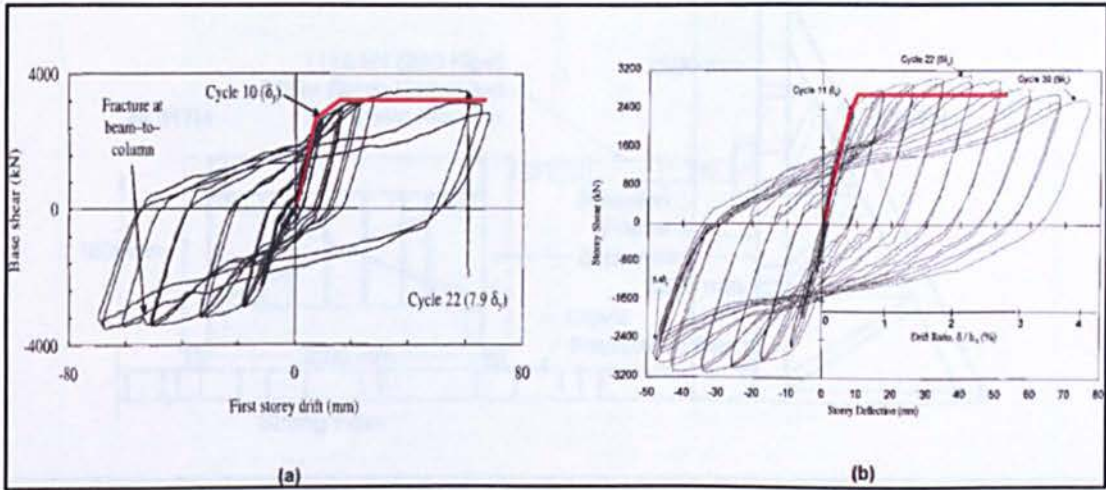


Figure 2.40: Comparison of M-PFI model prediction and experimental results (Kharrazi, 2004) from tests conducted at university of Alberta, (a) (Behbahanifard, 2003), (b) (Driver, 1997)

Kharrazi et al (2005) conducted shake table tests on DSPW and SF specimens. During the dynamic testing, the steel plate buckled elastically, and consequently diagonal tension fields developed in the steel plate. It was the first time that dynamic testing demonstrated yielding in the steel plate. A finite element model using explicit dynamic formulation was performed for analysis of specimens (Kharrazi, 2005). FE modelling of pushover, quasi-static and dynamic tests, demonstrated that numerical modelling of a ductile steel plate wall for different loading types provide reliable and effective results and confirms the finding of Behbahanifard et al (2003).

Berman and Bruneau (2005a, 2005b) conducted a number of quasi-static loading tests on one-bay, single-storey specimens with a boundary frame aspect ratio (L/h) of 2.0. All beam and column dimensions, as well as web-angle connections, were kept constant for all specimens to allow a more uniform comparison of structural characteristics such as strength, stiffness and seismic energy dissipation capacity. Figure 2.41 shows a typical test set-up.

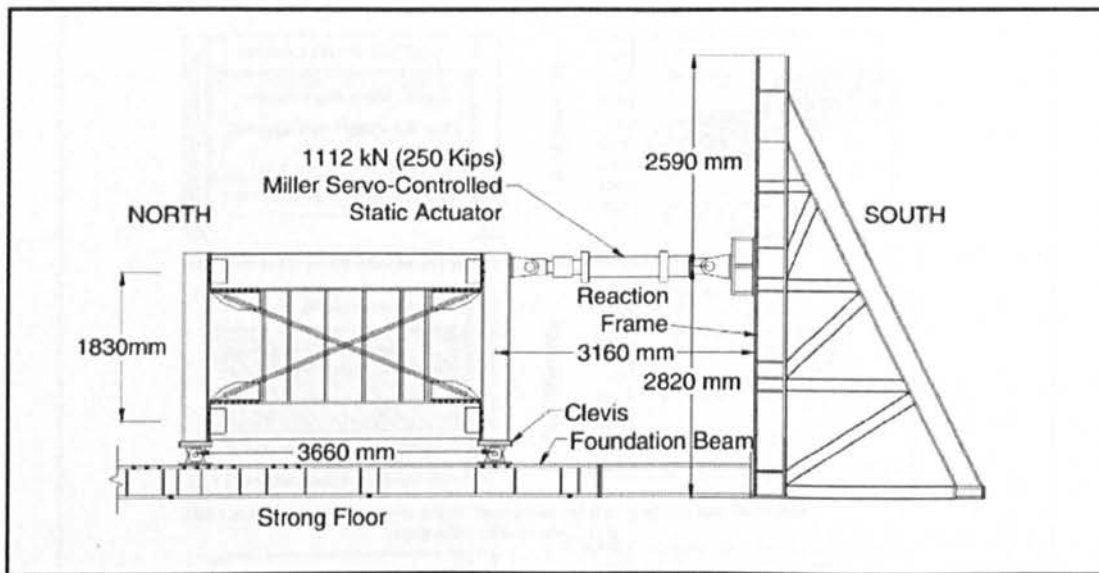


Figure 2.41: Typical test set-up for specimens tested (Berman and Bruneau, 2005a, 2005b)

Berman et al. (2005a) described and compared the results from cyclic testing of six specimens. The specimens incorporated four concentrically braced frames. Two specimens used cold-formed steel studs for in-plane and out-of-plane restraint of the brace, and two specimens were without bracing. In addition, two light-gauge steel plate shear walls, one with a flat steel plate and another with a corrugated steel plate were made. These two specimens were designed as seismic retrofit options for a four-storey steel-framed hospital structure with approximately half scale from the prototypes (Yang, 2002). Since the minimum available thickness of steel plate is several times greater than that required for the system, the light gauge materials were used as an alternative. This was to create a system strong enough to resist the design seismic loading and to be able to sufficiently dissipate the input energy to the system. All specimens were designed to meet major aims such as mobility, low impact on existing framing and significant increase in energy dissipation capacity. Figure 2.42 shows the specimen specifications and corresponding hysteresis curves of specimens tested by Berman et al (2005).

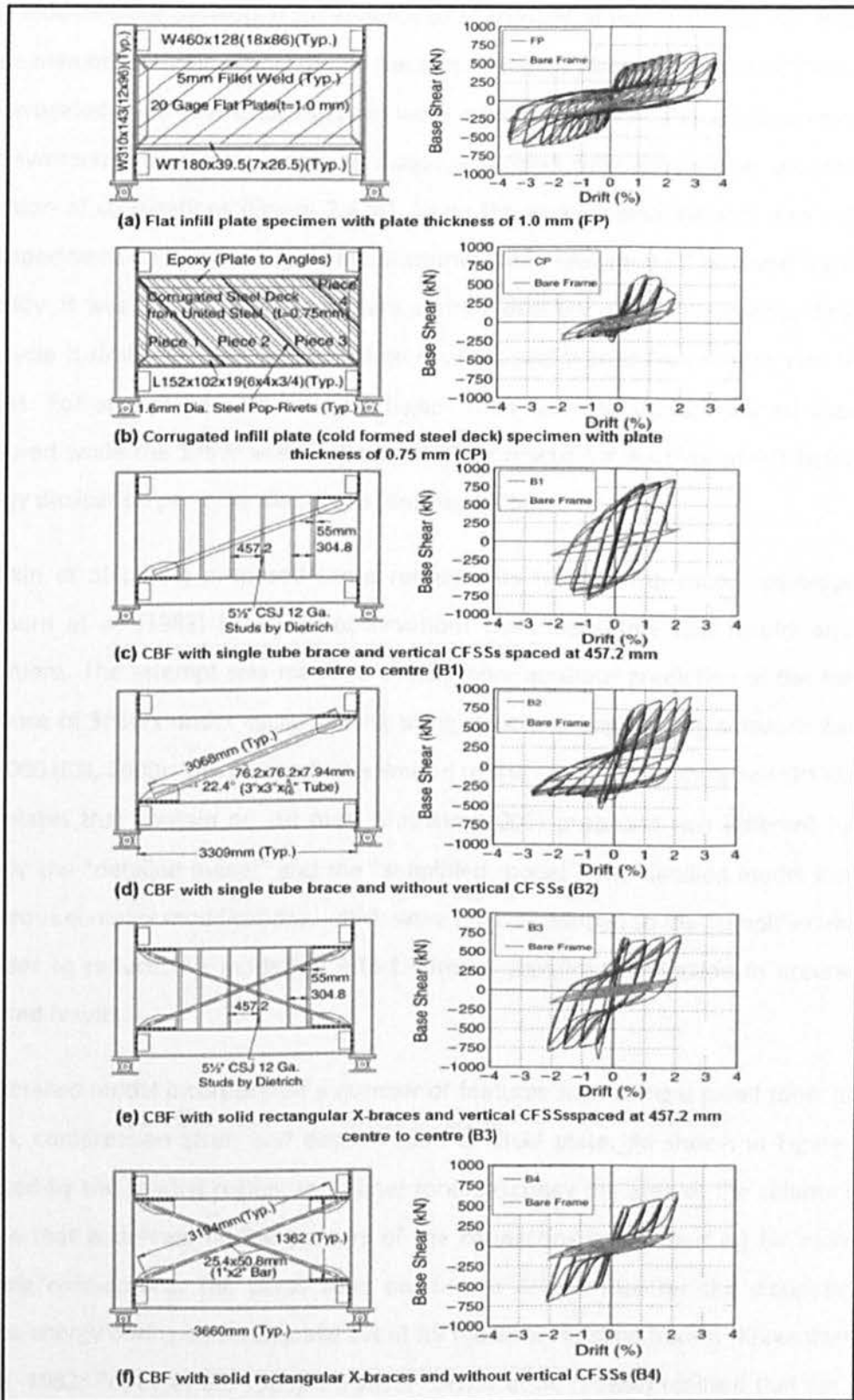


Figure 2.42: Test samples specifications and experimental hysteresis curves for specimens: (a) FP; (b) CP; (c) B1; (d) B2; (e) B3; (f) B4 (Berman, 2005-a)

CHAPTER 2: LITERATURE REVIEW

Strip models were developed for analysis of specimens. It was assumed that boundary frame members remain elastic during the test. The steel plate of specimen CP was made of corrugated plate where corrugations were orientated at 45°. This specimen exhibited anti symmetric hysteresis loops, as diagonal tension field action only developed in direction of corrugations (Figure 2.42b). Using the experimental results, they reported that specimens B3 had the largest initial stiffness, and specimen FP achieved the largest ductility. It was found that in specimens up to a ductility of 4.0, the energy dissipated per cycle is similar to SPSWs with flat steel plate, and braced frames with two tubular braces. For specimens with ductility higher than 4.0, the tubular braced specimen fractured while the SPSW with a flat steel plate reached a ductility of 9.0 before the energy dissipation per cycle decreased (Berma, 2005a).

Shishkin et al (2005) proposed same refinements to the strip model developed by Thorburn et al. (1983) based on observations from laboratory test results on SPSW specimens. The attempt was made to obtain more accurate prediction of the inelastic response of SPSWs under cyclic loading using structural engineering software package SAP2000 (CSI, 2000). This research was limited to the analysis of unstiffened SPSWs with thin plates that contain no cut-outs. Shishkin (2005) proposed two different models namely the "detailed model" and the "simplified model". The detailed model included numerous complex modifications, which were later developed to the "simplified model" in order to reduce the modelling effort without significant reduction in accuracy of analysed results.

The detailed model incorporated a number of features such as rigid panel zone, plastic hinges, compression strut, and deterioration of steel plate. As shown in Figure 2.43 depicted by the shaded region, this panel zone describes the area of the column cross section that is defined by the borders of the connecting beam ($d_b \times d_c$) for moment-resisting connections. The panel zone provides a ductile fuse for the dissipation of seismic energy during an earthquake event for moment resisting frames (Krawinkler and Popov, 1982; Popov et al., 1986). However, Driver et al. (1998a) realised that for their test specimens, the inelastic deformations in panel zones tended to remain small during the cyclic loading, and the panel zone regions perform elastically within elastic stage up

CHAPTER 2: LITERATURE REVIEW

to the peak wall capacity. The primary ductile fuses were formed within the steel plate. In order to achieve the actual behaviour of a panel zone in steel plate shear walls which expected to remain predominantly elastic, it was suggested that the beam and column elements within the panel zone be considered effectively rigid. It was found that for modelling purposes it is better to apply modulus of elasticity of 2×10^5 GPa or 1000 times the nominal values, for the elements within the panel zone. Such assumption was used in the proposed detailed model (Shishkin et al., 2005). It is worth to mention that following the forming of plastic hinges within the steel plate, if the system experiences large inelastic deformations, it is expected that the fuse development in the panel zones could appear in rigid beam-to-column connections.

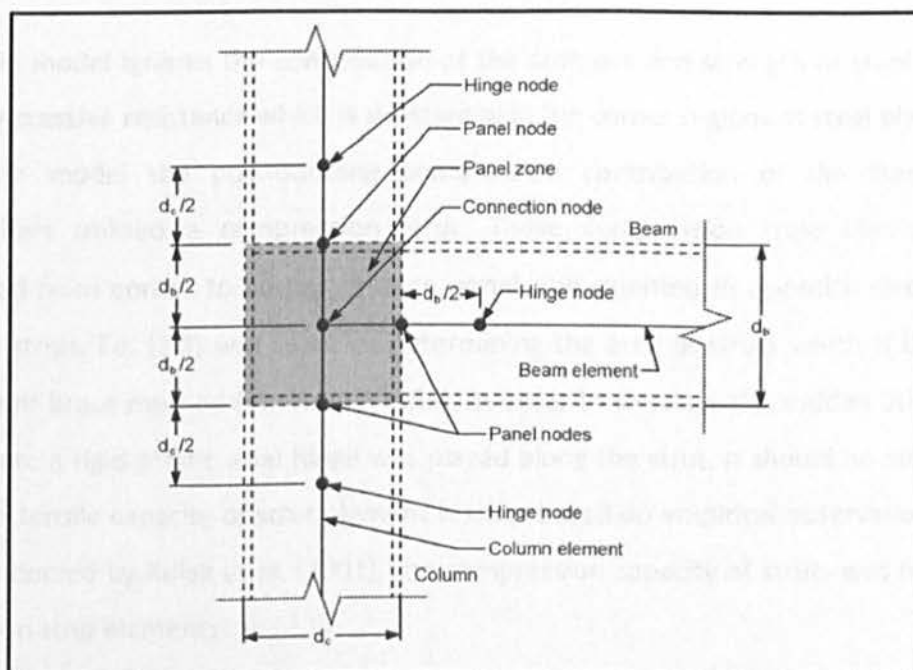


Figure 2.43: Typical frame-joint model detail for rigid connections

In order to simulate the inelastic behaviour of SPSWs, plastic hinges were utilised by Shishkin et al. (2005). The flexural plastic hinges were located at a distance of half of the member depth from the boundary of panel zone and axial plastic hinges were placed at discrete points along each of the pin-ended tension strips to simulate plastic behaviour of frame members and steel plate. Each hinge was considered to remain rigid until yielding commenced at that location. Up to yielding point of hinges elastic deformations occur for linear elements placed between hinges, thereafter, the overall behaviour of

CHAPTER 2: LITERATURE REVIEW

the system was affected by combination of distributed elastic member deformations and discrete hinge deformations according to hinge behaviour definitions

There are several methods for explaining the axial force-moment interaction. The following relationship was used by researchers to describe the interaction between axial force and moment (FEMA 356):

$$M_{pc} = 1.18ZF_y \left(1 - \frac{P}{A_c F_y} \right) \leq ZF_y \quad 2.9$$

where, F_y is the column yield stress, P is the axial load and Z is the column plastic modulus.

The strip model ignores the contribution of the stiffness and strength of steel plate to the compressive resistance which is substantial in the corner regions of steel plate. In an effort to model the post-buckling compression contribution of the steel plate, researchers utilised a compression strut. These compression truss elements are extended from corner to corner of each panel and oriented in opposite direction of tension strips. Eq. (2.2) was used for determining the area of struts which is based on equivalent brace method (Thorburn, 1983). In order to simulate the sudden buckling of steel plate a rigid-plastic axial hinge was placed along the strut. It should be mentioned that the tensile capacity of strut element is zero. Based on empirical observation of the test conducted by Kulak et al. (2001), the compression capacity of struts was set to 8% of tension strip elements.

Shishkin et al. (2005), located deterioration hinges only for two tension strips to include the effect of any possible tearing within the steel plate. Compression struts and deterioration strips are illustrated in Figure 2.44.

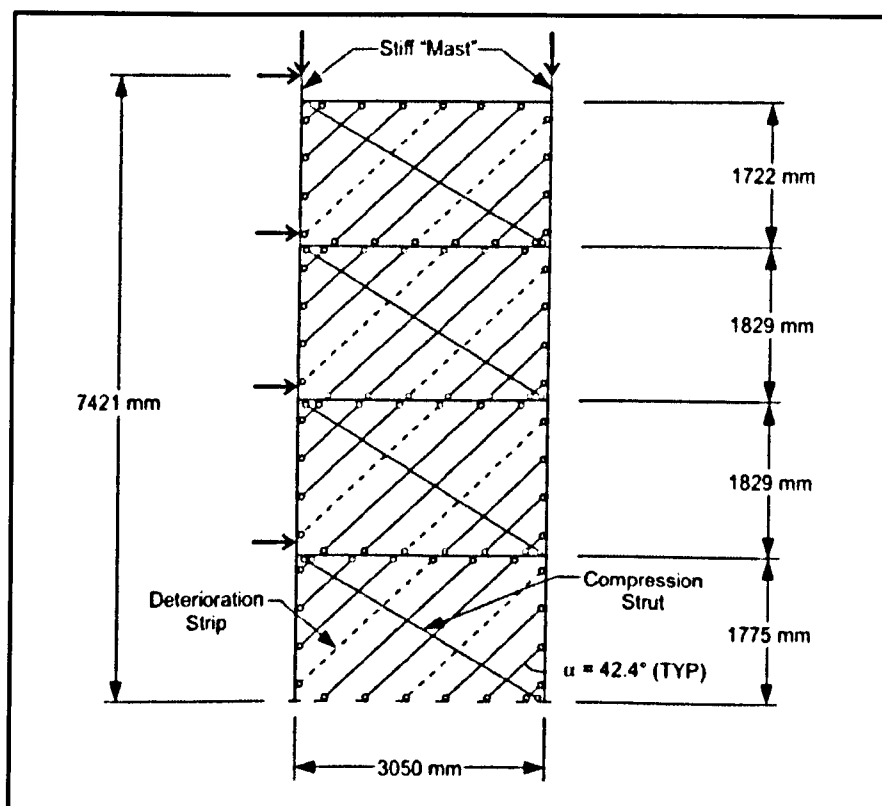


Figure 2.44: Compression struts and deterioration strips in detailed model proposed by Shishkin et al. (2005)

All parameters defined for detailed model were applied to the specimen developed by Driver et al. (1998a) and push-over analysis was performed.

Shishkin et al. (2005) attempted to simplify the parameters of detailed model. Modification in the position of plastic hinges in panel zone, reducing the number of nodes at the beam level, modelling all plastic hinges behaviour are modified parameters in simplified model. It was reported that each of above mentioned simplifications had small or negligible effect on analysis results. The results for simplified model were similar to detailed model and it was validated via comparing the results with several experimental works (Driver, 1997; Lubell, 1997; Timler, 1983). It was found that the modified strip model is relatively insensitive to variation of inclination angle of steel plate. They recommended that a value of $\alpha=40^\circ$ could be used for design of SPSWs. This value gives slightly conservative results. A comparison between results for two proposed models indicates that both models give the same initial stiffness. However, the simplified model lost 4% accuracy in predicting the ultimate capacity of the system.

CHAPTER 2: LITERATURE REVIEW

Purba (2006) carried out a series of finite element analysis on one-storey steel plate shear walls having multiple perforations within the steel plate. Variation in perforation diameters and different boundary conditions were investigated under a monotonic loading. The perforated-steel plate and the cut-out corner steel plate specimens tested by Vian (2005) were investigated in this research. Due to symmetrical conditions of loading and strip geometry a quadrant of full strip was modelled (Figure 2.45).

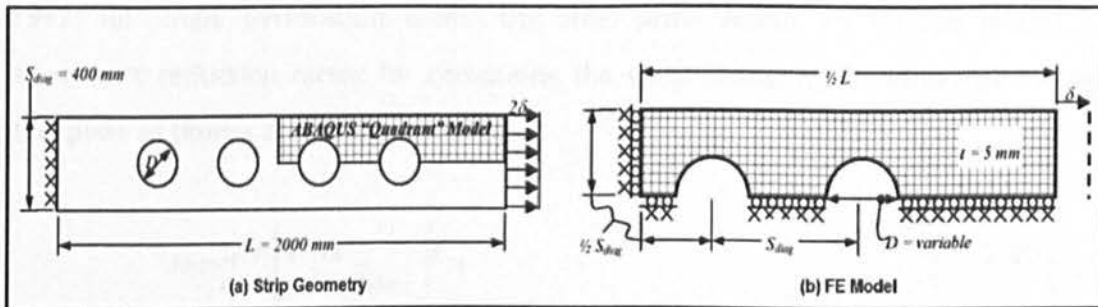


Figure 2.45: Scheme of (a) Strip geometry (b) FE model of Vian et al. (2005), developed by Purba (2006)

Isoparametric general-purpose shell elements (S4) were used to model both the steel plate and boundary frame members. Several FE mesh model developed (Purba and Bruneau, 2007) to find the appropriate mesh density to obtain accurate results. Considering the computation time efficiency, a $50 \times 50 \text{ mm}$ mesh size was selected for parametric study. Nonlinear push-over analysis was conducted on the FE model (Figure 2.46).

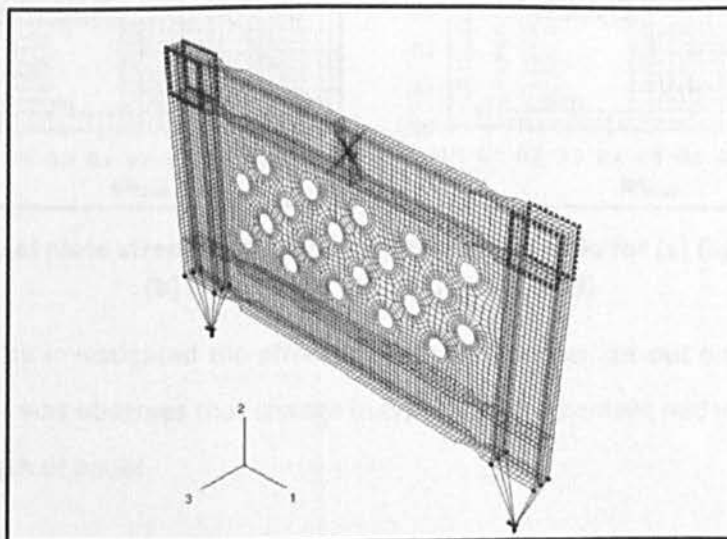


Figure 2.46 FE modelling of Vian et al. (2005) specimen by Purba (2006)

CHAPTER 2: LITERATURE REVIEW

Purba (2006) concluded that the results from individual perforated strip analysis are able to predict the performance of complete perforated SPSW if the diameter of holes is less than 60% of the strip width. It was reported that there is no interaction between adjacent strips to influence the stress distribution within the specific strip.

In order to approximate the shear strength of a multiple perforated steel plate, Purba (2006) developed the Eq. (2.5) which was proposed by Roberts and Sabouri-Ghomi (1992) for single perforation within the steel plate. Based on analysis results he proposed a reduction factor for computing the shear strength of multiple perforated steel plate as (Purba and Bruneau, 2009):

$$V_{yp,perf} = \left[1 - \alpha \frac{D}{S_{diag}} \right] V_{yp} \quad 2.10$$

where α is the proposed regression factor equal to 0.7. Figure 2.47 illustrates comparative plots for linear regression analysis according to Eq. (2.10).

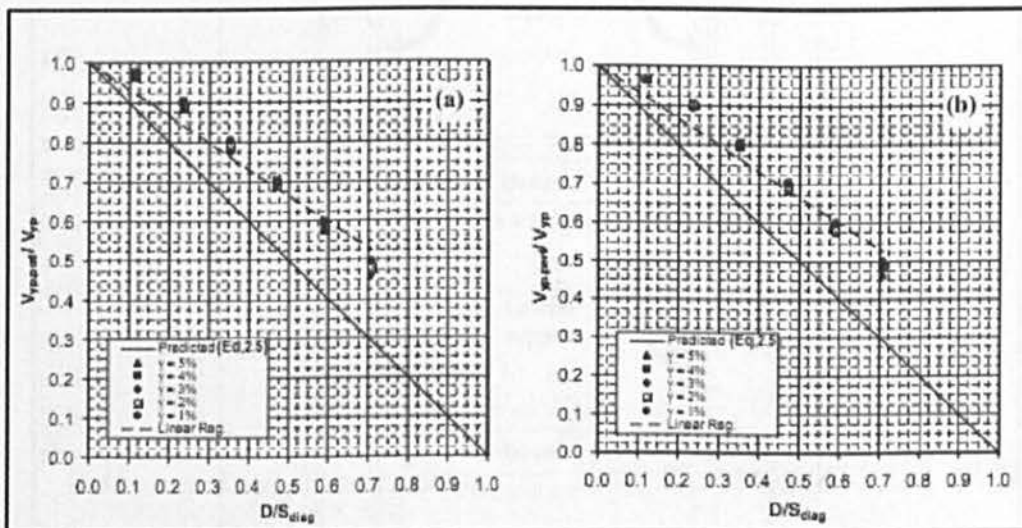


Figure 2.47: Steel plate strength ratio versus perforation ratio for (a) Rigid Floor mode, (b) Rigid Beam model (Purba, 2009)

Purba (2005) also investigated the effect of reinforced corner cut-out on shear strength of steel plate. It was observed that change in type of reinforcement had very small effect on shear strength of panel.

CHAPTER 2: LITERATURE REVIEW

Park et al (2007) conducted cyclic tests on five, three-storey specimens, 1/3 scale, with aspect ratio about 1.5. The effect of different range for steel plate thickness and variation in built-up vertical boundary members, namely strong columns (SC) and weak columns (WC) on overall behaviour of system were investigated. Strong and weak column sections were made of H-250×250×20×20 (built-up wide flange section, $H-d_c \times b_f \times t_w \times t_f$) and H-250×250×9×12, respectively, while beam sections were symmetrical for all specimens and were made of H-200×200×20×20. Thicknesses of the steel plates varied from 2 mm to 4 mm and were connected to frame members using fish plates. Figure 2.48 shows overall view of test specimens and corresponding test set-up.

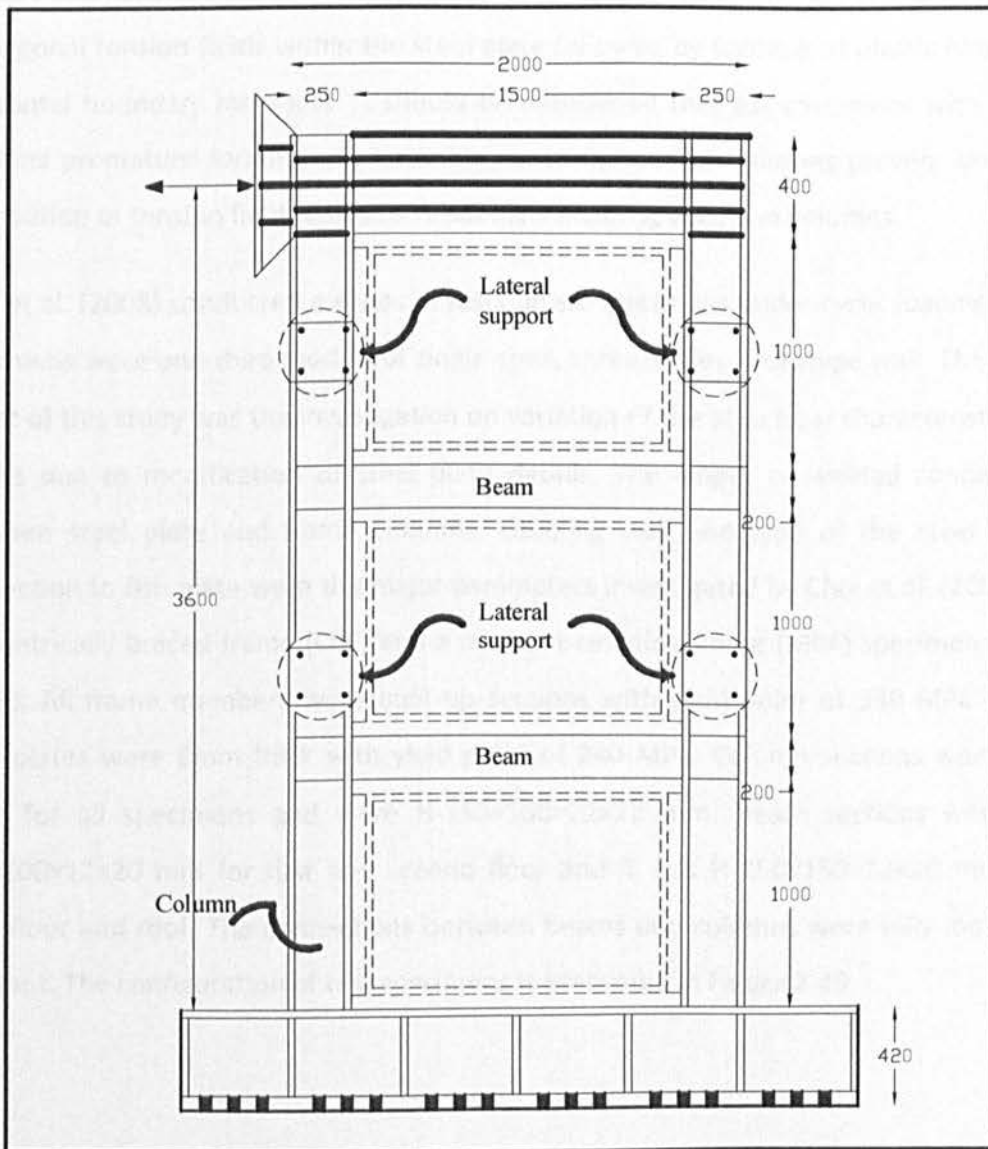


Figure 2.48: Scheme of test specimens (Park et al., 2007)

CHAPTER 2: LITERATURE REVIEW

Test results demonstrated that using weak column moves the system performance to flexural behaviour, which prevents the uniform distribution of diagonal tension fields. In other words, the columns need to be strong enough to anchor the forces applied by diagonal tension fields. Placing thicker steel plate in the frame with strong columns caused noticeable reduction in ductility of sample. The maximum drift for specimens with strong columns was 3.2%, while for specimens with weak columns it was 0.9%. Finite element analysis of specimens was implemented using ABAQUS software. The ultimate capacities underestimated for samples with strong columns, but good agreement was observed for specimens with weak columns (Park et al., 2007). Researchers concluded that shear deformation of specimens allows uniform distribution of diagonal tension fields within the steel plate followed by forming of plastic hinges in horizontal boundary members. It should be mentioned that for specimens with weak columns premature forming of plastic hinges at the end of columns prevent uniform distribution of tension fields and as a result local buckling occurs in columns.

Choi et al. (2008) conducted a series of tests on six specimens under cyclic loading. Test specimens were one-third models of single-span, three-storey prototype wall. The main target of this study was the investigation on variation of the structural characteristics of SPSWs due to modification of steel plate details. The length of welded connection between steel plate and frame columns, coupling wall and type of the steel plate connection to fish plate were the major parameters investigated by Choi et al. (2008). A concentrically braced frame (CBF) and a moment-resisting frame (MRF) specimen were tested. All frame members were built-up sections with yield point of 330 MPa while steel plates were 6mm thick with yield point of 240 MPa. Column sections were the same for all specimens and were H-150×150×22×22 mm. Beam sections were H-150×100×12×20 mm for first and second floor and it was H-250×150×12×20 mm for third floor and roof. The connections between beams and columns were fully moment resistant. The configuration of test specimens is presented in Figure 2.49.

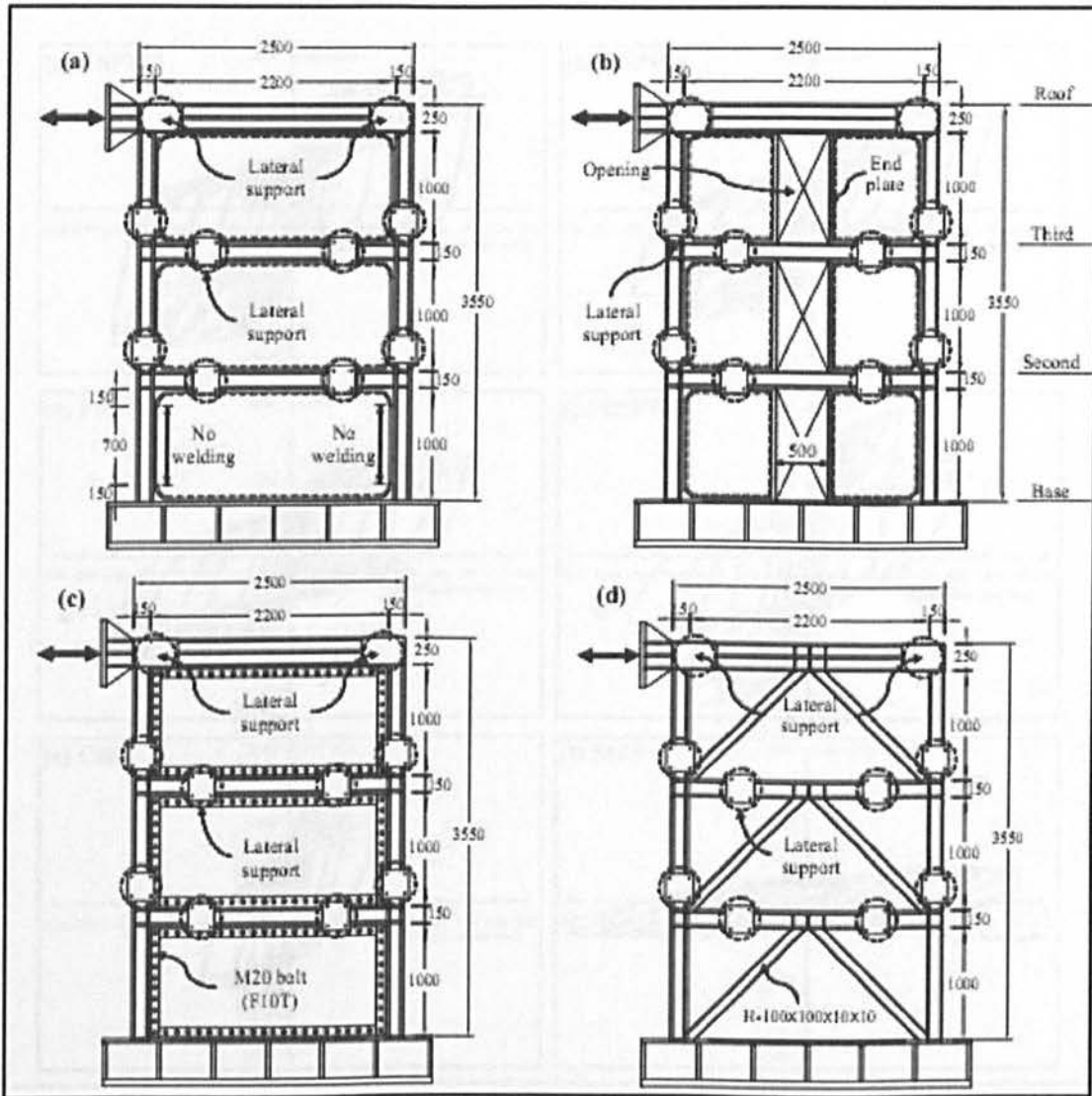


Figure 2.49: Different configurations of test specimens tested by Choi et al. (2008) for (a) Partially connected steel plate, FSPW4 specimen, (b) Coupled wall, FSPW5 specimen, (c) Bolt-connection, BSPW2 specimen, (d) CBF specimen

The beam and column sections for CBF and MRF specimens were the same as other specimens. The weight of braces (H-100×100×10×10) for CBF specimens were equal to the weight of steel plate used for FSPW2 specimens. All specimens were subjected to cyclic loading. Each cycle was repeated three times to reach the target displacement. Figure 2.50 presents the hysteresis behaviour of load-displacement curves for top storey of specimens.

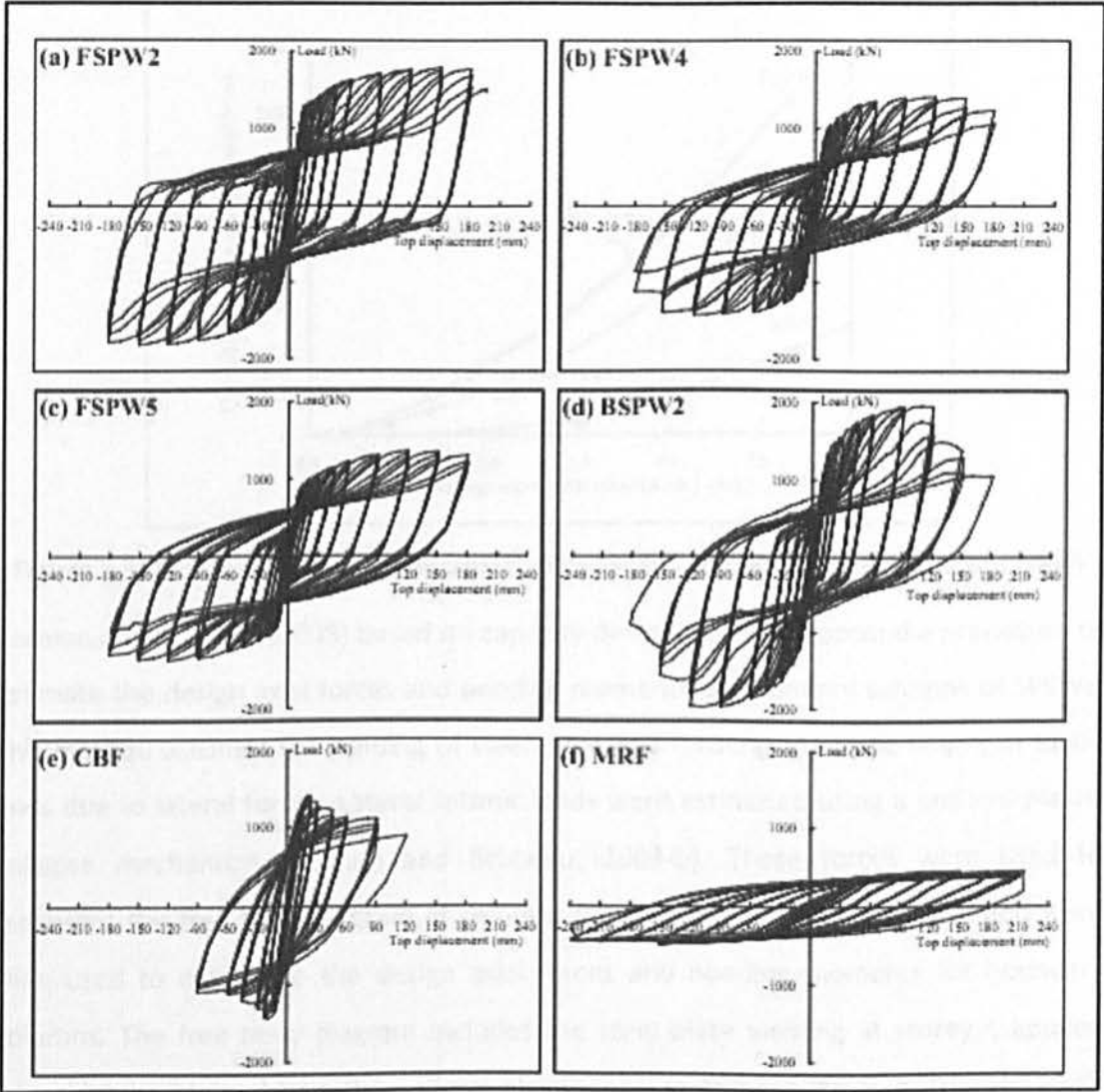


Figure 2.50: Load-top displacement relationships of test specimens for (a) FSPW2, (b) FSPW4, (c) FSPW5, (d) BSPW2, (e) CBF, (f) MRF tested by Choi et al. (2008)

Based on test observations the researchers reported that initial stiffness and ultimate capacity of FSPW2 and BSPW2 are slightly different. However, BSPW2 specimen exhibited less ductility than FSPW2 specimen. Due to existing restriction for developing of tension field action in BSPW4 and BSPW5 specimens, loading capacity of specimens were slightly less than FSPW2 specimen. Figure 2.51 shows cumulative energy dissipation capacity for specimens tested by Choi et al. (2008).

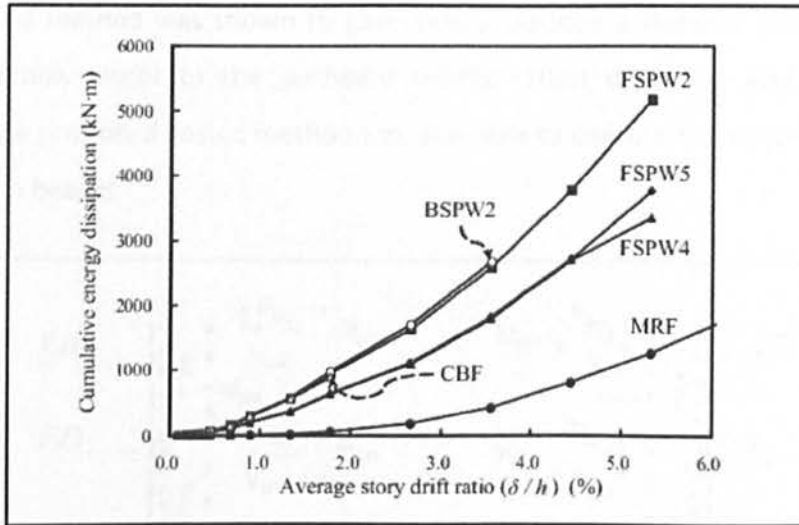


Figure 2.51: Cumulative energy dissipation capacity for specimens (Choi et al., 2008)

Berman and Bruneau (2008) based on capacity design method proposed a procedure to estimate the design axial forces and bending moments of boundary columns of SPSWs. This method assumes full yielding of steel plate and forming of plastic hinges at beam ends due to lateral forces. Lateral seismic loads were estimated using a uniform plastic collapse mechanism (Berman and Bruneau, 2003-b). These forces were used to represent the free body diagram of columns for a generic four-storey SPSW and were then used to determine the design axial forces and bending moments for boundary columns. The free body diagram includes the steel plate yielding at storey i , applied lateral loads obtained from the uniform plastic collapse mechanism, F_i , distributed loads to the columns, ω_{ycl} and ω_{xcl} , distributed loads to the beams, ω_{ybi} and ω_{xbi} , axial forces from the beams, P_{bli} , P_{bri} , moments from plastic hinging of the beams, M_{prli} and M_{prri} , and base reactions R_{yl} , R_{xl} , R_{yr} and R_{xr} (Figure 2.52).

To evaluate the adequacy of the proposed method, Berman and Bruneau (2008) designed two samples of four-storey SPSWs, one with constant and one with variable steel plate thickness denoted SPSW-C and SPSW-V, respectively. Column design loads also were computed based on two other available methods namely indirect capacity design method and the combined linear elastic computer program and capacity design concept refer to AISC 2005 seismic design provisions. The results, including column axial forces and bending moments from three design methods were compared with the results from nonlinear static pushover analysis for both SPSW-V and SPSW-C specimens.

CHAPTER 2: LITERATURE REVIEW

The proposed method was shown to give vertical boundary element design loads that are considerably closer to the pushover results rather than two above mentioned methods. The proposed design method was also able to capture the axial force-moment interaction in beams.

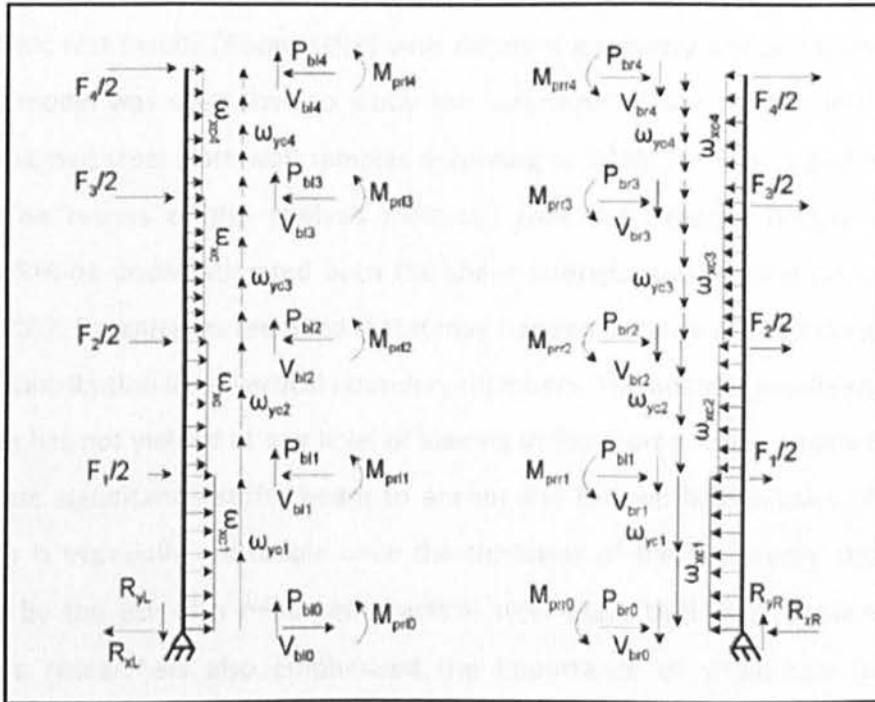


Figure 2.52 Free body diagram for vertical boundary members (Berma and Bruneau, 2008a)

Researchers noted that assuming of fully steel plate yielding over the entire height of the system on all floors would not be improbable in the taller structures. It was suggested that for tall buildings during earthquake event significant part of steel plate could remain in elastic area of loading. In such case the authors suggested that the column design forces could be reduced on similar way was proposed earlier by Redwood and Channagiri (1991). It is worth to mention that the proposed procedure is based on an assumed plastic collapse mechanism and linear model of one of the columns and as a result it does not involve non linear analysis.

Bhowmick et al. (2009) developed a nonlinear finite element method for investigating the behaviour of SPSW and different design approaches. The proposed model incorporated both geometry and material nonlinearities. Damping, strain rate and p-

delta effects were also included in proposed FE model. The model was created using ABAQUS/Standard (Hibbit, 2007) utilising four-node doubly-curved shell elements with reduced integration and an implicit time integration strategy for seismic analysis. The model was validated by comparing the finite element analysis results with the published cyclic quasi-static tests (Behbahanifard, 2003-b; Driver et al., 1998-a; Lubell et al., 2000) and dynamic test results (Rezai, 1999) with different geometry and configurations. The validated model was used then to study the behaviour of several ductile and limited ductile designed steel plate wall samples according to CAN/CSA S16-01 and NBCC 2005 criteria. The results of the analysis indicated that the capacity design method in CAN/CSA S16-01 underestimated both the shear strength and flexural demand at the base of SPSW. Researchers reported that it may happen because of neglecting the shear strength contribution from vertical boundary members. The analysis results showed that steel plate has not yielded at any level of loading in top storey which means there is no need to use significantly stiffer beam to anchor the tension field actions of top steel plate. This is especially noticeable once the thickness of the top storey steel plate is restricted by the use of a minimum practical steel plate thickness (Bhowmick et al., 2009). The researchers also emphasised the importance of strain rate in dynamic response of SPSWs based on results from other researchers (Manjoine, 1994; Krawinkler and Popov, 1982; Mahin et al., 1972; Gioncu, 2000). With higher strain rates the ductility of the steel plate shear wall reduces and the average flexural demand at the base of the wall is increased (Bhowmick et al., 2009).

In recent years the seismic design of structural systems is moving from simplified force-based deterministic methods towards performance-based seismic design (PBSD) techniques (Ghosh et al., 2009). Those techniques are using inelastic response parameters, such as ductility and hysteretic energy or combination of these parameters to quantify the damage of structures.

Ghosh et al. (2009) developed PBSD method for design of SPSWs for a four-floor frame with simple connections between beams and vertical boundary elements. This method considers the inelastic energy demand on structural system, and this energy is equated with the inelastic work done through the plastic deformations for a monotonic loading

up to the target drift. This method has already been used for the design of MRF (Lee, 2001; Leelathaviwat, 1998) and EBF systems (Chao, 2005; Ghosh et al., 2009) considered pinned connections between beams and columns, while the columns were fixed at their bases and were continuous along the height of the system (Figure 2.53).

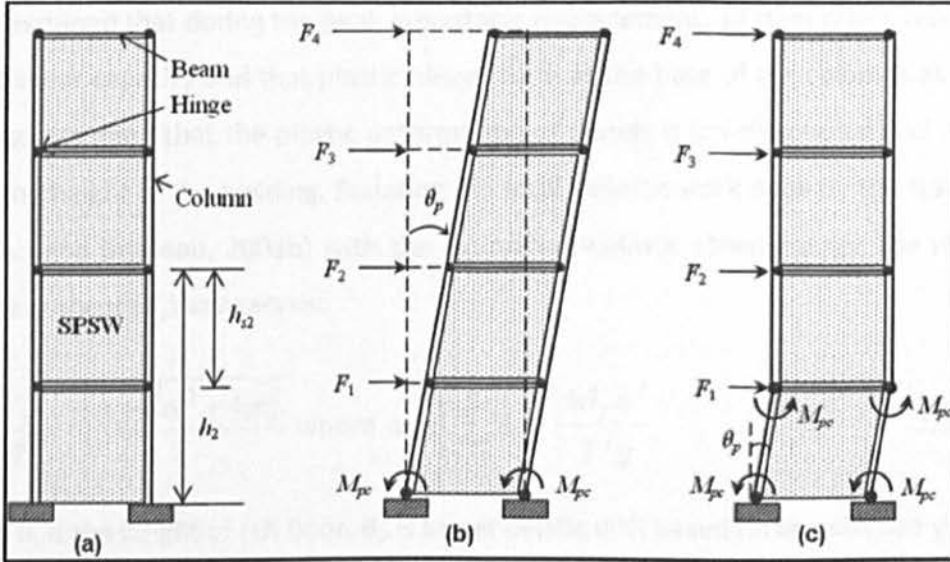


Figure 2.53: (a) Scheme of the SPSW (b) plastic hinge formation at the base of the boundary columns (c) soft ground storey (Ghosh et al., 2009)

The total strain energy of an inelastic system can be estimated from (Lee, 2001; Akiyama, 1985):

$$E_e + E_p = \gamma \left(\frac{1}{2} MS_v^2 \right) = \frac{1}{2} \gamma M \left(\frac{T}{2\pi} c_e g \right)^2 \quad 2.11$$

where E_e is elastic strain energy demand, E_p is plastic strain energy demand, γ is energy modification factor, M is total mass of the structure, T is fundamental natural period, S_v is pseudo velocity corresponding to T , C_e is elastic force coefficient and g is gravitational acceleration. The energy modification factor is a function of target ductility ratio of the system (μ_t) and ductility reduction factor (R) as follows:

$$\gamma = \frac{2\mu_t - 1}{R^2} \quad 2.12$$

The elastic force coefficient (C_e) is defined as follows:

$$C_e = \frac{A}{g} = \frac{V_e}{W} \quad 2.13$$

Where A is the design pseudo acceleration, V_e is the design (elastic) base shear and W is the seismic weight of the structure.

It was assumed that during the peak monotonic displacement, all steel plates reach their plastic shear capacity and that plastic hinges form at the base of the columns as well. It was also assumed that the plastic deformation of panels is uni-directional and uniform along the height of the building. Equating the total inelastic work done by the system W_p (Berman and Bruneau, 2003b) with the estimated inelastic strain energy, the required yield base shear (V_y) appears as:

$$\frac{V_y}{W} = \frac{-\alpha + \sqrt{\alpha^2 + 4\gamma c_e^2}}{2} \text{ where } \alpha = \left(\sum_{i=1}^n \lambda_i h_i \right) \frac{8\theta_p \pi^2}{T^2 g} \quad 2.14$$

Where h_i is the height of i th floor, θ_p is target plastic drift based on an assumed yield drift (θ_y) and λ_i represents the shear force distribution λ in the SPSW system and is equal to:

$$\lambda_i = \frac{F_i}{V_y} \quad 2.15$$

The thickness of steel plate at each storey level was obtained considering that plastic shear at each storey level to be carried out by corresponding steel plate of the floor.

$$t_i = \frac{2P_i}{0.95F_y L} = \frac{2V_i}{0.95F_y L} \quad 2.16$$

In this equation the plastic shear capacity of the plate (P_i) was calculated based on the multi-strip idealization (Thorburn, 1983). The coefficient of 0.95 in this equation represents the use of mean value of inclination angle of 45° instead of its real value. Gupta and Krawinkler (2000) also reported that the use of actual value of inclination angle of diagonal tension field action has insignificant effect on SPSW analysis results. Therefore the use of an average value of inclination angle was suggested for analysis and design of SPSWs.

Ghosh et al. (2009) utilised the recommendations given by Driver et al. (1997) for calculating of the base column moment capacity (M_{pc}), ensuring the formation of plastic hinges within the steel plate prior to columns.

$$M_{pc} = \frac{F_y t_1 h_1^2}{16} \tag{2.17}$$

It should be noted that as within the presented equations, steel plates are bearing the shear of stories and the shear resistance of vertical boundary members is neglected, the check of soft-storey formation is automatically satisfied.

Researchers applied the proposed method for the design of four-storey steel-frame structure with simple beam-to-column connections, and different aspect ratio of panels under strong motion records from the 1994 Northridge and 1995 Kobe earthquakes (Figure 2.54). The results indicated that the proposed displacement-based method is able to gain the target displacement ductility. However, the method needs to be validated for high-rise buildings and different earthquake scenarios to evaluate the P-Δ effects.

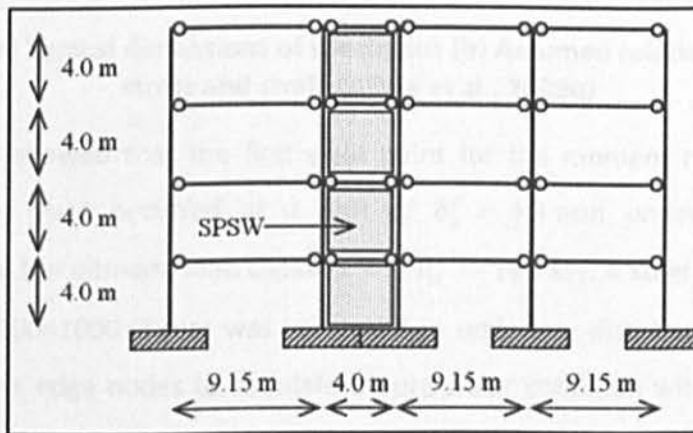


Figure 2.54: Scheme of the four-storey steel frame structures studied by Gosh et al.(2009) based on proposed method

Alinia et al. (2009b) carried out a series of finite element analysis on single-storey, single-bay SPSW specimens under lateral loading. ANSYS software was used for modelling and analysis of specimens to evaluate the interaction between boundary members and steel plates. All components of system were modelled using a four-node shell-181 element. This element has six degrees of freedom and is able to model both

material and geometrical nonlinearities. In order to distinguish the relative contribution of steel plate and boundary members on ultimate load bearing capacity of the system, the discrete frame and steel plate were analysed separately. In this study, the boundary members were supposed to be IPE160, and the thickness of the steel plate was 3 mm. Their material properties were $E_1=200$ GPa, $E_2=2$ GPa, $\nu=0.3$ with yield stress 240 MPa. The von Mises yield criterion was used for material yielding (Alinia et al., 2009b). Figure 2.55 shows the dimension of specimens and the assumed relationship between stress and strain for mild steel.

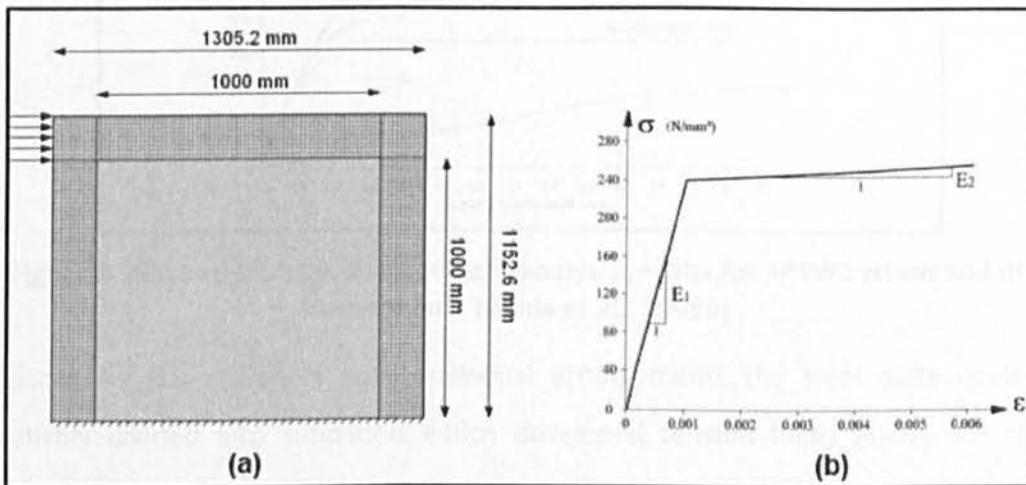


Figure 2.55: (a) Typical dimensions of specimens (b) Assumed relationship between stress and strain (Alinia et al., 2009b)

Analysis results showed that the first yield point for the moment resisting frame without a steel plate occurred at a drift of $\delta_y^F = 4.3$ mm under the load of $P_y^F = 81$ kN and the ultimate load capacity was $P_u^F = 160$ kN. A steel plate with the dimension of 1000×1000×3 mm was subjected to uniformly distributed shear load applied along the edge nodes to simulate a pure shear condition within the panel. The fixity of the boundary condition was defined by torsional rigidity of boundary frame members (Alinia et al., 2009b). The first yield point for steel plate occurred at drift of $\delta_y^P = 0.86$ mm under the load of $P_y^P = 146$ kN, and the ultimate load capacity was $P_u^P = 171$ kN. Analysis of the SPSW system incorporating steel plate and moment resisting frame subjected to the lateral load (similar to the aforementioned specimens) indicated that the first yield point occurred in the steel plate at $\delta_y^{infill} = 0.92$ mm, $P_y^{infill} = 192$ kN. The first yield point in boundary members

occurred at $\delta_y^{frame} = 1.429 \text{ mm}$, $P_y^{frame} = 270 \text{ kN}$. The combined ultimate load bearing capacity was $P_u^{SPSW} = 377 \text{ kN}$ which 25% is more than the summation of ultimate bearing load capacity for frame and detached steel plate. Figure 2.56 shows the analysis results for above mentioned case studies. It was concluded that there was an interaction effect between frame and steel plate (Alinia et al., 2009b).

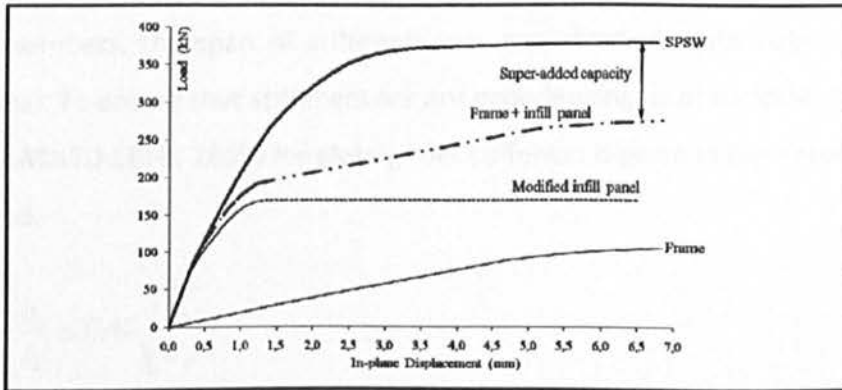


Figure 2.56: Load-inplane displacement analysis results for SPSW system and its components (Alinia et al., 2009b)

By using the flat stiffeners with individual arrangements the steel plate could be effectively divided into subpanels which developed tension fields across the shear panels. Alinia and Sarraf (2009a) carried out parametric study to determine the optimal dimension of stiffeners to propose appropriate design formulation. The study was focused on one-side flat stiffeners as shown in Figure 2.57.

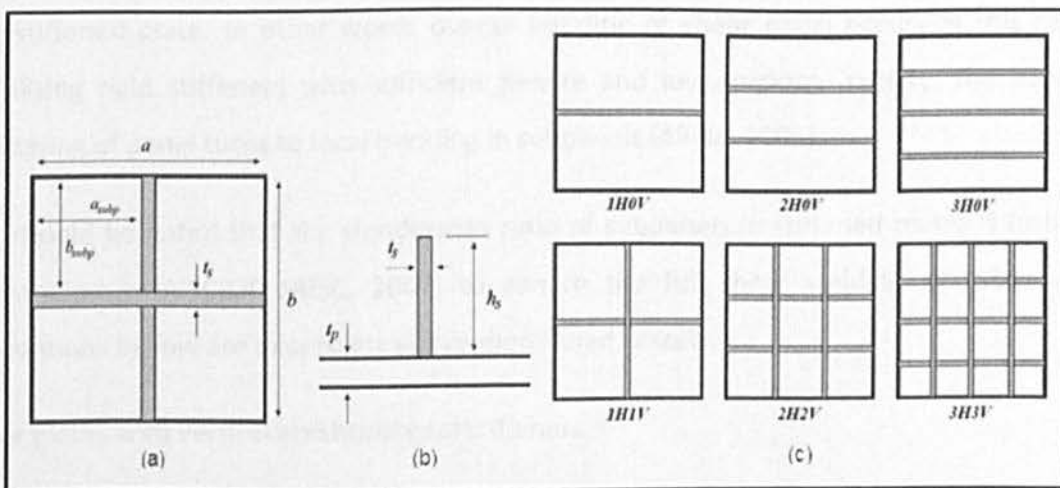


Figure 2.57: Scheme of geometrical specification of stiffened walls (a) Typical sub-plate dimensions, (b) Dimension of stiffeners (c) Various stiffener arrangements studied by Alinia and Sarraf (2009a)

CHAPTER 2: LITERATURE REVIEW

ABAQUS software was used for analysis of specimens. Plates were modelled by four-node S4R shell elements, and stiffeners were modelled by three-node B31 linear beam elements. Having six degrees of freedom for S4R elements initiates the out-of-plane behaviour of steel plates. The B31 element is better suited for simulation of linear elastic transverse shear deformations in accordance with Timoshenko beam theory, and allows for large axial strains. In order to prevent stress transmission between stiffeners and boundary members, the span of stiffeners was just short of plate edges (Alinia and Sarraf, 2009a). To ensure that stiffeners are not experiencing local buckling, the AASHTO provision (AASHTO-LRFD, 2005) for plate girder stiffeners is given in the equation below, was followed:

$$\frac{h_s}{t_s} \leq 0.48 \sqrt{\frac{E}{\sigma_y}} \quad 2.18$$

where, h_s is height of stiffener and σ_y is yield stress of stiffeners. In order to consider the weld-ability of material the following relation between steel plate and stiffeners thickness was also considered:

$$t_p \leq t_s < 5t_p$$

By using flexible stiffeners with low flexural rigidity, the buckling stresses increase. However, the buckling mode of the plate does not change in comparison to the unstiffened plate. In other words overall buckling of shear panel occurs in this case. Utilising rigid stiffeners with sufficient flexure and low torsional rigidity, the overall buckling of panel turns to local buckling in subpanels (Alinia, 2005).

It should be noted that the slenderness ratio of subpanels in stiffened plates is further restricted in AISC820 (AISC, 2007) to ensure the full shear yielding of subpanels. Equations bellow are expressing above mentioned criteria:

For plates with vertical and horizontal stiffeners

$$\frac{b_{subp}}{t_p} \leq 3.82 \sqrt{\frac{E}{\sigma_y}} \quad 2.19$$

CHAPTER 2: LITERATURE REVIEW

For plates with either vertical or horizontal stiffeners

$$\frac{b_{subp}}{t_p} \leq 2.88 \sqrt{\frac{E}{\sigma_y}} \quad 2.20$$

Based on the results from analysis, the researchers reported that there is no linear relation between optimal thickness and height of stiffeners. However, for different arrangements of stiffeners empirical equations were developed for evaluating the effectiveness of stiffeners by curve-fitting expressions. It was also reported that the optimal stiffeners are rigid enough to form nodal lines and that in the post buckling stage the subpanels behave as detached simply supported plates. Alinia et al. concluded that stiffeners prevent early overall buckling of shear panels. Stiffeners limit out-of-plane deformation of steel plate and improve elastic in-plane stiffness of shear panel. Furthermore it was concluded that in an optimal stiffener arrangement, the critical stresses of stiffened plates are equal to the critical stresses of individual subpanels (Alinia and Sarraf, 2009a).

Gholhaki and Sabouri-Ghomi (2009) conducted a research program to identify force modification factor for thin SPSWs. Two of one-bay three-storey specimens were constructed and subjected to hysteresis load according to ATC-24 protocol (Figure 2.58). The specimens were symmetrical with exception of beam to column connections. The beam-to-column connections were simple connection for one of the specimen (SPSW-S) and for the other specimen rigid connections (SPSW-R). Low yield steel plates 0.7 mm thick were used for all storeys of both specimens. Table 2.4 gives material properties of different members for specimens tested.

Table 2.4: Specification of material properties for specimens tested by Gholhaki and Sabouri-Ghomi (2009)

Members	F_y (MPa)	F_u (MPa)	E (GPa)
Steel plate	180	300	206
Column	366	550	206
Intermediate beams	310	446	206
End beam	366	550	206

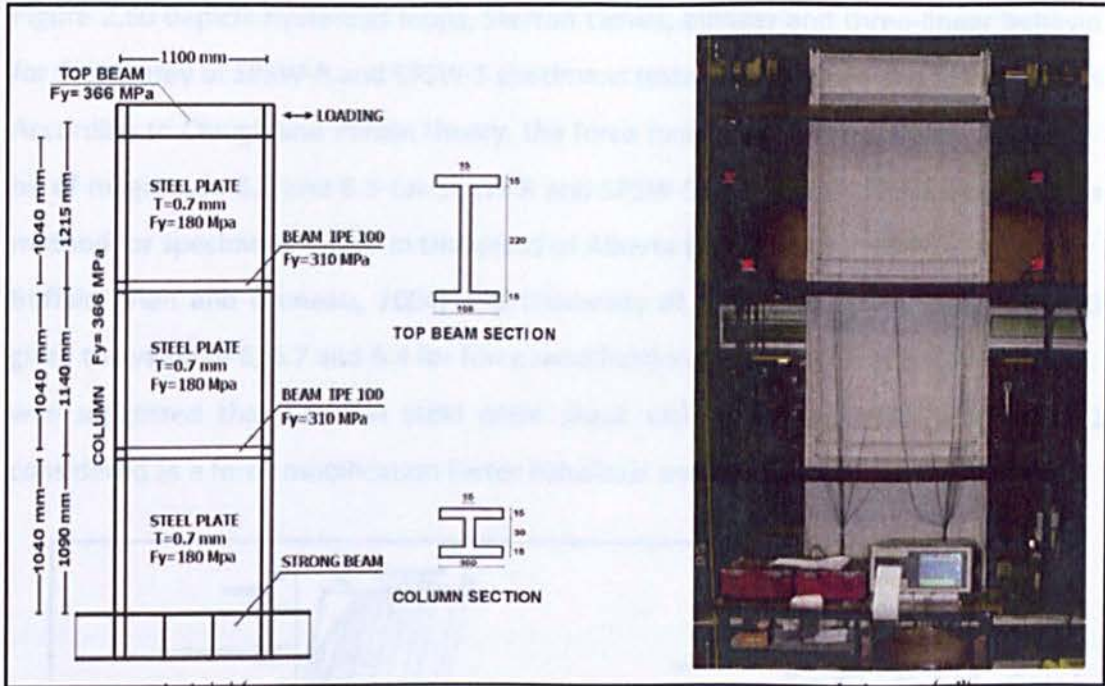


Figure 2.58: Scheme of three-storey SPSW specimen tested by Gholhaki and Sabouri-Ghomi (2009)

Based on Clough and Penzin theory (Clough and Penzin, 1993), the force modification factor (R) is defined as follows:

$$R = \frac{V_e}{V_{max}} = \frac{\delta_e}{\delta_y} = \frac{\delta_u}{\delta_y} \quad 2.21$$

where V_e is theoretical elastic base-shear and δ_u is ultimate displacement of specimen.

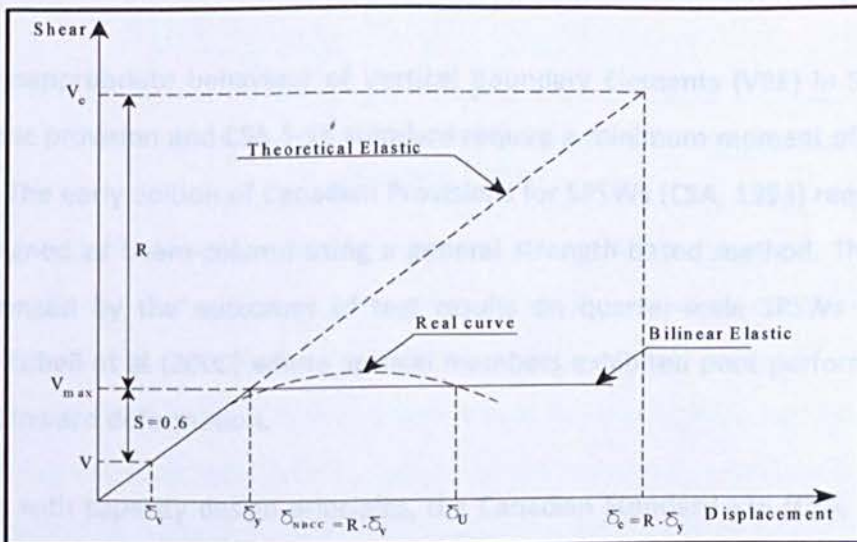


Figure 2.59 Elastic and plastic response of structures

CHAPTER 2: LITERATURE REVIEW

Figure 2.60 depicts hysteresis loops, Skelton curves, bilinear and three-linear behaviour for first storey of SPSW-R and SPSW-S specimens tested by Gholhaki and Sabouri-Ghomi. According to Clough and Penzin theory, the force modification factors were reported to be of magnitude 6.2 and 6.5 for SPSW-R and SPSW-S respectively. Following the same method for specimens tested in University of Alberta (Driver et al., 1998-a), University of Buffalo (Vian and Bruneau, 2004) and University of British Columbia (Kharrazi, 2005) gives the value of 6, 6.7 and 6.4 for force modification factor of corresponding frames. It was suggested that for thin steel plate shear walls the magnitude of 6 could be considered as a force modification factor (Gholhaki and Sabouri-Ghomi, 2009).

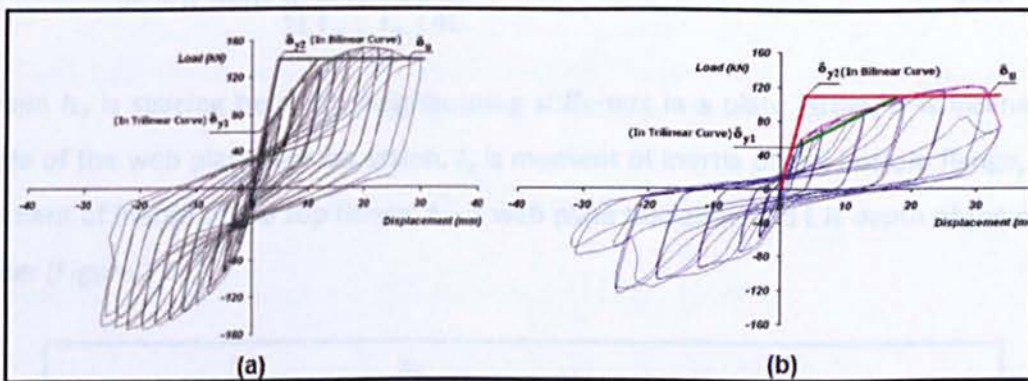


Figure 2.60: Hysteresis and multi linear behaviour of first floor for (a) SPSW-R specimen (b) SPSW-S specimen tested by Gholhaki and Sabouri-Ghomi (2009).

2.2.3. Recent advances on steel plate shear Walls (from 2010 onward)

To avoid inappropriate behaviour of Vertical Boundary Elements (VBE) in SPSWs, the AISC seismic provision and CSA S-16 standard require a minimum moment of inertia for the VBEs. The early edition of Canadian Provisions for SPSWs (CSA, 1994) required VBEs to be designed as beam-column using a general strength-based method. This method was challenged by the outcomes of test results on quarter-scale SPSWs specimens tested by Lubell et al (2000) where vertical members exhibited poor performance and significant inward deformation.

Consistent with capacity design principles, the Canadian Standard S16 (CSA, 2001) and AISC seismic provisions (AISC, 2005c) require Horizontal Boundary Elements (HBEs) and

CHAPTER 2: LITERATURE REVIEW

VBEs to be designed to remain elastic while the steel plates are fully yielded, with the exception of plastic hinges at the ends of HBEs and at the base of VBEs (Qu and Bruneau, 2010-b). In order to make sure that VBEs are sufficiently stiff, CSA S16-01 introduced the flexibility factor, ω_t , which was proposed previously developed by analytical procedure for plate girders. Wagner (1931) derived the governing fourth-order ordinary differential equation for the local flange deflections. This equation was derived based on modelling each flange of the plate girder as a continuous beam on an elastic foundation (Wagner, 1931). The flexibility factor for plate girders is defined as below:

$$\omega_t = h_{si} \sin \alpha \sqrt[4]{\left(\frac{1}{I_u} + \frac{1}{I_o}\right) \frac{t_{wi}}{4L}} \tag{2.22}$$

Where h_{si} is spacing between neighbouring stiffeners in a plate girder, α is inclination angle of the web plate tension action, I_u is moment of inertia of the bottom flange, I_o is moment of inertia of the top flange, t_{wi} is web plate thickness and L is depth of the plate girder (Figure 2.61).

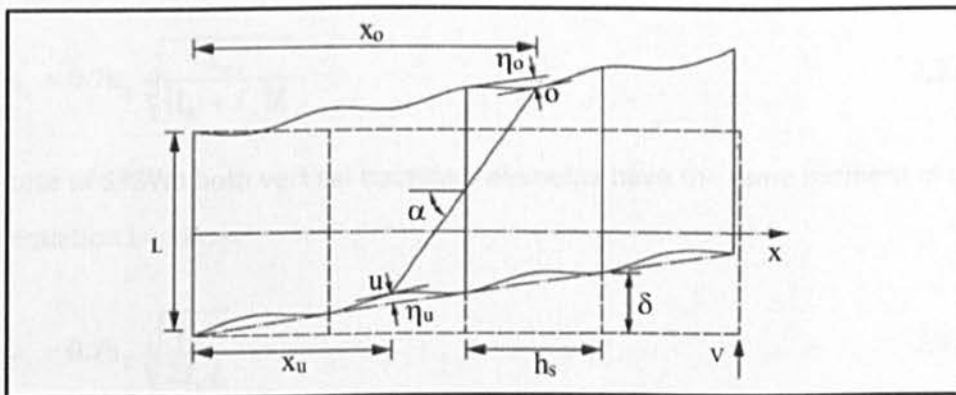


Figure 2.61: Deformation of a cantilever plate girder under transverse load (Wagner, 1931)

The relation between stress uniformity ratio $\sigma_{mean}/\sigma_{max}$, where σ_{mean} and σ_{max} indicates the mean and maximum value of the web tension load components parallel to the stiffener respectively, and the flexibility factor ω_t , is presented in Figure 2.62. For the smaller value of the flexibility factor, which means the plate girder has relatively stiff flanges, the stress uniformity ratio $\sigma_{mean}/\sigma_{max}$ is approximately equal to 1.0 indicating the development of a uniform tension field. The shape of the curves indicates that with an increase in the flexibility factor the stress uniformity ratio decreases, which mean due

to flexibility of the flanges a less uniform tension field, could be developed within the web of plate girder.

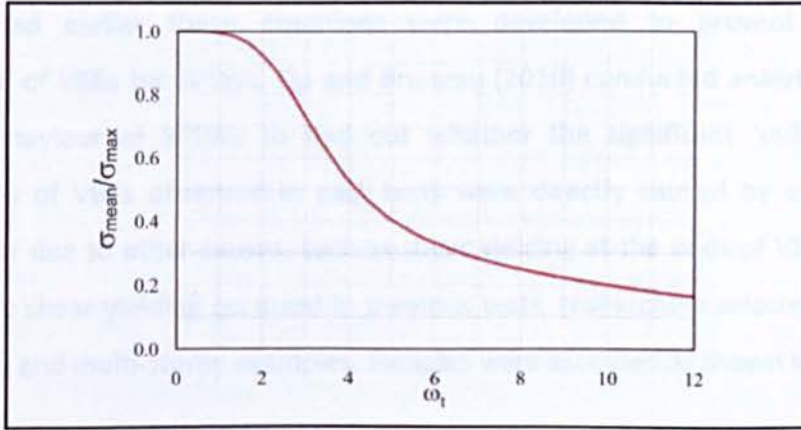


Figure 2.62: The relationship between flexibility factor and stress uniformity ratio developed by Qu and Bruneau (2010).

For simplicity, by assuming $\alpha=45^\circ$ and approximate equivalency $\left(\frac{1}{I_u} + \frac{1}{I_o}\right) = \frac{4}{(I_u + I_o)}$

the flexibility factor is simplified as follows (Kuhlen et al., 1952) :

$$\omega_t \approx 0.7h_s \sqrt[4]{\frac{t_{wi}}{(I_u + I_o)L}} \quad 2.23$$

In the case of SPSWs both vertical boundary elements have the same moment of inertia, I_c , this equation becomes:

$$\omega_t = 0.7h_s \sqrt[4]{\frac{t_{wi}}{2I_cL}} \quad 2.24$$

Based on information provided by Montgomery and Medhekar (2001), CSA S16 limited the flexibility factor to a maximum value of 2.5. Imposing the maximum value of 2.5 on Eq. (2.24) leads to the following requirement which was first implemented in the CSA S16-01:

$$I_c \geq \frac{0.00307t_{wi}h_s^4}{L} \quad 2.25$$

This requirement was adopted in the USA National Earthquake Hazard Reduction Program (NEHRP) provisions for seismic regulations for new buildings and other

CHAPTER 2: LITERATURE REVIEW

structures, also known as FEMA 450 (FEMA, 2003), and also the AISC seismic provisions (AISC, 2005c).

As mentioned earlier these equations were developed to prevent undesirable performance of VBEs for SPSWs. Qu and Bruneau (2010) conducted analytical research on VBEs behaviour of SPSWs to find out whether the significant ‘pull-in’ inelastic deformations of VBEs observed in past tests were directly caused by excessive VBE flexibilities or due to other causes, such as shear yielding at the ends of VBEs. To check whether VBE shear yielding occurred in previous tests, researchers selected number of single-storey and multi-storey examples. Samples were assessed as shown in Table 2.5.

Table 2.5: Evaluation of VBE shear and strength requirements (Qu and Berman, 2010b)

Case	Researcher	Specimen Identification	Number of Stories	Scale	Aspect Ratio ^c (L/h)	α (°)	ω_b	V_n (kN)	$V_{pushover}$ (kN)	$V_{u-design}$ (kN)	Shear Yielding
(i) single-story specimen											
1	Lubell et al. (2000)	SPSW2	1	1:4	1.00	37.4	3.35	75	108	113	Yes
2	Berman and Bruneau (2005)	F2	1	1:2	2.00	44.8	1.01	932	259	261 ^d	No
(ii) multi-story specimen ^a											
3	Driver et al. (1998)	^b	4	1:2	1.58	43.4	1.73	766	1361	1458	Yes
4	Park et al. (2007)	SC2T	3	1:3	1.46	44.4	1.24	999	676	1064	No
5		SC4T	3	1:3	1.46	44.1	1.44	999	984	1383	No
6		SC6T	3	1:3	1.46	43.9	1.58	999	1218	1622	Yes
7		WC4T	3	1:3	1.46	45.0	1.62	560	920	1210	Yes
8		WC6T	3	1:3	1.46	45.0	1.77	560	1151	1461	Yes
9	Qu et al. (2008)	^b	2	1:1	1.00	41.3	1.95	2881	1591	2341	No
10	Lee and Tsai (2007)	SPSW N	2	1:1	0.66	38.8	2.53	968	776	955	No
11		SPSW S	2	1:1	0.66	36.5	3.01	752	675	705	No

^a For multi-story specimens, VBEs at the first story are evaluated.
^b Not applicable.
^c Using the first-story height.
^d The plastic moments applied at the VBE ends are equal to the strength of web-angle beam-to-column flexible connections.

Comparing $V_{pushover}$ to $V_{u-design}$ confirms that using free body diagram equation for estimating of VBE shear requirement $V_{u-design}$, gives a conservative design shear force. On the other hand comparing V_n to $V_{pushover}$ reveals that samples 1, 3, 6, 7 and 8 should have experienced shear yielding during their tests. This prediction is consistent with experimental observations. It was concluded that there is no relation between flexibility factor and significant inward deformations (Qu and Berman, 2010b).

Berman (2011) designed and evaluated the behaviour of 3, 9, 14 and 20 storey buildings with SPSWs lateral load resisting system using nonlinear response history. Buildings

were subjected to ground motions representing different hazard levels. The results were then compared with code-designed SPSWs. The main purpose of the study was to investigate the seismic behaviour of SPSWs having various configurations when designed in accordance with the provisions. Designing of vertical boundary elements based on capacity design method (Berman and Bruneau, 2008a) can be quite conservative in comparison with nonlinear response history for taller SPSWs where simultaneous yielding of all steel plates and horizontal boundary elements is unlikely (Berman, 2011). The strip model was used to simulate SPSW behaviour, where the steel plate was represented by discrete tension-only strips and the VBEs and HBEs were represented by beam elements. The cyclic load-displacement behaviour of the tension-only truss elements utilized in this research is demonstrated in Figure 2.63. The inclination angle of the diagonal tension field α was computed using Eq. (2.1).

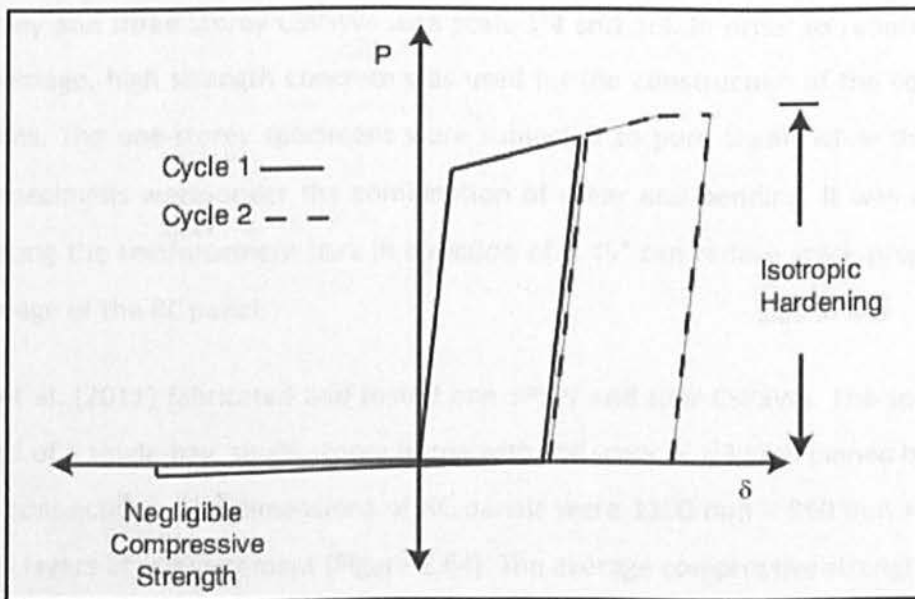


Figure 2.63: The scheme of strip element cyclic axial load behaviour (Berman, 2011)

Berman (2011) reported that code-designed SPSWs are capable of meeting drift limitations when subjected to ground motions which simulate the design loading. It was also reported that the steel plates resist between 60% and 80% of the storey shear and the rest is resisted by VBEs. It was found that distribution of storey shear is independent of hazard level and panel aspect ratio.

CHAPTER 2: LITERATURE REVIEW

The concrete composite steel plate shear walls were originally introduced by Astaneh-Asl in 2000. Since then a number of experimental work and theoretical research has been conducted about this type of SPSW (Astaneh-Asl, 2000; Astaneh-Asl, 2001-c; Astaneh-Asl, 2002; Zhao and Astaneh-Asl, 2003; Zhao and Astaneh-Asl, 2004; Arabzadeh et al., 2011; Zhao and Astaneh-Asl, 2007; Guan, 2008; Rahai and Alipour, 2009; Lanhui et al., 2011).

Rahai et al. (2009) performed an analytical study and experimental tests on the one-storey CSPSWs. According to the test results they concluded that increasing the shear studs spacing reduces the slope of the load-displacement curve. It was also concluded that increasing of stud spacing improves the ductility of specimens. This trend continues up to a certain amount of stud spacing and beyond that ductility of specimen remains approximately constant. Arabzadeh et al. (2011) conducted experimental research on one-storey and three-storey CSPSWs with scale 1:4 and 1:3. In order to reduce the RC panel damage, high strength concrete was used for the construction of the composite specimens. The one-storey specimens were subjected to pure shear, while the three-storey specimens were under the combination of shear and bending. It was reported that placing the reinforcement bars in direction of $\pm 45^\circ$ can reduce crack propagation and damage of the RC panel.

Lanhui et al. (2011) fabricated and tested one SPSW and four CSPSWs. The specimens consisted of a single-bay, single storey frame with the scale of 1:3 with pinned beam-to-column connections. The dimensions of RC panels were 1100 mm \times 950 mm \times 60 mm with two layers of reinforcement (Figure 2.64). The average compressive strength of 150 mm concrete cubes was 330 N/mm². For all specimens the shear wall was only connected to the frame beam, and there was no connection between shear wall and columns. Researchers concluded that RC panels effectively prevent the out-of-plane buckling of the shear panel. It was also found that for CSPSWs the load bearing capacity, ductility and energy dissipation capacity all increased.

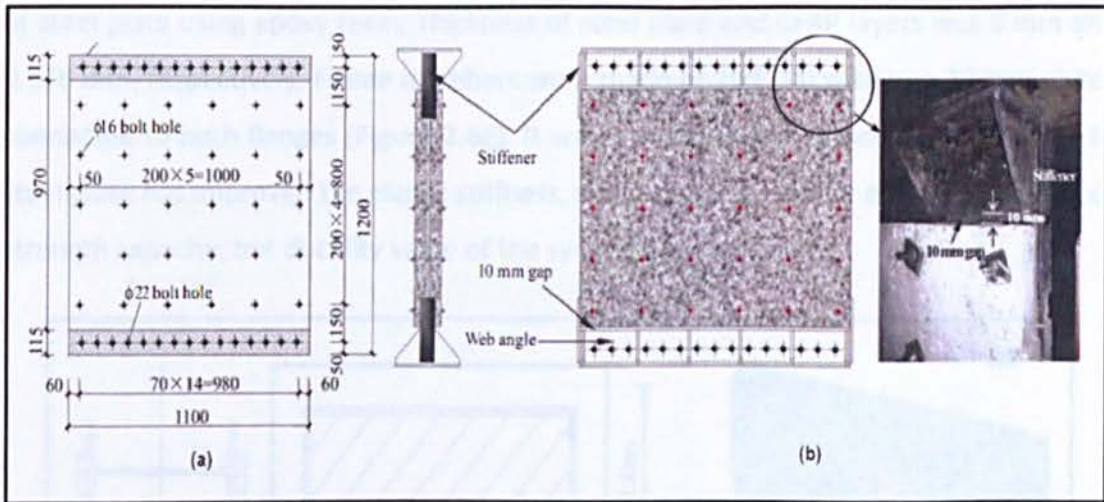


Figure 2.64: (a) Configuration of steel plate (b) Detail of CSPSW tested by Lanhui et al. (2011)

Rahai et al. (2011) conducted FE analysis of one-storey FRP-composite steel plate shear wall to find the optimum angle of fibres for strengthening of shear panel. Steel plate was strengthened using CFRP wrap covering the whole plate. The failure of CFRP material was considered utilising the Hashin failure criteria in ABAQUS software. It was concluded that the optimum angle of the fibres is $\theta=35^\circ$ and this is measured from horizontal direction (Figure 2.65). It was also reported that the shear strength of FRP-composite SPSW in comparison with pure SPSW is increased, while the ductility of the shear panel is decreased.

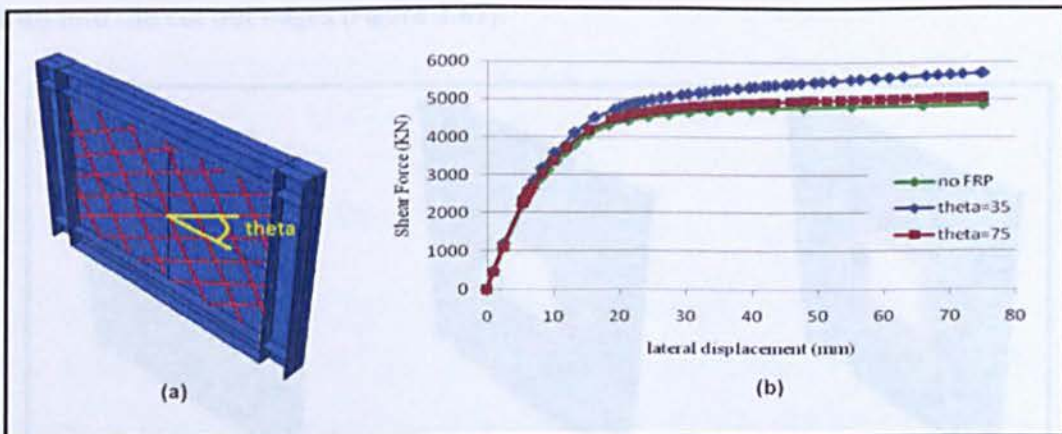


Figure 2.65: (a) Fibre directions angle (b) FE results for of SPSW strengthened with two 0.5 mm plies for two different fibre directions (Rahai et al, 2011)

Hatami et al. (2011) conducted an experimental study and numerical modelling of one-storey SPSW strengthened with CFRP material. The CFRP layer was applied to both sides

of steel plate using epoxy resin. Thickness of steel plate and CFRP layers was 3 mm and 0.176 mm, respectively. Frame members were made of 2IPE200 with two 12 mm plates connected to both flanges (Figure 2.66). It was concluded that attaching CFRP layers to steel plate has improved the elastic stiffness, shear capacity, energy dissipation and over strength capacity, but ductility value of the system has decreased.

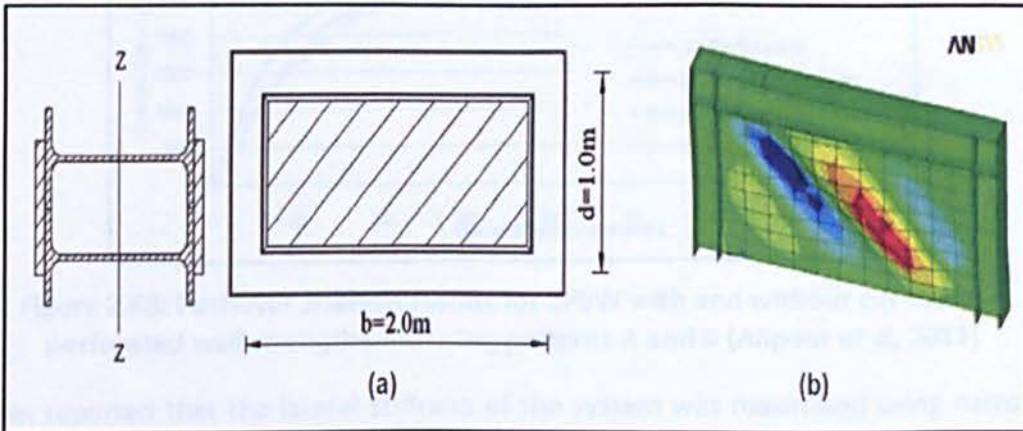


Figure 2.66: (a) Scheme of test specimen dimensions (b) FE modelling of specimen (Hatami et al, 2011)

Alipour et al. (2011) conducted numerical study on effectiveness of FRP strips as perforation boundary elements. In this study, FRP strips were attached to square perforated edges. The effect of FRP strip thickness, width and material type on SPSW behaviour was also studied. Three different patterns were used for attaching the FRP strips into the cut out edges (Figure 2.67).

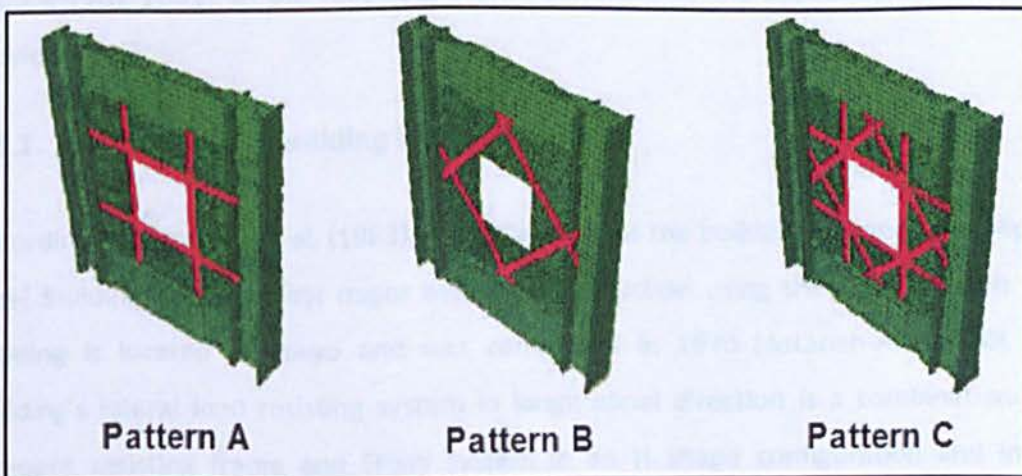


Figure 2.67: Three different configuration of cut-out edge strengthening using FRP strip material (Alipour et al, 2011)

Figure 2.68 shows pushover analysis results for SPSW with and without perforation. The results for perforated and strengthened wall with FRP strips using patterns A and B are also shown in this figure.

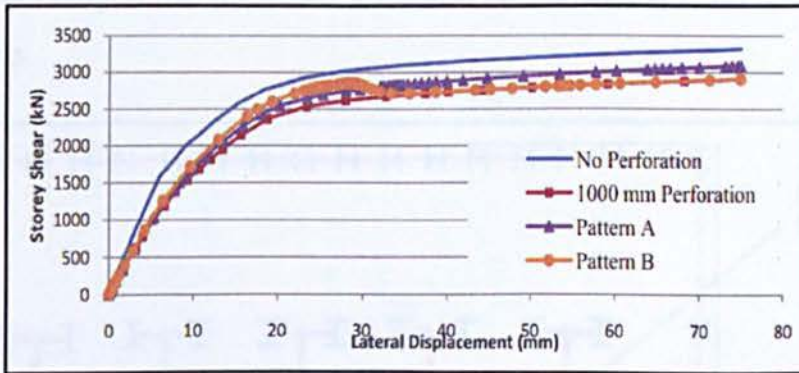


Figure 2.68: Pushover analysis results for SPSW with and without cut-out and perforated wall strengthened using patterns A and B (Alipour et al, 2011)

It was reported that the lateral stiffness of the system was maximised using narrower and thicker strips while the strength and energy dissipation were maximised with wider and thinner strips (Alipour et al, 2011).

2.3. Practical applications and case studies of Steel plate shear walls

Since 1970's stiffened and un-stiffened SPSWs have been used as the primary lateral load resisting system in new construction of buildings and for the rehabilitation of existing structures. In some cases, the SPSWs were constructed as composite elements (Astaneh-Asl, 2001). In the following a brief summary of the applications of SPSWs is provided.

2.3.1. 20-storey office building in Tokyo, Japan

According to Thorburn et al. (1983), it is believed that the building referred to as Nippon Steel Building, was the first major building construction using the SPSW system. This building is located in Tokyo and was completed in 1970 (Astaneh-Asl, 2000). The building's lateral load resisting system in longitudinal direction is a combination of a moment resisting frame and SPSW system in an H shape configuration and in the transverse direction is comprised of only a SPSW system. The steel plate panels consist of 2.74 m by 3.71 m steel plates with thickness ranged from 7.8 mm to 12.7 mm. Steel

plates are stiffened in horizontal and vertical direction using steel channels. During the design procedure it was decided that the gravity loads were excluded as load from SPSW system. It was also assumed that the design lateral load will be resisted by walls without developing buckling in the steel plates. Figure 2.69 shows the typical plan of Nippon Steel Building.

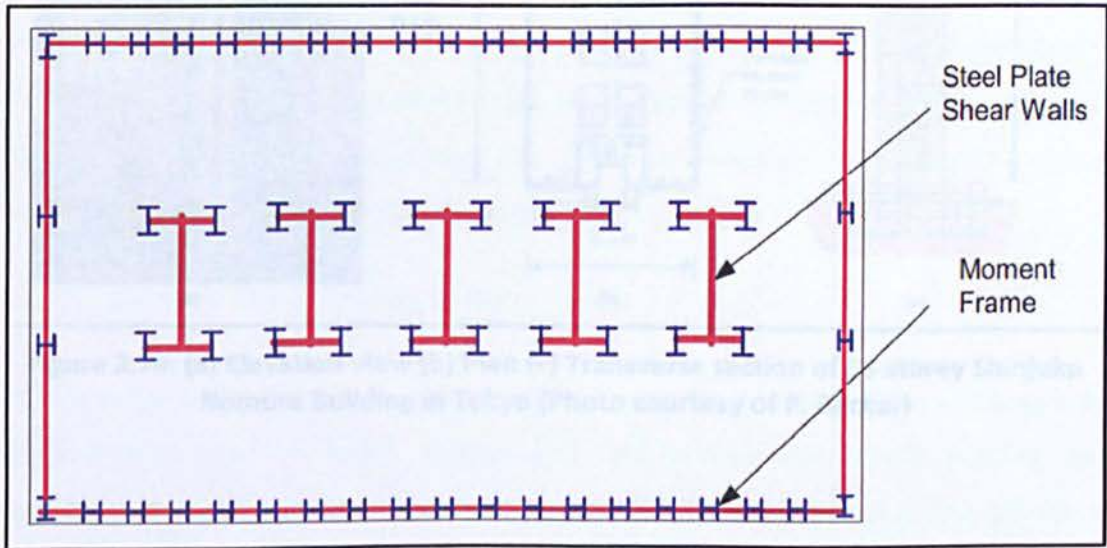


Figure 2.69: Typical floor plan of Nippon Steel Building

2.3.2. 53-storey high-rise building in Tokyo

This 53-storey building is called Shinjuku Nomura Building and located in Tokyo. The structure was initially designed using reinforced concrete shear walls. However, according to Engineering News Record (1978), due to a patent problem, the R/C walls were replaced with SPSWs (Figure 2.70). This structure consisted of moment resisting perimeter frames and T-shape stiffened SPSWs. The steel plate panels were approximately 3 m in height and 5 m in length. The wall panels were vertically stiffened on one side and horizontally stiffened on the other side. The panels were connected to H-steel columns and boundary box sections by bolted connections.

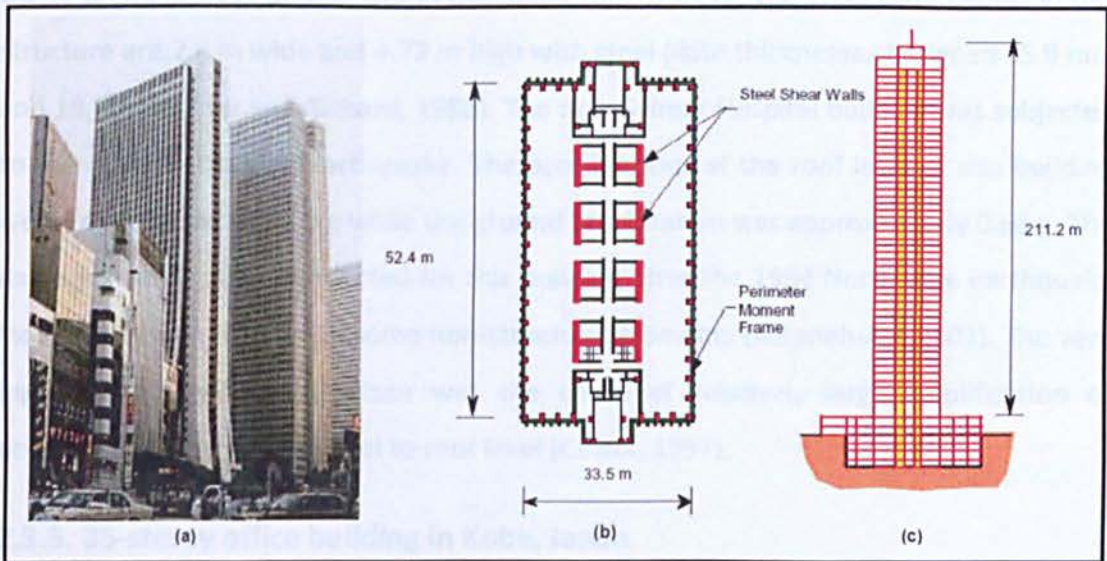


Figure 2.70: (a) Elevation view (b) Plan (c) Transverse section of 53-storey Shinjuku Nomura Building in Tokyo (Photo courtesy of P. Becker)

2.3.3. 30-storey hotel in Dallas, Texas

The 30-storey Hyatt Regency Hotel in Dallas, Texas is a good example of the efficient application of SPSWs in areas with low seismicity but with relatively high wind loads. This building has a steel braced frame in longitudinal direction and SPSWs in transverse direction. In this structure SPSWs were designed to carry about 60% of the tributary gravity load while the wide flange boundary columns designed to resist the remaining 40%. Designers claimed that by using SPSWs as a gravity load carrying element 30% of steel has been saved (Troy and Richard, 1988).

2.3.4. 6-storey hospital in Los Angeles, California

The Olive View Hospital in Sylmar, California, is a good example of SPSWs used in an important structure, and is in a relatively high seismic zone. The existing hospital building is a replacement for the reinforced concrete Olive View Hospital that had partially collapsed during the 1971 San Fernando earthquake and had to be demolished. The new Sylmar Hospital building is designed to resist the gravity load entirely through a

steel space-frame and to resist lateral load through reinforced concrete shear walls in the first two storeys and SPSWs in the upper four storeys. The steel plate panels in this structure are 7.6 m wide and 4.72 m high with steel plate thicknesses between 15.9 mm and 19.1 mm (Troy and Richard, 1988). The new Sylmar Hospital building was subjected to the 1994 Northridge earthquake. The accelerations at the roof level of this building were found to exceed 2.3 g while the ground acceleration was approximately 0.66 g. The damage investigation conducted for this building after the 1994 Northridge earthquake indicated severe damage in some non-structural elements (Astaneh-Asl, 2001). The very high stiffness of this structure was the cause of relatively large amplification of acceleration from ground level to roof level (Celebi, 1997).

2.3.5. 35-storey office building in Kobe, Japan

The 35-storey office building in Kobe, Japan is one of the most important buildings with SPSW system in a very highly seismic area. The construction of this building was completed in 1988 and was subjected to the 1995 Kobe earthquake. The structural system of this building is a dual system consisted of steel moment frames and shear walls. The shear walls in the three basement levels are reinforced concrete and in the first and second floors of the building the walls are composite shear walls constructed of steel and reinforced concrete. Above the second floor, the walls are stiffened SPSWs. Figure 2.71 shows framing plan and typical frames of this building.

Several damage assessments on this building were conducted after the 1995 Kobe earthquake. It was reported that only minor damage has occurred in building which consisted of local buckling in sub-panels of the stiffened SPSW at the 26th storey. A permanent roof drift of 225 mm was evident in the northern plane, and a 35 mm drift in the western plane. The results of the post-earthquake inelastic analysis of this structure indicated that the soft storeys may have been formed at the floors between the 24th and 28th level of the building. From the post-earthquake inelastic analyses the maximum storey drift was determined to be about 1.7% at the 29th floor of the N-S frame (Fujitani et al, 1996).

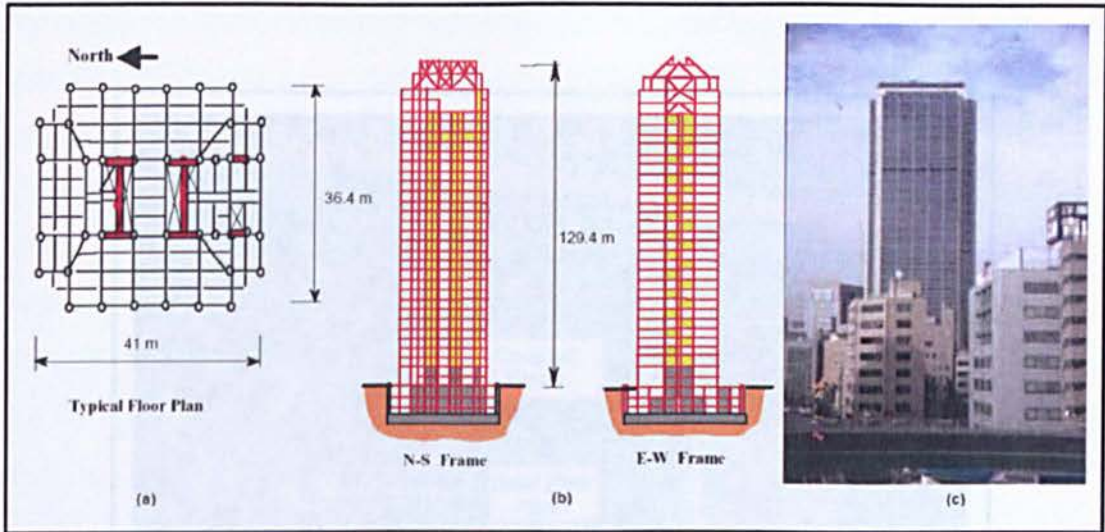


Figure 2.71: (a) Floor plan (b) elevation section (c) Photo of 35-storey Kobe building (Photo courtesy of C.E. Ventura)

2.3.6. 24-storey building in Seattle, Washington

The typical floor framing of the U.S. Federal Courthouse in Seattle consists of steel deck and/or concrete floors supported on wide flange beams and columns. The lateral load-resisting consists of a core with four large concrete-filled tubs (CFT) at its corners and steel plate shear walls and coupling beams connecting the circular sections to each other in one direction and steel braced frame in the other. The four round concrete-filled tubes carry the gravity load in the interior of the building. The H-shaped columns within the steel box core are not designed to carry gravity load but are designed to be the main part of the lateral-load resisting system. At the four corners of the core, the concrete-filled steel pipe columns anchor the SPSWs and resist the intense forces being applied to the shear walls (Figure 2.72). This can be considered as a dual system incorporating SPSWs and special moment-resisting frames.

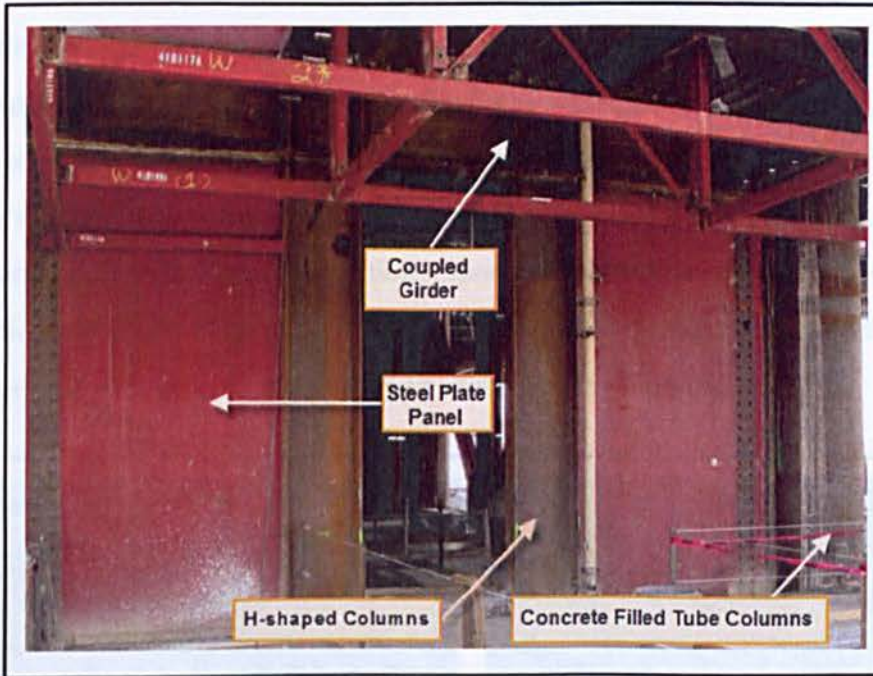


Figure 2.72: Coupled SPSW under construction regarding to 24-storey US Courthouse Building, Seattle, Washington

2.3.7. 26- and 31-storey buildings in Japan

In recent years Low Yield Point (LYP) steel plate shear walls have been developed and employed successfully in Japan. According to Yamaguchi et al. (1998) the LYP steel used in this structure had a yield point of approximately 80 to 120 MPa, a tensile strength of 200 to 300 MPa and the percentage elongation at fracture exceeding 50%. Dimensions of shear panels were 3 m in height and 4.5 m in width and 6 mm to 25 mm thick steel plate which were stiffened in both horizontal and vertical directions.

2.3.8. 56-storey L.A. Live hotel and residences building in California

The 56-storey L.A. Live hotel and residences tower is located in down town Los Angeles. This building uses an advanced steel plate shear wall system to resist lateral loads. The lateral load resisting system of this building originally had been designed to be concrete shear walls. However, based on reviewing the conceptual design of building in 2006,

heavy 760 mm thick concrete shear walls were replaced with much lighter 6 mm to 25 mm thick steel plate shear walls. The project commenced on November 2007 and the cut-out time frame was early 2010. VBEs and HBEs are designed to permit the web plates to develop significant diagonal tension fields and reach their expected yield stress within the entire panel while dissipating energy. By using the SPSW system the structure's weight was reduced by 35% which also replaced a heavy and complex deep foundation system with a mat foundation. Elevation view and construction procedure of this building is shown in Figure 2.73. Changing from concrete to steel plate shear walls saved time, reduced weight, and reclaimed usable space (Kristeva, 2010).

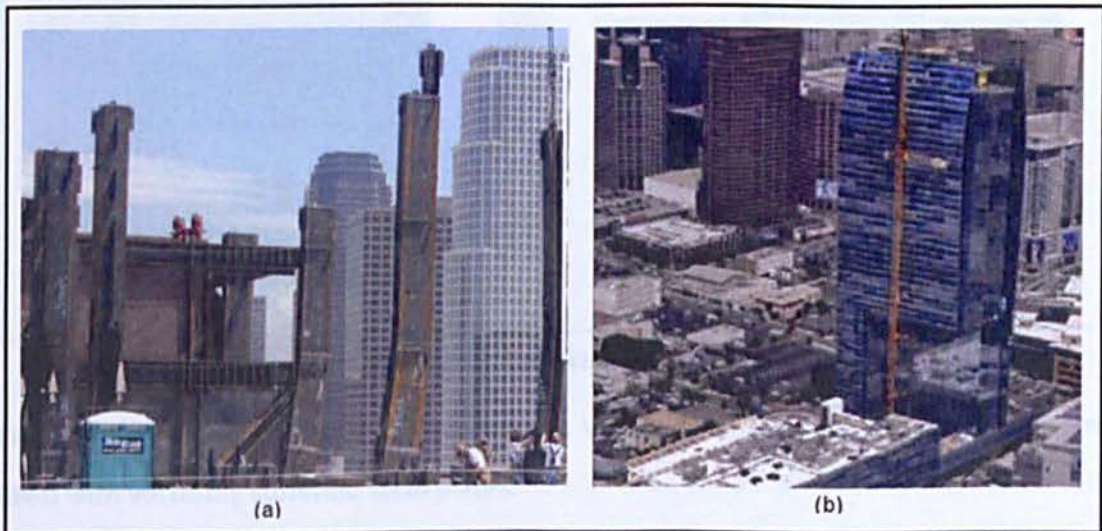


Figure 2.73: (a) Steel plate shear walls under construction (b) Elevation view of 56-storey L.A. Live hotel and residence building (Photo courtesy of AEG and Gensler)

2.3.9. 75-storey Jinta Tower in Tianjin, China

The 330 meter tall 75-storey Jinta Tower in Tianjin, China, is the tallest building in the world to contain slender steel plate shear walls. SPSWs are used as the primary lateral load resisting system in this office building (Figure 2.74). The lateral load resisting system for the Jinta tower can be classified as a frame-shell wall system, with perimeter and core ductile moment-resisting frames, and core SPSWs linked together with outrigger and belt trusses (Lee et al., 2010). Figure 2.74 shows scheme of outrigger truss for Jinta tower. The design of un-stiffened SPSWs requires that no gravity load has been

CHAPTER 2: LITERATURE REVIEW

considered to be carried by un-stiffened SPSW panels (CAN/CAS S16-01 2001), hence a modified slender SPSW with vertical stiffened channels was used in this building. To ensure that vertical stiffeners act as buckling stiffeners primarily, not as columns, 100 mm gap was incorporated between ends of stiffeners and the horizontal boundary elements (Figure 2.75).

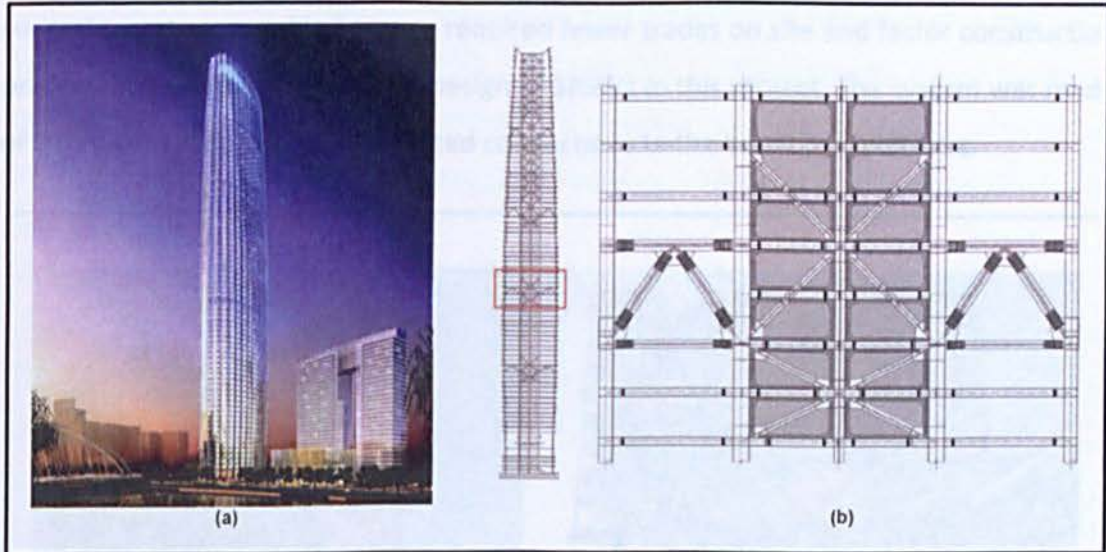


Figure 2.74: (a) The architectural impression (b) Outrigger truss of Jinta tower

The SPSW system consists of CFT columns as VBEs and wide flange beams as HBEs, infilled with vertically stiffened steel plates.

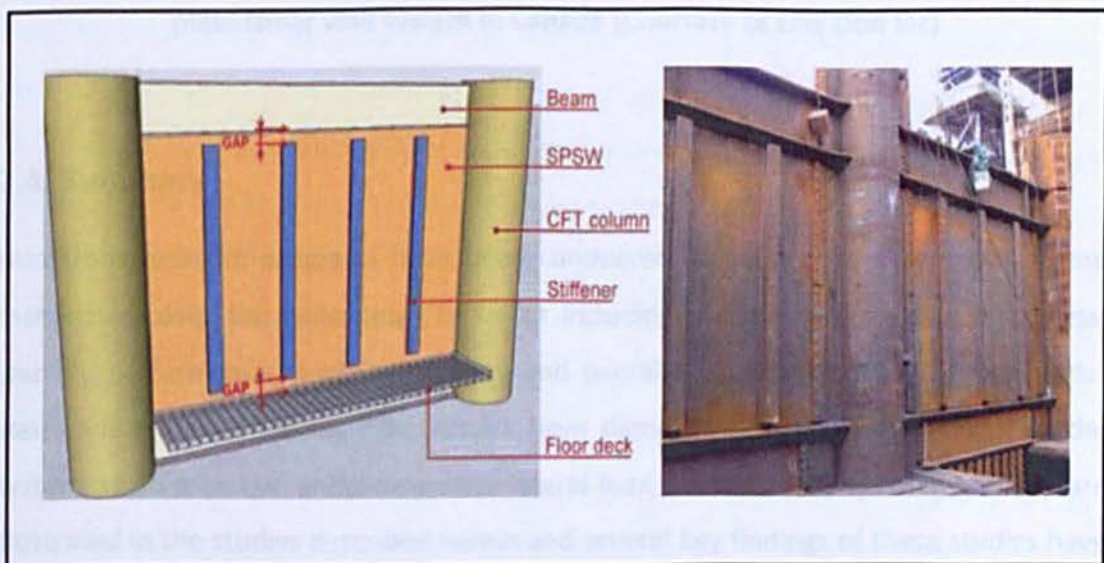


Figure 2.75 Stiffened shear panels adopted in Jinta tower

2.3.10. Airport control tower of Edmonton international airport, Canada

This project was the first time a SPSW system had been specified for an air traffic control tower. Figure 2.76 shows the SPSW system utilised as the lateral load resisting system for the combined airport traffic control tower and office building structure at the Edmonton international airport in Alberta. Using SPSW system, instead of reinforced concrete, was reasonable because required fewer trades on site and faster construction process. The wind load governed design of SPSWs in this project. The system was made of 5 mm thick steel plates with bolted connections to the boundary members.

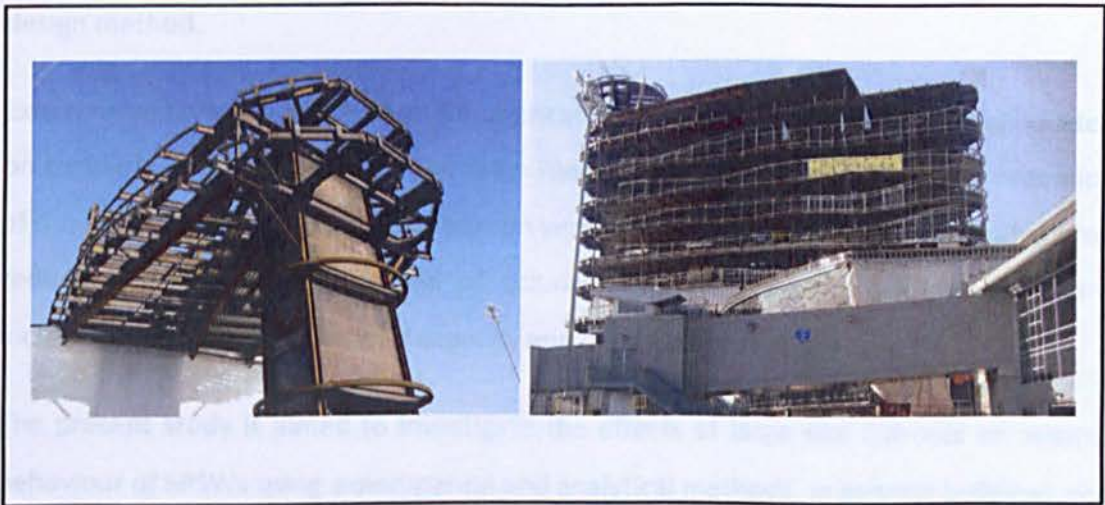


Figure 2.76: Construction of Edmonton International Airport's control tower with steel plate shear wall system in Canada (Courtesy of Ellis Don Inc)

2.4. Summary

Numerous research programs have been conducted on steel plate shear walls. These researches cover the wide range of topics including investigation on elastic stiffness, stability performance, ductility capacity and overall response of SPSW system under static and dynamic loading. The results have demonstrated the effectiveness of the system as an effective and economical lateral load resisting system. Many results are illustrated in the studies described herein and several key findings of these studies have been presented and discussed. Research studies on the seismic behaviour, response and performance of SPSWs leads to advanced analysis and design methodologies for

CHAPTER 2: LITERATURE REVIEW

engineering purposes. Although the strip model proposed by Thorburn et al. (1983) is an effective model for push over analysis of SPSW system, the model has not provided accurate results for cyclic dynamic analysis. The strip model neglects the steel plate buckling resistance and thus the dominant action is the post-buckling strength from diagonal tension field action.

The design of SPSWs is done in accordance with a number of design guides and design standards such as AISC 341-05, AISC 2007 and CSA S16-09. Capacity design method is accepted in current standard and provisions. However, to better understand the system behaviour a number of research projects have concentrated on the performance based design method.

Experimental (Vian et al .2005) and numerical studies (Purba, 2006) has been conducted on regularly perforated SPSWs. The main function of perforated infill plate is reduction of the effects of diagonal tension fields on vertical boundary members. This strategy can reduce flexural stiffness demand of columns for SPSW system without significant increasing of ultimate shear load capacity and initial stiffness of the system.

The present study is aimed to investigate the effects of large size cut-outs on seismic behaviour of SPSWs using experimental and analytical methods. In general buildings, the doors, windows and lift entrances are sometimes located within the shear walls. In such cases by introducing large size cut-outs within the steel plate span, the ultimate shear load capacity and initial stiffness of the system could be reduced significantly. Using coupled wall system or stiffening of the shear panels are two alternatives for enhancing the system performance against lateral loads. In part of this research improving seismic performance of SPSW systems with and without cut-outs using GFRP laminates is investigated. Using composite panels the main parameters of seismic behaviour of system is improved and the contribution of beam element for anchoring the diagonal tension field is increased and as result, the flexural stiffness demand of column is reduced. In other part of this research improving seismic performance of SPSW system with cut-outs using flat steel stiffeners is investigated by analytical methods and experimental results. The accuracy of FE method for optimal design of steel stiffeners is confirmed with comparison the FE and corresponding test results.

3. FINITE ELEMENT SIMULATION TECHNIQUE FOR SPSWs

3.1. Introduction

Over the last two decades, finite element method has been adopted by numerous researchers to study the behaviour of steel plate shear walls. The finite element models of specimens are initially developed to provide a fundamental understanding of their behaviour. Due to the highly non-linear behaviour of SPSWs and severe convergence difficulties in implicit analysis, a dynamic explicit scheme was found to provide an accurate solution for quasi-static applications.

In part of this chapter cyclic loading with an increasing displacement history is applied to specimens in accordance with ATC-24 protocol. The number of cycles applied at each amplitude is based on the ATC-24 recommendation. An eigen-value buckling analysis is initially performed to model the buckling shape of specimens. Then the buckling mode shape is introduced to FE model to account for the initial imperfection of specimens. The established models incorporate both material and geometrical non-linearity. Displacement control solution strategy is used for all quasi-static analyses and the accuracy of the finite element model is then validated by comparing the FE results with the experimental data of specimen tested under the quasi-static loading by Kharrazi in 2005.

In the following sections the development of finite element method for SPSW systems is discussed. Several FE models were prepared to simulate the structural behaviour such as

CHAPTER 3: FINITE ELEMENT SIMULATION TECHNIQUE FOR SPSWS

initial stiffness, post-yield stiffness and ultimate capacity of the system during pushover and cyclic loading procedure. In this study, the commercially available ABAQUS software, which is a multipurpose, linear and nonlinear finite element analysis program, is used. ABAQUS software is one of the well suited packages for solving highly non-linear engineering problems. It contains an extensive library of elements that can model virtually all structural material behaviours.

3.2. Finite Element Model

ABAQUS model is composed of several different components that together describe the physical problem to be analysed and the results to be obtained. At a minimum the analysis model consists of discretized geometry, element section properties, material data, load and boundary conditions, analysis type, and output requests. All these characteristics will be discussed in detail for specimens in next chapters. A complete ABAQUS analysis usually consists of three distinct stages: pre-processing, simulation, and post-processing. These three stages are linked together by files as shown below (Hibbitt et al.; 2007):

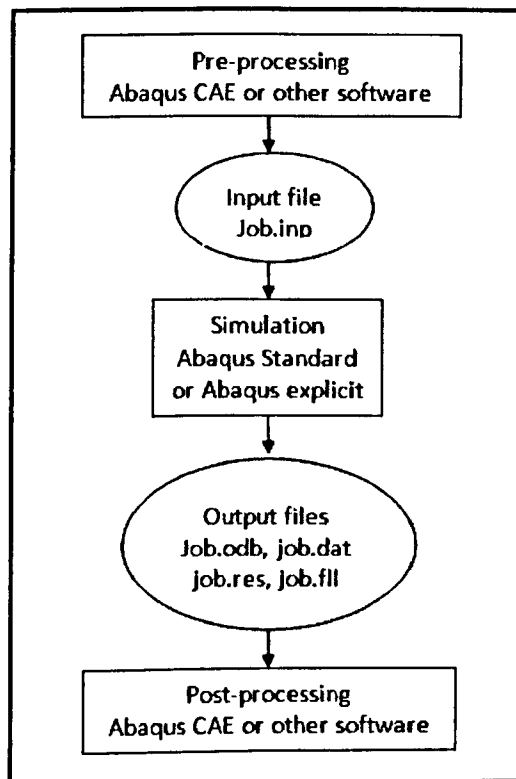


Figure 3.1: Connection of three distinct stages in ABAQUS (Hibbitt et al.; 2007)

ABAQUS consists of two main analysis modules namely ABAQUS/Standard and ABAQUS/Explicit. ABAQUS/Standard is a general-purpose analysis product that can solve a wide range of linear and non-linear problems such as quasi-static analysis and high-speed dynamics and multi-physics response of components. ABAQUS/Standard solves a system of equations implicitly at each solution increment. ABAQUS/Explicit is a special-purpose analysis product that uses an explicit dynamic finite element formulation. It marches a solution in small time increments without solving a coupled system of equations at each increment. In other words solution procedure for nonlinear problems requires iterations for ABAQUS/Standard but does not require iterations for ABAQUS/Explicit method.

In the following sections the static implicit method and its relevant convergence challenges with respect to SPSW analysis and the explicit finite element method with existing issues regarding to quasi-static simulation of a SPSW are described.

3.3. Implicit finite element method and convergence problem

For an implicit solution the equation of equilibrium at the end of the load increment is the difference between externally applied loads and internal node point forces. Since the internal nodal point forces depend on the history of nodal point displacements, an iterative process is needed to solve this equation of equilibrium for the exact configuration of the system. In general, the equation of equilibrium at the end of load increment, at time $t+\Delta t$ can be written as:

$$\underline{R}_{t+\Delta t} - \underline{F}_{t+\Delta t} = 0 \quad 3.1$$

where $\underline{R}_{t+\Delta t}$ is the vector of externally applied loads and the vector of $\underline{F}_{t+\Delta t}$ represents the internal nodal point forces.

During the analysis of SPSWs the sudden buckling of steel plate in early stage of loading and the re-orientation of diagonal tension field during the loading and unloading procedures causes the local instability of the system. This manner of the system capitalises the convergence problem. The convergence problem of implicit method was observed during the pushover analyses and as a result it was time consuming at extreme

deformation stages. For most analyses the size of increment had to be reduced to a value less than 10^{-5} to achieve the convergence (Maleki, 2004). This increment rate is reasonable for an explicit scheme but not for a multiple iteration implicit method. Due to poor performance of the implicit finite element method, the explicit dynamic method was adopted as an efficient approach for the analysis of steel plate shear wall systems.

3.4. Explicit finite element method

The explicit finite element method was originally developed to analyse dynamic events within a rapid loading scenario. With proper considerations such as the control of kinetic energy level, this method is also used for quasi-static problems that include contact problems, post buckling behaviour, highly nonlinear geometry and material properties and also material degradation and failure. In fact due to small velocities of different parts of specimen during a quasi-static simulation, the kinetic energy is negligible. Generally, the kinetic energy of the deformable materials should not exceed typically 5% to 10% of its internal energy during most of the quasi-static simulation (Hibbitt et al., 2007).

3.4.1. Dynamic explicit method – stability limitation

The most common explicit time integration operator used in nonlinear dynamic analysis is probably the central difference method. The central difference method is a conditionally stable algorithm (Bathe, 1996). It is used as a time integrator accepting that the amount of time during which the model can be developed, keeping the error bounded, should be less than the stability limit. The stability limit is defined by highest frequency of the system, ω_{max} . Without and with presence of damping in the model, the stability limit is defined by equations 3.2 and 3.3, respectively.

$$\Delta t_{stable} = \frac{2}{\omega_{max}} \quad 3.2$$

$$\Delta t_{stable} = \frac{2}{\omega_{max}} \left(\sqrt{1 + \xi^2} - \xi \right) \quad 3.3$$

Where, ξ is the fraction of critical damping in the mode with the highest frequency.

CHAPTER 3: FINITE ELEMENT SIMULATION TECHNIQUE FOR SPSWs

In ABAQUS/Explicit, a small amount of damping in the form of bulk viscosity is always added to the model to control the high frequency oscillations. As can be seen from equation 3.3, damping reduces the stable time increment and requires more time for the analysis. The simple method for determining the stability limit, both conservative but realistic, was adopted by ABAQUS/Explicit. The highest frequency, based on the element-by-element method is higher than the highest frequency of the global model. Therefore, a stable time increment based on element-by-element calculation is smaller than the global value and is a more conservative estimate. The highest frequency of an element is associated with the dilatational mode, and the critical time increment is given by:

$$\Delta t_{\text{stable}} = \frac{L_e}{C_d} \quad 3.4$$

where, L_e is the smallest characteristic length of the element and C_d is the dilatational wave speed of the material defined as:

$$C_d = \sqrt{\frac{E}{\rho}} \quad 3.5$$

where, E is the modulus of elasticity and ρ is the density of the material.

Equations 3.4 and 3.5 indicate that the material properties and the size of the FE mesh are two main parameters that can dominate the critical time increment. The stiffer the material the higher the wave speeds, resulting in a smaller stable time increment. Since the modulus of elasticity is constant, the critical time depends only on the smallest element size in the FE mesh. The element size is suggested to be kept as large as possible providing the accuracy of analysis is acceptable. If the smallest element dimension and the wave speed of the material are known, the stability limit of analysis can be estimated.

3.4.2. Evaluation of Quasi-Static Solution

The most general method to evaluate whether a response of a system is quasi-static or not is defined by the energy balance equation as indicated below:

$$E_I + E_V + E_{FD} + E_{KE} - E_W = E_{TOTAL} = 0.0$$

3.6

where,

E_I : internal energy including both elastic strain energy and plastic work,

E_V : energy absorbed by viscous dissipation,

E_{FD} : friction energy (energy dissipated by frictional forces in a contact problem),

E_{KE} : kinetic energy,

E_W : work done by external forces,

E_{TOTAL} : total energy of the system.

In order to verify the acceptance of quasi-static solution the ratio of the kinetic energy history, E_{KE} , to the internal energy history, E_I , should be relatively small throughout the analysis.

Generally, a smooth loading history should produce smooth energy results. If smooth loading procedure causes oscillating or noisy energy results, the quality of the simulation may be considered unacceptable or inadequate. Since the energy ratio alone is not capable to show such behaviour, the kinetic energy history itself is an indicator of any smooth or noisy behaviour. If the kinetic energy does not exhibit quasi-static behaviour, the velocity histories of some critical nodes need to be monitored to find cause of any high kinetic energy.

3.5. Description of the FE model for quasi-static testing

3.5.1. Element selection

In order to capture the local buckling of SPSW components, particularly local buckling of beam and column flanges, the steel plate and boundary members were modelled with shell elements. Most of the continuum and plate elements in ABAQUS/Explicit are based on an updated Lagrangian formulation. This formulation updates the nodal coordinates at the beginning of each increment to reflect the current positions in space. All shape

CHAPTER 3: FINITE ELEMENT SIMULATION TECHNIQUE FOR SPSWs

functions and derivatives were re-evaluated based on these updated nodal coordinates. Since the steel plate experiences considerably large magnitude deformations and strains, this formulation is useful and effective.

A general purpose four-node doubly-curved shell element S4R from ABAQUS/Explicit element library is used for modelling of specimens. The S4R is a reduced integration element and counts for finite membrane strains and large rotations. Each node of this element provides six degrees of freedom, three rotations (θ_x , θ_y , θ_z) and three translations (u_x , u_y , u_z) which are defined in a global coordinate system. The S4R employs one integration point on its mid-surface to form the element internal force vector. The default number of integration points through the thickness of this element is five, which makes it sufficient for simulating the elastic-perfectly plastic response of shell structures. This element is a reduced integration element which gives more accurate results and significantly reduced running time if the elements are not distorted. In order to prevent the stress concentration in simulation procedure, all concentrated loads and boundary conditions were distributed to a number of nodes.

3.5.2. Geometry and initial imperfection

The measured dimensions of specimens are used for creating the FE models. However, the fish plates used for connection of steel plate to boundary members are not modelled. In other words, it was assumed that steel plate is connected directly to the boundary members. Generally, all SPSW systems have some initial deformations during fabrication of members, welding of specimens, placing of steel plate and eccentricity of fish plate connections. Any initial deformation of steel plate can significantly affect the in-plane shear stiffness of specimen in comparison with system with fully flat steel plate. Therefore, during the construction of finite element model for each specimen, the initial imperfection of steel plates was considered. It is assumed that the steel plates have an initial imperfection pattern corresponding to the first buckling mode of the steel plate loaded in a way similar to that used in the related test. The maximum out-of-plane deformation considered for the imperfection is set to 0.1 mm of the lowest buckling mode as suggested from the experimental results by Kharrazi (2005). Figure 3.2 shows

the scheme of initial imperfection pattern used in the development of the FE model of specimens.

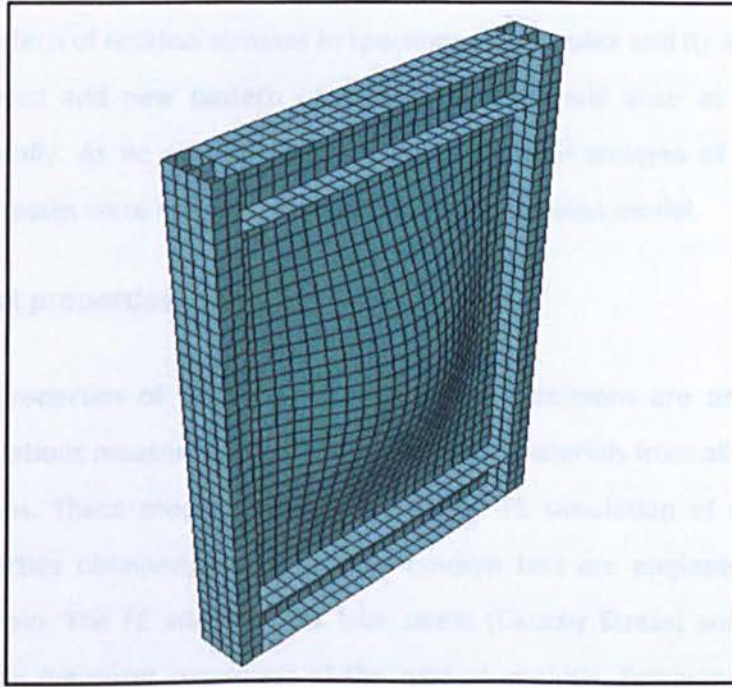


Figure 3.2: Scheme for deformed shape of the lowest buckling mode

3.5.3. Loading and boundary conditions

In order to simulate the rigid boundary at the base of the shear wall specimen, all nodes at the base of models are fully fixed. Lateral bracing of specimens are simulated by restraining the out of plane displacement of top beam at both sides of the beam. The horizontal load is applied to top beam through thick plate welded to the top beam at position where quasi-static loading was applied to the test specimen. The effect of the thick plate in the finite element model was considered by uniform displacement of nodes of area corresponding to thick plate position using the cyclic regime utilised in the quasi-static tests.

3.5.4. Residual stresses

Residual stresses are present in all fabricated steel elements and are usually produced due to welding and forced installation. Different cooling during the manufacture of hot-rolled structural steel sections, rolling of shapes and plates are also producing residual

stresses in the steel components. Residual stresses in steel plate shear walls can be created during the manufacturing procedure of hot-rolled sections, welding of beams to columns and welding of fish plates to boundary members and to steel plates. The distribution pattern of residual stresses in specimens is complex and its initial magnitude will be dissipated and new pattern of residual stresses will arise as the steel plate deforms plastically. As no measurement of initial residual stresses of specimens was taken, these stresses were not considered in the finite element model.

3.5.5. Material properties

The material properties of different parts of SPSW specimens are determined from stress-strain relations measured from tensile testing of materials from all components of SPSW specimens. These properties are used in the FE simulation of specimens. The material properties obtained from a tension coupon test are engineering stress and engineering strain. The FE analysis uses true stress (Cauchy Stress) and true strain as stress and strain measures regardless of the type of analysis. Following equations are applicable to obtain true stress-strain from tension coupon test results (Lubliner, 1990)

$$\sigma_{\text{true}} = \sigma_{\text{nominal}}(1 + \epsilon_{\text{nom}}) \quad 3.7$$

$$\sigma_{\text{ln}}^{\text{pl}} = \ln(1 + \epsilon_{\text{nom}}) \cdot \frac{\sigma_{\text{true}}}{E} \quad 3.8$$

where, E is the modulus of elasticity, σ_{nom} is the nominal (engineering) stresses and ϵ_{nom} is the nominal (engineering) strain obtained from material tests. The true stress-strain behaviour of the material is used to model the characteristics of the material both in pushover and cyclic quasi-static analysis.

For pushover analysis of each specimen the isotropic hardening model was selected because this model enables the use of a multi-linear representation of the stress-strain curve. For the quasi-static modelling, many stress and strain reversals are involved during the process, and the Bauschinger effect becomes an important issue. As a result the kinematic hardening flow rule was selected. The Bauschinger effect is characterised by a reduced yield stress upon load reversal after plastic deformation has occurred during the initial loading. The linear kinematic hardening component takes this effect in

CHAPTER 3: FINITE ELEMENT SIMULATION TECHNIQUE FOR SPSWs

to account, but considering a nonlinear component is more beneficial as it improves the shape of the cycles.

One of the important characteristics for FE model is the meshing. A too coarse mesh may result in non-conservative answers, particularly when the local buckling governs the system's behaviour. However, a too fine mesh increases the numerical errors and demand for computational analysis, so there is a limit for how fine the mesh can be made. A rule of thumb for shell elements is that there should be at least six elements in the expected half wavelength of a buckle (Brescia, 2010).

3.5.6. Displacement control analysis

In this research displacement control strategy is adopted in both pushover and cyclic analysis of specimens. In order to estimate the shear capacity of SPSW system properly, the solution strategy is expected to be capable of tracing the response of the system near the initial elastic buckling limit point and beyond it. The graph of load response of SPSW system near to the limit point is entirely flat and a very small increment of load results in a very big displacement response. In addition, in a load control method applying additional small load that is larger than the steel plate shear wall capacity leads to an unstable dynamic solution. Therefore, in pushover and cyclic analysis of SPSW system a displacement control method is beneficial because the load level can be adjusted based on displacement level within stage next to the limit point. In ABAQUS/Explicit the available control approach is to apply the history of displacement to one or more nodes separately.

After the definition of geometrical and mechanical properties, the assemblage of the different parts that constituted the sections is required. Subsequently, tie constraints are created between the boundary members and steel plate. The amplitude of the displacements is applied in accordance with adopted loading protocol.

3.6. Validation of the FE modelling

The finite element model was validated by comparing published test results with the corresponding FEA results. The model is based on a nonlinear dynamic formulation and

CHAPTER 3: FINITE ELEMENT SIMULATION TECHNIQUE FOR SPSWs

an explicit strategy is used to obtain the results from the model at each increment without any iteration. The model is used to simulate the behaviour of the one-storey ductile steel plate shear wall. The pushover analysis and cyclic behaviour results are used as a basis of comparison with the test results of the specimen conducted by Kharrazi (2005). Initial stiffness, yielding point, the inclination angle of diagonal tension field, the ultimate capacity of the system, and the pinching of hysteresis loops are parameters that have been used to validate the finite element model.

Kharrazi's specimen was a 60% scale model of an inner residential building core, with floor-to-floor and column-to-column spacing of 1800 mm and 1362 mm respectively. Frame column and beam members were constructed from hollow steel section and wide flange steel section, respectively. The steel plate was made of nominal 0.7 mm thick cold-rolled steel sheet. The overall geometry of specimen and detail of fish plate connection are illustrated in Figure 3.3 and Figure 3.4, respectively. In this study the specimen is labelled as DSPW-1 and SPSW-0.7 for test and FEA model respectively.

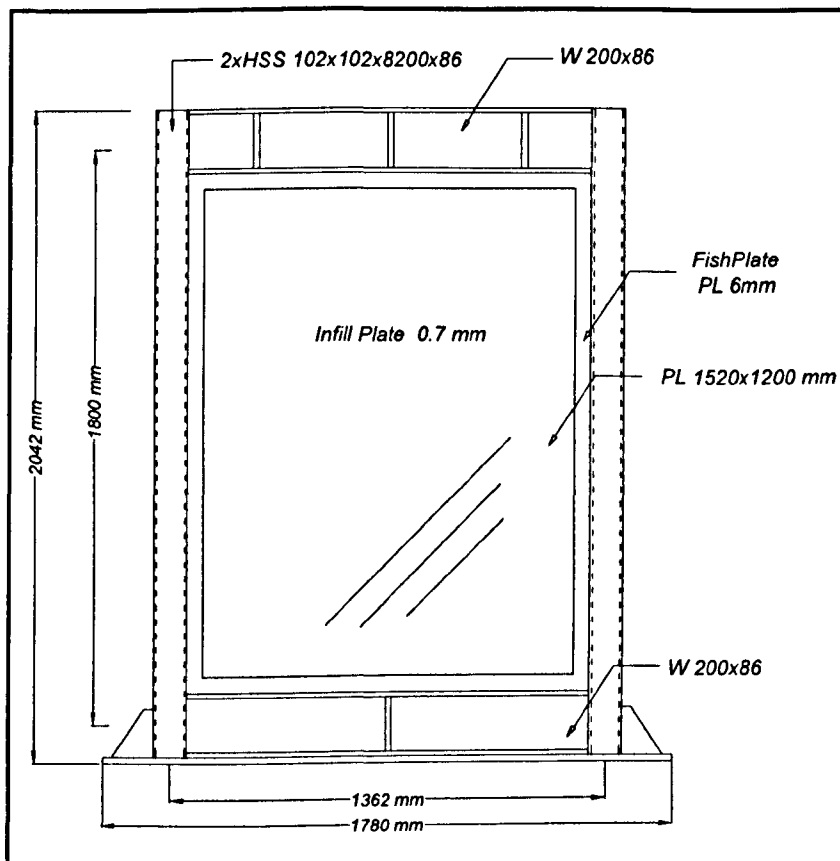


Figure 3.3: Dimensions of the single storey DSPW-1 specimen tested by Kharrazi, 2005

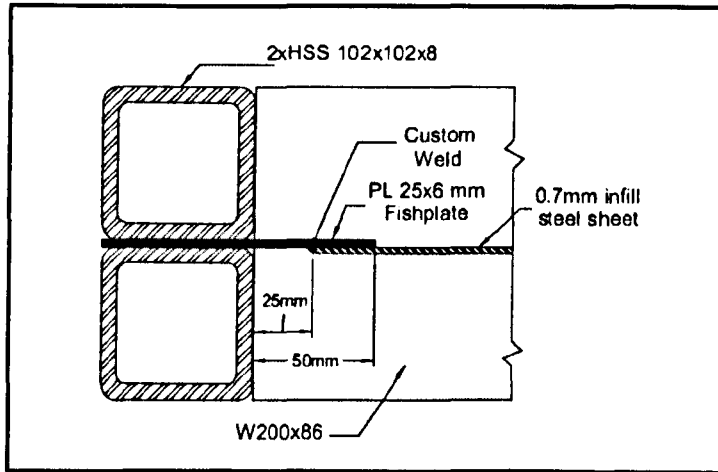


Figure 3.4: Fish plate connection detail for DSPW-1 specimen (Kharrazi, 2005)

Table 3.1 gives a summary of material properties for different components of specimens determined from coupon tensile testing.

Table 3.1: Summary of material properties determined from coupon tensile testing (Kharrazi, 2005)

Member	Yield Strength (MPa)	Ultimate Strength (MPa)
HSS 102X102X8 (averaged)	481	523
W200X86 (based on flange results)	318	468
Fish Plate	376	513
Steel Sheet	246	361

In order to determine how accurately the developed finite element model is capable of capturing the stiffness and the capacity of the DSPW-1 test specimen, pushover and cyclic analysis is carried out using the finite element model of specimen considering the criteria described earlier in this chapter. Figure 3.5 illustrates the scheme of provided finite element model based on overall geometry and dimensions, given in Figure 3.4, configuration, depicted in Figure 3.3 and material properties, given in Table 3.1, for DSPW-1 specimen.

The 'S4R' shell element with 50×50 mm mesh size was selected to model the specimen. To simulate the rigid boundary at the base of the specimen, all nodes at the base of model were fixed. To simulate the lateral bracing system during the quasi-static test, the out-of-plane displacements at the top of both sides of beam were restrained. During the test, the horizontal load at the top of the specimen was applied through a thick adaptor plate welded to the top flange of the upper beam. To simulate the effect of the adaptor plate in the FE model, the nodes of an area representing the adaptor plate was uniformly displaced (Figure 3.5).

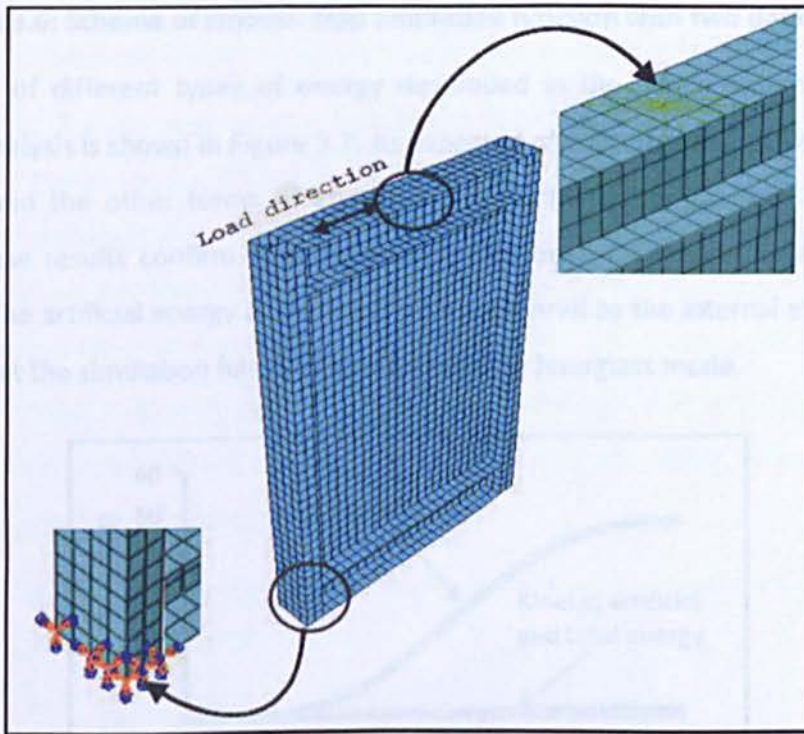


Figure 3.5: FE model developed in accordance with DSPW-1 specimen

3.6.1. Pushover analysis of SPSW test specimen

Pushover analysis of DSPW-1 specimen is carried out using the explicit method. A frequency analysis of test specimen indicated that the period of the first buckling mode is 0.3011 seconds (3.3208 HZ). The total time of the analysis was set at about three times the period of the first mode. The initial time increment of the model which is function of mesh size and material properties was obtained as 8.132×10^{-6} seconds. The model was loaded using smooth amplitude function. Accordingly, the velocity and acceleration are zero at the beginning and end of each loading step (Figure 3.6).

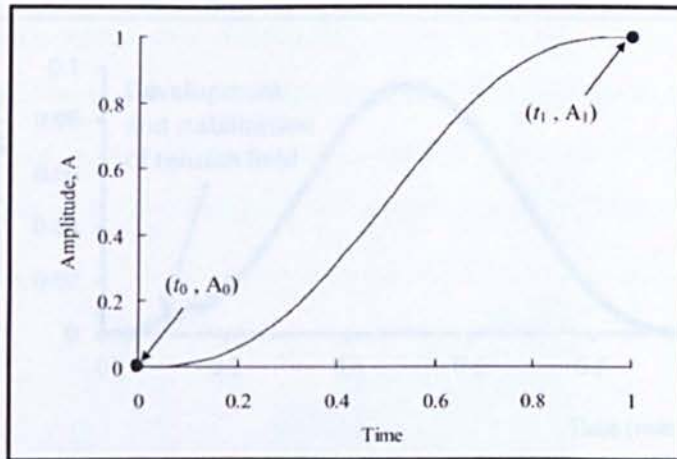


Figure 3.6: Scheme of smooth step amplitude function with two data points

The history of different types of energy developed in the whole system during the pushover analysis is shown in Figure 3.7. As expected, the internal and external energies are equal and the other forms of energy are negligible in comparison with internal energy. These results confirm that the analysis has been carried out in a quasi-static condition. The artificial energy is also negligible compared to the internal energy, which indicates that the simulation has not been affected by hourglass mode.

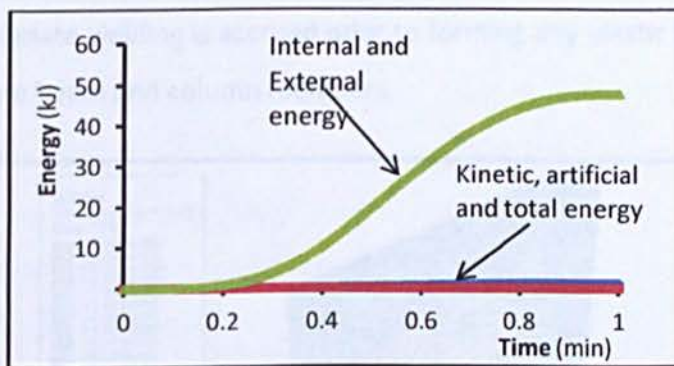


Figure 3.7: Energy history of the pushover analysis of SPSW-0.7 model

Figure 3.8 presents the kinetic energy versus time curve. The curve indicates that the kinetic energy varies smoothly over time as expected when a tension field is developing in the steel plate of the SPSW-0.7 specimen. Once the diagonal tension field develops the kinetic energy increases rapidly. This behaviour was observed during the test and was accompanied by loud popping sound and rapid out-of-plane deformations in the steel plate.

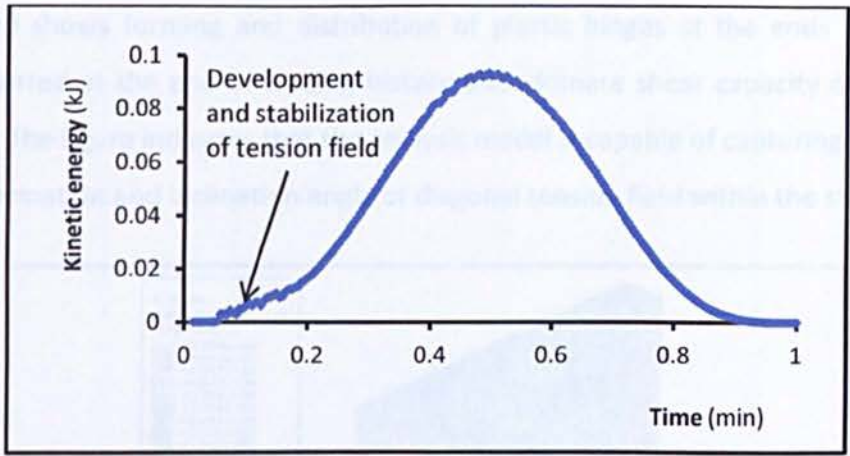


Figure 3.8: Kinematic energy history of the pushover analysis for SPSW-0.7 model

The increasing displacement was applied to the nodes located on the upper flange at mid-length of the top beam. This monotonic loading regime continued until it reached a value beyond the displacement at which the test specimen reached its ultimate capacity by forming of plastic hinge at ends of columns. Figure 3.9 illustrates forming and uniform development of diagonal tension field in the steel plate and the state of stresses developed in all parts of test specimen in accordance with von Mises criteria. It is clear that steel plate yielding is accrued prior to forming any plastic hinges at the ends of boundary frame beam and column members.

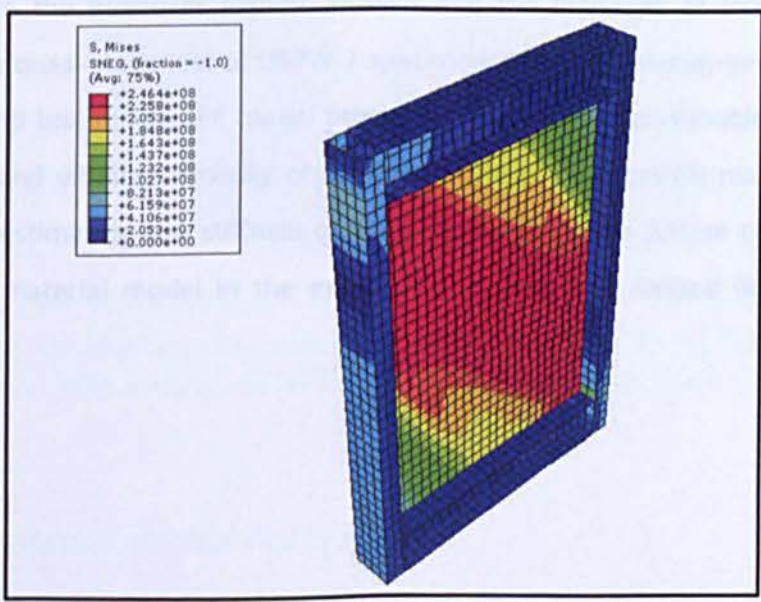


Figure 3.9: Contour plot of stresses for SPSW-0.7 specimen in accordance with von Mises stress criteria at early stage of loading

CHAPTER 3: FINITE ELEMENT SIMULATION TECHNIQUE FOR SPSWS

Figure 3.10 shows forming and distribution of plastic hinges at the ends of columns which occurred at the end of loading history and ultimate shear capacity of SPSW-0.7 specimen. The figure indicates that the analysis model is capable of capturing the out-of-plane deformation and inclination angle of diagonal tension field within the steel plate.

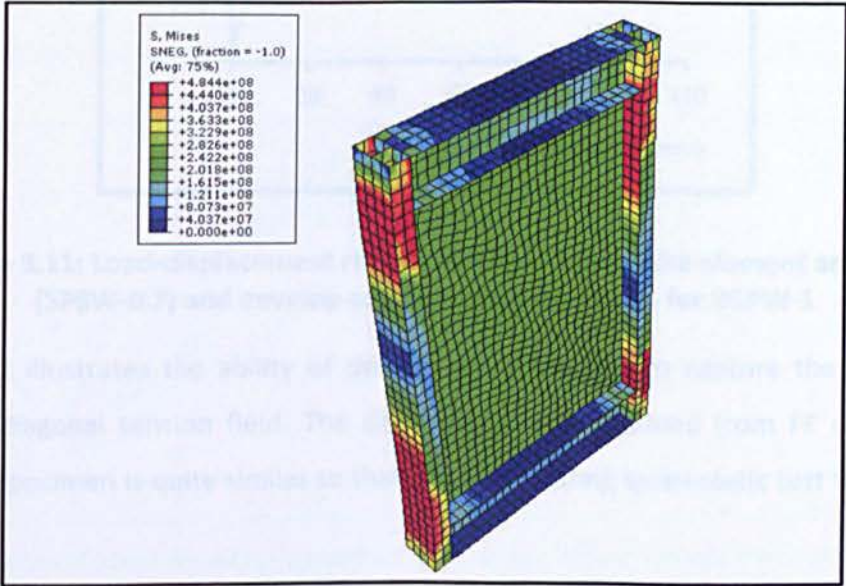


Figure 3.10: Von Mises counter plate for SPSW-0.7 specimen at the final stage of loading

Figure 3.11 shows the load-displacement diagram of the SPSW-0.7 finite element model obtained from the pushover explicit analysis and the envelope of hysteresis curves attained from quasi-static test of DSPW-1 specimen. There is good agreement between FE analysis and test results. FE model provides adequate and reasonable prediction of the stiffness and ultimate capacity of specimen. One of the possible reasons for slight difference in estimating wall stiffness or overall capacity of the system could be due to the bi-linear material model in the explicit FE analysis that limited flexibility in the simulation.

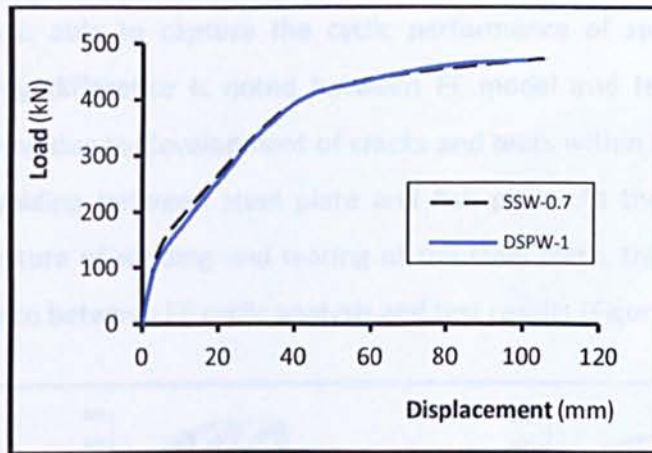


Figure 3.11: Load-displacement results obtained from finite element analysis (SSW-0.7) and envelop of hysteresis test results for DSPW-1

Figure 3.12 illustrates the ability of developed FE method to capture the inclination angle for diagonal tension field. The deformed shape obtained from FE analysis for SPSW-0.7 specimen is quite similar to that observed during quasi-static test for DSPW-1 specimen.

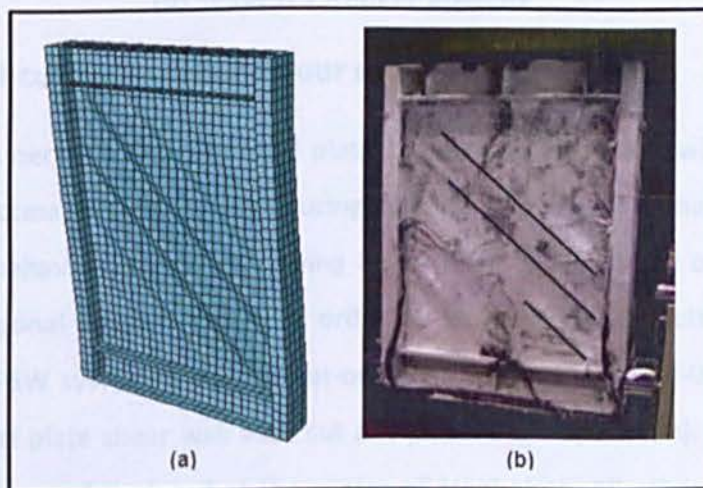


Figure 3.12: Comparison of tension field development; (a) During loading of the specimen in FE analysis for SPSW-0.7; (b) During quasi-static for DSPW-1

3.6.2. Cyclic analysis of SPSW test specimen

In order to evaluate the efficiency of a SPSW system under cyclic loading, the finite element model should be capable of simulating the cyclic response of the system. The

developed model is able to capture the cyclic performance of specimen. However, gradually increasing difference is noted between FE model and test specimen. This probably is occurring due to development of cracks and tears within the steel plate and fracture of the welding between steel plate and fish plate. As the FE model is not simulating the fracture of welding and tearing of the steel plate, this can be the main reason for difference between FE cyclic analysis and test results (Figure 3.13).

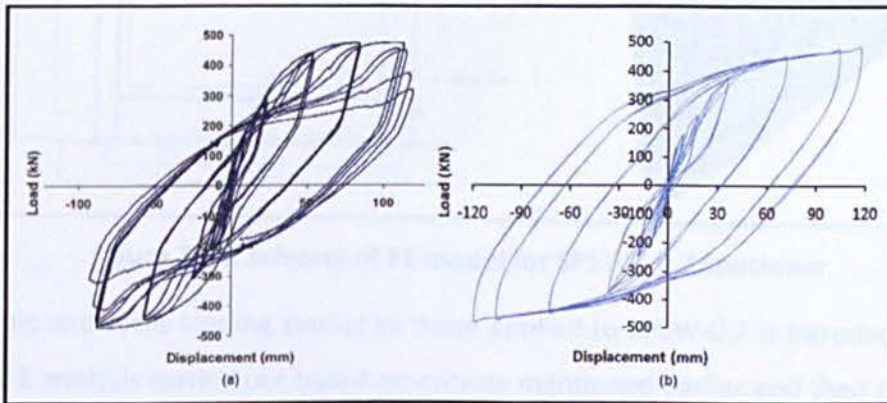


Figure 3.13: Load-displacement hysteresis loop of (a) DSPW-1 from quasi-static test (b) SPSW-0.7 from FE analysis

3.7. Effects of cut-outs on behaviour of SPSW systems

Sometimes it is necessary part of steel plate to be cut-out to place windows, doors or even to have access to services. Introducing cut-outs to steel plate may undermine the post buckling behaviour of system owing to weakening the ability of steel plate for developing diagonal tension fields. In order to evaluate the effects of cut-outs on behaviour of SPSW system, a circular cut-out is introduced to SPSW-0.7 specimen and denoted as steel plate shear wall with cut out (SPSWC-0.7 specimen). The diameter of cut-out is 500mm and is placed at the centre of steel plate. All other parameters and characteristics are assumed to be similar to SPSW-0.7 specimen (Figure 3.14).

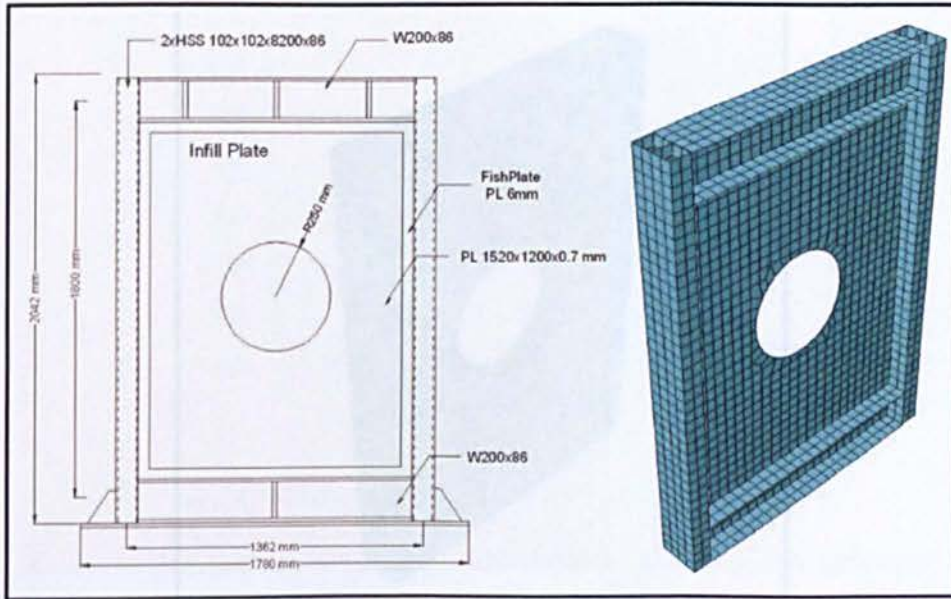


Figure 3.14: Scheme of FE model for SPSWC-0.7 specimen

Monotonic and cyclic loading similar to those applied to SPSW-0.7 is introduced to the system. FE analysis carried out based on criteria mentioned earlier and then the results were compared with the specimen without cut-out. The results show reduction in initial stiffness and ultimate load bearing capacity of specimen as expected. In the mean time energy dissipation capacity of the system is reduced and out-of-plane deformation of steel plate is increased. Deformed shape and hysteresis behaviour of SPSWC-0.7 specimen is shown in Figure 3.15 and a contour plot of stress distribution of system is illustrated in Figure 3.16.

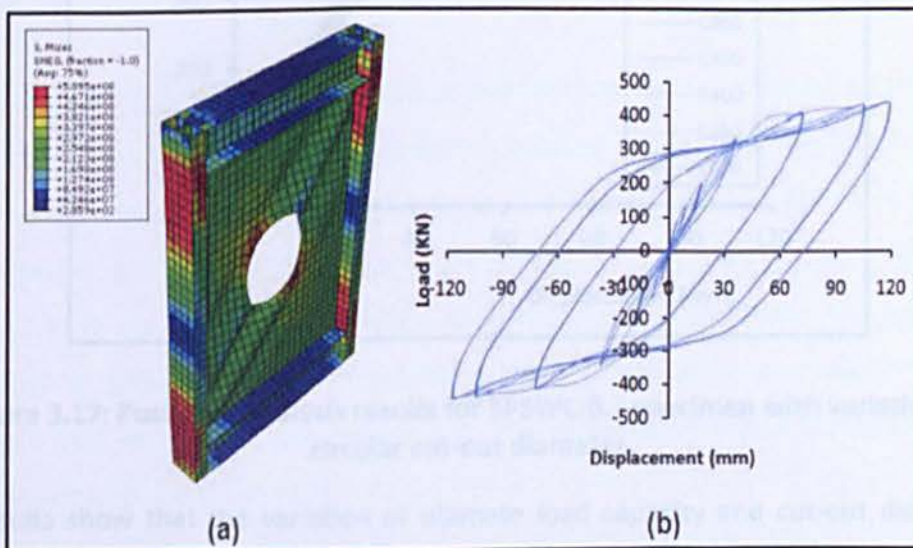


Figure 3.15: (a) Deformed shape and; (b) hysteresis loop for SPSWC-0.7 specimen

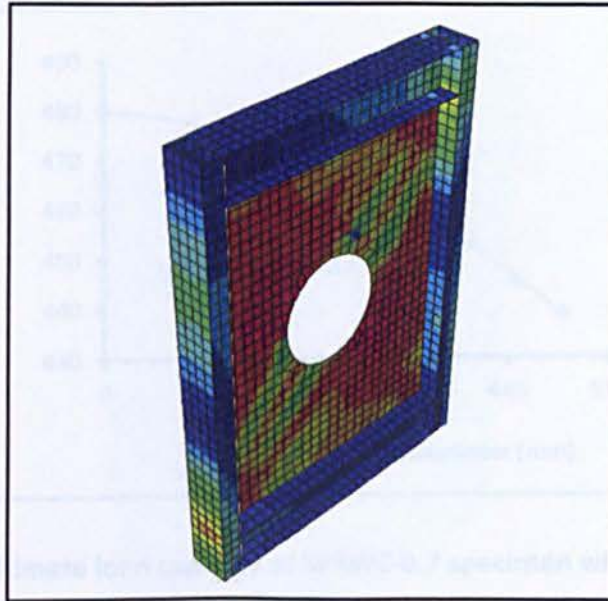


Figure 3.16: Contour plot of stress distribution for SPSWC-0.7 specimen

A variety of circular cut-outs with different diameter have been considered in order to establish the relation between the diameter and the ultimate load capacity of the system. FE analyses were carried out on seven specimens where the only difference was diameter of cut-outs. The pushover analysis results are presented in Figure 3.17.

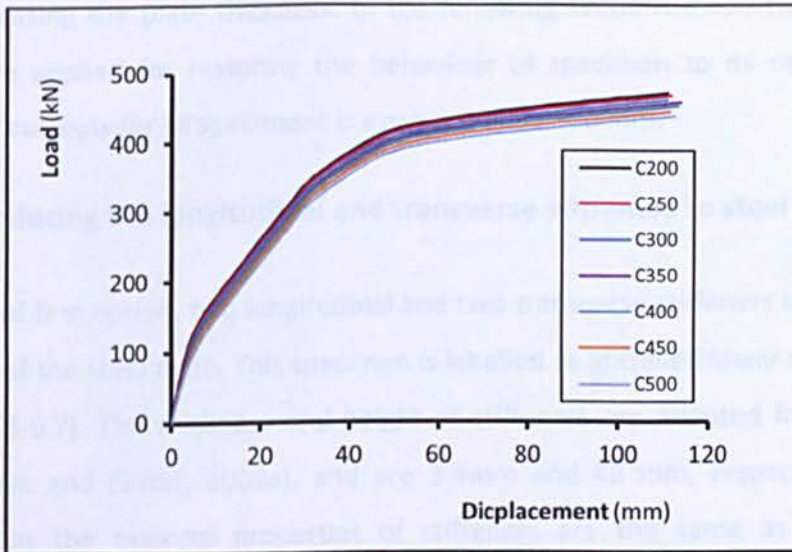


Figure 3.17: Pushover analysis results for SPSWC-0.7 specimen with variation of circular cut-out diameter

The results show that the variation of ultimate load capacity and cut-out diameter is described by a second-degree relationship as shown in Figure 3.18:

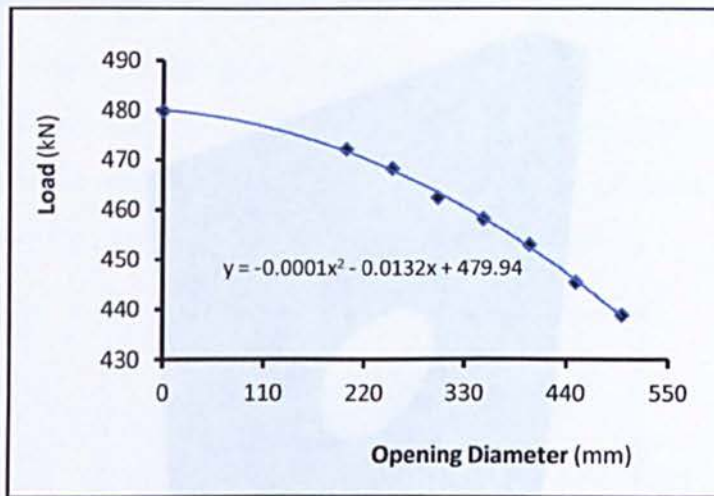


Figure 3.18: The ultimate load capacity of SPSWC-0.7 specimen with different cut-out diameters

3.8. Restoring the behaviour of SPSW systems with cut-outs

When there is a need for an opening in the steel plate shear wall system, there are two options to restore the system to its initial characteristics: by introducing stiffeners and/or increasing the plate thickness. In the following sections these two mentioned methods are applied for restoring the behaviour of specimen to its original values. Diameter of cut-outs for all specimens is assumed to be 500 mm.

3.8.1. Introducing the longitudinal and transverse stiffeners to steel plate

In the case of first option, two longitudinal and two transverse stiffeners were attached to one side of the steel plate. This specimen is labelled as Stiffened Shear wall with Cut-out (SPSWCS-0.7). The thickness and height of stiffeners are adopted from literature review (Alinia and Sarraf, 2009a), and are 3.4mm and 46 mm, respectively. It was assumed that the material properties of stiffeners are the same as steel plate's properties. In order to prevent direct transition of stress from boundary elements to stiffeners and precluding their interaction, the stiffeners are not connected to the boundary elements (Figure 3.19).

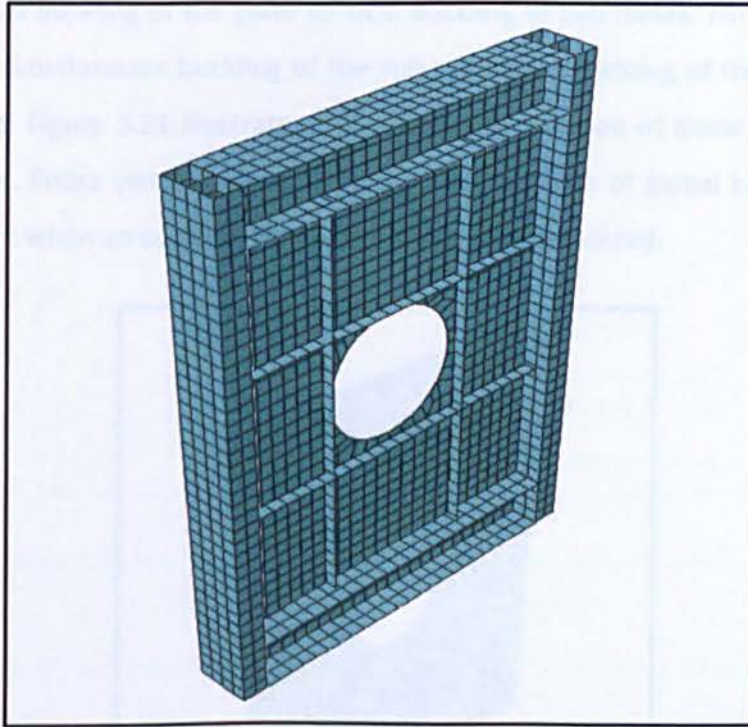


Figure 3.19: Scheme of FE model for stiffened SPSW with cut-out using

Figure 3.20 presents the position of stiffeners and the hysteresis loops for SPSWCS-0.7 specimen.

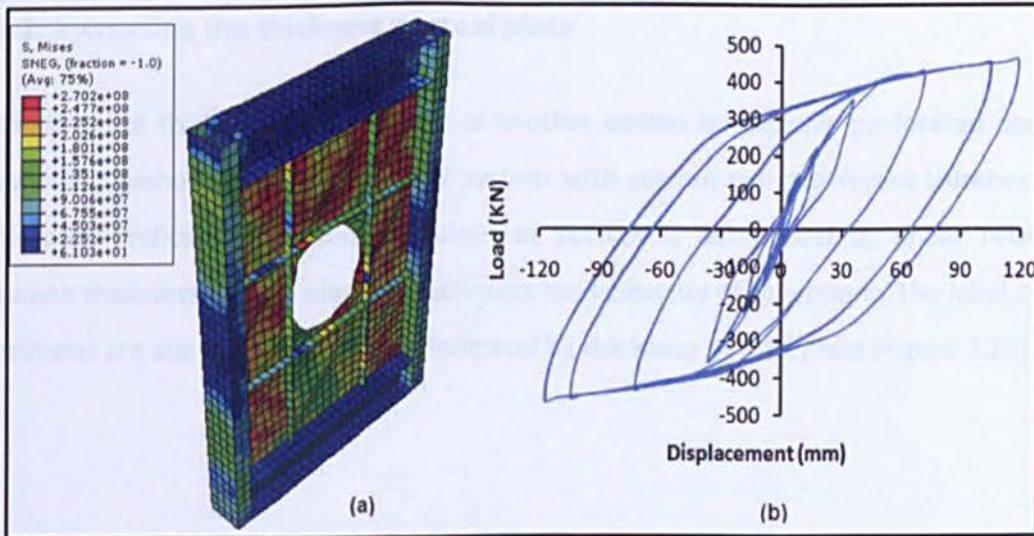


Figure 3.20: (a) Deformed shape and; (b) hysteresis behaviour for SPSWCS-0.7 specimen

Stiffeners are acting as a lateral support for steel plate and increase the critical shear stresses of sub-plates. Using the stiffeners could improve the system behaviour by increasing ductility and capacity of energy dissipation. The application of stiffeners

changes overall buckling of the plate to local buckling of sub-plates. For optimal design of stiffeners, simultaneous buckling of the sub-plates and yielding of the materials will be considered. Figure 3.21 illustrates the uniform distribution of shear stresses within the sub-plates. Entire yielding of sub-plates and prevention of global buckling of steel plate is evident when an optimal design of stiffeners is considered.

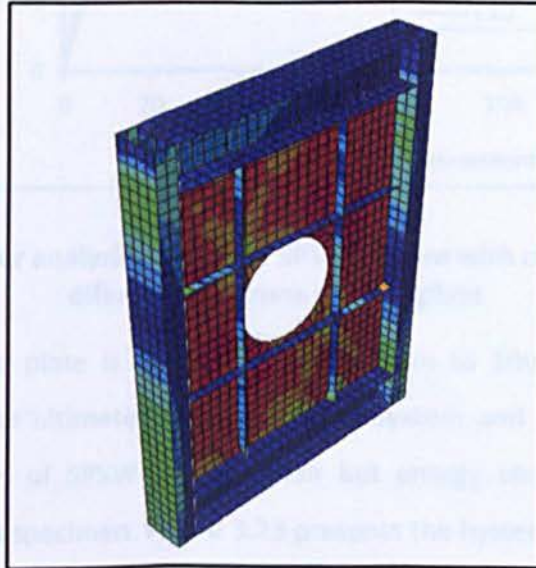


Figure 3.21: Entire yielding of sub-plates for SPSWCS-0.7 specimen

3.8.2. Increasing the thickness of steel plate

Increasing the thickness of steel plate is another option to improve perforated plate's behaviour. Pushover analysis of SPSW system with cut-out using different thickness of steel plate indicates that the behaviour of system is dominated by linear relation between thickness of steel plate and ultimate load capacity of specimens. The label of all specimens are started with "t" letter followed by thickness of infill plate (Figure 3.22).

Figure 3.23: (a) Deformed shape and (b) Hysteresis loops for SPSWC-1 specimen

Figure 3.24 compares the load-displacement results of FE models for all specimens discussed above under monotonic loading. It is obvious that if the main objective of the designer is to keep the stiffness and/or ultimate load capacity of perforated wall as the

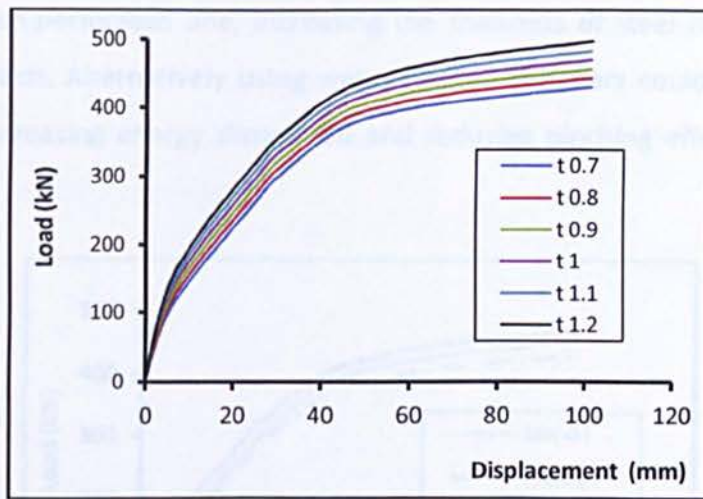


Figure 3.22: Pushover analysis results for SPSW system with circular cut-outs using different thickness of steel plate

Once thickness of the plate is increased from 0.7mm to 1mm which is labelled as SPSWC-1 specimen the ultimate load capacity of system and the stiffness would be increased to the level of SPSW-0.7 specimen but energy absorption would still be relatively less than this specimen. Figure 3.23 presents the hysteresis curve loops for this sample.

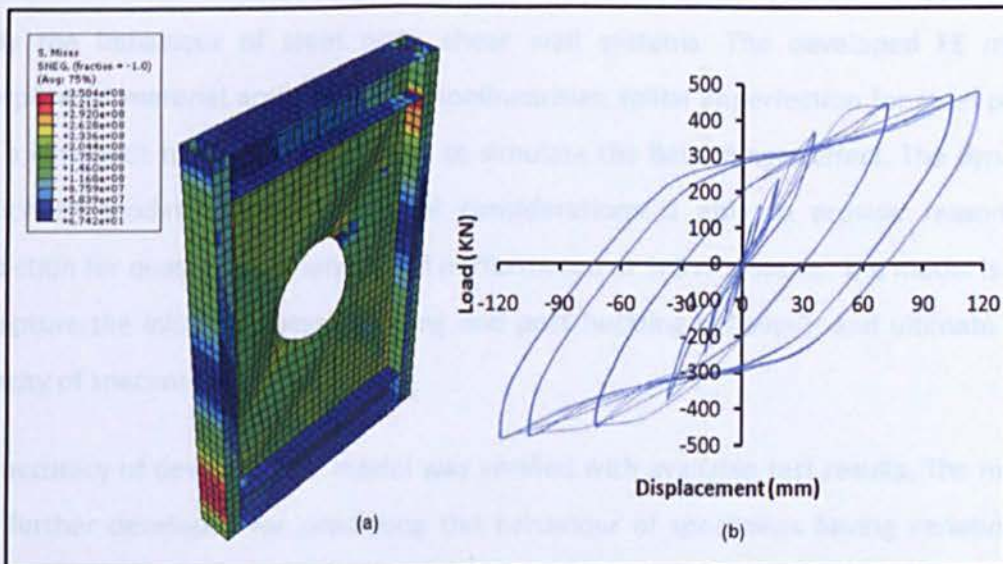


Figure 3.23: (a) Deformed shape and (b) Hysteresis loops for SPSWC-1 specimen

Figure 3.24 compares the load-displacement results of FE models for all samples discussed above under monotonic loading. It is obvious that if the main objective of the designer is to keep the stiffness and/or ultimate load capacity of perforated wall at the

same level of un-perforated one, increasing the thickness of steel plate could be an effective approach. Alternatively using well designed stiffeners could have significant influence on increasing energy dissipation and reducing pinching effect on hysteresis curves.

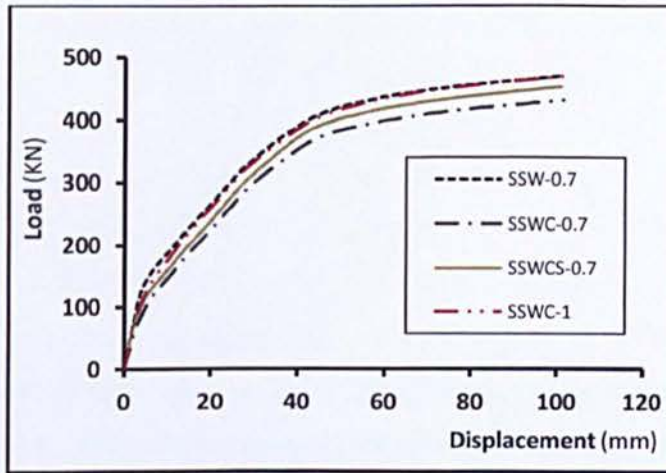


Figure 3.24: Comparative results for push-over analysis of specimens

3.9. Summary

The nonlinear explicit finite element method is found to be very effective approach to study the behaviour of steel plate shear wall systems. The developed FE model incorporated material and geometric nonlinearities, initial imperfection for steel plates and a kinematic hardening subroutine to simulate the Bauschinger effect. The dynamic explicit FE model with some special considerations is able to provide reasonable prediction for quasi-static analysis and performance of SPSW systems. The model is able to capture the initial stiffness, buckling and post buckling behaviour and ultimate load capacity of specimens.

The accuracy of developed FE model was verified with available test results. The model was further developed for predicting the behaviour of specimens having variation of circular cut-outs in the centre of steel plate. In addition two different alternatives were studied to restore the performance of perforated specimens. Using thicker steel plates and/or introducing longitudinal and transverse stiffeners to steel plate were applied in the model. However, there are no published test results to confirm the accuracy of

CHAPTER 3: FINITE ELEMENT SIMULATION TECHNIQUE FOR SPSWs

developed method to predict the behaviour of perforated and strengthened system. For this reason the planned experiments in this research are designed to cover different types of specimens including SPSW systems with and without cut-outs and corresponding improved specimens.

4. EXPERIMENTAL

TEST SET-UP

4.1. Introduction

This chapter comprises two main parts. The first part covers design and construction of the loading system and corresponding components including the rigid box for connecting screw jack to the reaction frame, support-structure for holding and connecting gear box and motor to the screw jack, connection parts for loadcell, loading plate, connection plate, rigid clamps, and lateral bracing system. The second part mainly covers the instrumentation of test specimens and data acquisition system.

To obtain performance data and validate design assumptions for FE modelling of stiffened and non-stiffened specimens, nine specimens of single-storey SPSW comprising two solid specimens (W1 and W2), three GFRP-steel sandwich shear walls (W1G1, W1G2 and W1G3), two specimens with cut-outs (W1O and W2O), two stiffened specimens with cut-outs (W1OG and W2OS), and finally one frame-only specimen (F) were constructed and tested under cyclic load. The size of specimens was determined based on the capacity of the testing equipment and availability of facilities. The capacity of reaction frame was assessed for maximum applied load during the testing. A loading system was designed to apply cyclic quasi-static load and a lateral bracing was designed to prevent the out-of-plane buckling of test specimens. The specimens' geometry design was mainly dictated by the size of the reaction frame and limitations imposed by the testing facilities. Possible configurations for edge connections of fish plates were studied and a moment-resisting connection was considered between beam and columns.

4.2. Material tests

In order to determine the material properties of boundary members and steel plates, a series of tests were conducted on representative samples of materials used in specimens. Tests included coupon tensile testing of flange and web samples of universal Beam 126x76x13 members used for boundary beam and columns. Coupon tensile tests were also conducted on samples of the steel plates and fish plates.

The instrumentation on the tensile coupon test consisted of two uniaxial strain gauges. The first strain gauge was mounted parallel to the direction of applied load and the second one was mounted in the direction perpendicular to the applied load. The data from this configuration of strain gauges are used for calculation of Poisson's ratio. The strains were also monitored continuously by an attached extensimeter. This device was used to generate a continuous load-deflection plot for specimens and also as a check on the calculated strains. Figure 4.1 presents the coupon tension test procedure for steel materials. Data acquisition system, measurement of sample dimensions using micrometer, installation of sample into the universal tensile test machine, rupture of sample and outline of the load-displacement diagram for sample which is created using flange part of universal section are shown in this picture.

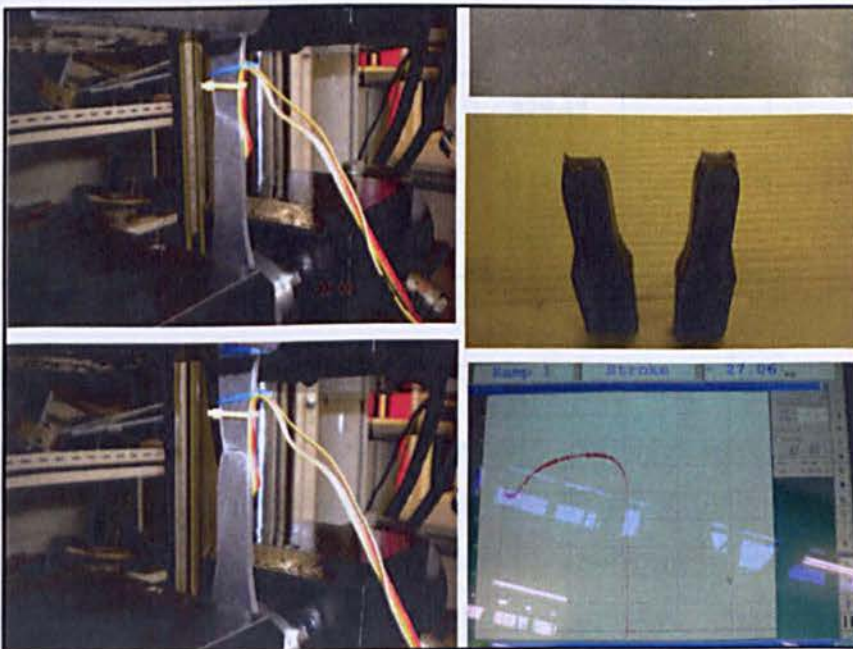


Figure 4.1 Coupon tensile test procedure for steel materials

CHAPTER 4: EXPERIMENTAL TEST SET UP

The summary of coupon tensile test values is presented in Table 4.1 for all samples.

Table 4.1: Summary of material properties determined from coupon testing

Member	Width average* mm	Thickness average mm	Yield Strength MPa	Ultimate Strength MPa	average Yield Strength MPa	Ultimate Strength average MPa
Universal Beam 126x76x13 based on flanges results	20.1	6.76	354	539.04	356	542
	20.08	7.04	359	546.73		
	20.04	6.95	355	540.43		
Universal Beam 126x76x13 based on web results	20.07	4.71	338	513.85	342	521
	20.03	4.74	347	527.92		
	20.05	4.63	342	520.84		
Fish Plates	20.09	3.384	369	483.45	372	485
	20.04	3.32	375	488.03		
	20.02	3.326	372	484.33		
Steel plates Type I	20.373	0.670	241	351.94	242	355
	20.12	0.673	245	359.60		
	20.6	0.671	241	352.72		
Steel plates Type II	20.09	1.41	205	329.47	212	337
	20.04	1.42	220	341.57		
	20.05	1.40	213	341.64		

*Average values are taken from multiple readings along the length of the sample.

4.3. Test specimen specifications and construction procedure

In this research single-storey steel plate shear wall specimens were constructed and tested. Each specimen was a 1/3 scaled model, with height of 1025 mm and width of 1090 mm. Frame's members (beam and columns) were constructed from universal section 126 × 76 × 13. The steel panel was constructed from two different types of cold-rolled steel sheets with nominal thickness of 0.675 mm and 1.4 mm. The configuration

CHAPTER 4: EXPERIMENTAL TEST SET UP

of specimens differed principally in the type of steel plate material used for each panel. The variations include thickness of steel plates, introducing cut-outs into steel plates and using sandwich shear panels. Figure 4.2 illustrates the overall geometry of test specimens.

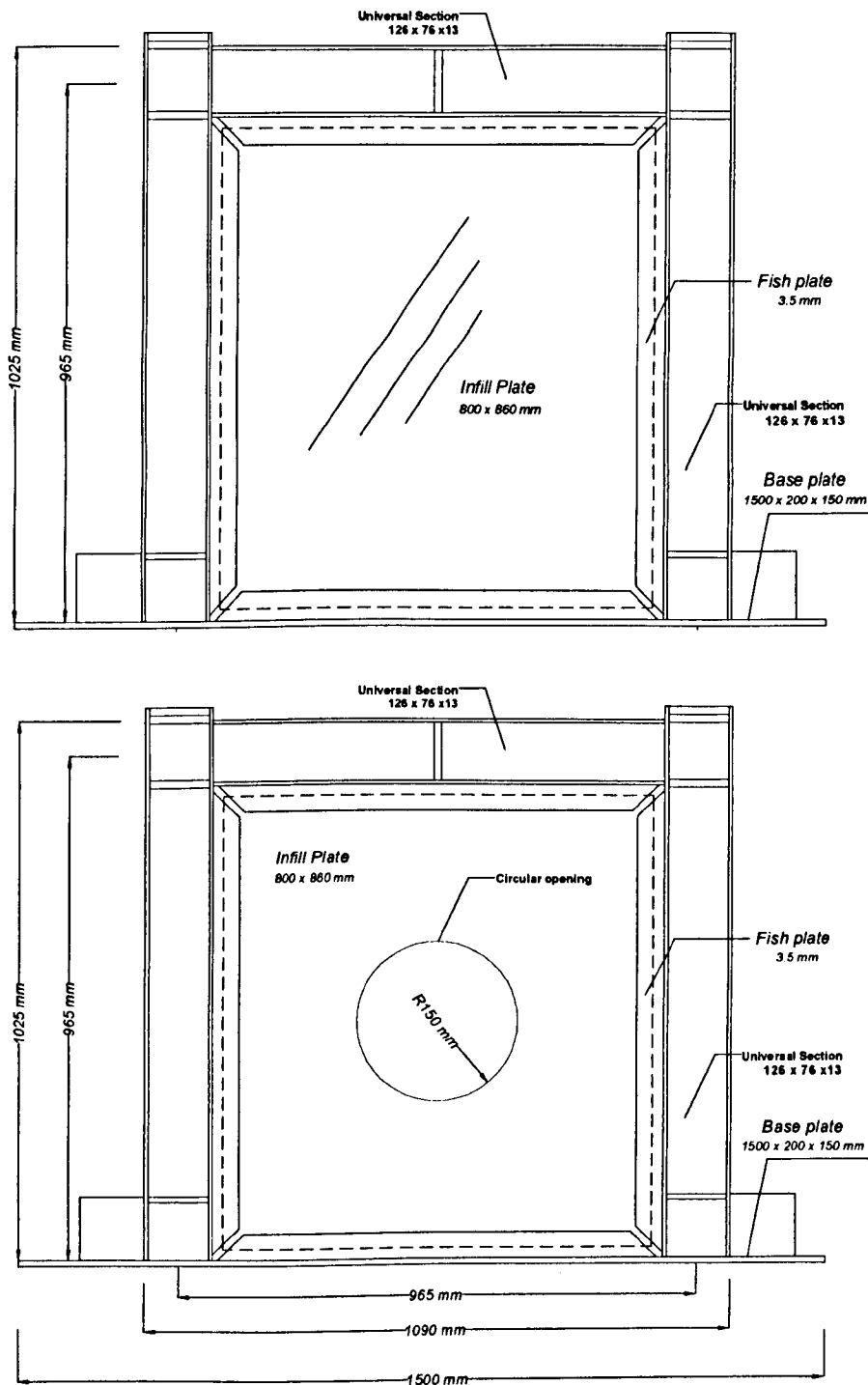


Figure 4.2: Overall geometry and dimensions for single-storey test specimens

CHAPTER 4: EXPERIMENTAL TEST SET UP

Figure 4.3 shows the configuration and dimension of main and secondary fish plates' connections. In this research an innovative type of fish plate, namely secondary fish plates are used. This type of connection provides proper friction between fish plates and steel panels which is more effective for transferring the shear load between elements.

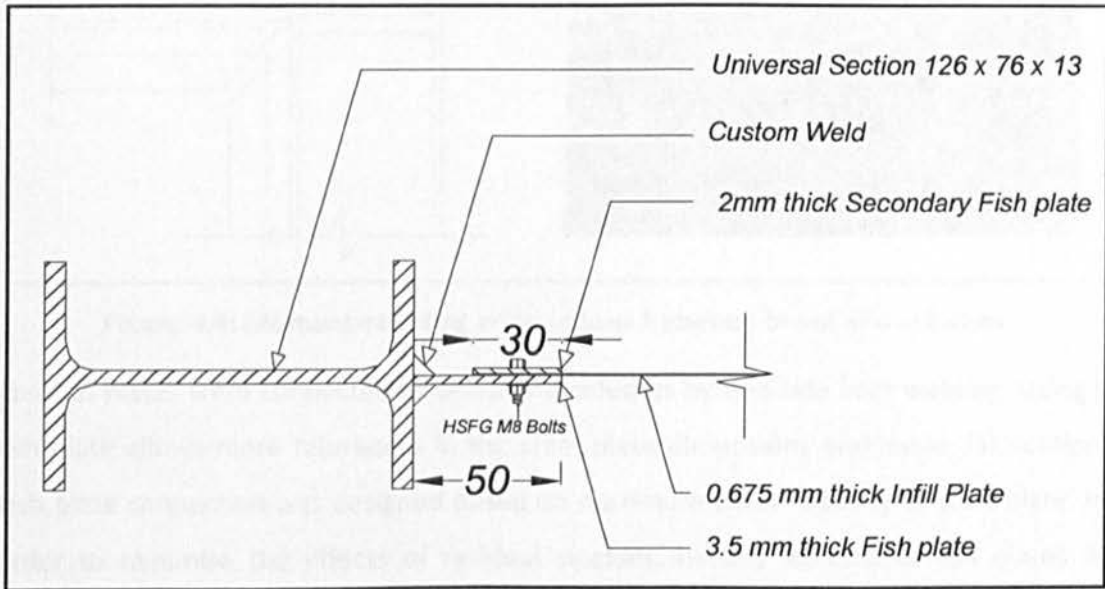


Figure 4.3: Detailed view for dimensions and type of connection between steel plate and boundary elements

In order to provide full moment-resisting connections between frame's boundary members, moment-resisting connections are designed and applied to beam-to-columns connections. Figure 4.4 illustrates the rigid connection conducted between beam and column for test specimens utilising Shielded Metal Arc (SMA) weld. The beam flanges were rigidly connected to the column flange using fully penetrated groove welding. The beam web was connected to the column flange using two-side fillet welding. Furthermore, the edges of connection plates were properly treated for this type of connection. During the test program the exact magnitude of the perpendicular angle between beam and column connections was monitored. Moment-resisting connection could provide sufficient stiffness for beam-column joints and alternatively prevents premature tearing of the steel plate at the edge of steel plate.

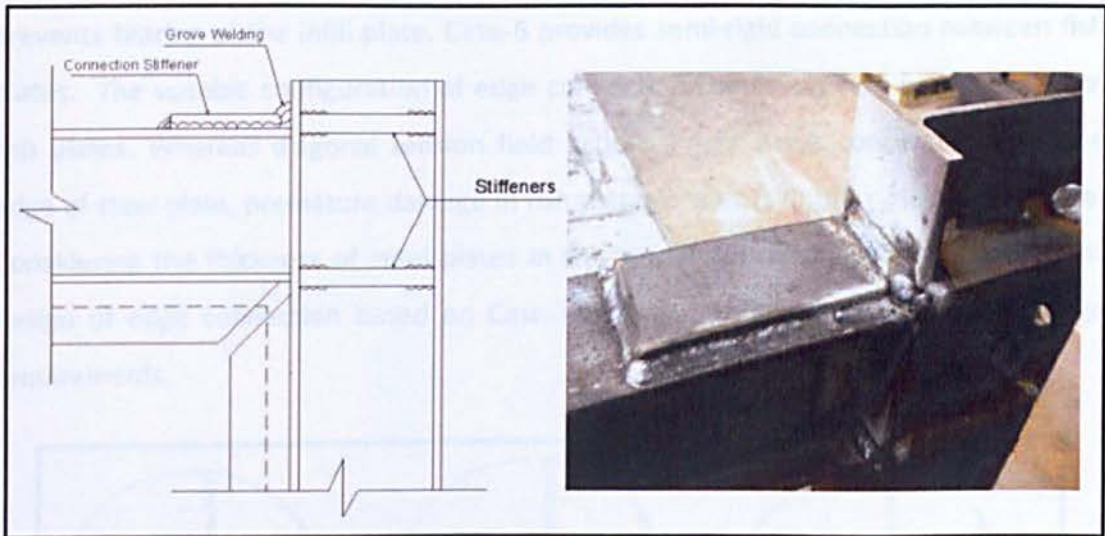


Figure 4.4: Moment-resisting connections between beam and columns

The fish plates were connected to beam and columns by two-side fillet welding. Using a fish-plate allows more tolerances in the steel plate dimensions and easier fabrication. Fish plate connection was designed based on maximum shear capacity of steel plate. In order to minimise the effects of residual stresses, initially welding of fish plates to boundary members was conducted as intermittent weld and after cooling the remaining gaps were welded (Figure 4.5).



Figure 4.5: Connection of fish plate to boundary members using intermittent fillet welding on both sides of fish plate

In order to design proper connection at the edge of test specimens, several options were considered (Figure 4.6). Case-1 provides deformable connection between fish plates which prevents premature buckling of fish plates. Case-2 and case-3 provide a rigid connection between fish plates. Case-4 and case-5 provide deformable edge connection between fish plates, However existence of attached plate to infill plate

CHAPTER 4: EXPERIMENTAL TEST SET UP

prevents tearing of the infill plate. Case-6 provides semi-rigid connection between fish plates. The suitable configuration of edge connection should prevent early damage of fish plates. Whereas diagonal tension field actions imply stress concentration to the edge of steel plate, premature damage in fish plates prevents entire yield of steel plate. Considering the thickness of steel plates in this research it was finally concluded that design of edge connection based on Case-1 is more practical and meets the design requirements.

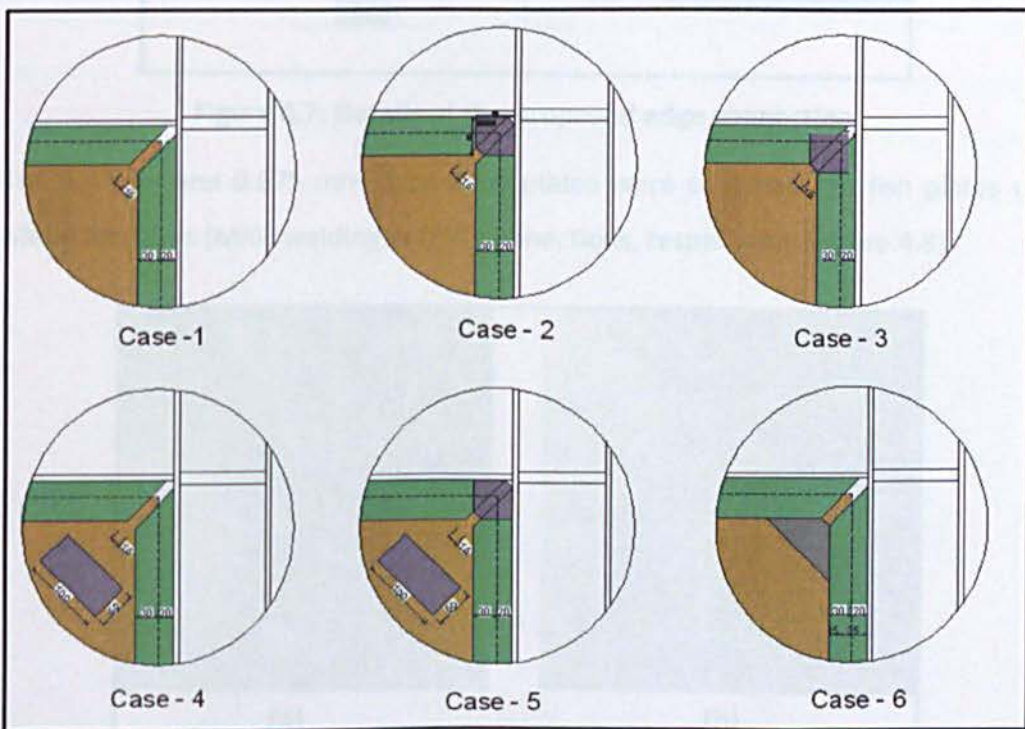


Figure 4.6: Different edge connection of test specimens (measurements in mm)

All specimens were designed and constructed according to details shown in Figure 4.7. It is worth mentioning that the test results confirmed the behaviour of specimens at the edge connections is as expected. The capability of designed connection prevents occurrence of early damage for fish plates and premature tears of steel plate.

Since steel plates are very thin, the handling and welding require special considerations are required for handling in this research, for welding of steel plate to fish plates and stiffeners to steel plate that welding process. MIG welding uses an arc of electricity to create a small cavity between a continuously fed electrode (+ the wire fed welding gun) and a cathode (- the metal being welded, the metal) enclosed by the steam circuit, along

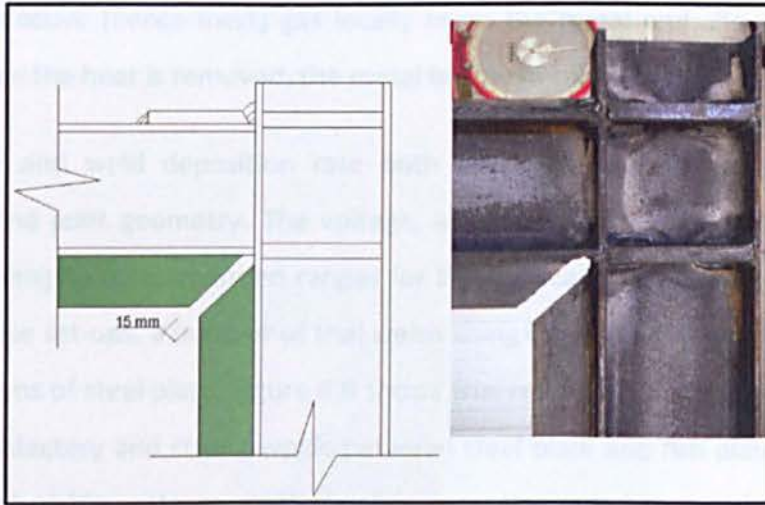


Figure 4.7: Details of the proposed edge connection

The 1.4 mm and 0.675 mm thick steel plates were connected to fish plates using Metal Inert Gas (MIG) welding or bolt connections, respectively (Figure 4.8).

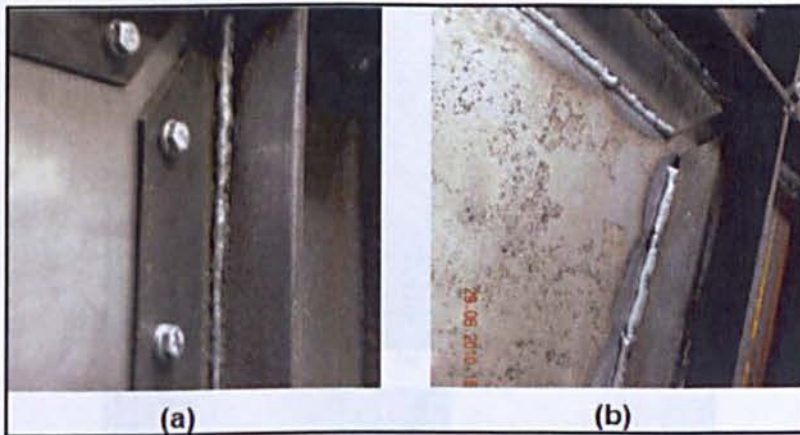


Figure 4.8: Connection of steel plates to fish plates (a) Using HSFG bolts for 0.675 mm thick steel plate and (b) Using MIG weld for 1.4 mm thick steel plates

HSFG bolt connections were pre-tensioned to prevent premature slip of the bolt connections due to friction. The bolt sizes and spacing were designed to resist diagonal tension action until plastic hinges were fully formed within the steel plate.

Since steel plates are very thin, for handling and welding issues special considerations are required for handling. In this research, for welding of steel plate to fish plates and stiffeners to steel plate MIG welding is used. MIG welding uses an arc of electricity to create a short circuit between a continuously fed anode (+ the wire-fed welding gun) and a cathode (- the metal being welded). The heat produced by the short circuit, along

CHAPTER 4: EXPERIMENTAL TEST SET UP

with a non-reactive (hence inert) gas locally melts the metal and allows them to mix together. Once the heat is removed, the metal begins to cool and solidify.

Weld quality and weld deposition rate both are influenced by variety of welding parameters and joint geometry. The voltage, wire speed and gas flow are set by the welder according to recommended ranges for the application before welding. In order to finalise these set-ups, a number of trial welds using 0.6 mm wires were conducted on strips specimens of steel plate. Figure 4.9 shows trial results of different welding set-ups to obtain satisfactory and strong welds between steel plate and fish plates with proper penetration of welding. However, the welding was controlled to avoid any burning of steel plate during the welding. The maximum length of welding for each Pulse was limited to 70 mm to absorb the energy supplied in the form of heat generated in welding process.

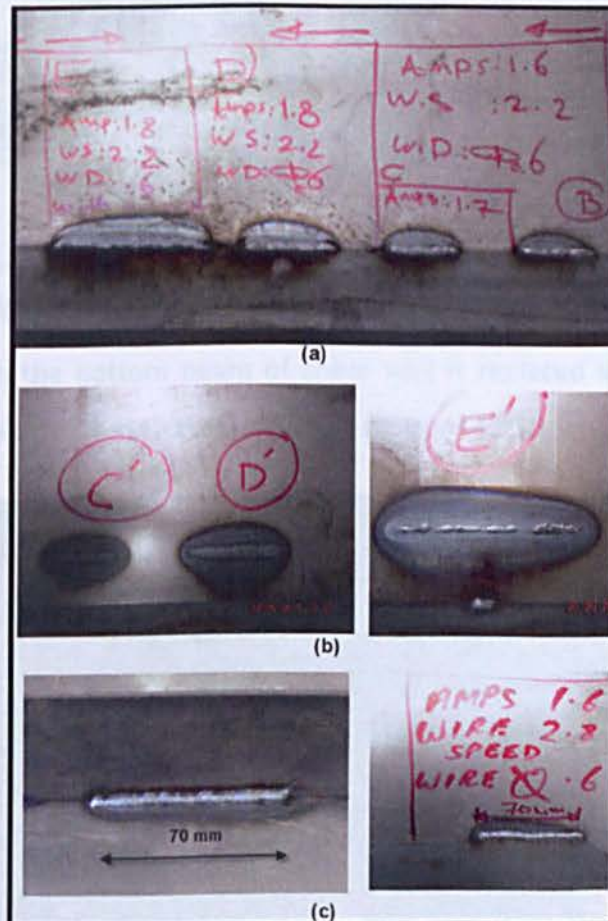


Figure 4.9 Different trials for welding of steel plate to fish plates and stiffeners to steel plate using MIG welding

CHAPTER 4: EXPERIMENTAL TEST SET UP

A coupon specimen was made and tested according to afore mentioned procedure. The test results of this prototype specimen showed desirable performance of welded joints and indicated that the proposed MIG weld set-up is suitable for connecting the stiffeners to steel plate and steel plate to fish plates (Figure 4.10).

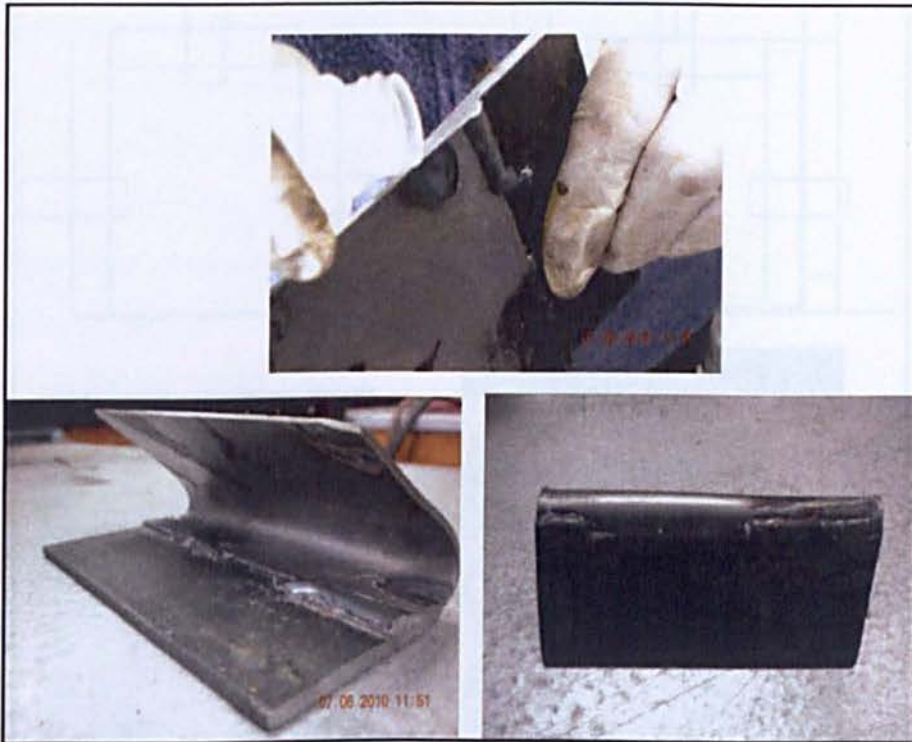


Figure 4.10: Testing of welding joint by MIG welding

In present research the bottom beam of shear wall is replaced with base plate. This configuration is similar to those in real structures (Figure 4.11).

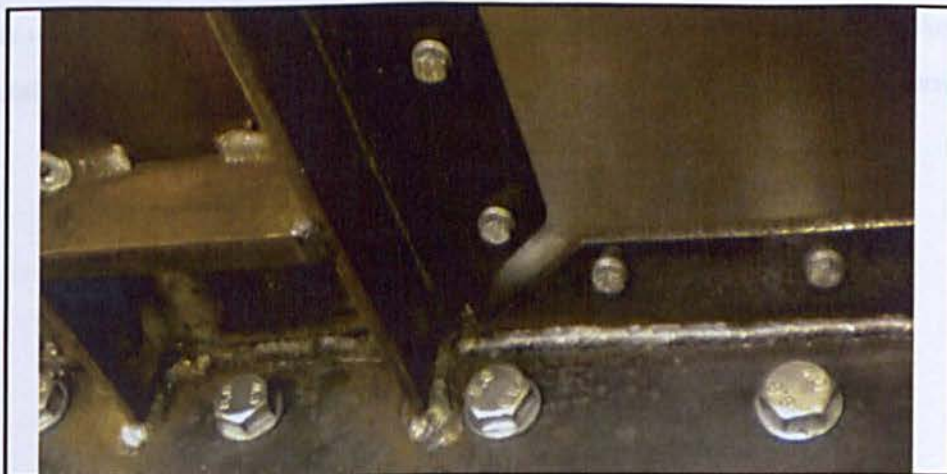


Figure 4.11 Connection of steel plate to boundary members via fish plate

CHAPTER 4: EXPERIMENTAL TEST SET UP

In order to reduce the size tolerance of specimens during the welding operation, a jig was designed and constructed as shown in Figure 4.12. By using this frame, the required time for specimens' construction was reduced effectively.

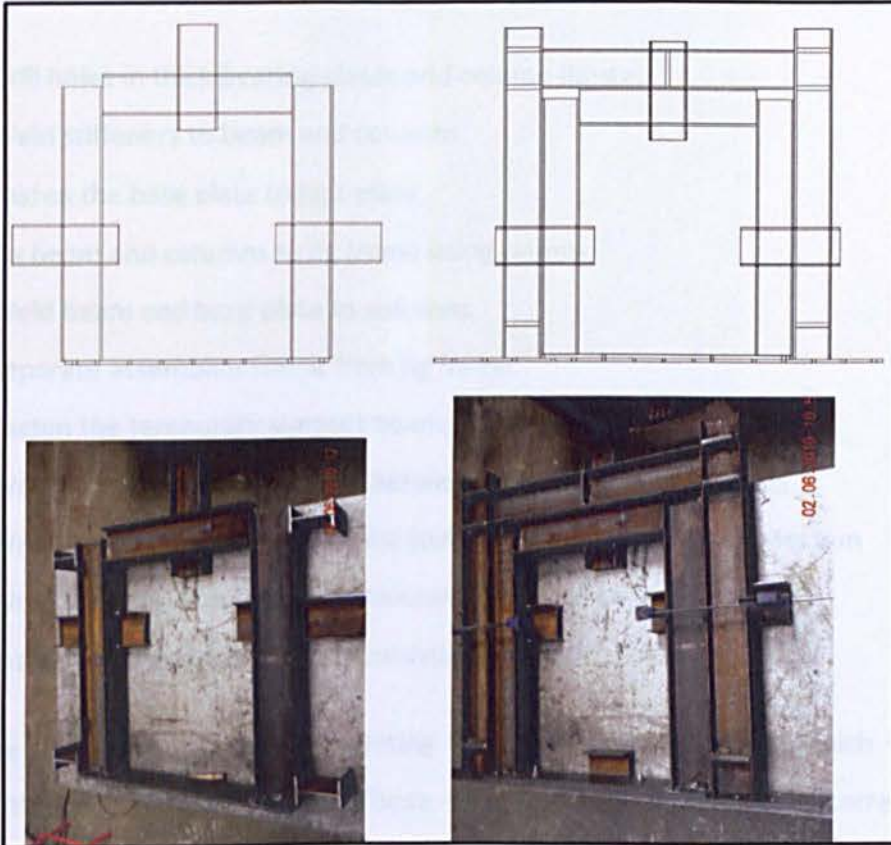


Figure 4.12: Jig frame was designed and constructed to improve the efficiency of specimen's construction

Columns were connected to the base plate using fillet welding all around the web and flanges of columns. In order to create an entirely stiff connection between column and base plate, two stiffeners were welded to column's flanges and base plate (Figure 4.13).



Figure 4.13: Utilising stiffener to create sufficient connection between column and base plate

CHAPTER 4: EXPERIMENTAL TEST SET UP

All the specimens were entirely constructed in Kingston University structural engineering laboratory. This allowed for complete control of the assembly process. All welding was done by a qualified welder. The construction sequence for all specimens was as follows:

- Drill holes in thick bearing plates and column flange,
- Weld stiffeners to beam and columns,
- Fasten the base plate to jig's plate,
- Fix beam and columns to jig frame using clamps,
- Weld beam and base plate to columns,
- Separate assemblies frame from jig frame,
- Fasten the temporary support beam to the base plate of specimen,
- Weld the connector stiffeners between columns and base plate,
- Weld the connection plate at the joint of beam-to-column connection
- Weld the fish plates to beam, columns and base plate,
- Install shear panel to moment resisting frame.

There are few more steps for completing the specimen construction which varies for each of the individual specimens. These steps are later explained in corresponding chapters.

The specimens were placed in the reaction frame and fastened to the reaction frame by twenty 14 mm diameter and ten 10 mm diameter HSFG bolts. In order to prevent stress concentration in the base plate around the area that columns are connected to base plate, eight clamp plates were designed and constructed. These plates were fastened to reaction frame using 16 mm diameter HSFG bolts. Figure 4.14 gives more details for connection of specimens to reaction frame. To increase friction, the contact surfaces between the base plate and test frame were cleaned prior to installation.

4.4. Lateral supporting systems

In order to prevent any possible buckling of specimens during testing, a proper lateral bracing system was designed. The lateral bracing system consists of four square hollow sections (SHS) placed on each side of the specimen. Two SHS are placed on each side of the specimen laterally (Figure 4.14). The SHS are connected to the specimen using HSFGB bolts and clamped plates. The SHS are connected to the specimen using HSFGB bolts and clamped plates. The SHS are connected to the specimen using HSFGB bolts and clamped plates.

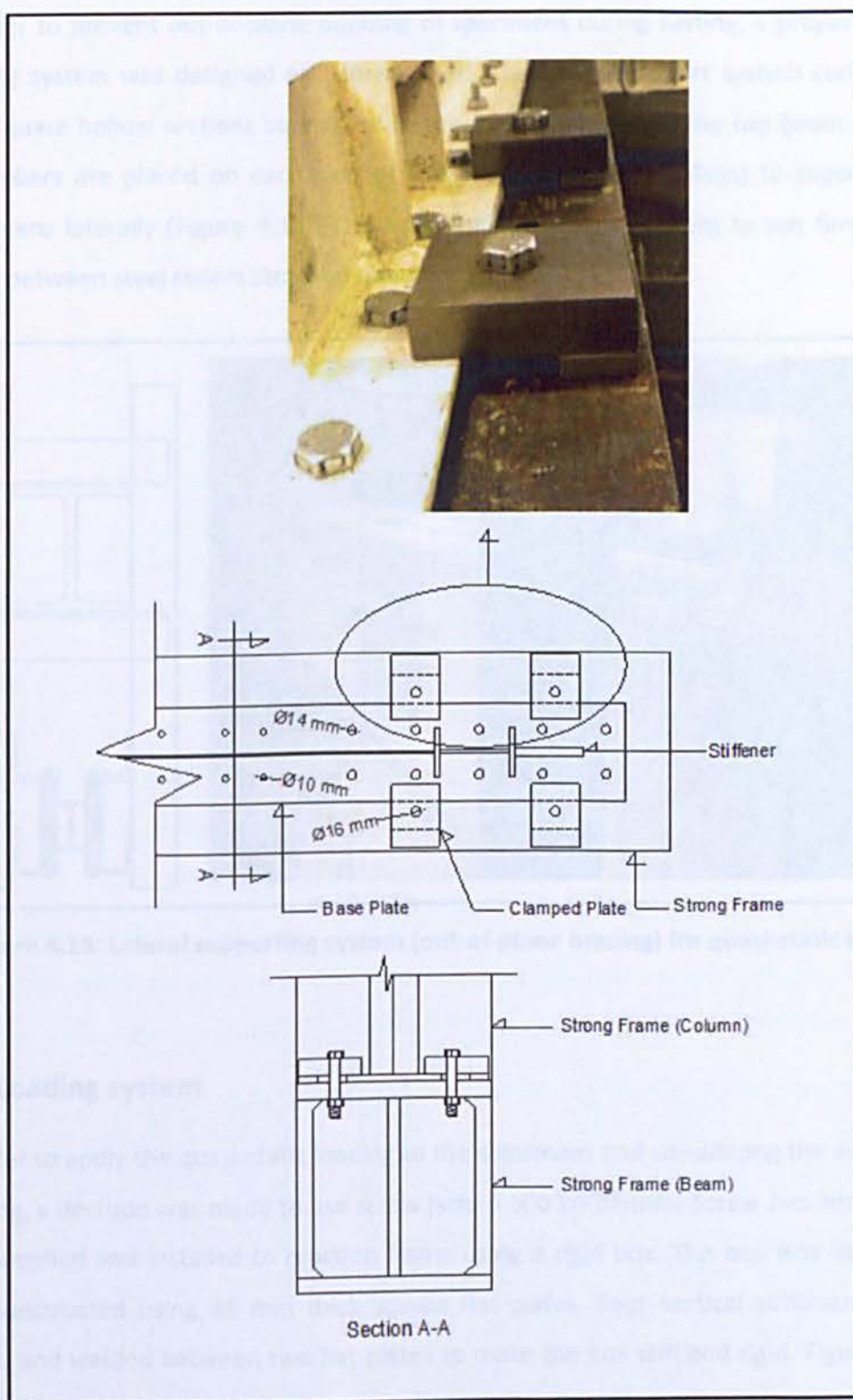


Figure 4.14: Specimens' connection to the reaction frame using HSFGB bolts and clamped plates

4.4. Lateral supporting system

In order to prevent out-of-plane buckling of specimens during testing, a proper lateral bracing system was designed and constructed. The lateral support system consists of four square hollow sections connected to the reaction frame on the top beam so that two rollers are placed on each side of specimens (total four rollers) to support the specimens laterally (Figure 4.15). This set-up allows test specimens to run firmly and freely between steel rollers attached to hollow sections.

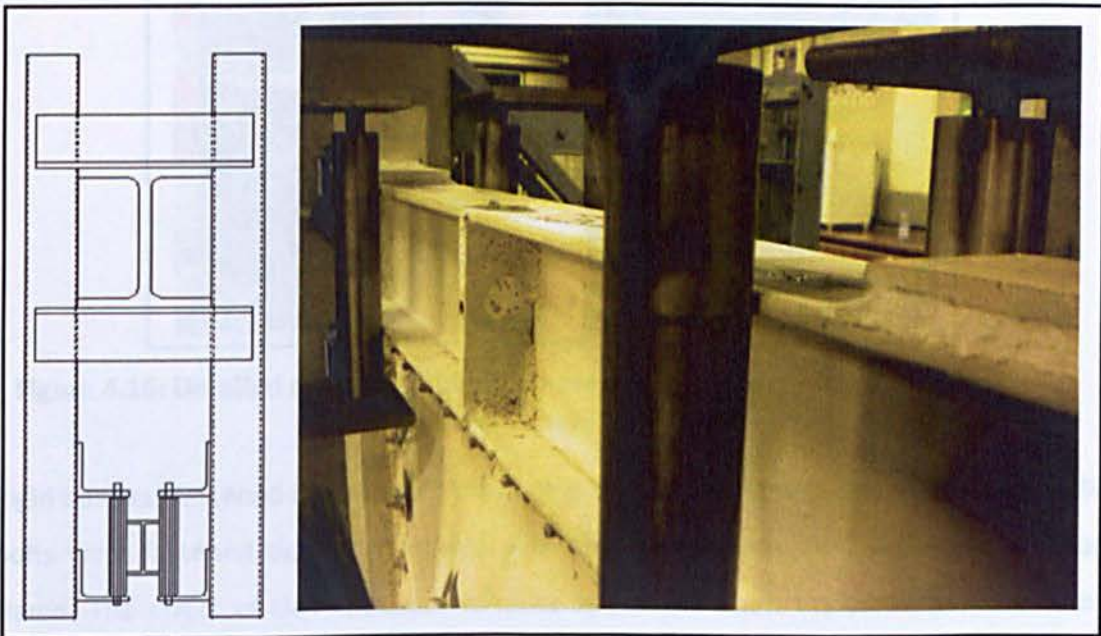


Figure 4.15: Lateral supporting system (out-of-plane bracing) for quasi-static tests

4.5. Loading system

In order to apply the quasi-static loading to the specimens and considering the available funding, a decision was made to use screw jack. A 500 kN Benziler Screw Jack model BD was supplied and installed to reaction frame using a rigid box. This box was designed and constructed using 35 mm thick square flat plates. Four vertical stiffeners were placed and welded between two flat plates to make the box stiff and rigid. Figure 4.16 shows detailed design and manufactured rigid box.

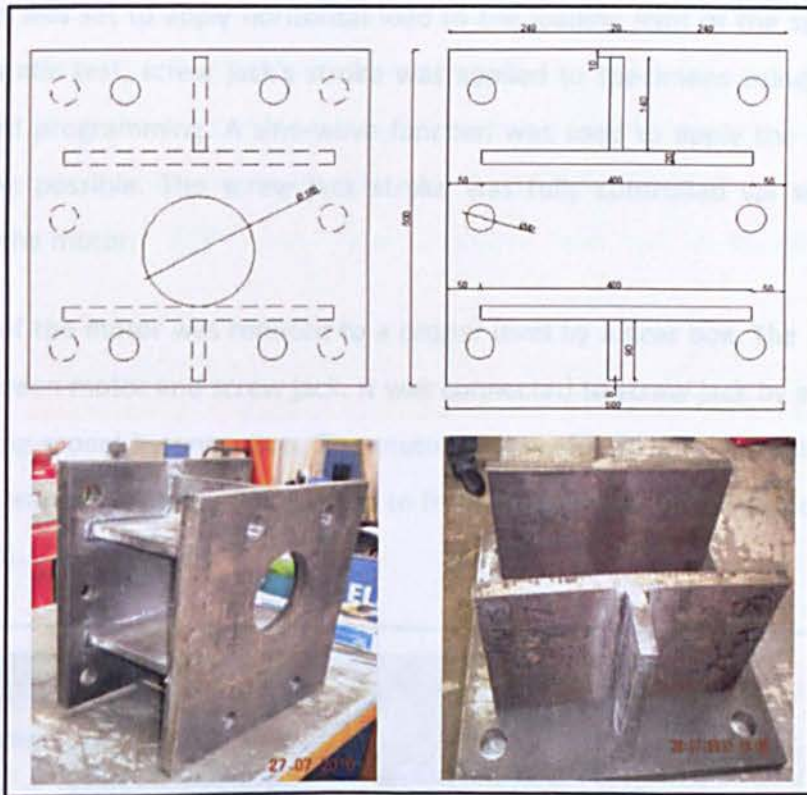


Figure 4.16: Detailed design and manufactured rigid connection box (all dimensions in mm)

Rigid box was fastened to reaction frame using six HSFG bolts with diameter 42 mm. The bolts were fastened tightly to provide sufficient friction between plates and reaction frame. The effect of this operation is most important when the screw jack pulls the specimens. Figure 4.17-a shows connection of rigid box to reaction frame. When connection between rigid box and reaction frame was accomplished, screw jack was fastened to rigid box using four HSFG bolts with diameter of 42 mm (Figure 4.17-b).

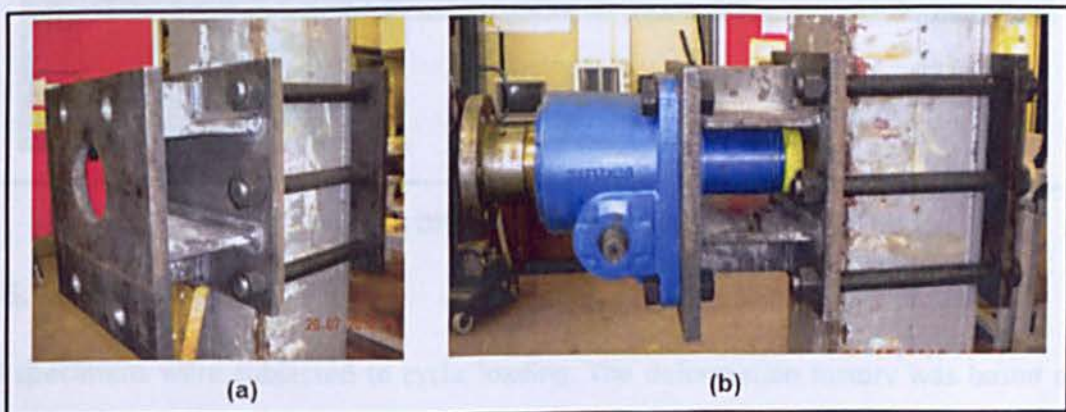


Figure 4.17: Connection of rigid box and screw jack to reaction frame

CHAPTER 4: EXPERIMENTAL TEST SET UP

The system was set to apply horizontal load to the loading joint of the specimens. For the quasi-static test, screw jack's stroke was applied to specimens using inverter and user-defined programming. A sine-wave function was used to apply the cyclic load as smoothly as possible. The screw jack stroke was fully controlled via signal sent by inverter to the motor.

The speed of the motor was reduced to a proper level by a gear box. The gear box was placed between motor and screw jack. It was connected to screw jack by a flexible gear type coupling model X connection. The motor was equipped with a cooling system to prevent increase of heating in motor due to frequently and long time use of the system (Figure 4.18).



Figure 4.18 Different parts of loading unit

4.6. Loading history

All specimens were subjected to cyclic loading. The deformation history was based on established guidelines for simulating earthquake loading (Applied Technology Council,

1992). Each cycle was repeated to reach the target displacement. Twenty-eight loading cycles were applied to the test specimens, of which sixteen cycles were in the inelastic range. The tests were terminated when the system could not sustain more loads and failed. The recommended loading (deformation) history in this testing program consists of stepwise increasing deformation cycles (Multiple Step Test) as illustrated in Figure 4.19.

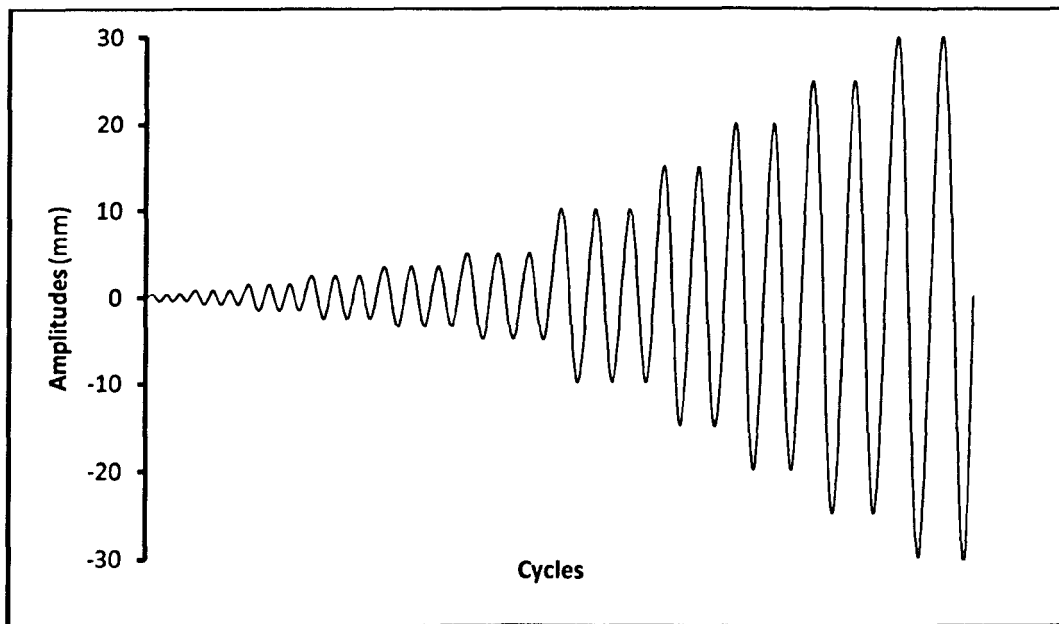


Figure 4.19: Deformation history for quasi-static test of specimens according to ATC-24 protocol

4.7. Instrumentation and data acquisition

To measure the applied load, the screw jack was equipped with a F204 universal loadcell with a maximum capacity of 500 kN. The F204 is ideally suited to bi-directional engineering force measurements. In order to provide a proper connection between the loadcell and connector shafts, two locking nuts were designed and manufactured. Locking nuts prevent loosening of connections under cyclic loading of system. Figure 4.20 shows the connection of loadcell to corresponding parts of loading system.

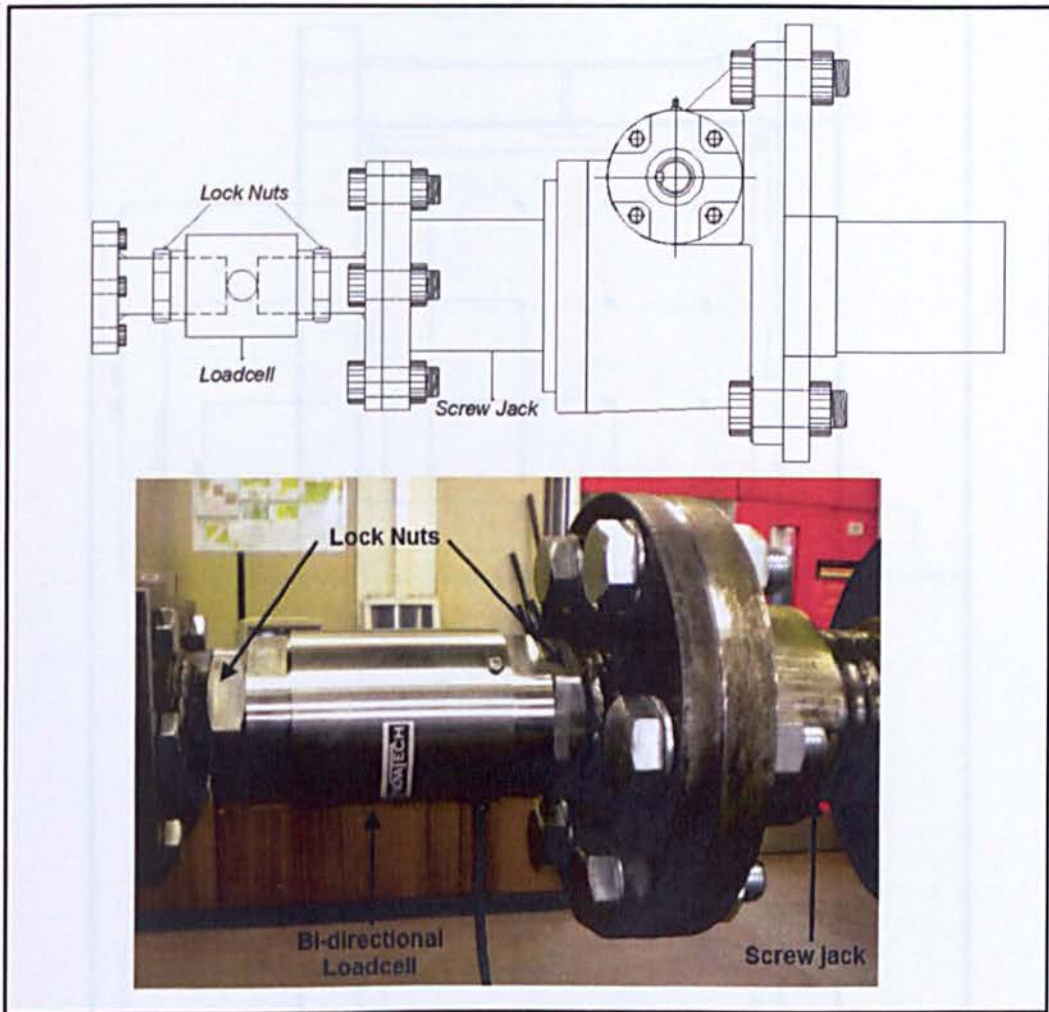


Figure 4.20: Connection of Loadcell to corresponding parts of loading system using locking nuts

Six types of data acquisition were used during the test procedure to fully describe any strain and deflection data. These comprised rosette strain gauges, uni-axial strain gauges, dial gauge, LVDTs, CDSs and infrared thermal camera.

Rosette strain gauges were mounted on the diagonal direction and half upper part of shear panels. The variation in direction and magnitude of the principal strains on the infill panels were studied using data recorded from rosettes installed on the steel plate. The major principal strains, direction of the major principal strain (angle measured from the vertical axis), and the maximum shear strain were calculated at each rosette strain gauge location (compressive and tensile strains are considered negative and positive, respectively). Analysis of this data was used to capture the occurrence of any yielding scenario in the steel plate.

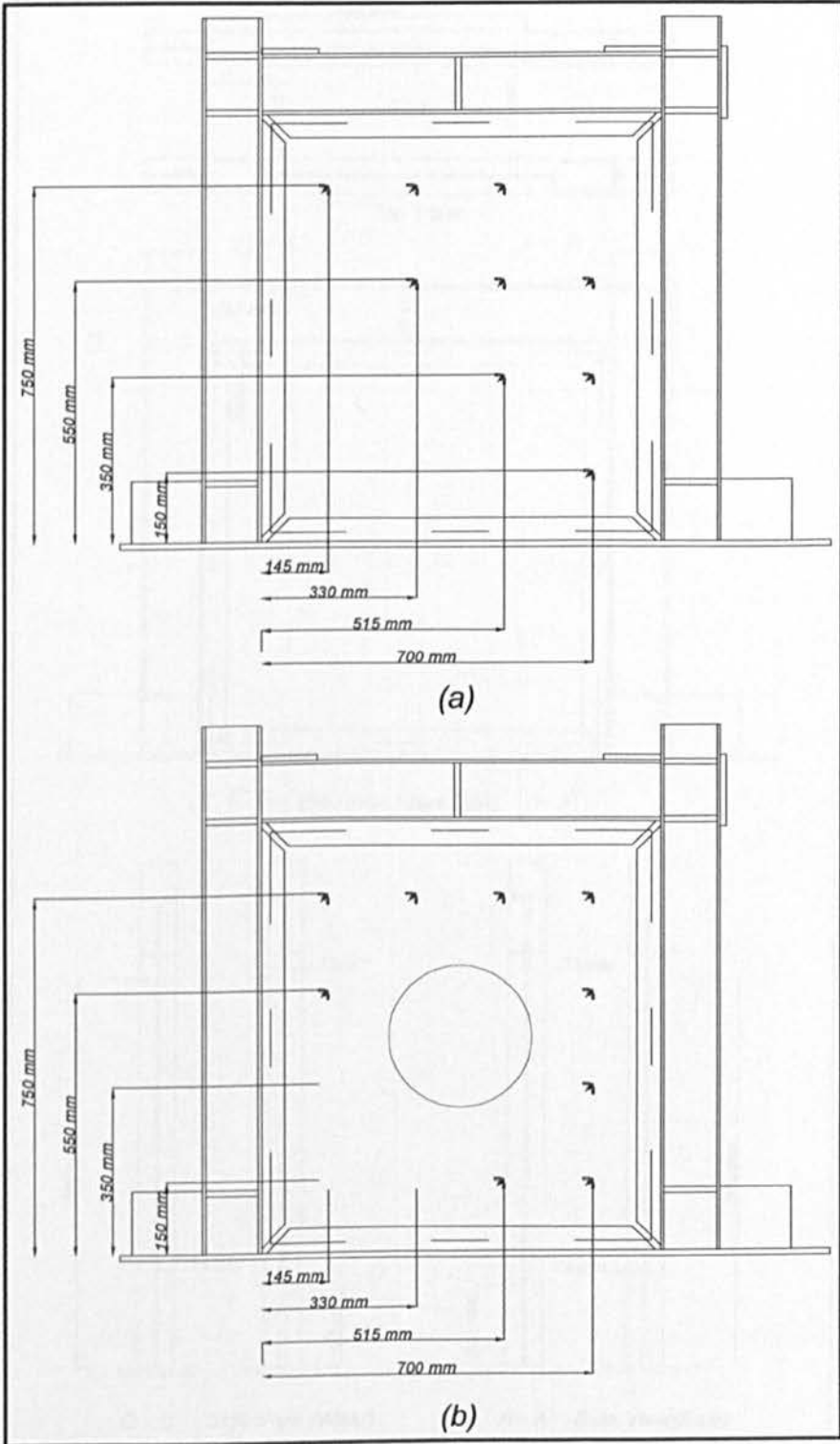


Figure 4.21: Locations of rosette strain gauges within the shear panel for test specimens (a) without cut-out (b) with cut-out

Figure 4.22 illustrates the locations of uni-axial strain gauges on the inner and outer flanges of beam and columns of the specimens.

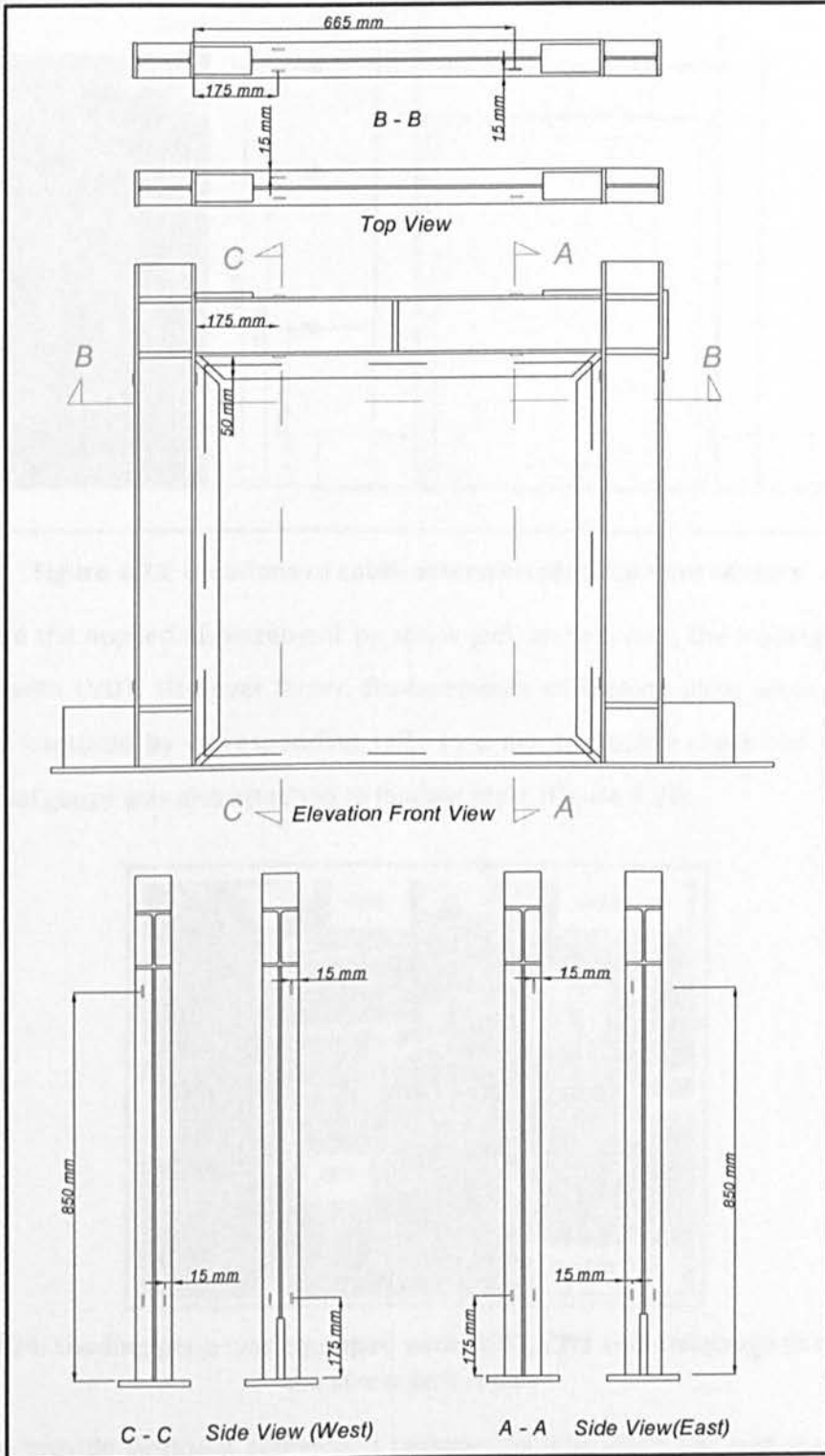


Figure 4.22: Un-axial Strain gauge locations on flanges of beam and columns

Cable-extension displacement sensors (CDS) were connected to columns at the most critical positions to capture deformations (Figure 4.23). This instrumentation layout was identical for all specimens.

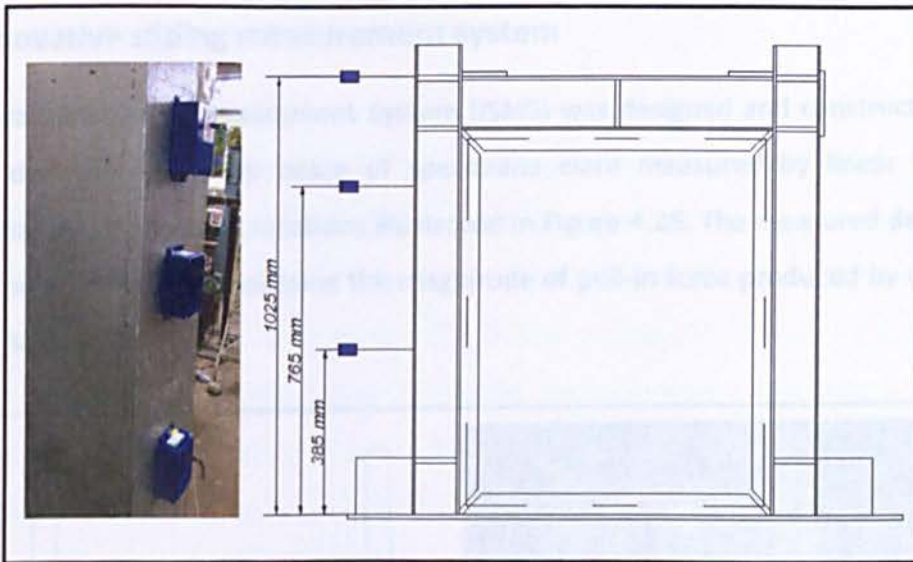


Figure 4.23: Locations of cable-extension displacement sensors

To measure the applied displacement by screw jack up to 5 mm, the loading plate was equipped with LVDT. However larger displacements of loading plate were controlled using data captured by corresponding CDS. In order to double check the screw jack stroke, a dial gauge was also attached to loading plate (Figure 4.24).

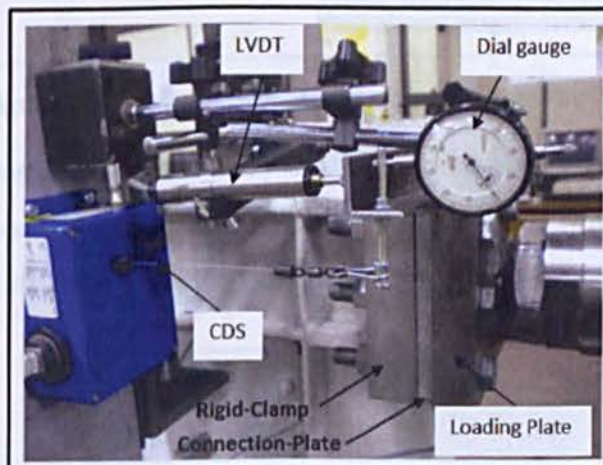


Figure 4.24: Loading plate was equipped with LVDT, CDS and dial gauge to measure the screw jack stroke

In order to provide sufficient connection between loading plate and test specimens in addition to connection plate that was welded to the outer flange of column, two Rigid-Clamps were also utilised. These two clamp-plates were designed and manufactured to preclude fracture of welding exhibited between connection plate and column when specimen is subjected to tensile load.

4.8. Innovative sliding measurement system

An Innovative Sliding Measurement System (ISMS) was designed and constructed. The vertical deflections for top beam of specimens were measured by linear variable differential transformers at locations illustrated in Figure 4.25. The measured deflection values could be used for assessing the magnitude of pull-in force produced by diagonal tension field action.

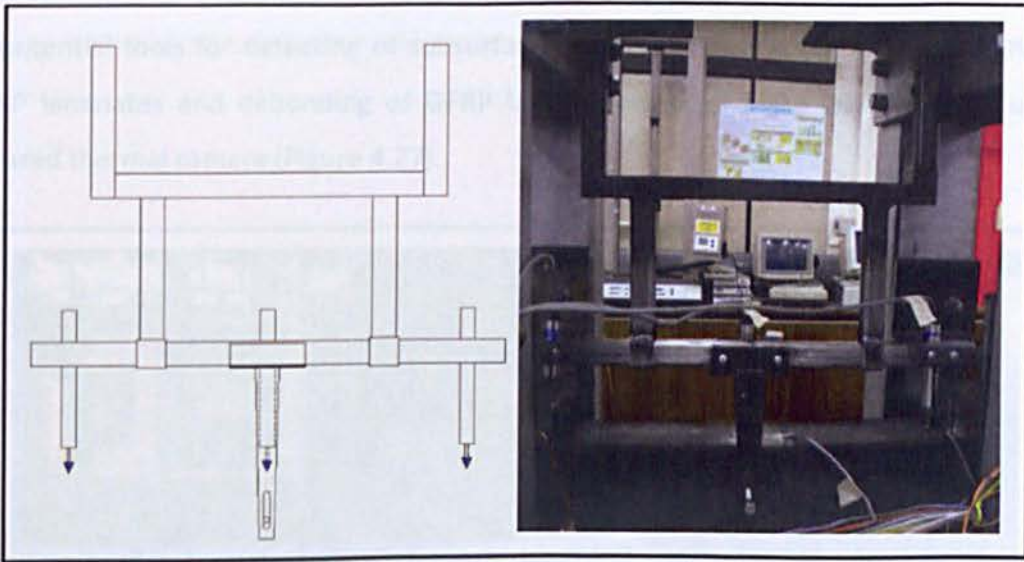


Figure 4.25: Innovative sliding measurement system

Out-of-plane buckling of infill panel was measured for the number of specimens during tests on only a few occasions. This was accomplished by manually measuring the profile from a temporarily attached timber was used as a reference (Figure 4.26).



Figure 4.26: Manually measurement of out-of-plane buckling of steel plate

4.9. Thermal imaging using infrared camera

A thermographic camera or thermal camera is a device that forms an image using infrared radiation. Instead of the 450–750 nanometre range of the visible light camera, infrared cameras operate in wavelengths as long as 14,000 nm (14 μm). Thermography is used in this case as a non-destructive test method. Thermographic camera is able to measure temperatures of surfaces without having a physical contact to them. Non destructive test (NDT) techniques such as infrared thermal camera have been developed as potential tools for detecting of subsurface defects. In this research delaminating of GFRP laminates and debonding of GFRP layers from steel plate was detected using infrared thermal camera (Figure 4.27).

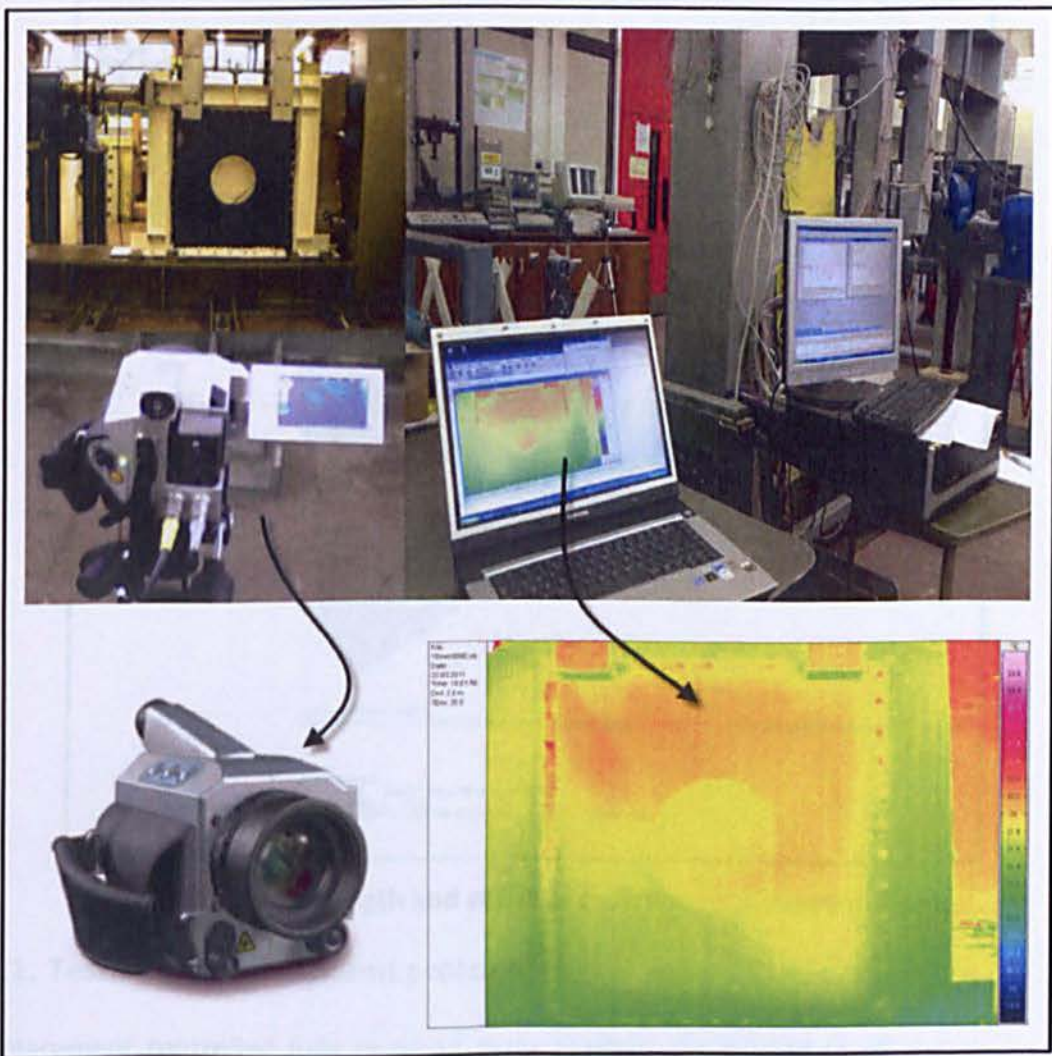


Figure 4.27: Infrared thermal camera is used for capturing delaminating and debonding of GFRP composite layers

4.10. Assessment of reaction frame

The existing reaction frame in structure laboratory was modelled and analysed for maximum load that may be applied during the testing procedure. As built dimensions of the frame is used for modelling of reaction frame in commercial software ABAQUS. Shell elements are used for modelling of the all components (Figure 4.28). The analysis results show that the frame is strong enough to meet necessary requirements for safe use of the frame and sufficiently stiff so the measurement of deflections of test specimens will not be effected from deformations of the frame. It should be noted that the reaction frame has been assessed for current research program and should be re-assessed for the future tests.

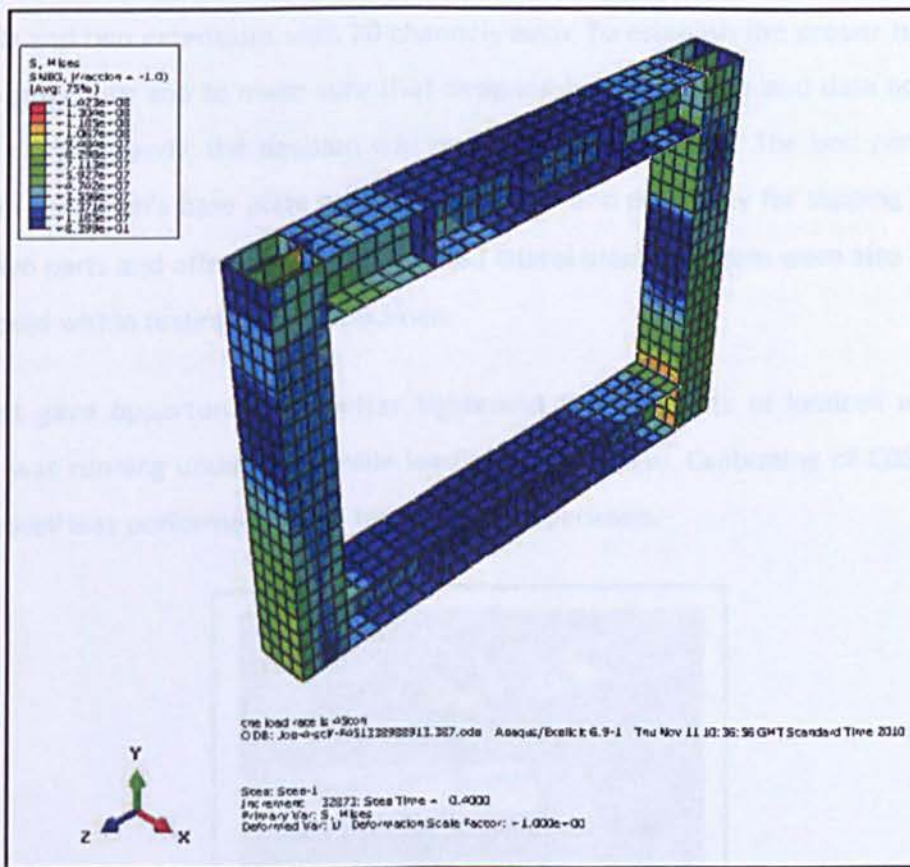


Figure 4.28: The strength and stiffness assessment of reaction frame

4.11. Testing procedures and protocol

Displacement controlled fully reversed cyclic loading was applied to all specimens. A loading strategy for testing was derived by following the method outlined in the Applied

Technology Council ATC-24 protocol for experiments using quasi-static cyclic loading. The specimens were loaded with a single in-plane load at the beam centre line level. The specimens cyclically loaded with gradually increasing deflection increments according to ATC-24 protocol up to 2.5% drift (25 mm). The specimens were subjected to 28 fully reversed cycles to reach the 2.5% drift. The displacement amplitudes were repeated three times up to 10 mm storey drift and then just two times to reach the ultimate capacity of the specimens.

4.12. Trial test specimen (T)

All measurement instruments, equipments and devices were connected to computer via a data logger system model DT85_G with 55 channels including main data logger with 15 channels and two extensions with 20 channels each. To establish the proper running of testing procedure and to make sure that designed loading system and data acquisition system work properly, the decision was made to run a trial test. The bolt connections between specimen's base plate and reaction frame and possibility for slipping between these two parts and effectiveness of installed lateral bracing system were also aimed to be checked within testing of trial specimen.

This test gave opportunity for better tightening the lock nuts of loadcell when the system was running under the tensile loading (Figure 4.29). Calibrating of CDSs, LVDTs and loadcell was performed within testing of this specimen.



Figure 4.29: Tightening the lock nuts when system is running under tensile loading

CHAPTER 4: EXPERIMENTAL TEST SET UP

Figure 4.30 shows the general test set up for trial specimen.

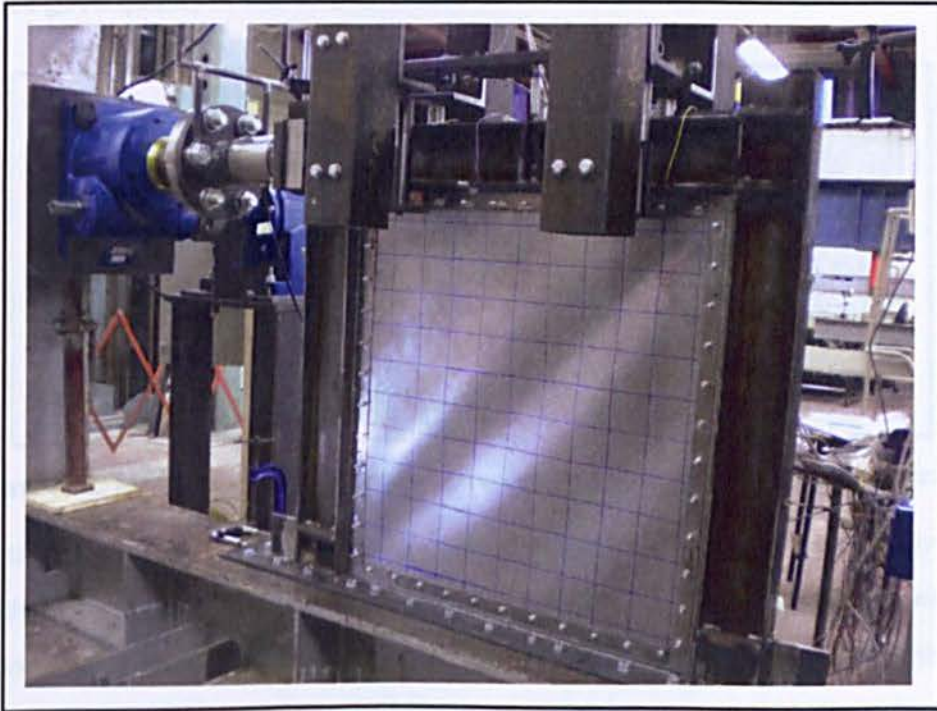


Figure 4.30: General configuration of test set up for trial specimen

In order to double check the CDS devices calibration some locations were simultaneously equipped using LVDT devices. In addition to this within the main testing program parallel usage of these two devices was planned (Figure 4.31).

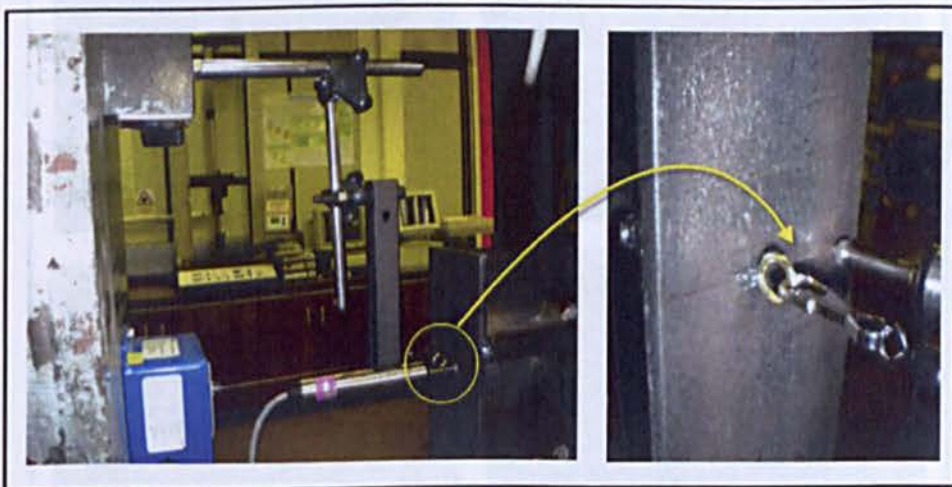


Figure 4.31: Double check for CDS devices calibration using LVDT

The base plate is fully fixed to the reaction frame using HSFG bolts. However, to ensure that there is no slipping between base plate and reaction frame, the base plate is

CHAPTER 4: EXPERIMENTAL TEST SET UP

equipped with a LVDT device that was placed in loading direction. The monitored results confirmed good quality of the connection between these two parts (Figure 4.32).

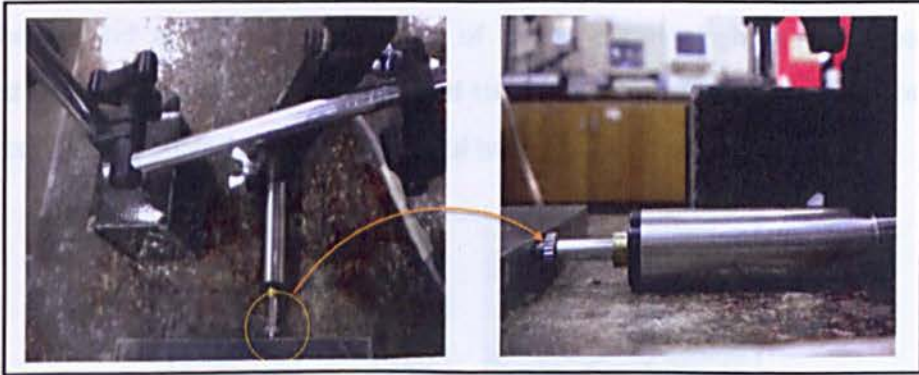


Figure 4.32: Monitoring any slippage between test specimen and reaction frame

One of the most important issues that occurred during the testing of trial specimen was the uplift of base plate. This event happened at the both ends of base plate when the corresponding column was under tensile loading. Having a close look to this event revealed that the bolts were secured but shear fracture occurred in the nuts grooves (Figure 4.33).

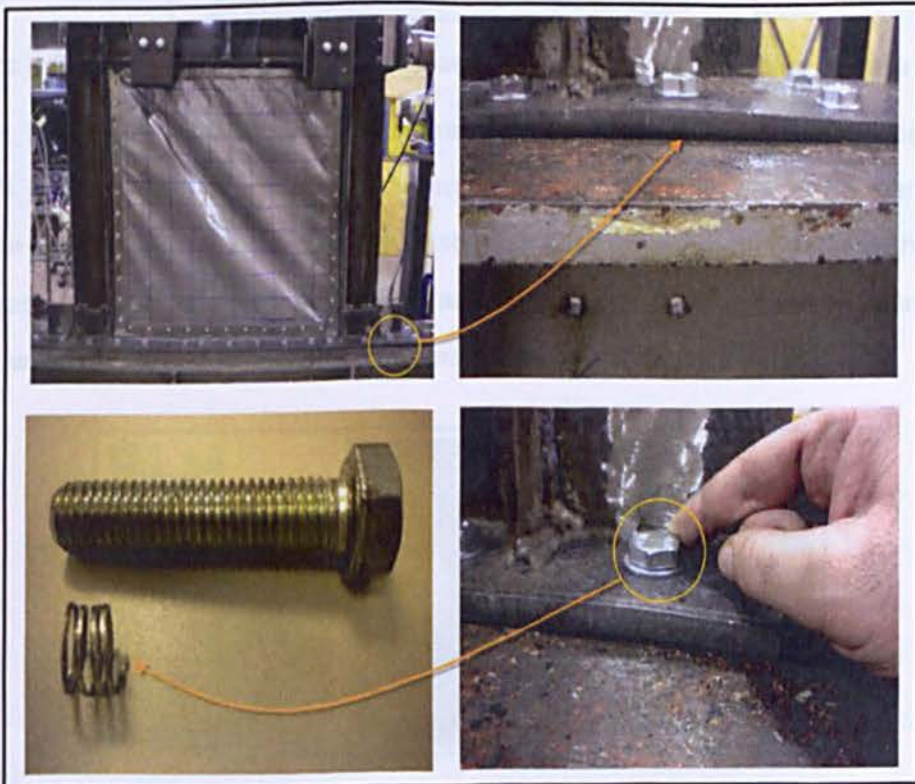


Figure 4.33: Occurrence of shear fracture in nut

CHAPTER 4: EXPERIMENTAL TEST SET UP

In light of the above considerations, two actions were taken. Utilising longer nuts (the minimum required length for nuts were calculated to be 16 mm length) which can prevent shear fracture in nuts grooves. In practice the length of available nuts was 40 mm. The second action was employing of clamp plates. Eight clamp plates were provided and were symmetrically attached to the reaction frame (Figure 4.34). These actions completely solved the uplift issues of base plates for all tests.

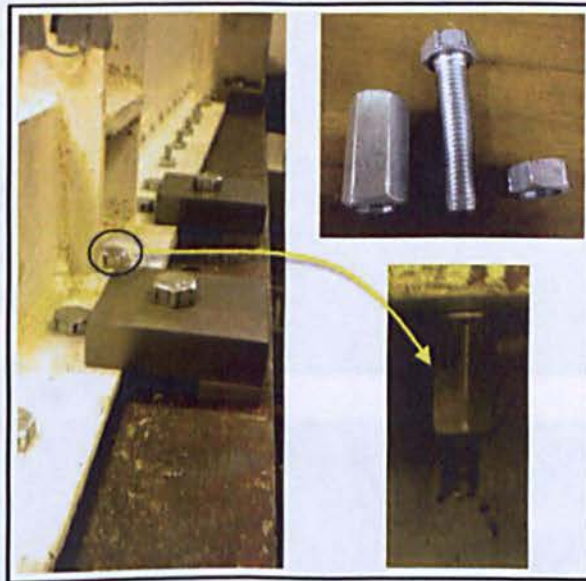


Figure 4.34: Utilising longer nuts and clamps precluded any uplifting of base plate

In order to provide stiff loading plate and to keep this plate entirely connected to column's outer flange precluding occurrence of any damage on welding particularly when the loading plate is loaded in tensile stage, a pair of rigid clamp plates with specific configuration were designed and manufactured. Figure 4.35 shows the damage of welding which occurred at final stage of tensile loading for trial specimen.



Figure 4.35: Utilising rigid clamp plates prevent damage of welding at location of connection between loading plate and column's outer flange

It was possible that the spindle of screw jack accidentally rotates during the loading period. In order to prevent this occurrence, an anti rotation hanger was designed and constructed. The hanger resisted any rotational freedom of spindle and could guarantee that no rotation could be applied to the test specimens. Figure 4.36 shows different parts of anti rotation hanger system.



Figure 4.36: Anti rotation hanger prevents any rotation to be applied to the test specimens

Based on maximum shear capacity of 0.675 mm thick steel plate, M6 bolts could transfer the shear loads between steel plate and fish plates. Using M6 connectors for trial specimen could not prevent premature stretching of steel plate at the connections of steel plate and fish plates (Figure 4.37). This is because utilising M6 bolts did not supply enough friction between steel plate and fish plates (main fish plates and secondary fish plates). As a result the decision was made to use M8 connectors instead of M6 for main tests, because pre-tensile capacity of M8 was enough to provide effective friction between connection plates.

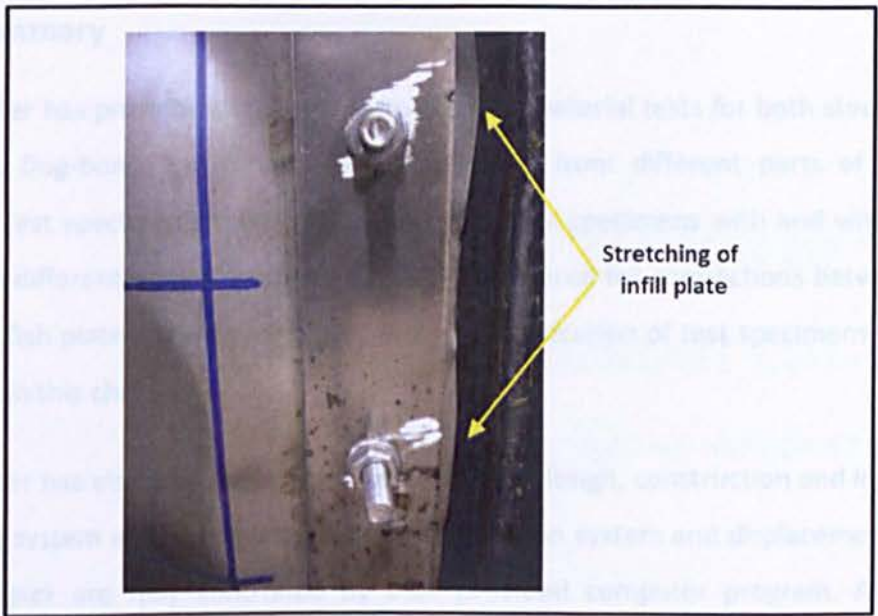


Figure 4.37: Premature stretching of steel plate at connections to the fish plates

In all test specimens, 46 eight millimetre HSFG bolts were used to connect the steel plates and fish plates. Trial specimen was loaded in accordance with ATC-24 protocol. The hysteresis behaviour of this specimen for cyclic loading test is shown in Figure 4.38.

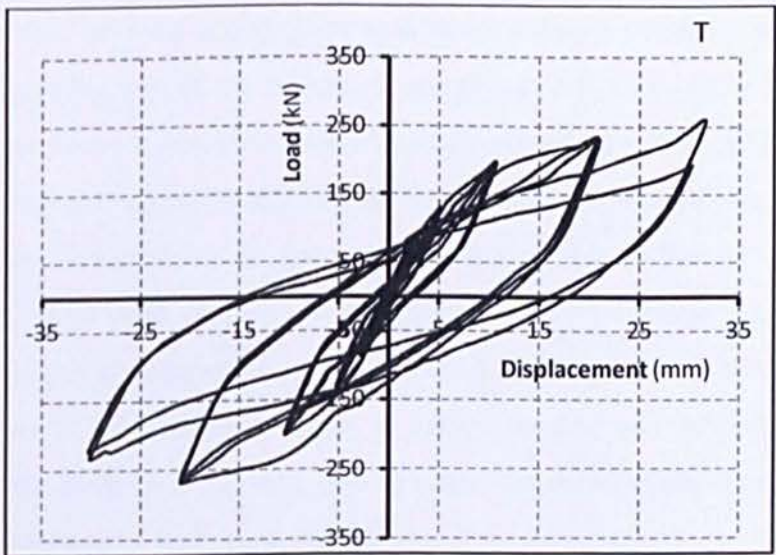


Figure 4.38: Hysteresis behaviour of Trial specimen

It is worth mentioning that although this graph is affected by uplifting of base plate, it gives a rough idea on main test specimen's behaviour. This test and corresponding results were useful to improve the test set up and the specimen's construction configuration.

4.13. Summary

This chapter has provided detailed information for material tests for both steel and FRP materials. Dog-bone specimens were constructed from different parts of universal sections. Test specimen's specifications are given for specimens with and without cut-outs. Two different types of connections are considered for connections between steel plate and fish plates. The welding procedure for fabrication of test specimens has been explained in this chapter.

This chapter has also provided brief information for design, construction and installation of loading system and lateral bracing. Data acquisition system and displacement control of screw jack are fully controlled by user provided computer program. A Siemens inverter provides required signals for geared motor to apply displacements dictated by user defined program which is defined based on ATC-24 protocol.

Finally this chapter has reviewed requirements for precise testing program via launching a cyclic test on a trial specimen.

5. SEISMIC BEHAVIOUR OF SPSW SYSTEMS WITHOUT CUT-OUTS

EXPERIMENTAL AND NUMERICAL STUDY

5.1. Introduction

This chapter comprises two main sections, quasi-static tests and FE analysis of SPSW specimens without cut-outs. The specimens to be tested were placed inside the reaction frame and were tightened to the bottom beam of reaction frame using 30 HSCG bolts and eight clamp plates. After application of a small warming up cycle of displacement to check the instrumentation and capturing zero reading for LDSs and CDSs, the main test proceeded. The quasi-static cyclic test on specimens provided detailed information on the stress flow and yield patterns in the steel plate and surrounding members, in addition to load and displacement data at specified locations. Due to the slow speed of testing, important observations related to failure modes was monitored. Ductility, stiffness, energy dissipation capacity, and strength degradation are some of the most important characteristics to be assessed.

The testing procedures and corresponding results for frame-only specimen and all other specimens without cut-outs are included in this chapter. Preliminary test specimen's analysis for estimating required power of screw jack is done for all tests. Experimental works are followed by FE analysis of the specimens.

5.2. Preliminary analysis of test specimens

Before starting testing of specimens, a preliminary nonlinear pushover analysis was performed by Abaqus software. As result of high demands to the computational analysis of steel shear, walls mainly due to shear buckling and local instabilities in the steel plate, monotonic loading was applied to estimate the envelope of load-displacement response

Based on the preliminary analysis, the capacity of specimens was estimated in the range of 150-350 kN. At ultimate capacity, the displacement at the top of the specimen, relative to the base, was estimated in the range of 25 to 35 mm.

5.3. Test results and discussion of frame-only specimen (F)

A moment resisting frame without steel plate with specifications given in Figure 5.1 was designed and constructed. Detail and specification of this frame remains the same for all test specimens.

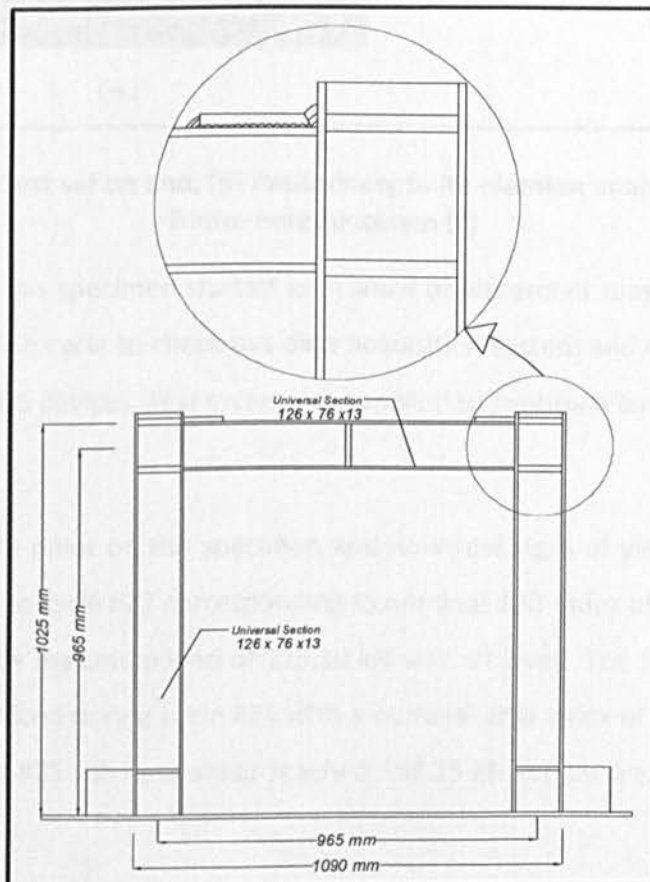


Figure 5.1: Specifications of frame-only specimen

5.3.1. Behaviour of frame-only specimen during the test

The moment-resisting frame, without the steel plate was constructed and subjected to the quasi-static cyclic load in accordance with ATC-24 protocol. Test set up for this specimen is shown in Figure 5.2-a. The preliminary push over analysis results (Figure 5.2-b) were used to estimate the capacity of the frame-only specimen.

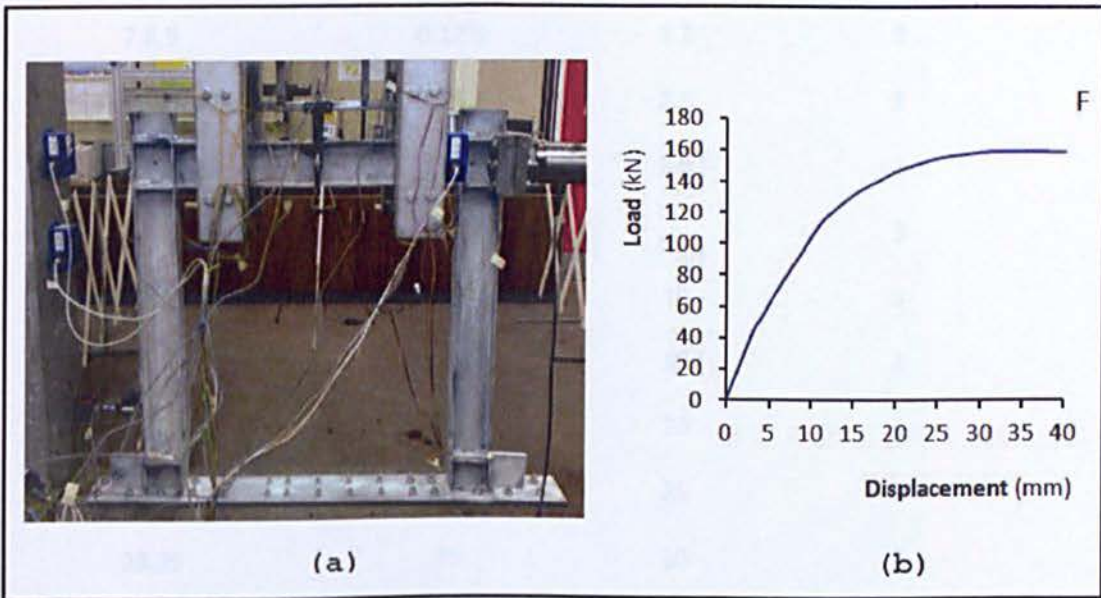


Figure 5.2: (a) Test set up and, (b) Preliminary finite element analysis results for frame-only specimen (F)

Test program for this specimen started with small displacement magnitude of 0.2 mm. This is a warming up cycle to check out data acquisition system and taking zero reading for all LVDT and CDS devices. Test cycles were applied to specimen based on magnitudes given in 5.1.

No flaking of white paint on the specimen and no visual signs of yielding of specimen were observed up to cycle #23 corresponding to nominal drift index of 1.5%. At this level of displacement the maximum load of 125.10 kN was achieved. The first significant sign of yielding was noticed during cycle #24 with a nominal drift index of 19.41 mm. During the cycles #24 and #25 the base shear reached 148.25 kN corresponding to storey drift of 20 mm.

5.1: Loading amplitudes used for quasi-static test of frame-only specimen in accordance with ATC-24 protocol

Test Cycle	Nominal Drift Index	Nominal Displacement (mm)	Number of Input Cycles
1,2,3	0.04%	0.4	3
4,5,6	0.08%	0.8	3
7,8,9	0.12%	1.2	3
10,11,12	0.25%	2.5	3
13,14,15	0.35%	3.5	3
16,17,18	0.5%	5	3
19,20,21	1%	10	3
22,23	1.5%	15	2
24,25	2%	20	2
26,27	2.5%	25	2
28,29	3%	30	2
30,31	3.5%	35	2
32	4%	40	1

During the cycles #26 and #27 with a nominal drift index of 2.4% an appearance of plastic hinges was noticed at the bottom of the right column. Audible cracking sounds were heard from specimen during cycle #28 and further investigation revealed a fracture in the weld of the column-to-base plate stiffener (Figure 5.3).

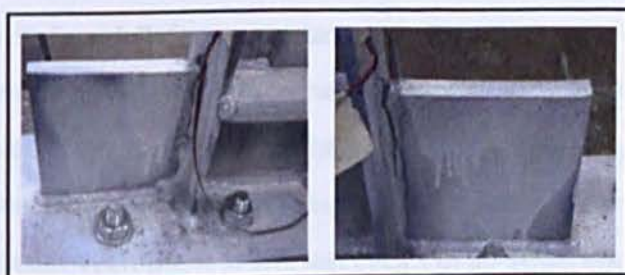


Figure 5.3: Fracture in the weld connection of column-to-base plate stiffeners at both columns of the frame-only specimen

At cycle #29 (a nominal drift index of 3%) a maximum load of 159.2 kN was achieved. During the cycles #30 and #31 with a nominal drift index of 3.5% a maximum shear load of 155.77 kN was reached. Cycle #32 was the last cycle with drift index of 40 mm applied to specimen. A maximum base shear of 151.66 kN was achieved during this cycle. Plastic hinges were fully developed at the bottom of both columns (Figure 5.4).

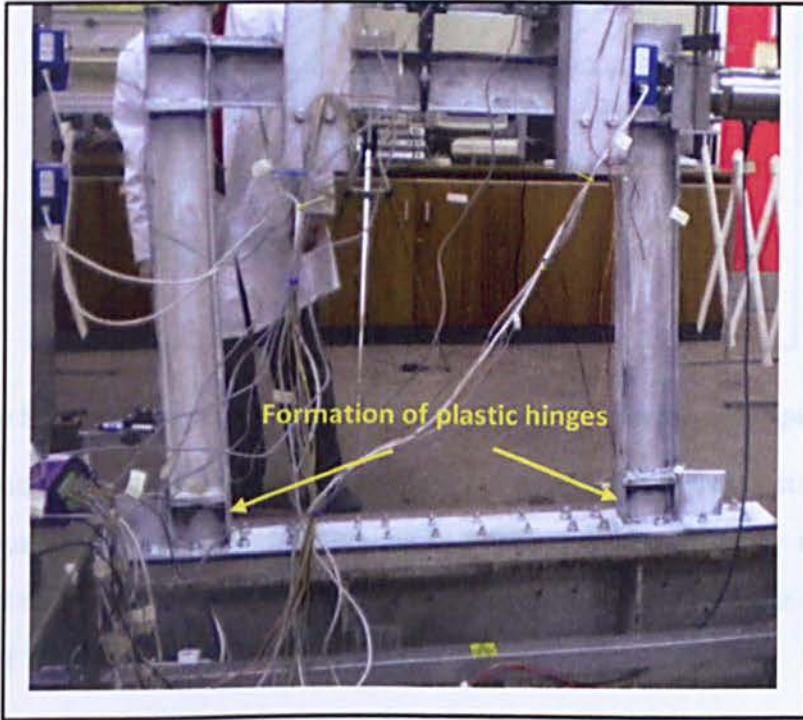


Figure 5.4: Plastic hinges were noted at the bottom of both columns

5.3.2. Load displacement behaviour of frame-only specimen

Figure 5.5 illustrates the hysteretic behaviour of F specimen recorded during the quasi-static test. The specimen was cyclically loaded with gradually increasing displacement magnitudes shown in **Error! Reference source not found.**. During the test program a maximum displacement of 40 mm was achieved prior to termination of the test. The maximum load achieved for each cycle of the same storey drift dropped a little for the first few set of cycles. However, at higher displacement levels the strength degradation was more noticeable between the first and last cycles of an equal displacement.

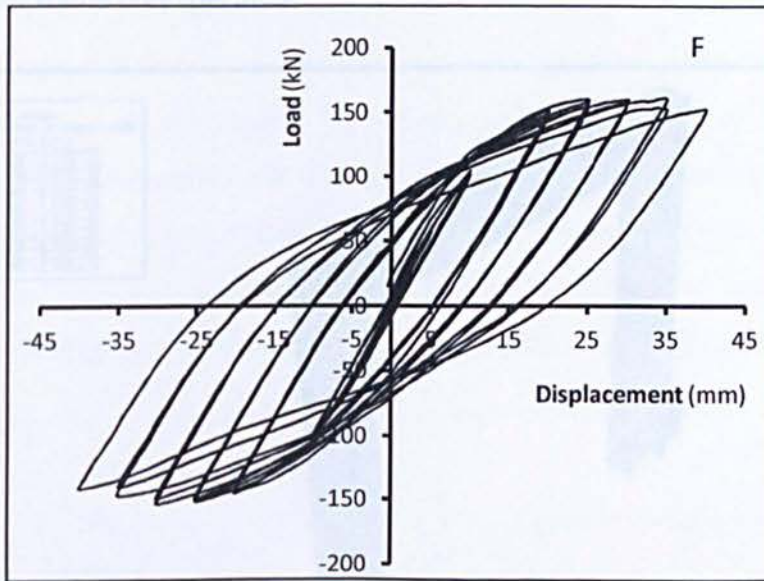


Figure 5.5: Testing results for hysteresis behaviour of frame-only specimen

From the load-displacement diagram illustrated in Figure 5.6, the frame started to yield at a shear load of 108.07 kN corresponding to adrift of 8.54 mm storey displacement and reached total yield by developing plastic hinges at the bottom of the columns at a shear load of 159.62 kN with a storey displacement of 35 mm.

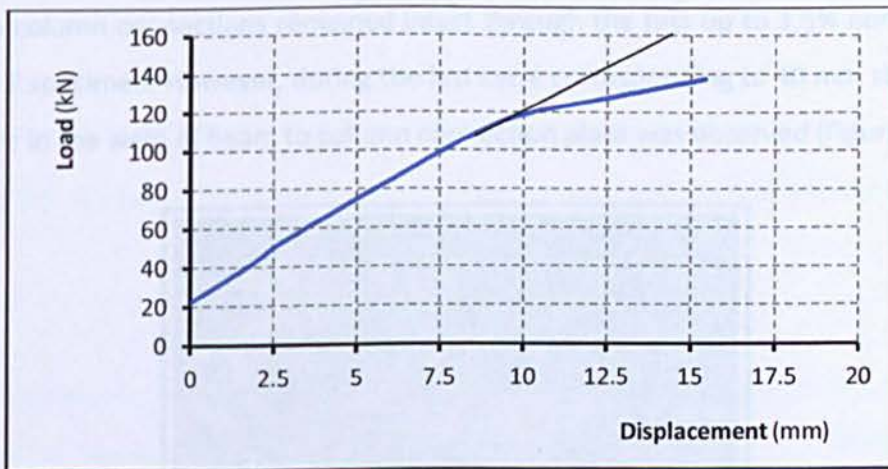


Figure 5.6: Yield point of frame-only specimen based on Load-displacement diagram

Based on data from strain gauges, the columns reached yielding plateau and developed plastic hinges. These hinges formed at the positions predicted by the FE analysis. The beam section did not experience any deformation and no visual yielding was observed.

Counter graph based on von Misses stress distribution and corresponding scale is shown in Figure 5.7 for frame only specimen.

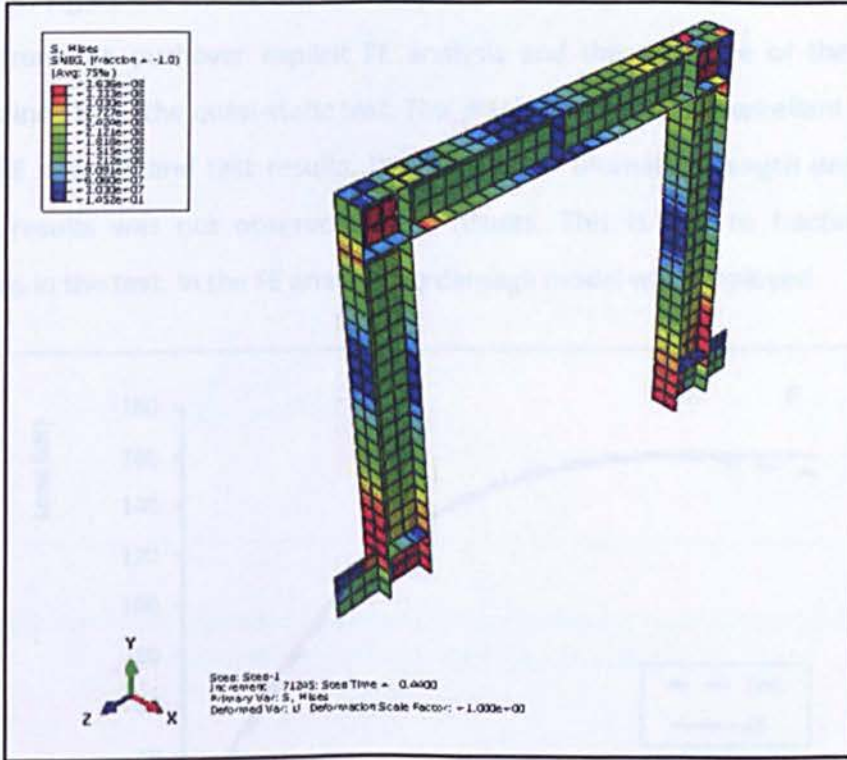


Figure 5.7: Formation of plastic hinges at the bottom of columns as was estimated by FEA results

Beam to column connections remained intact through the test up to 3.5% nominal drift index of F specimen. However, during the last cycle corresponding to 40 mm storey drift a fracture in the weld of beam to column connection plate was observed (Figure 5.8).



Figure 5.8: Fracture in weld of beam to column connection plate during the last cycle of testing for frame-only specimen

5.3.3. Finite Element Analysis for frame-only specimen (F)

Numerical model of tested specimen was performed based on the procedure described in chapter 3. Figure 5.9 shows the load-displacement diagram of open frame specimen obtained from the pushover explicit FE analysis and the envelope of the hysteresis curves attained from the quasi-static test. This diagram indicates an excellent agreement between FE analysis and test results. Degradation of ultimate strength demonstrated with test results was not observed in FE results. This is due to fracture in weld connections in the test. In the FE analysis no damage model was employed.

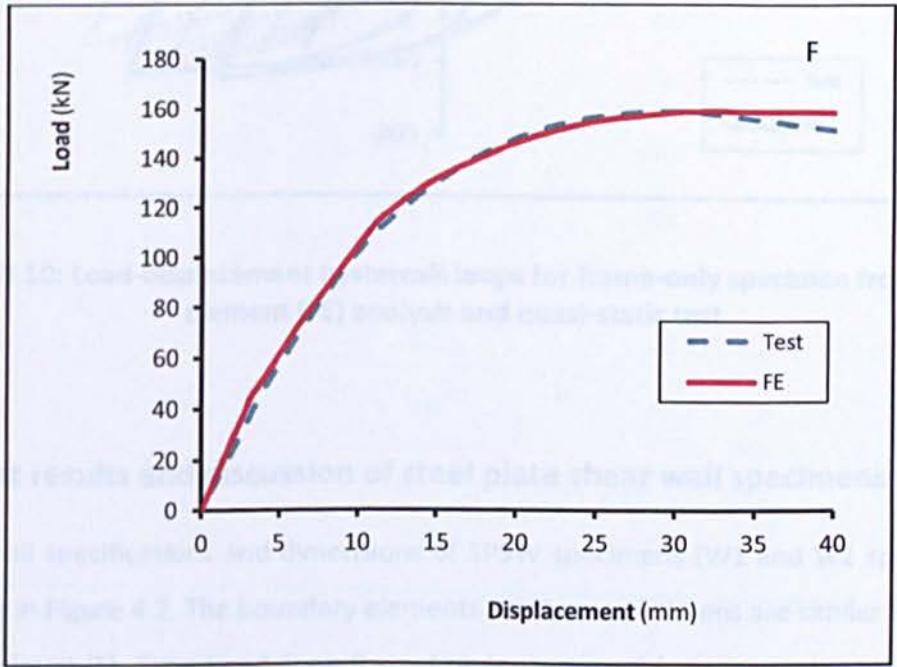


Figure 5.9: Pushover finite element load-displacement results and test quasi-static response for frame-only specimen

The load-displacement hysteresis curves of FE analysis and quasi-static test results are compared in Figure 5.10. This figure indicates a gradual reduction on stiffness of the system after each cycle in test results. This reduction was not observed in FE model as no damage model was used in the FE model and effects of residual stresses ignored.

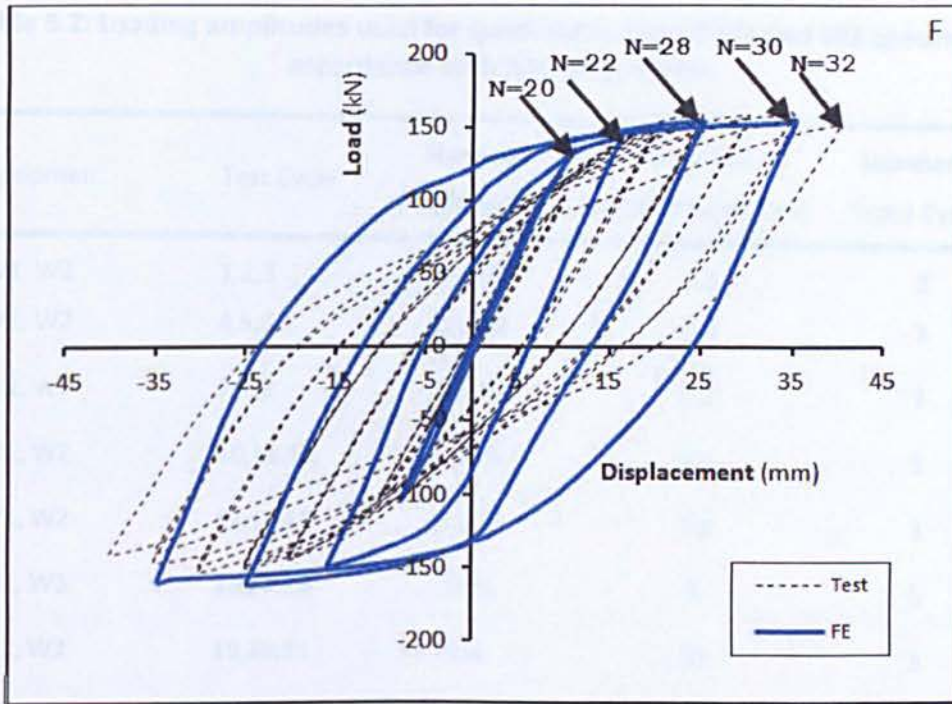


Figure 5.10: Load-displacement hysteresis loops for frame-only specimen from finite element (FE) analysis and quasi-static test

5.4. Test results and discussion of steel plate shear wall specimens

The overall specifications and dimensions of SPSW specimens (W1 and W2 specimens) are given in Figure 4.2. The boundary elements for these specimens are similar to frame-only specimen (F). Type I and Type II steel plates are used for construction of W1 and W2, respectively. Each steel plate is connected to fish plates using M8 bolts for both specimens. The only difference between W1 and W2 is the thickness of steel plates. The cyclic displacement loads with different amplitudes were applied to specimens in accordance with ATC-24 protocol. As shown in Table 5.2 both specimens are subjected to the same loading history up to nominal drift index of 3.5%. The maximum loading capacity of 249.13 kN and 275.14 kN was gained for W1 and W2 specimen during the amplitude of 30 mm, respectively.

Table 5.2: Loading amplitudes used for quasi-static test of W1 and W2 specimens in accordance with ATC-24 protocol

Specimen	Test Cycle	Nominal Drift Index	Nominal Displacement (mm)	Number of Input Cycles
W1, W2	1,2,3	0.04%	0.4	3
W1, W2	4,5,6	0.08%	0.8	3
W1, W2	7,8,9	0.12%	1.2	3
W1, W2	10,11,12	0.25%	2.5	3
W1, W2	13,14,15	0.35%	3.5	3
W1, W3	16,17,18	0.5%	5	3
W1, W2	19,20,21	1%	10	3
W1, W2	22,23	1.5%	15	2
W1, W2	24,25	2%	20	2
W1, W2	26,27	2.5%	25	2
W1, W2	28,29	3%	30	2
W1	30	3.5%	35	1
W2	30,31	3.5%	35	2

5.4.1. Test results and discussion of W1 specimen

The W1 specimen is constructed with 0.675 mm thick steel plate. Figure 5.11-a shows general view of test set up and connection of specimen to the reaction frame. The preliminary FE analysis of this specimen gives estimation on monotonic behaviour of W1 as illustrated in Figure 5.11-b. According to this graph the maximum capacity of specimen is estimated to be about 280 kN.

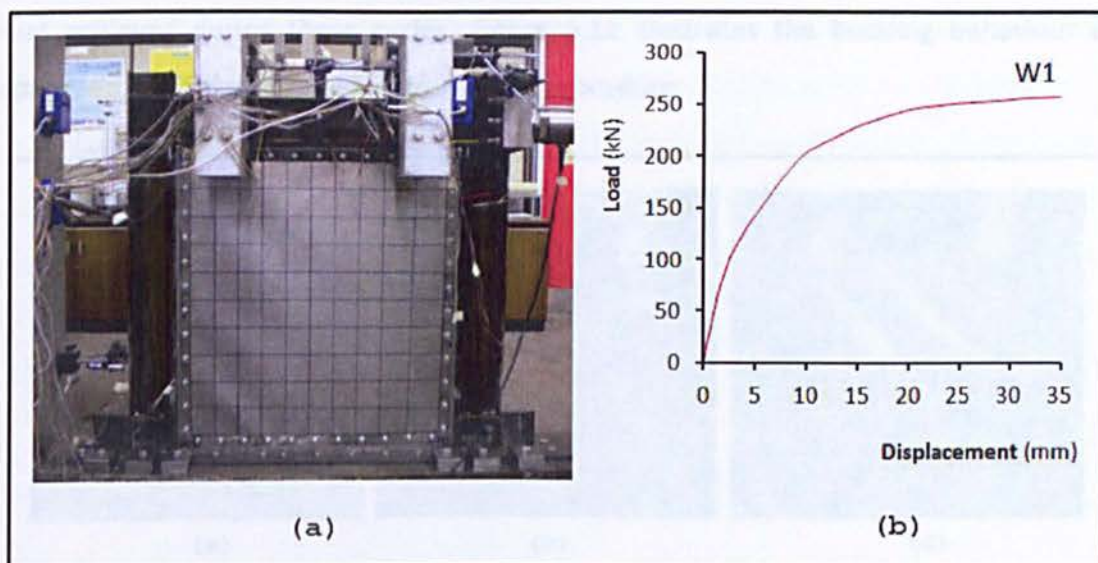


Figure 5.11(a) Test set up and, (b) Preliminary finite element analysis results for W1 specimen

5.4.1.1. Behaviour of W1 during the test

The response of specimen up to a nominal drift index of 0.12% was linear. During these nine cycles no visual sign of steel plate buckling was observed. During cycles #7 to #9 formation of diagonal tension field was noted within the steel plate. The first cycle that followed elastic buckling and minor sign of yielding within the steel plate was cycle #10. During cycles #10 to #12 the base shear reached 84.89 kN corresponding to nominal drift index of 0.25%. Considerable elastic buckling deformation was observed during cycles #13 to #15. A maximum shear load of 106.97 kN was achieved corresponding to maximum storey drift of 3.5 mm.

During cycles #16 to #18 plate popping noises were heard. All three cycles of 5 mm displacement amplitude were accompanied with plate popping sound as the specimen passed through its initial position. Visible stretching at the centre of the steel plate was observed and a maximum base shear of 134.76 kN was reached during these cycles. At the nominal drift index of 1% including cycles #19 to #21 a distinct tension field and extensive yielding developed within the steel plate. A maximum base shear of 195.14 kN

was achieved during these cycles. Figure 5.12 illustrates the buckling behaviour of specimen at different stages of the loading procedure.

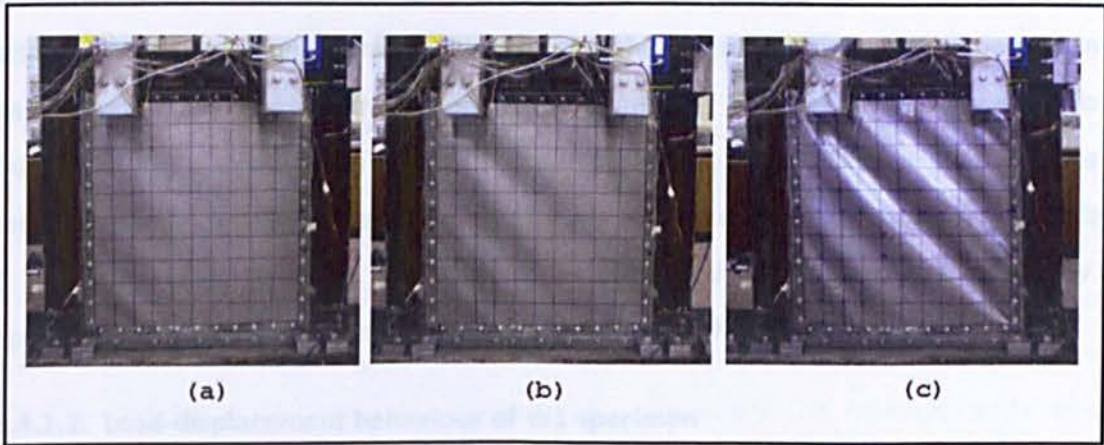


Figure 5.12: W1 (a) after the first nine cycles (b) in cycle #14 considerable elastic deformation (c) in cycle #20 distinct tension field and extensive yielding of steel plate

At the nominal drift index of 1.5% including cycles #22 and #23 a fracture in the weld of the fish plate to right column connection was observed. A maximum base shear load of 232.03 kN was gained for this amplitude. During cycles #24 and #25 the length of weld fracture was extended to 30% of the length of column. Figure 5.13 shows fracture of weld connection between fish plate and right column. During these cycles the base shear reached 246.93 kN corresponding to a nominal storey drift of 2%.

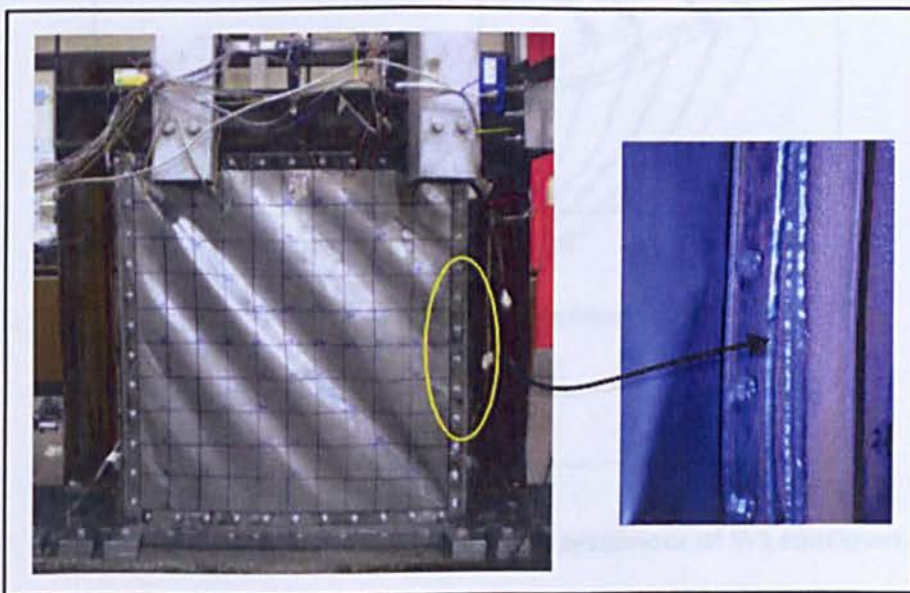


Figure 5.13: Weld fracture of connection between fish plate and right column for W1 specimen

A plastic hinge was first noted at the bottom of the left column during cycle #26. Plastic hinge was also noted at the bottom of right column during cycle #27. A maximum base shear of 250.40 kN corresponding to storey drift of 25 mm was reached. Plastic hinges also developed at all four corners of the columns during cycles #28 and #29. A maximum base shear of 249.13 kN corresponding to nominal drift index of 3% was achieved for this amplitude. The specimen during cycle #30 sustained 243.04 kN shear load. The test terminated due to development of plastic hinges at both ends of the columns. Appendix B gives the stress analysis results of steel plate and boundary members for W1 specimens. This figure illustrates the yield of columns at the bottom part.

5.4.1.2. Load-displacement behaviour of W1 specimen

The relation between storey shear and storey drift (load-displacement relation) is a key point for investigating the behaviour of cyclically loaded systems. Figure 5.14 illustrates the hysteresis behaviour recorded during the quasi-static test for W1 specimen. As shown in this figure the hysteresis loops are stable and robust. A maximum base shear of 249.13 kN corresponding to storey drift of 30 mm was achieved prior to termination of the test.

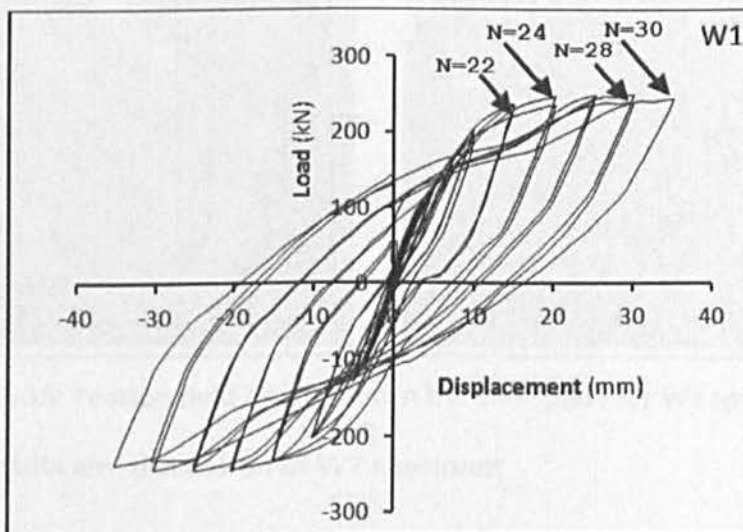


Figure 5.14: Testing results for hysteresis behaviour of W1 specimen

The steel plate began to exhibit first yield at approximately 165 kN corresponding to a 7.5 mm displacement drift. The steel plate then yielded completely at approximately

203 kN corresponding to a 10 mm storey drift. The maximum out-of-plane buckling of specimen reached 25 mm corresponding to a 20 mm storey drift. The W1 specimen withstood a total load level of 249.13 kN and storey drift of 35 mm. The test was halted once the plastic hinges developed at all four bottom corners of columns.

The inclination angle of the tension field in the steel plate was obtained by measuring the angle at the crest of the buckle waves (relative to the vertical) by assuming that the angle of inclination corresponded to the orientation of the buckle waves. Since the SPSW specimen's response exhibited minor unsymmetrical behaviour, the inclination angle of tension field was measured as the load was applied in each direction and the average was taken to obtain the tension field orientation. The measurements were conducted at nominal drift indices of 0.25%, 0.5% and 1%. Figure 5.15 provides a scheme of the buckles for both pulling and pushing of W1 at nominal drift index of 0.5%. The measured orientation of the tension field at nominal drift indices of 0.25%, 0.5% and 1% were in the range from 41° to 43°.

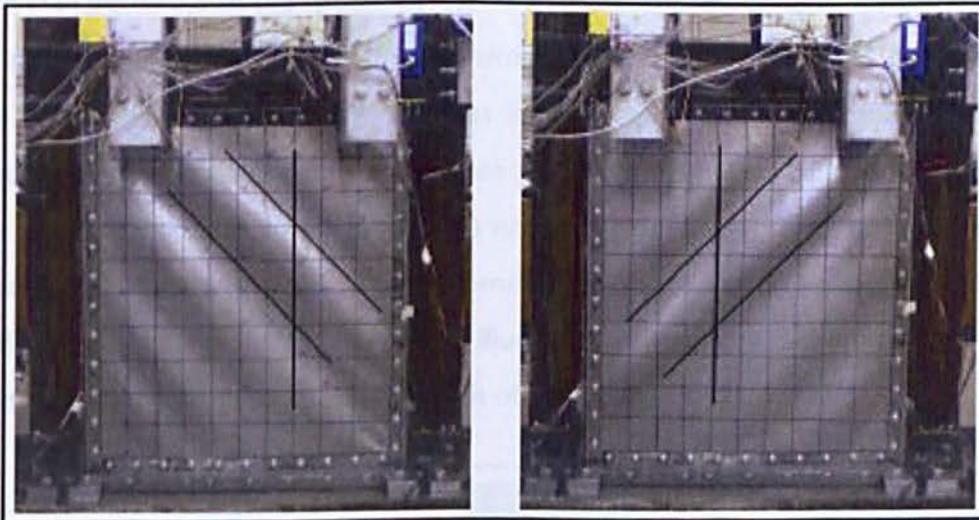


Figure 5.15: Tension field orientation in the steel plate for W1 specimen

5.4.2. Test results and discussion of W2 specimen

The only difference between W1 and W2 is type of steel plate. For construction of W2 specimen the type II steel plate with thickness of 1.4 mm is utilised. The other specifications and loading history of specimen except the last cycle is similar to W1 specimen. Figure 5.16 shows general view of test set up and preliminary FE results for

W2 respectively. Based on these results a maximum base shear of 280 kN is estimated for final stage of loading for this specimen.

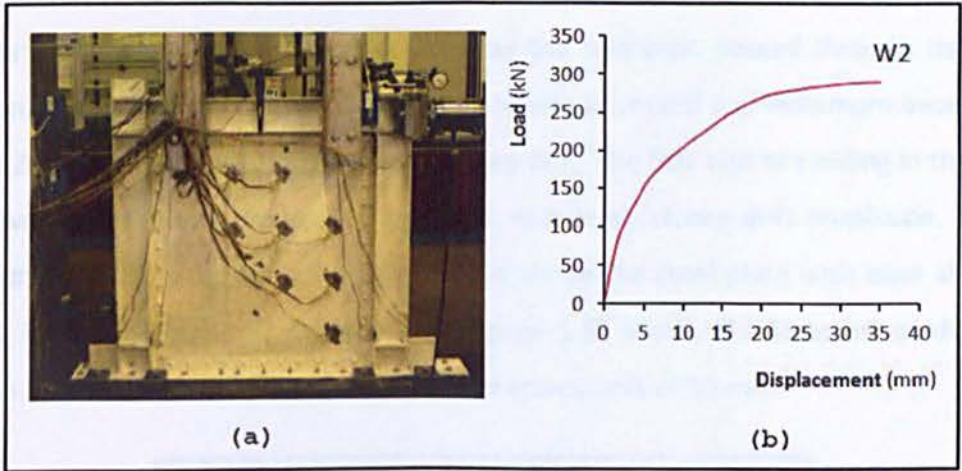


Figure 5.16: (a) Test set up and, (b) Preliminary finite element analysis results for W2 specimen

5.4.2.1. Behaviour of W2 specimen during the test

The overall behaviour of W2 specimen is similar to W1. The response of specimen during the first nine cycles was linear with a maximum base shear of 53.94 kN. No flaking of white paint which could be considered as indication for plastic deformations on the boundary members and steel plate was observed. During the cycles #10 to #12 the base shear reached 90.63 kN corresponding to nominal drift index of 0.25%. Formation of diagonal tension fields and initial noises produced as result of steel plate buckling was noted during this amplitude. Figure 5.17 illustrates initiation of diagonal tension field within the steel plate during the storey drift of 2.5 mm.

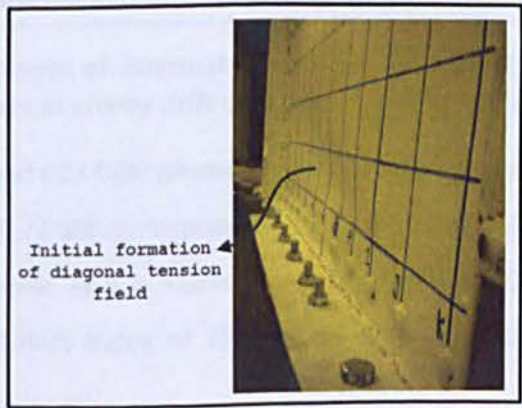


Figure 5.17: positioning of diagonal tension field within the steel plate for W2

CHAPTER 5: SEISMIC BEHAVIOUR OF SPSW SYSTEMS WITHOUT CUT- OUTS

Considerable elastic buckling deformation was observed during cycles #13 to #15 with maximum shear load of 111.13 kN and storey drift of 3.5 mm. During the third cycle of this amplitude flaking of white paint was noted on the steel plate. During cycles #16 to #18 very loud popping noises were heard as the specimen passed through its initial position. Diagonal stretching of the steel plate was observed and maximum base shear of 138.26 kN was achieved for the 5 mm storey drift. The first sign of yielding in the steel plate was noted during cycles #17 and #18 with 5mm storey drift amplitude. During cycles #19 to #21 extensive yielding occurred within the steel plate with base shear of 206.92 kN at nominal drift index of 1%. Figure 5.18 shows development of diagonal tension field and deformation of steel plate at storey drift of 10 mm.

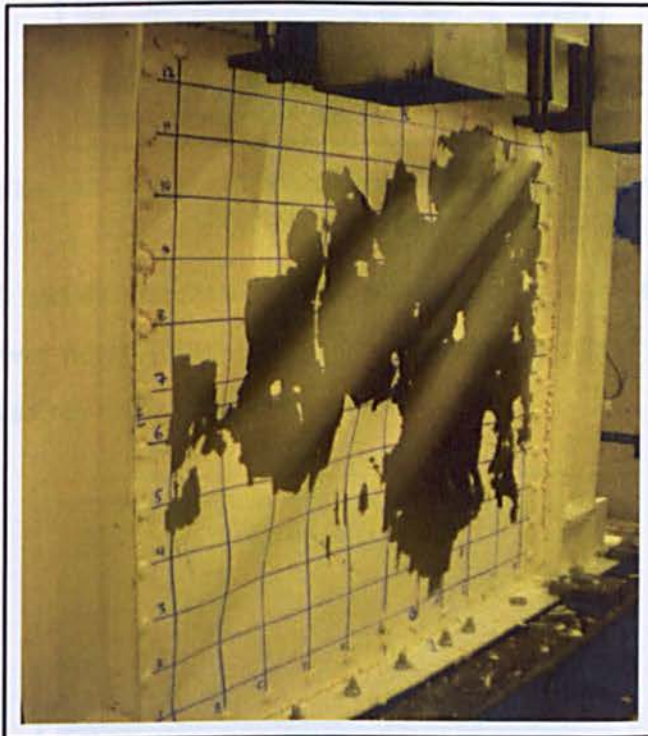


Figure 5.18: Development of diagonal tension field and yield zone within the steel plate at storey drift of 10 mm for W2 specimen

During the cycles #22 and #23 fully plastic behaviour was observed in the steel plate and base shear reached 246.73 kN corresponding to 15 mm storey drift. Cycles #24 and #25 were applied to specimen and a maximum base shear 267.62 kN was achieved for corresponding nominal drift index of 2%. Out of plane buckling deformation of steel

plate was extensively increased during these cycles (Figure 5.19). An investigation of connections revealed that up to 20 mm storey drift all weld connections were intact.

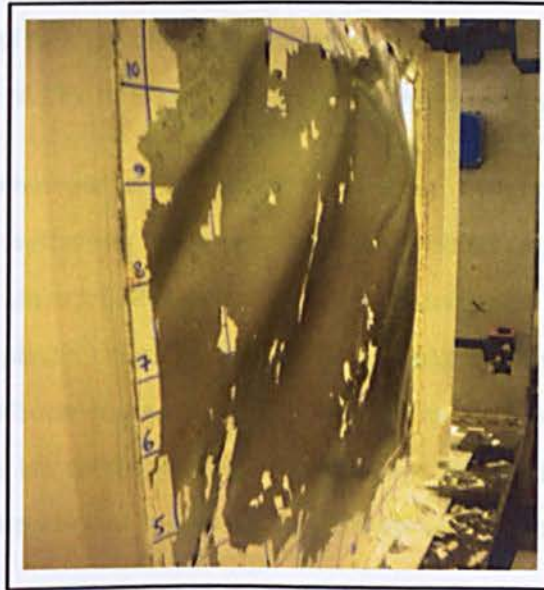


Figure 5.19: Massive out-of-plane deformation of steel plate at storey drift of 20 mm for W2 specimen

During cycles #26 and #27 fracture of weld connection between base plate and left column stiffener was noted (Figure 5.20). A maximum base shear of 276.53 kN was reached at 25 mm storey drift during these cycles.

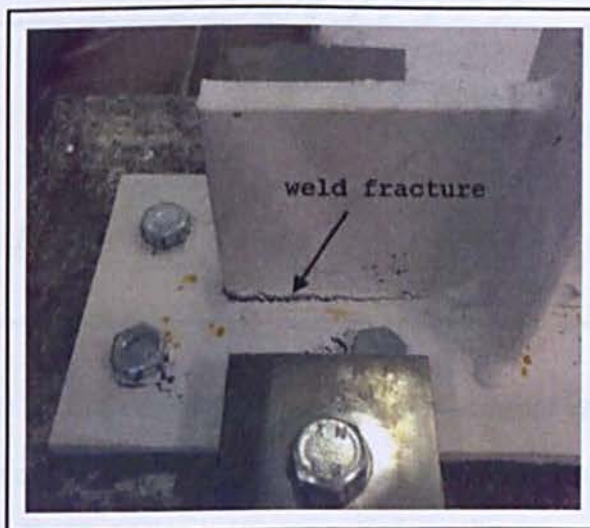


Figure 5.20: Fracture of weld connection between base plate and left column stiffener at a nominal drift index of 2.5% for W2

CHAPTER 5: SEISMIC BEHAVIOUR OF SPSW SYSTEMS WITHOUT CUT- OUTS

Formation of plastic hinges at the bottom of columns was noted first time during cycles #28 and #29 corresponding to nominal drift index of 3%. A maximum base shear of 280.55 kN was reached during these cycles. During the next amplitude with storey drift of 35 mm formation of fully plastic hinges developed at all four corners of the column. A maximum base shear of 275.14 kN was achieved for this amplitude.

Load-displacement behaviour of W2 which is recorded during the quasi-static test is given in Figure 5.21. Hysteresis loops are stable and robust during the test procedure and a maximum base shear of 280.55 kN was reached during 30 mm storey drift. Due to development of fully plastic hinges at the bottom of columns, the maximum base shear capacity for next amplitude decreased to 275.14 kN. The steel plate began to yield first at approximately 135 kN corresponding to a 4.9 mm storey displacement. The steel plate then yielded completely at approximately 190 kN corresponding to 9 mm drift.

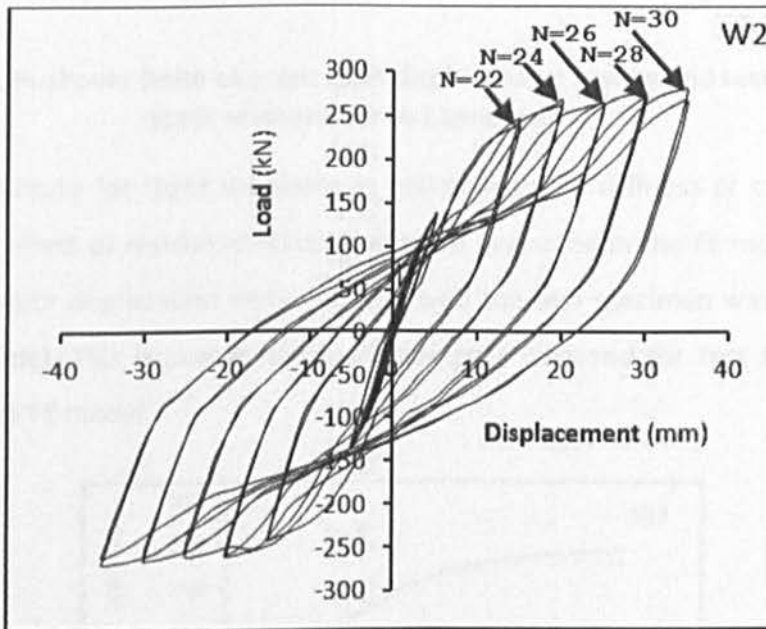


Figure 5.21: Testing results for hysteresis behaviour of W2 specimen

The inclination angle of the tension field was obtained similar to measurement done for W1. In other words these angles were measured as the load was applied in each direction and the average was taken to obtain the tension field orientation. The measured orientation of the tension field at nominal drift indices of 0.25%, 0.5% and 1% were in the range from 38° to 40° for W2.

5.4.3. Finite element analysis of W1 and W2 specimens

Figure 5.22 and Figure 5.23 show the load-displacement diagram of the W1 and W2 specimens obtained from the pushover explicit analysis and the envelope of the hysteresis curves attained from the quasi-static test. Figure 5.22 and Figure 5.23 show that that FE models provide adequate prediction of the stiffness of both specimens.

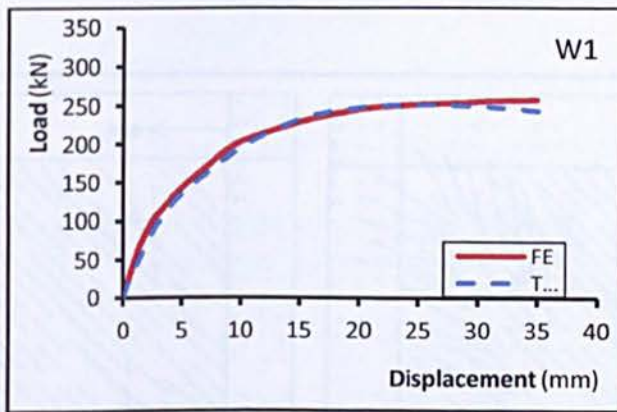


Figure 5.22: Pushover finite element load-displacement results and test quasi-static response for W1 specimen

One possible cause for slight variations in estimating wall stiffness or overall capacity could be the effect of residual stresses that were neglected in the FE model. The post-ultimate strength degradation demonstrated with the test specimen was not observed in the FE model. This is due to the weld fractures occurred for test specimens not included in the FE model.

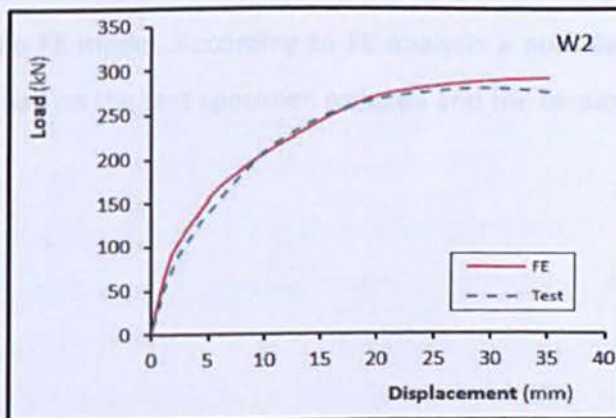


Figure 5.23: Pushover finite element load-displacement results and test quasi-static response for W2 specimen

Once the W1 and W2 models were loaded up to the yielding load of the steel plate, the vector plot of the maximum in-plane principal stresses at the mid-surface of their elements were extracted and they are plotted in Figure 5.24. Angles measured from the vector plot range from 38° to 45°. The inclination angle of tension field at yield point of steel plate during the test ranged from 41° to 43°. The angle of inclination of the tension field predicted using Eq. (2.4) was 42.30° and 40.77° for W1 and W2 specimens, respectively.

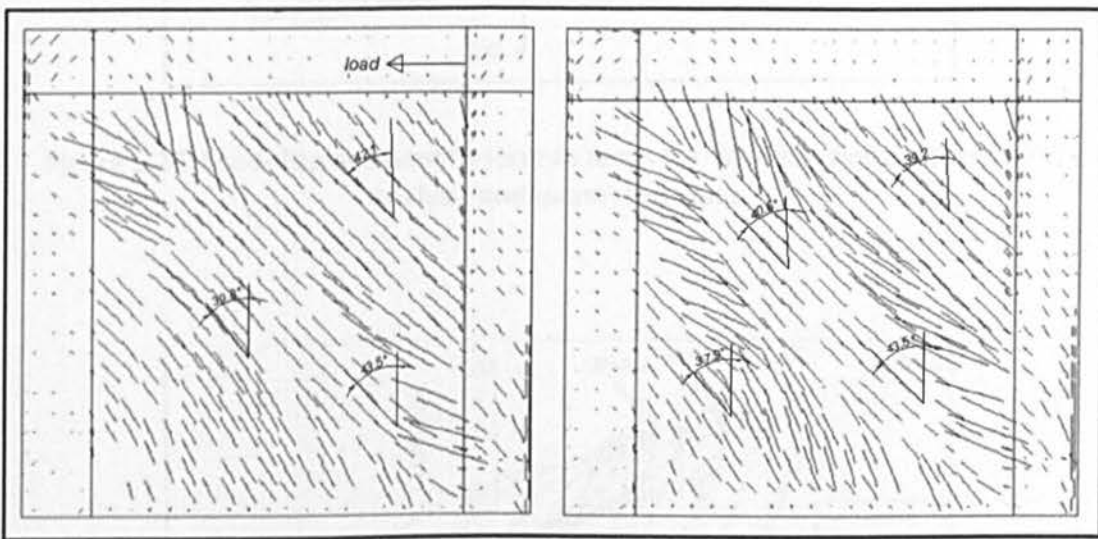


Figure 5.24: In-plane maximum principle stresses at the mid-surface of the elements of W1 (left) and W2 (right) at the applied drift of 10 mm

The load-displacement hysteresis results of both FE analysis and quasi-static test are shown in Figure 5.25 and Figure 5.26. A notable stiffness reduction occurred during the reloading phase until development of the tension field in the steel plate. This behaviour was simulated in the FE model. According to FE analysis a notable change in stiffness occurred once the load on the test specimen reduced and the tension field of steel plate had disappeared.

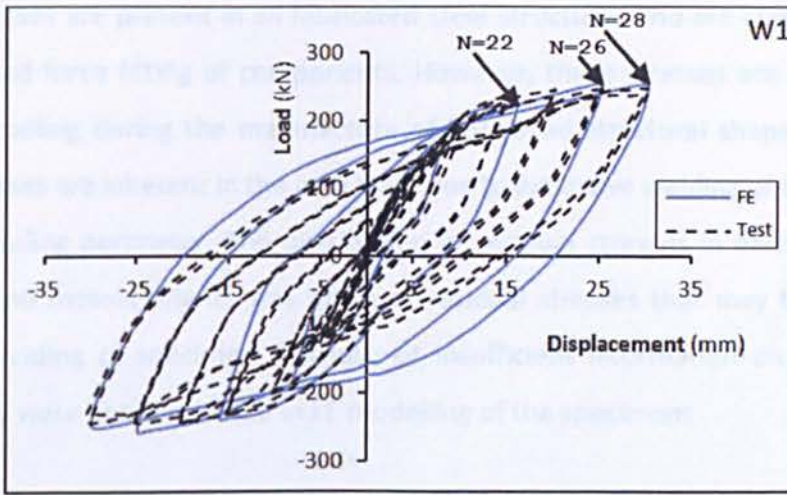


Figure 5.25: Load-displacement hysteresis loops for W1 from finite element (FE) analysis and quasi-static test

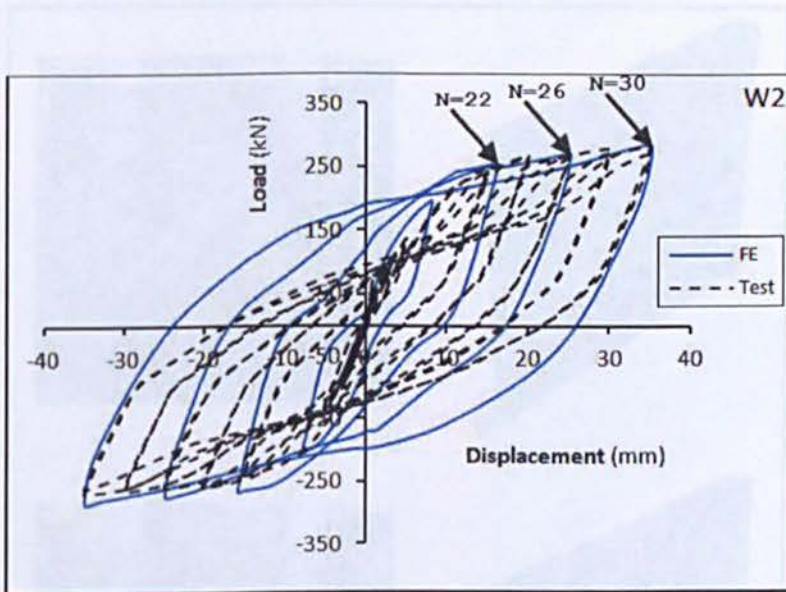


Figure 5.26: Load-displacement hysteresis loops for W2 from finite element (FE) analysis and quasi-static test

The FE models reasonably captured the cyclic performance of each specimen. Gradually increasing differences were noted between the test results and FE response once drift value increased beyond 2%. This is due to development of weld fractures in the specimens. Considering that the size of these cracks increased with loading cycles, a gradual stiffness reduction was observed in the experimental responses which FE model did not simulate.

Residual stresses are present in all fabricated steel structures and are commonly result of welding and force fitting of components. However, these stresses are also result of differential cooling during the manufacture of hot-rolled structural shapes. Significant residual stresses are inherent in the infill plate due to extensive welding of the infill plate to its surrounding perimeter. The distribution of residual stresses in each specimen is complex, so no measurements was taken of residual stresses that may have resulted from each welding of specimen. Because of insufficient information on the residual stresses, they were not considered in FE modelling of the specimens.

The deformed configuration of the W1 and W2 specimens at full development of the tension field during loading and neutral state of each specimen is compared to that of the FE results in Figure 5.27 and Figure 5.28

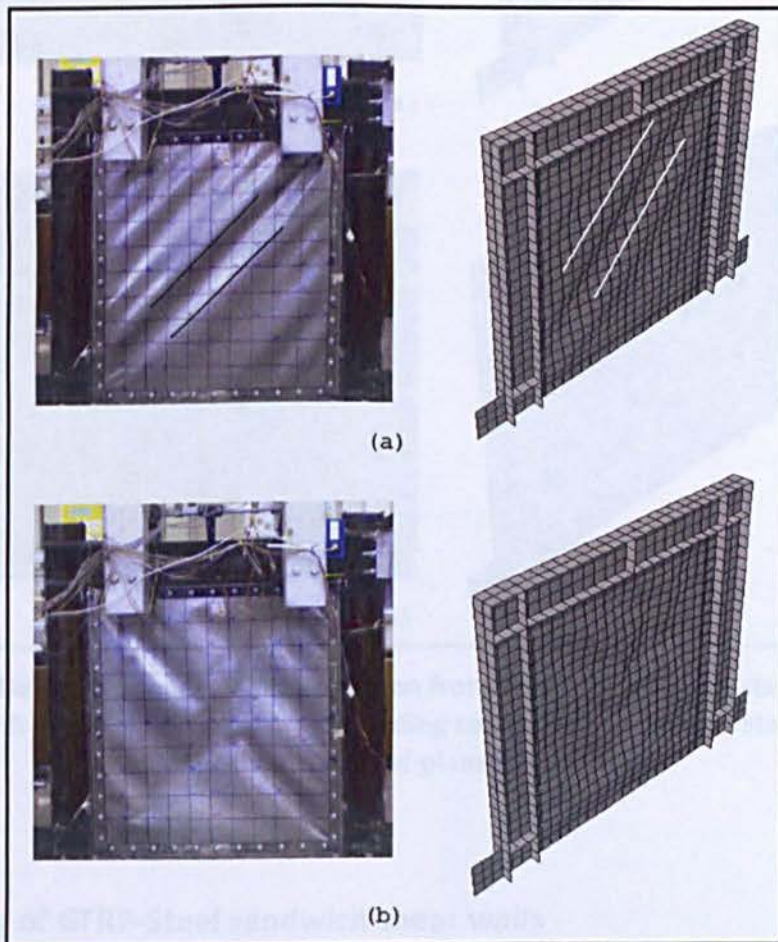


Figure 5.27: Deformed shape of W1 specimen from analysis and quasi-static test at the nominal drift index of 2% cycle, (a) for loading toward (b) for neutral state including steel plate with out-of-plane deformation

The deformed shapes obtained from FE analysis were similar to those observed during the quasi-static tests. The deformed configuration and number of buckle waves of the steel plate were similar for both FE and test results.

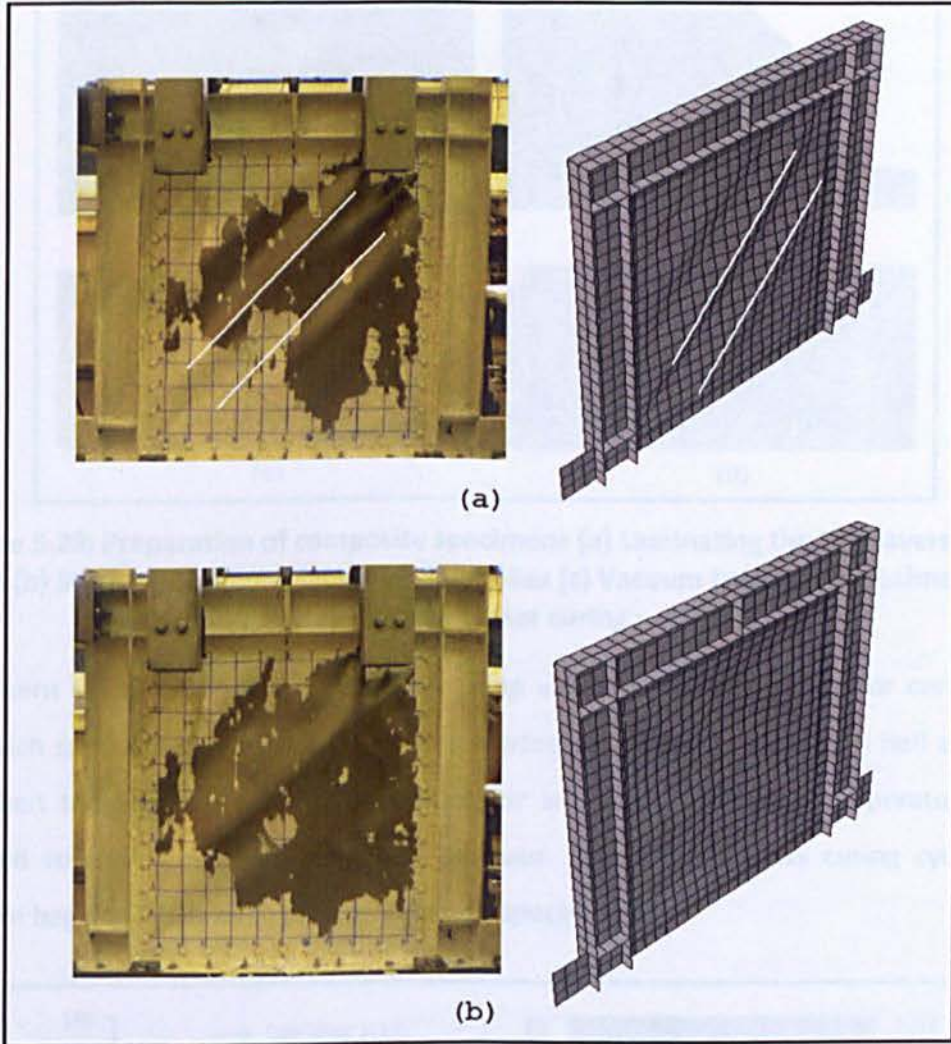


Figure 5.28: Deformed shape of W2 specimen from analysis and quasi-static test at the nominal drift index of 2% cycle, (a) for loading toward (b) for neutral state including steel plate with out-of-plane deformation

5.5. Testing of GFRP-Steel sandwich shear walls

GFRP-steel Sandwich Shear Wall (GSSW) was manufactured by laminating unidirectional glass fibres to the steel plate. During manufacturing of sandwich plates both sides of

CHAPTER 5: SEISMIC BEHAVIOUR OF SPSW SYSTEMS WITHOUT CUT- OUTS

steel plate were cleaned by acetone and then the GFRP plies (MULTIPREG E722) laid down on both sides of steel plate. Figure 5.29 shows stacking of second layers of GFRP ply and vacuum bagging technique for manufacturing of sandwich specimen.

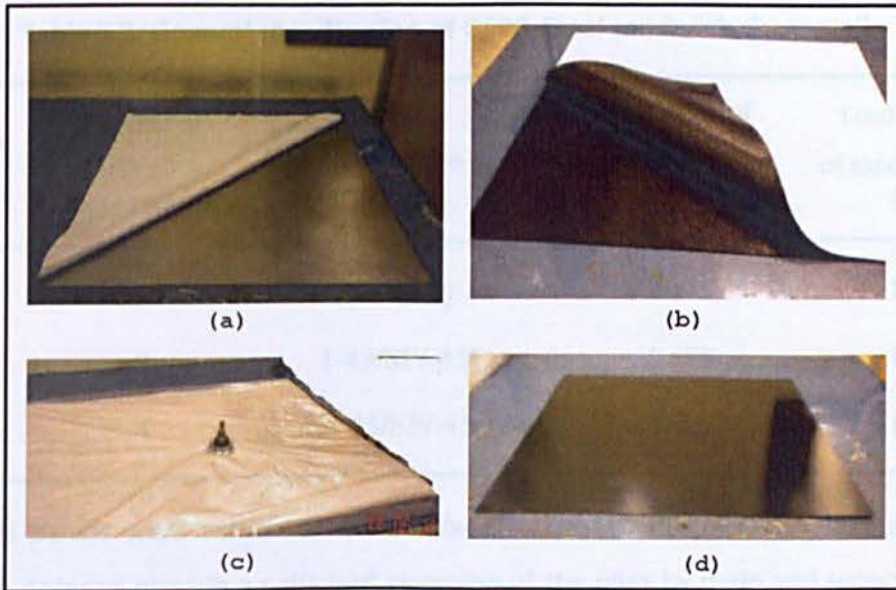


Figure 5.29: Preparation of composite specimens (a) Laminating the first layers of plies (b) Stacking of second layers of GFRP plies (c) Vacuum bagging of specimens (d) Specimen after curing

Specimens were then cured in an oven using vacuum bag technique. For curing the sandwich specimens, sandwich panel was heated up gradually to 120° in half an hour and then temperature was kept constant for an hour. Finally the temperature was reduced to room temperature in half an hour. Figure 5.30 shows curing cycle and vacuum bagging in the oven for the sandwich specimens.

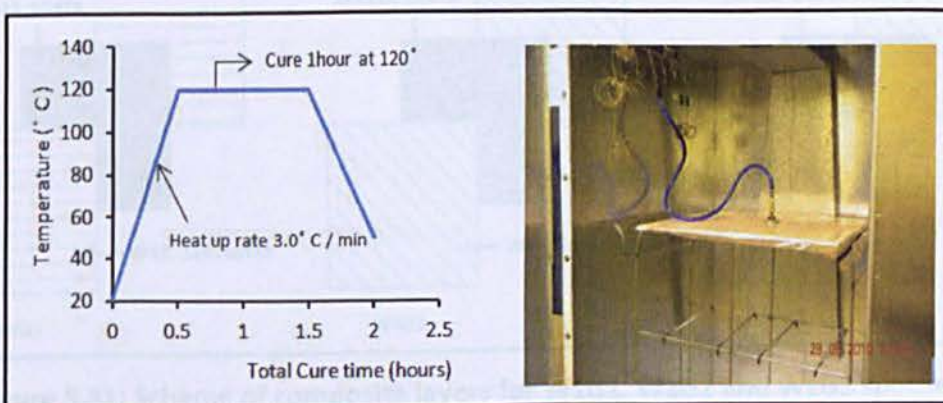


Figure 5.30: Scheme of (a) Curing cycle (b) Vacuum bagging inside the oven for GSSW specimens

CHAPTER 5: SEISMIC BEHAVIOUR OF SPSW SYSTEMS WITHOUT CUT- OUTS

Table 5.3 gives the number of ply layers installed to steel plate, orientation of plies relative to horizontal and the thickness of sandwich panels for W1G1, W1G2 and W1G3 specimens.

Table 5.3: General specification of GFRP-Steel sandwich shear walls

Specimen label	Number of GFRP ply layers	Fibres orientation (degree)	Thickness of steel plate (sp) (mm)	Total thickness of sandwich panel (mm)
W1G1	2	[0/SP/0]	0.675	1.275
W1G2	2	[-45/SP/-45]	0.675	1.275
W1G3	4	[+45/-45/SP/-45/+45]	0.675	1.875

Sandwich panels were attached to fish plates utilising M8 bolts and secondary fish plates. In order to provide a sufficient clamping of the plies by main and secondary fish plates 3M scotch-weld adhesive (9323 B/A structural adhesive) was applied between sandwich panel and fish plates. This type of connection was used to make sure that if any separation between steel plate and composite laminates occurs prior to the rupture of fibres the composite laminates will be able to participate during the applied displacements. Figure 5.31 shows the orientation of fibres for W1G1, W1G2 and W1G3 specimens.

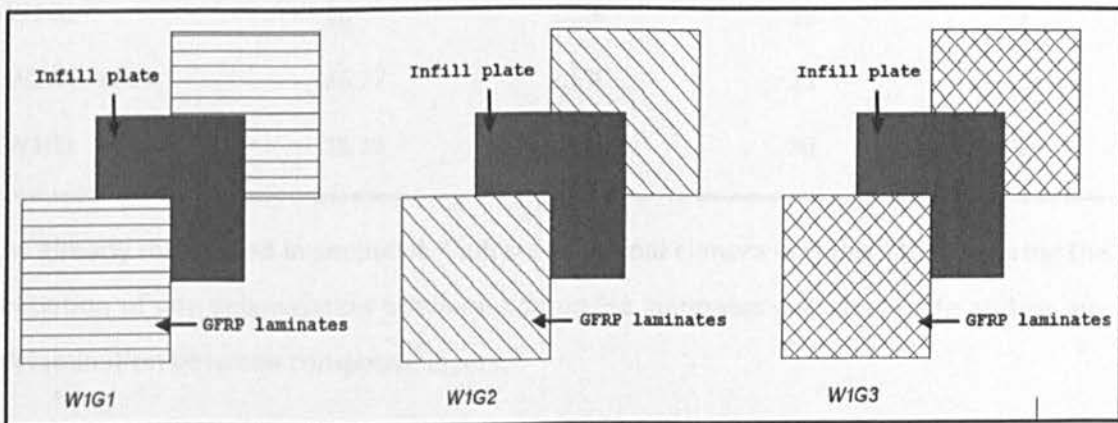


Figure 5.31: Scheme of composite layers for W1G1, W1G2 and W1G3 specimens

CHAPTER 5: SEISMIC BEHAVIOUR OF SPSW SYSTEMS WITHOUT CUT- OUTS

Specimens were subjected to fully reversed quasi-static cyclic loading according to ATC-24 protocol loading requirements. Table 5.4 shows number of cycles (a), Nominal drift index (b), applied amplitudes (c), and number of test cycles for applied amplitudes (d) for W1G1, W1G2 and W1G3 specimens.

Table 5.4: Loading amplitudes used for quasi-static test of W1G1, W1G2 and W1G3 specimens in accordance with ATC-24 protocol

Specimen	(a) Number of Test Cycles	(b) Nominal Drift Index	(c) Applied Amplitudes (mm)	(d) Number of Test Cycles for Each Amplitude
W1G1, W1G2, W1G3	1,2,3	0.04%	0.4	3
W1G1, W1G2, W1G3	4,5,6	0.08%	0.8	3
W1G1, W1G2, W1G3	7,8,9	0.12%	1.2	3
W1G1, W1G2, W1G3	10,11,12	0.25%	2.5	3
W1G1, W1G2, W1G3	13,14,15	0.35%	3.5	3
W1G1, W1G2, W1G3	16,17,18	0.5%	5	3
W1G1, W1G2, W1G3	19,20,21	1%	10	3
W1G1, W1G2, W1G3	22,23	1.5%	15	2
W1G1, W1G2, W1G3	24,25	2%	20	2
W1G2	26	2.5%	25	1
W1G1,W1G3	26,27	2.5%	25	2
W1G1	28,29	3%	30	2

As already mentioned in section 4.9 infrared thermal camera was used for capturing the initiation of any delamination between composite laminates and steel plate and/or any delamination between composite layers.

5.5.1. Test results and discussion of W1G1 specimen

The sandwich panel of W1G1 contains steel plate type I and one layer of GFRP plies on both sides of the steel plate. The plies were laid down in zero degree relative to horizontal direction [0/SP/0]. Total thickness of sandwich panel was 1.275 mm for this specimen. Figure 5.32-a shows test set up and corresponding instrumentation for W1G1 before loading of the specimen. The preliminary analysis for monotonic loading of W1G1 specimen gives an estimation of 300 kN for driving the loading point of specimen to nominal drift index of 3% (Figure 5.32-b).

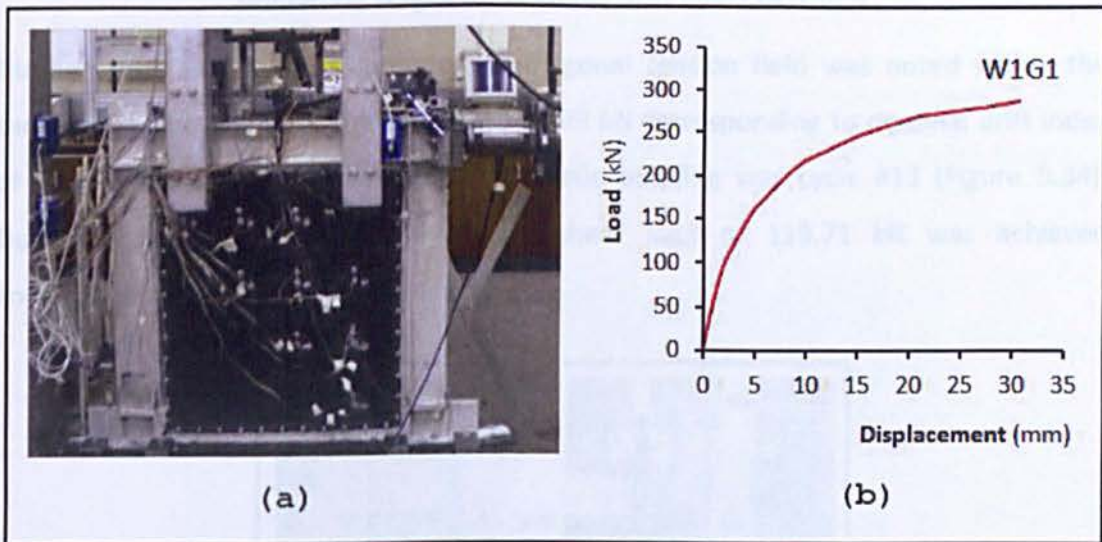


Figure 5.32: (a) Test set up and, (b) Preliminary finite element analysis results for W1G1 specimen

5.5.1.1. Behaviour of W1G1 specimen during the test

The response of specimen up to a nominal displacement of 1.2 mm was linear. However, a sign of non-linear behaviour was noted during the unloading stages of cycles #7 to #9 (Figure 5.33). Nonlinear behaviour of specimen at the early stage of loading could be related to the initial local plastic deformations in zones with stress concentrations. During these cycles a maximum shear load of 49.42 kN was achieved.

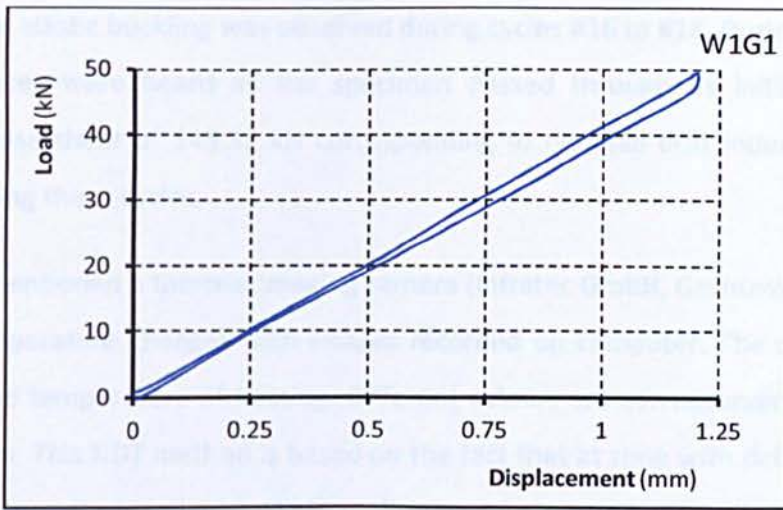


Figure 5.33: Linear and non-linear behaviour of W1G1 specimen during loading and unloading stages for nominal drift index of 0.12%

During cycles #10 to #12 formation of diagonal tension field was noted within the sandwich panel. The base shear reached 92.99 kN corresponding to nominal drift index of 0.25%. The first cycle that followed elastic buckling was cycle #13 (Figure 5.34). During cycles #13 to #15 a maximum shear load of 119.71 kN was achieved corresponding to storey drift of 3.5 mm.



Figure 5.34: Initiation of elastic buckling noted during cycle #13 for W1G1 specimen

Considerable elastic buckling was observed during cycles #16 to #18. During these cycles popping noises were heard as the specimen passed through its initial position. A maximum base shear of 149.32 kN corresponding to nominal drift index of 0.5% was reached during these cycles.

As already mentioned a thermal imaging camera (Infratec GmbH, Germany) was used to monitor temperature changes with images recorded on computer. The colour scale is indicating the temperature of heating. Different colours are corresponding to different temperatures. This NDT method is based on the fact that at zone with delamination the thermal conductivity is reduced. With application of external heating the temperatures of the surface of the FRP material are increasing faster for delaminated zones in comparison with others.

Evaluation of monitored images of sandwich panel captured by infrared camera shows that up to storey drift of 5mm no delamination has occurred between steel plate and composite laminates (Figure 5.35).

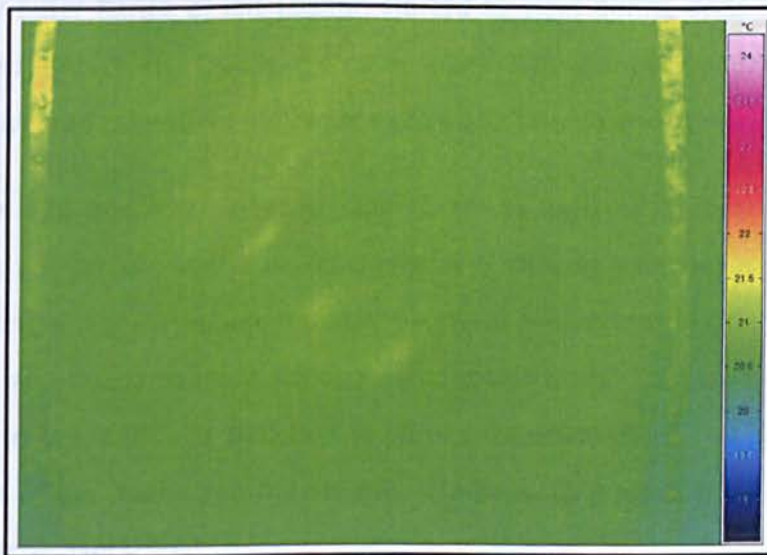


Figure 5.35: Scheme of sandwich panel's image captured by infrared camera at storey drift of 5mm

At the nominal drift index of 1% during cycles #19 to #21 a distinct tension field with maximum base shear of 211.25 kN was gained in specimen. During the amplitude of 15 mm the first sign of debonding between steel plate and GFRP plies was detected by infrared camera. The damaged area was located at the top of the sandwich panel (Figure

5.36). A maximum storey shear of 249.57 kN was achieved for cycles #22 and 23 corresponding to 15 mm storey drift.

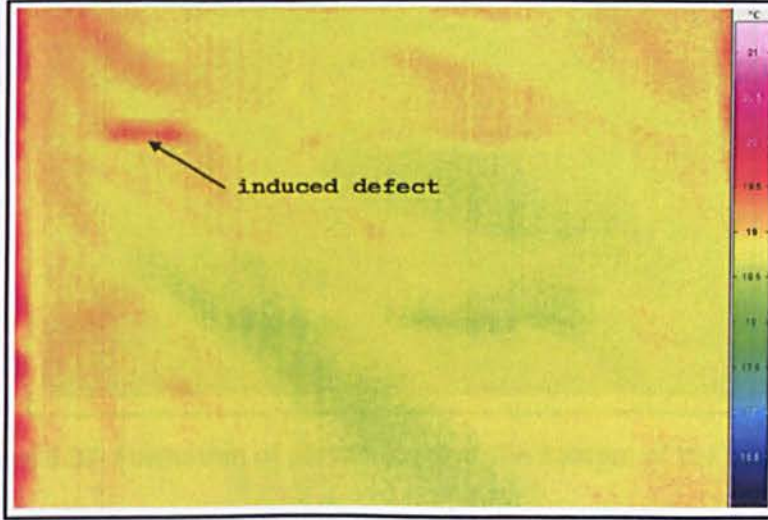


Figure 5.36: Location of debonding of GFRP ply and steel plate

At the nominal drift index of 2% first sign of yielding was noted at the bottom of the columns. Outer flange of right column reached yielding level during cycle #24 and subsequently outer flange of left column started to yield during cycle #25 once base shear reached 271.89 kN. During cycles #24 and #25 the delamination which was captured by infrared camera during cycles #22 and #23 became visible.

During cycles #26 and #27 corresponding to storey drift of 25 mm plastic hinges developed at the bottom of the columns (Figure 5.37) and a maximum base shear of 274.79 kN was gained. Formation of plastic hinges at the bottom of columns caused an increase for vertical component of diagonal tension field. This component applies tension load in perpendicular direction of glass plies orientation. This type of loading causes failure of the matrix and fibre-matrix interface. As a result the GFRP laminates start to tear in parallel strips.

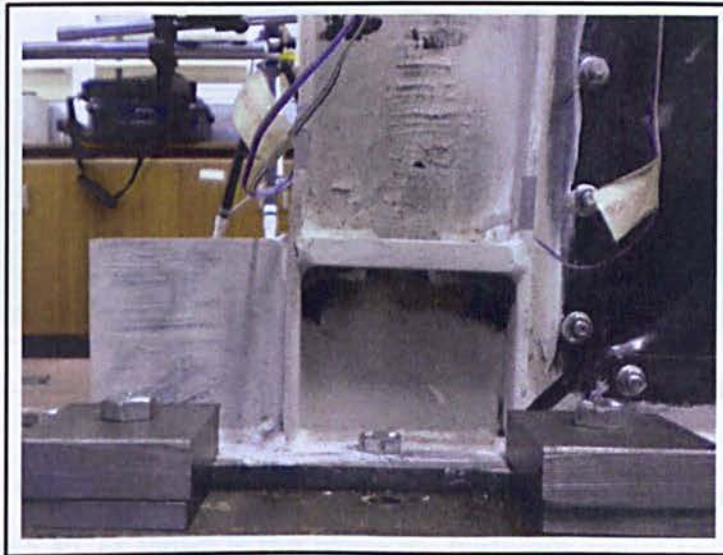


Figure 5.37: Formation of plastic hinge at the bottom of the column

The state of specimen at storey drift of 25 mm is depicted in Figure 5.38. The out-of-plane deformation of composite panel for W1G1 specimen is significantly less than the out-of-plane deformation of steel plate for W1 specimen at the same level of storey drift.

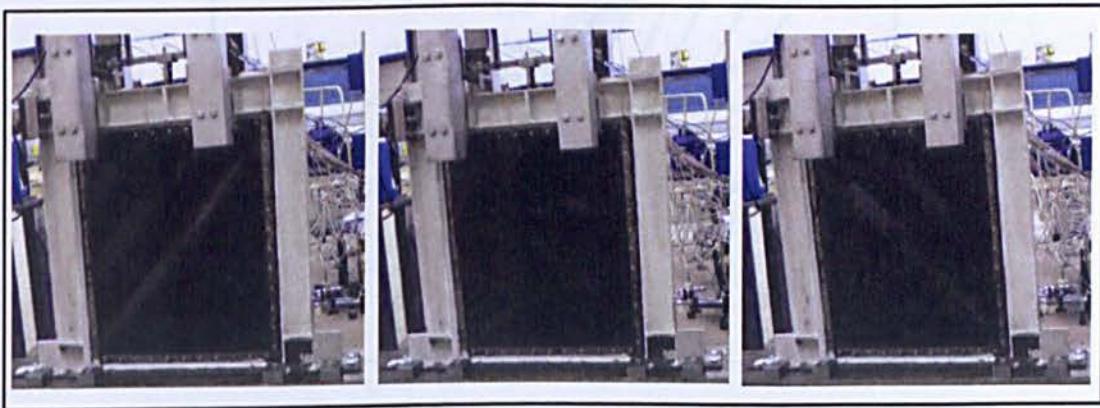


Figure 5.38: State of GFRP-sandwich panel W1G1 at the storey drift of 25mm

During cycles #28 and #29 plastic hinges formed at storey levels of columns. A maximum shear load of 263.24 kN was gained corresponding to nominal drift index of 3%. During cycle #29 entire GFRP laminates were delaminated in both sides of steel plate. However, due to clamping of plies between fish plates, the glass fibres still were able to carry the applied load in tension. Testing of W1G1 specimen was terminated once the plastic hinges were fully developed at both ends of the columns during cycle #29. The state of composite panel during cycle #29 is shown in Figure 5.39.

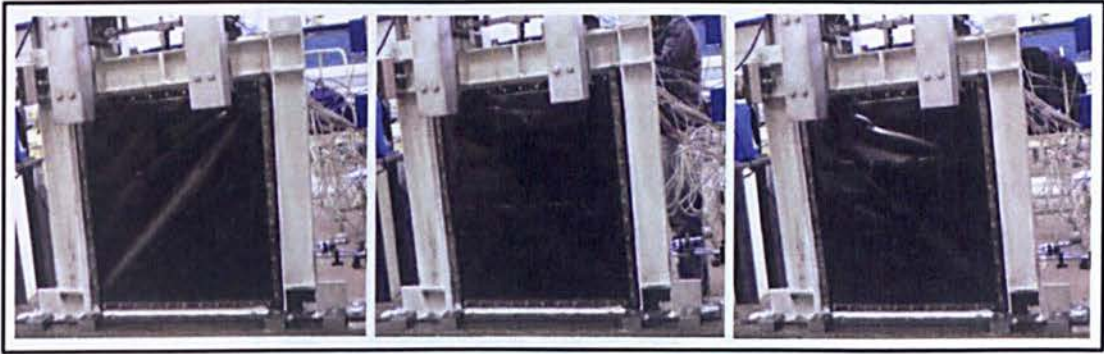


Figure 5.39: Sate of composite panel for W1G1 specimen during cycle #29 Load-displacement behaviour of W1G1 specimen

The hysteresis behaviour curves for W1G1 specimen during the quasi-static test is shown in Figure 5.40. As shown in this figure the hysteresis curves are relatively stable and robust. A maximum base shear of 275.24 kN corresponding to storey drift of 30 mm was achieved prior to termination of the test.

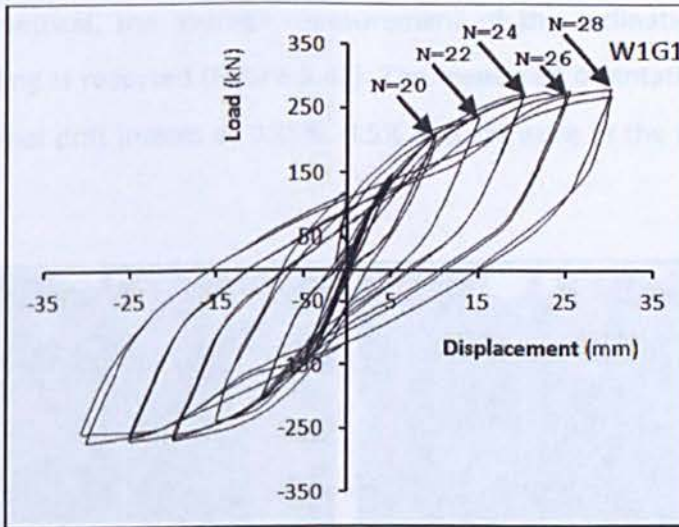


Figure 5.40: Testing results for hysteresis behaviour of W1G1 specimen

The sandwich panel began to buckle first at approximately 105 kN corresponding to a 3 mm displacement. The initiation of delamination between steel plate and GFRP plies was detected by infrared camera at displacement of 15 mm and then was visible at storey drift of 20 mm. Tearing of GFRP laminates occurred during cycles #24 to #29 in parallel strips. The tearing paths were in the matrix of laminates and were accelerated once plastic hinges formed at bottom and subsequently at the top part of the columns. Figure 5.41 illustrates strips of composite plies after termination of the test.

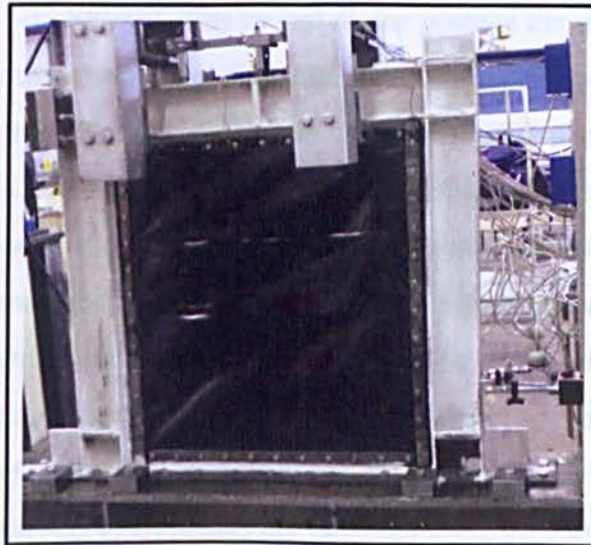


Figure 5.41: Tearing of GFRP plies along the fibres orientation in W1G1 specimen

The inclination angle of the tension field in sandwich panel was obtained by measuring the angle at the crest of the buckle waves (relative to the vertical). As the specimen became unsymmetrical, the average measurement of the inclination angle in both direction of loading is reported (Figure 5.42). The measured orientation of the tension field at the nominal drift indices of 0.25%, 0.5% and 1% were in the range from 39° to 45°.

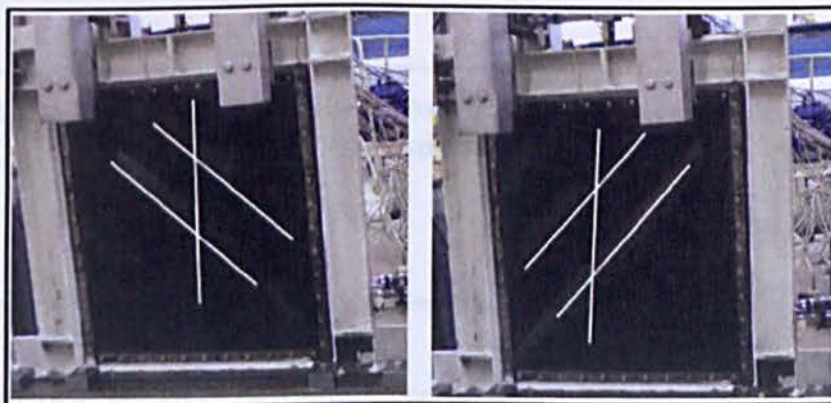


Figure 5.42: Tension field orientation in the sandwich panel for W1G1 specimen

5.5.2. Test results and discussion of W1G2 specimen

Sandwich panel W1G2 contained steel plate type I and one layer of GFRP plies on both sides of the steel plate. The plies were laid down in the 45 degree relative to the

horizontal direction [-45/SP/-45]. This caused during pushing the specimen by screw jack GFRP plies on the both sides of steel plate are under the tensile load. This configuration was set up to study the effect of compressive strength of GFRP plies on the behaviour of steel plate. To keep symmetrical out-of-plane deformation of steel plate composite laminates were introduced to both side of the steel plate. Total thickness of sandwich panel was 1.275 mm for this specimen. Figure 5.43-a shows test set up and corresponding instrumentation for W1G2 before loading of the specimen. According to the preliminary finite element analysis for W1G2 specimen approximately a maximum load of 320 kN and 250 kN is required for pushing and pulling of the specimen respectively. The preliminary FEA results are depicted in Figure 5.43-b.

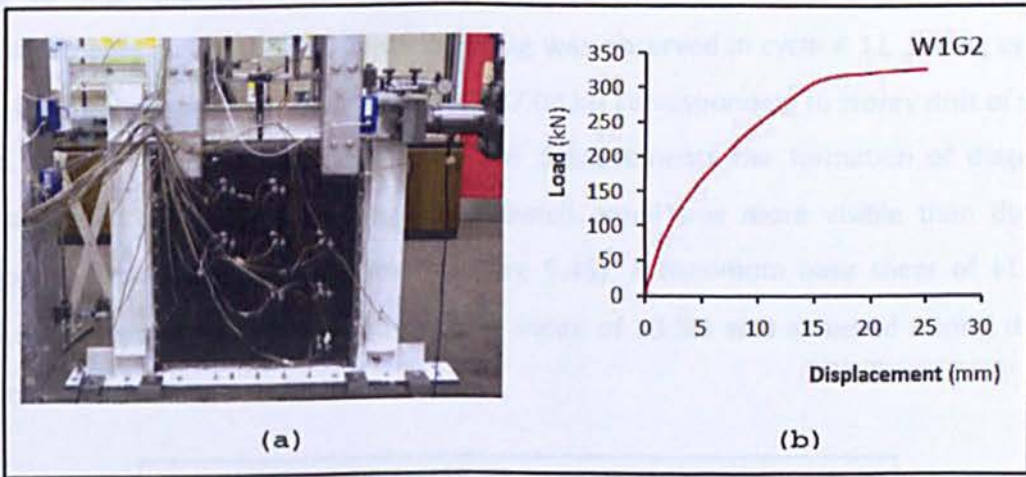


Figure 5.43: (a) Test set up and, (b) Preliminary finite element analysis results for W1G2 specimen

5.5.2.1. Behaviour of W1G2 specimen during the test

W1G2 specimen behaved differently during applying the positive and negative displacement load at storey level. This is mainly due to specific configuration of sandwich panel. During the cycles #1 to #9 the response of specimen is non linear for positive displacement. However, its response was linear for negative displacements. This response of specimen is depicted in Figure 5.44 during cycle #8. Maximum base shears reached +50.07/-48.02 kN corresponding to storey drift of ± 1.2 mm.

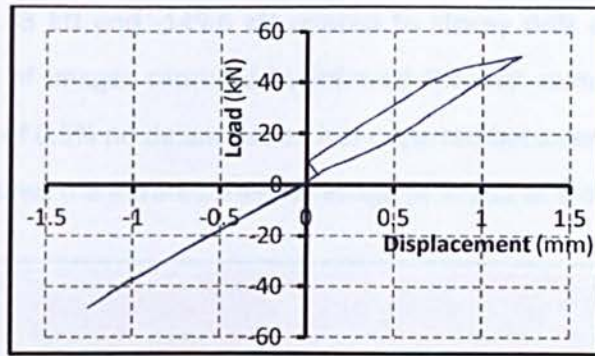


Figure 5.44: Different behaviour of W1G2 specimen for positive and negative storey drift of 1.2 mm during cycle #8

During first nine cycles no visual sign of steel plate buckling was observed. During cycles #10 to #12 the specimen start to exhibit non-linear behaviour for negative displacements as well. Minor elastic buckling was observed in cycle # 11. During cycles #10 to #12 the base shear reached +95.4/-87.04 kN corresponding to storey drift of ± 2.5 mm. During cycles #13 to #15 for positive displacements the formation of diagonal tension field and elastic buckling of sandwich panel was more visible than during negative displacements of specimen (Figure 5.45). A maximum base shear of +132/-115.67 kN corresponding to nominal drift index of $\pm 3.5\%$ was achieved during these cycles.

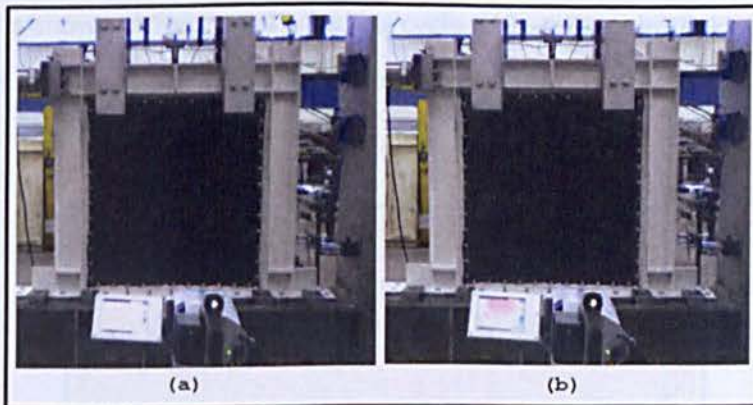


Figure 5.45: Formation of diagonal tension field and elastic buckling of W1G2 specimen during cycle #14 corresponding to storey drift of (a) +2.5 mm (b) -2.5 mm

Considerable elastic buckling was observed during cycles #16 to #18 corresponding to storey drift of 5 mm. During these cycles popping noises were heard when the specimen passed through its initial position mainly in negative amplitude area. Maximum base

shear reached 171.43 kN and -149.6 kN related to storey drift of +5 mm and -5mm, respectively. Study of images captured by infrared thermal camera proves that up to nominal drift index of 0.5% no delamination has occurred between steel plate and GFRP plies. Figure 5.46 shows the infrared thermal image of W1G2 at storey drift of 5mm.

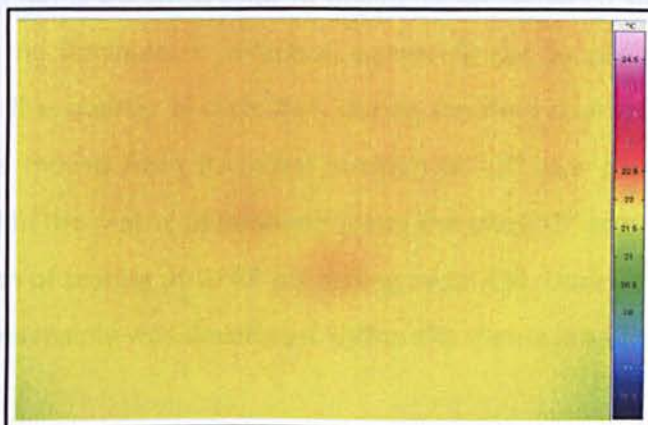


Figure 5.46: Infrared thermal image of sandwich panel W1G2 specimen during cycle #18

During cycles #19 to #21 corresponding to nominal drift index of $\pm 1\%$ maximum base shear of +266.12/-205.18 was attained. The first sign of damage between steel plate and GFRP plies was captured by infrared thermal camera at the storey drift of 15 mm during cycles #22 and #23 and maximum base shear of +308.45/-229.63 kN. The location of delamination is shown in Figure 5.47. During cycle #23 white paint flaking was observed at the bottom of the left side column and first sign of yield was noted at outer flange of column.

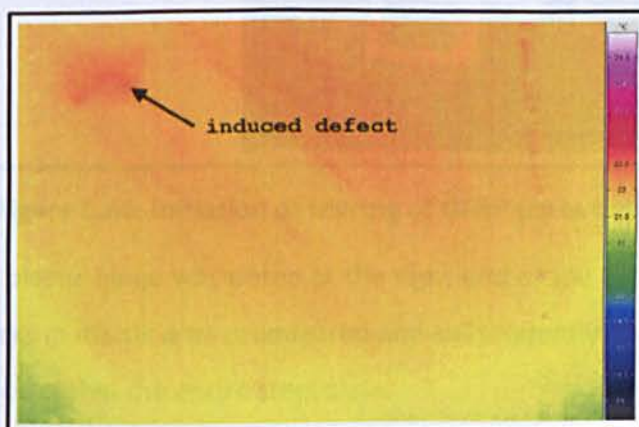


Figure 5.47: Location of delamination between steel plate and GFRP plies W1G2 specimen during cycle # 23

During cycles #24 and #25 plastic hinges developed at bottom part of both columns. Maximum base shear of +311.58/-239.68 kN was reached corresponding to storey drift of ± 20 mm. During cycle #24 GFRP plies started to rupture at the position that within previous amplitude was captured by infrared thermal camera. It is worth mentioning that the tearing of fibres occurred prior to delamination between steel plate and GFRP plies. Tearing of the laminate in direction perpendicular to ply orientation initially started during the first quarter of cycle #24. During the third quarter of cycle #24, when the specimen was moved from its initial position to -20 mm storey drift tearing of laminate occurred in the matrix of laminate along the plies 45° orientation. Figure 5.48 shows the initiation of tearing of GFRP ply during cycle #24. During the following cycles tearing of laminates mainly was developed within the matrix area than tearing of GFRP plies.

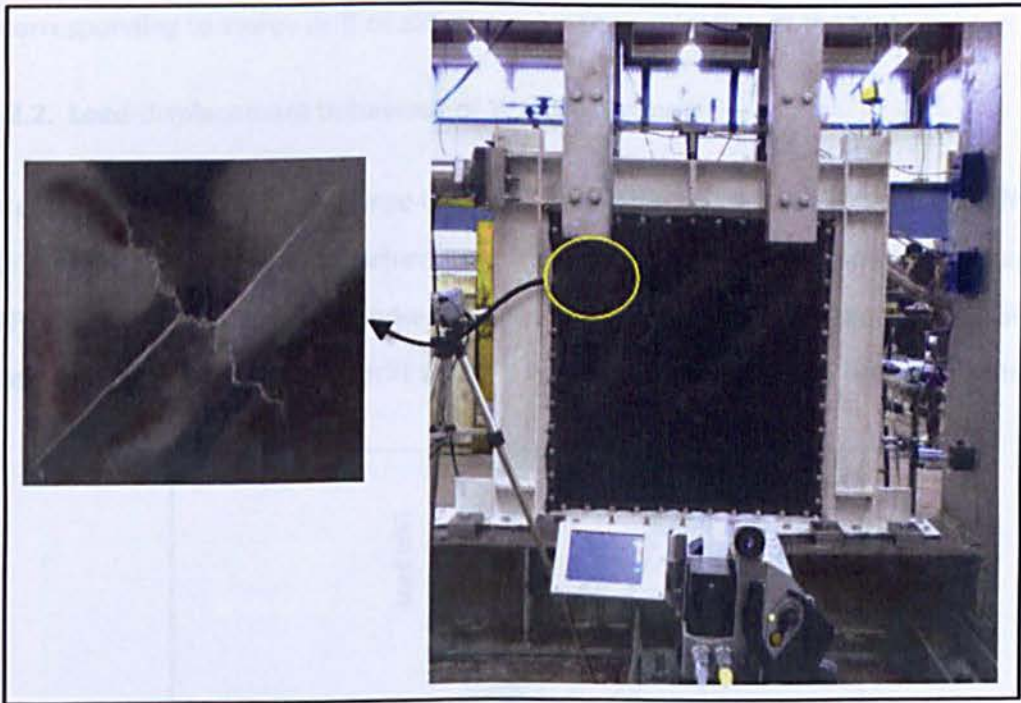


Figure 5.48: Initiation of tearing of GFRP ply in both

During cycle #26 a plastic hinge was noted at the right end of the beam (Figure 5.49). In the mean time cracks in matrix area propagated and subsequently delamination of GFRP plies were developed within the entire steel plate.



Figure 5.49: Formation of plastic hinges at the end of beam

The test was terminated due to formation of plastic hinges at the bottom of the columns and end of the beam during cycle #26. Maximum base shear reached +288.37/-224.93 kN corresponding to storey drift of ± 25 mm prior to termination of the test.

5.5.2.2. Load-displacement behaviour of W1G2 specimen

Hysteresis curves for cyclic response of W1G2 during the quasi-static test are depicted in Figure 5.50. Non-symmetrical behaviour of specimen is due to unbalanced lay-up of GFRP plies for construction of sandwich panel. Maximum base shear reached 311.58 kN corresponding to 20 mm storey drift whilst it was -239.68 kN at storey drift of -5 mm.

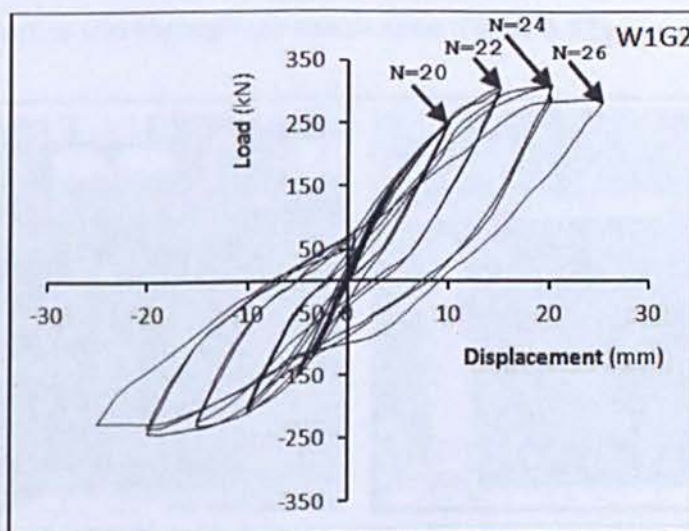


Figure 5.50: Hysteresis behaviour of W1G2 during the quasi-static test

Diagonal tension field and elastic buckling of sandwich panel first was noted in fibre orientation of sandwich panel during cycle #13 and then in the non-fibred direction of panel during cycle #15. The average inclination angle measured for nominal drift index of 0.25%, 0.5% and 1% in both loading directions varies in range 41° to 47° and 40° to 45° for reinforced and non-reinforced direction of sandwich panel. Figure 5.51 illustrates the measured inclination angles for both reinforced and non-reinforced direction of sandwich panel.

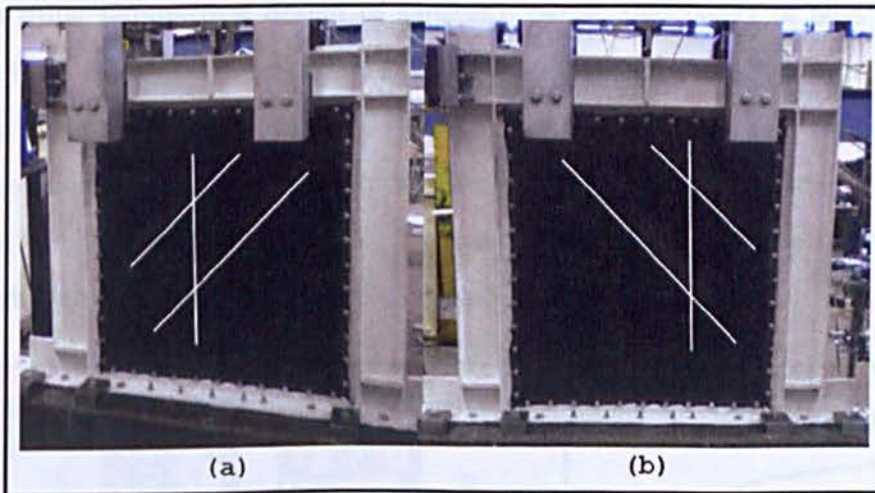


Figure 5.51: Variation of inclination angle between (a) reinforced direction and (b) non-reinforced direction of sandwich panel for W1G2 specimen

Formation of plastic hinges was noted at storey drift of 20 mm when the specimen was loaded in ply direction. By reversing the load direction at 20 mm displacement plateau the laminates start to tear through the matrix zone (Figure 5.52).

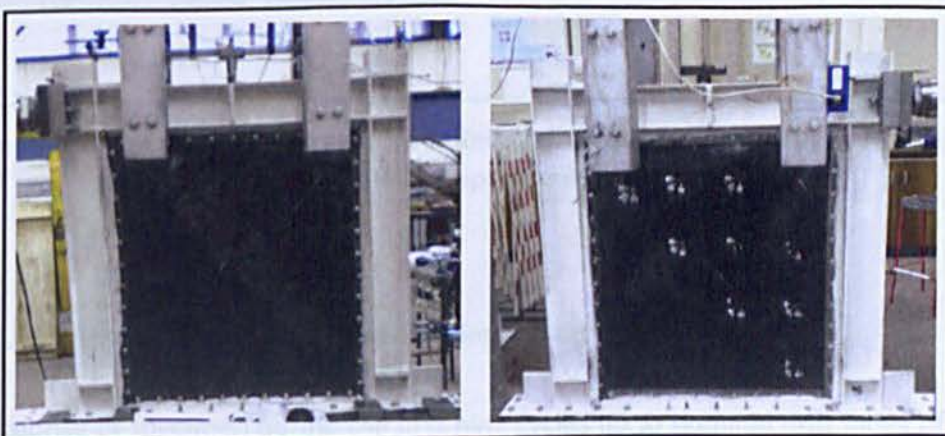


Figure 5.52: Tearing of GFRP plies due to stretching of the steel plate in direction perpendicular to fibres for W1G2

The test was terminated due to development of plastic hinges at the column bottom and end of beam at nominal drift index of 2.5%.

5.5.3. Test results and discussion of W1G3 specimen

W1G3 specimen was designed based on the response of W1G1 and W1G2 specimens and corresponding test results. Two main goals were considered for design of GFRP lay-up to inhibit tearing in matrix area and to prevent premature damage of boundary members using symmetrical design of sandwich panel. Two layers of plies were laid down on both sides of steel plate in $\pm 45^\circ$. Sandwich panel was 1.875 mm thick with configuration of [+45/-45/SP/-45/+45]. Figure 5.53-a shows general test set up view for W1G3 specimen. Preliminary FE monotonic analysis of specimen estimates a maximum 330 kN of load requirement for driving the loading point to target displacement of 25 mm. Results for this analysis are given in Figure 5.53-b.

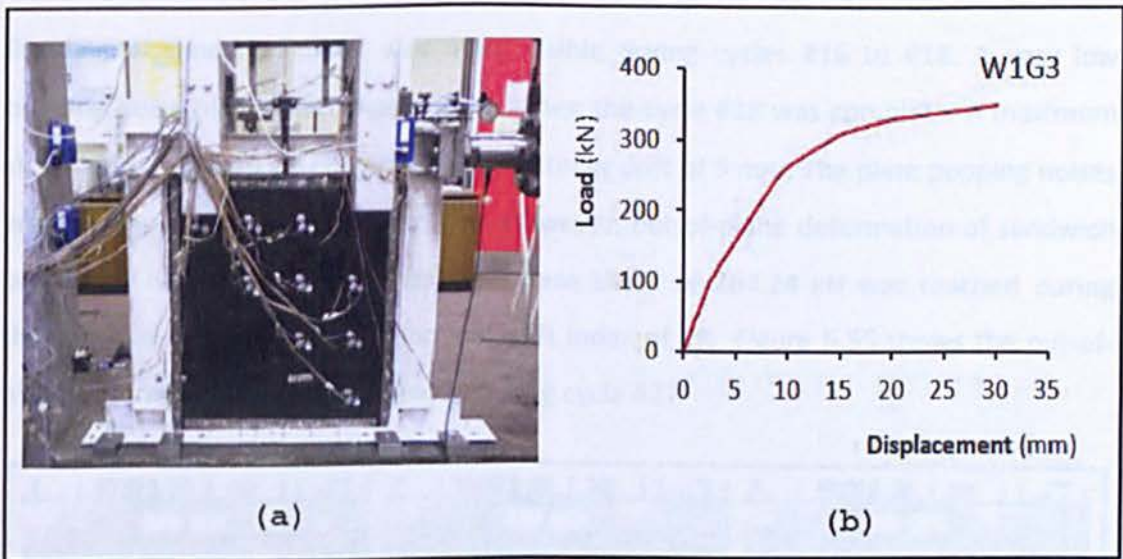


Figure 5.53: (a) Test set up and, (b) Preliminary finite element analysis results for W1G3 specimen

5.5.3.1. Behaviour of W1G3 specimen during the test

The response of specimen during the first nine cycles up to nominal drift index of 0.12% is linear (Figure 5.54). During these nine cycles there is no visual sign of sandwich panel

buckling. A maximum base shear reached 59.56 kN during cycle #9. During cycles #10 to #12 formation of diagonal tension field was noted. A maximum base shear reached 108.89 kN corresponding to 2.5 mm storey displacement. The first cycle that elastic buckling observed was cycle #13. During cycles #13 to #15 the base shear reached 143.05 kN corresponding to nominal drift index of 0.35%.

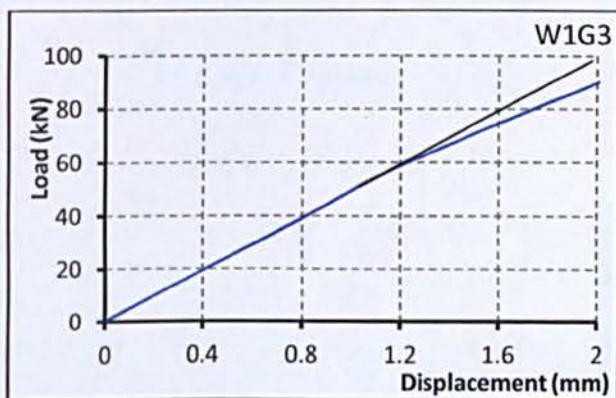
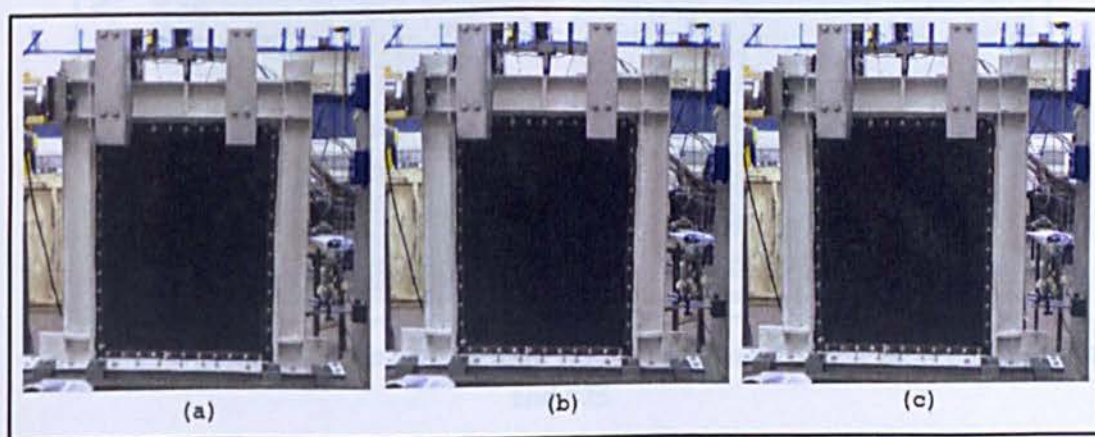


Figure 5.54: Linear behaviour of W1G3 up to storey drift of 1.2 mm

Buckling of sandwich panel was more visible during cycles #16 to #18. A very low popping noise of the plate was noticed when the cycle #18 was complete. A maximum shear load of 179.79 kN corresponding to storey drift of 5 mm. The plate popping noises were strong during cycles # 19 to #21. However, out-of-plane deformation of sandwich panel was not noticeable. A maximum base shear of 267.24 kN was reached during these cycles corresponding to nominal drift index of 1%. Figure 5.55 shows the out-of-plane deformation of sandwich panel during cycle #21.



**Figure 5.55: The shape of sandwich panel W1G3 specimen during cycle #21
(a) storey drift of +10 mm (b) initial position (c) storey drift of -10 mm**

During applying the displacement amplitude of 15 mm the first sign of induced defect was detected by thermal imaging system. The location of induced defect during the cycle #23 is depicted in Figure 5.56 . A maximum base shear 312.37 kN reached during the cycles # 22 and #23.

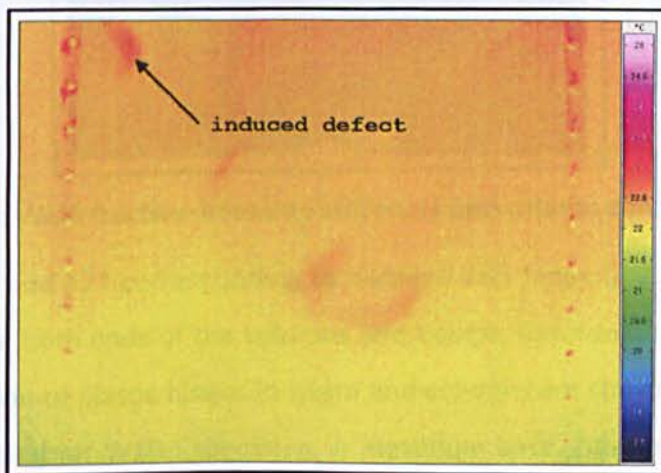


Figure 5.56: Location of possible induced defect during story drift of 15 mm

During the nominal drift index of 2% the first sign of yielding was noticed at bottom part of left column. During the first cycle of this amplitude, cycle #24, the GFRP laminates started to tear at the position that was captured by infrared thermal image during cycle #23. During cycle #24 the tearing of plies occurred on the other side of sandwich panel (Figure 5.57). A maximum base shear reached 324.66 kN during this amplitude.

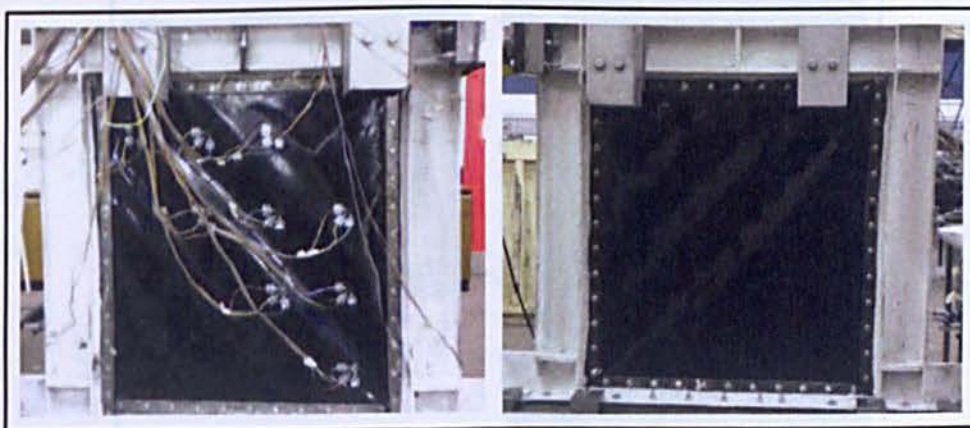


Figure 5.57: Tearing of GFRP plies at both sides of sandwich panels during cycles #24 and #25

During storey drift of 20 mm weld fracture occurred between both stiffeners and column connections during cycle #25 (Figure 5.58).



Figure 5.58: Weld fracture between stiffeners and column connections

During cycles #26 and #27 corresponding to nominal drift index of 2.5%, plastic hinges were developed at both ends of the columns and beams. Deformed shape of sandwich panel and formation of plastic hinges in beam and columns are shown in Figure 5.59 at final stage of loading for W1G3 specimen. A maximum base shear reached 289.47 kN corresponding to storey drift of 25 mm. An investigation on weld connections at the end of this test indicated that except fracture in the weld between stiffeners and columns, other welds remained intact.

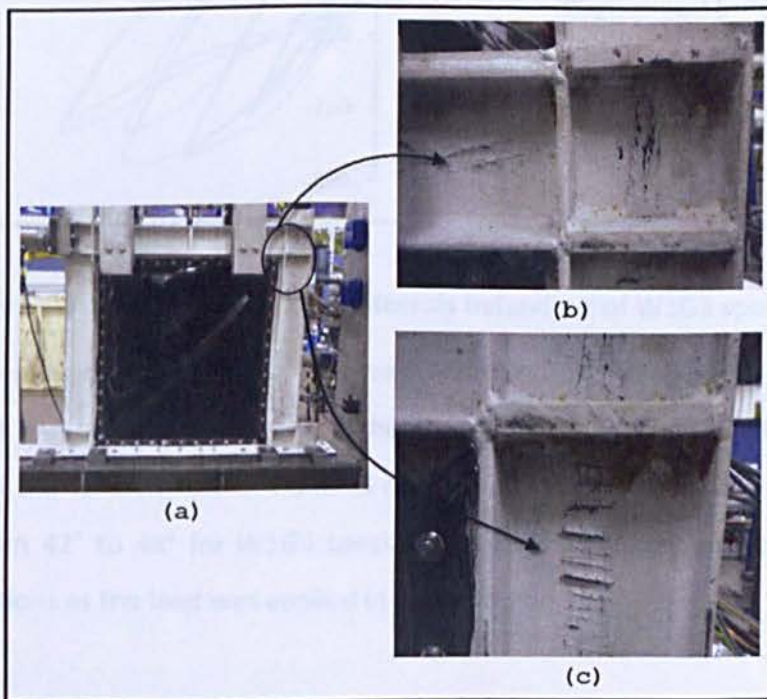


Figure 5.59: (a) State of sandwich panel during the final loading cycle and development of plastic hinges at the end part of (b) Beam and (c) Columns

5.5.3.2. Load-displacement behaviour of W1G3 specimen

The hysteresis response of W1G3 specimen during quasi-static test is relatively stable and symmetric (Figure 5.60). Maximum base shear was reached 324.66 kN corresponding to nominal drift index of 2%. Considerable elastic buckling of sandwich panel and development of diagonal tension field within the panel was noticed at storey drift level of 5 mm. Up to storey drift of 15 mm no degradation of maximum base shear was observed. Once the GFRP plies started tearing during cycle #24, degradation of maximum shear capacity of specimen was observed.

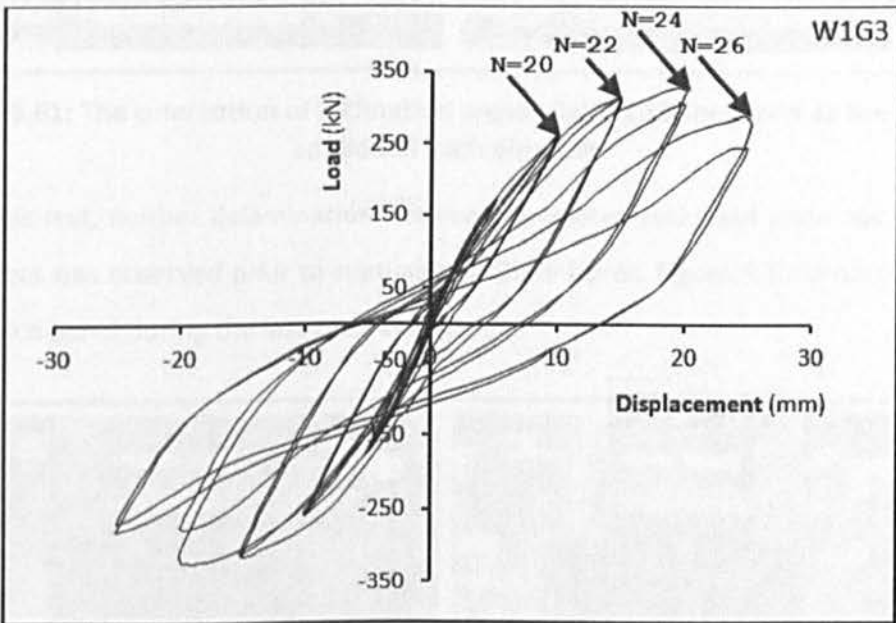


Figure 5.60: Testing results for hysteresis behaviour of W1G3 specimen

The inclination angle of the tension field was recorded as the load was applied in each direction and the average reported as the tension field orientation. The measured orientation of the tension field at nominal drift indices of 0.25%, 0.5% and 1% were in the range from 42° to 48° for W1G3 specimen. Figure 5.61 illustrates the inclination angle orientations as the load was applied in each direction.

5.5.3. Finite element analysis results for W1G1, W1G2 and W1G3 specimens

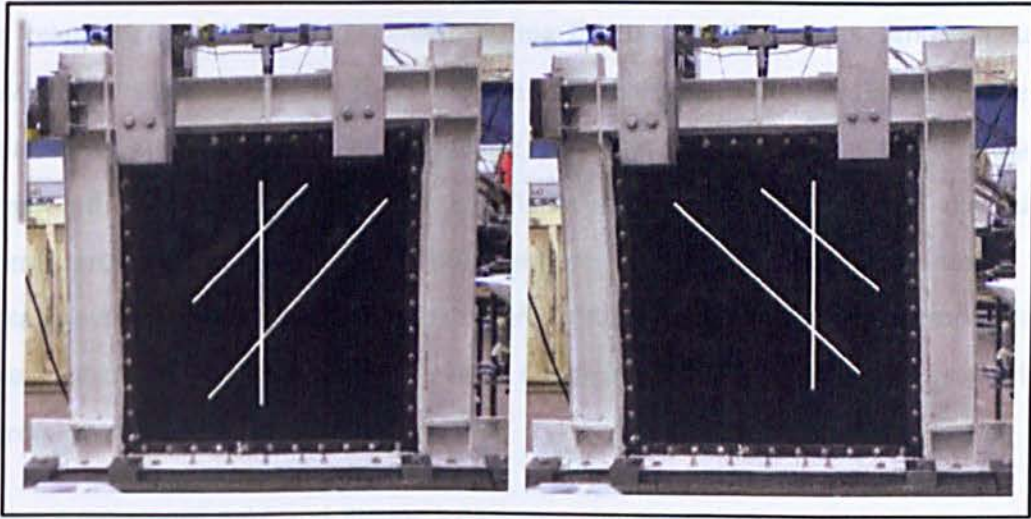


Figure 5.61: The orientation of inclination angles for W1G3 specimen as the load is applied in each direction

During this test, neither delamination between laminates and steel plate nor between GFRP layers was observed prior to rupturing of GFRP fibres. Figure 5.62 shows the state of sandwich panel during the last cycle of the test.

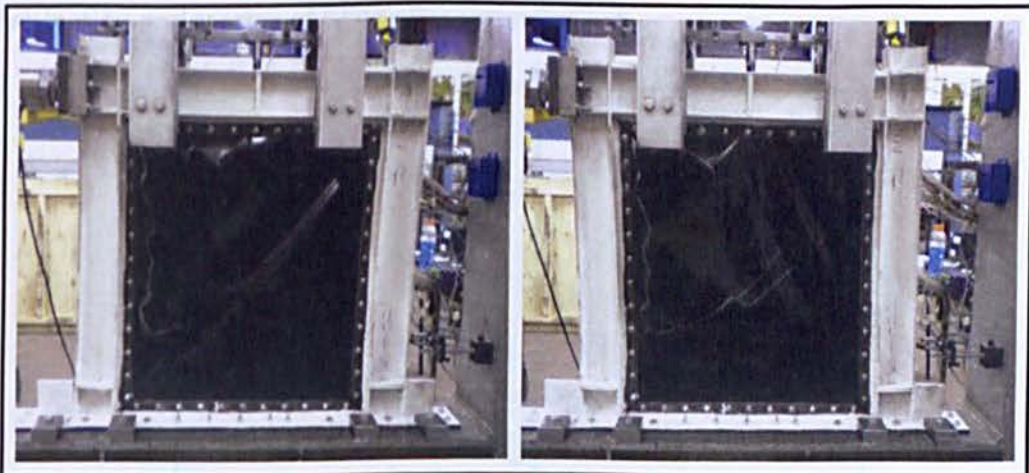


Figure 5.62: Tearing of GFRP plies at nominal drift index level of 2.5% for W1G3 specimen

This test was terminated due to development of plastic hinges at the end part of columns and beams during the last cycle.

Figure 5.63: Comparison of experimental results of the four test specimens subjected to 7.6 and 10.4% drift levels for W1G3 specimen

5.5.4. Finite element analysis results for W1G1, W1G2 and W1G3 specimens

The response of sandwich specimens during the test program was simulated using ABAQUS software. A perfect bond was assumed between GFRP laminates as well as between steel plate and GFRP laminate. Failure of GFRP material in FE model is considered using the Hashin failure criteria in ABAQUS software. When the failure criteria are met in an element, the element is removed from the model and subsequently the element stiffness is omitted in the following steps. Orthotropic elastic behaviour is defined by introducing elastic coefficients (E_{11} , E_{22} , G_{12} and ν_{12}) in a local coordinate system.

Figure 5.63, Figure 5.64 and Figure 5.65 show the load-displacement diagram of the W1G1, W1G2 and W1G3 specimens obtained from the envelope of the hysteresis curves attained from cyclic explicit FE analysis and the quasi-static test results. Based on Figure 5.63, Figure 5.64 and Figure 5.65, it is shown that FE models provide adequately reasonable estimation of the stiffness and maximum base shear capacity of the specimens. However, the test and FE results are matching up to maximum load where delamination and tearing of GFRP plies are extended.

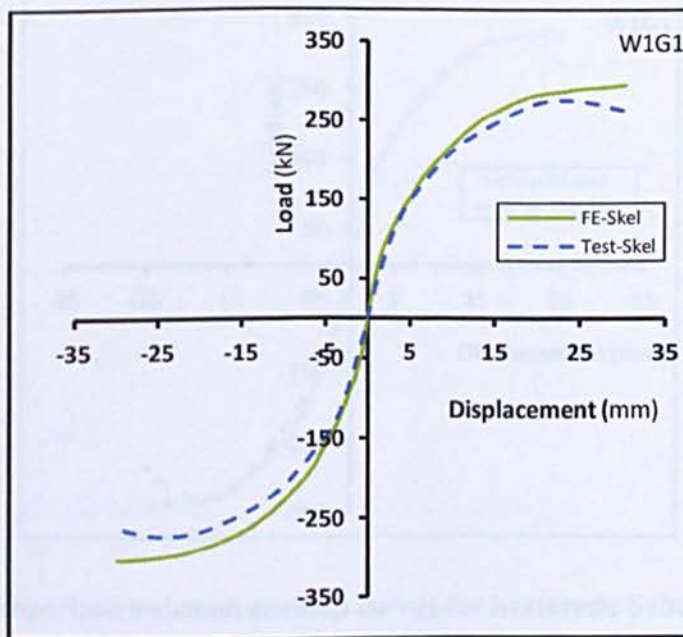


Figure 5.63: Comparison between envelop curves for hysteresis behaviour of FE and test results for W1G1 specimen

Gradually increasing difference was noted between the test and FE results for W1G1 specimen due to early rupture of laminates within the matrix zone.

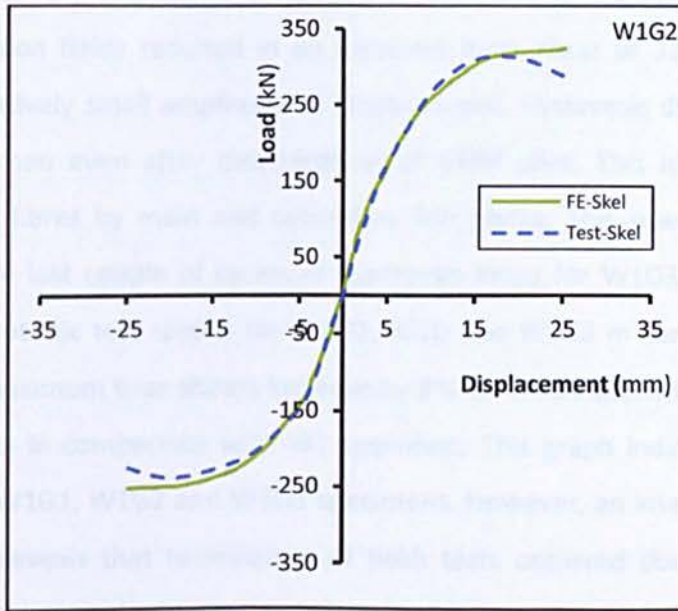


Figure 5.64: Comparison between envelop curves for hysteresis behaviour of FE and test results for W1G2 specimen

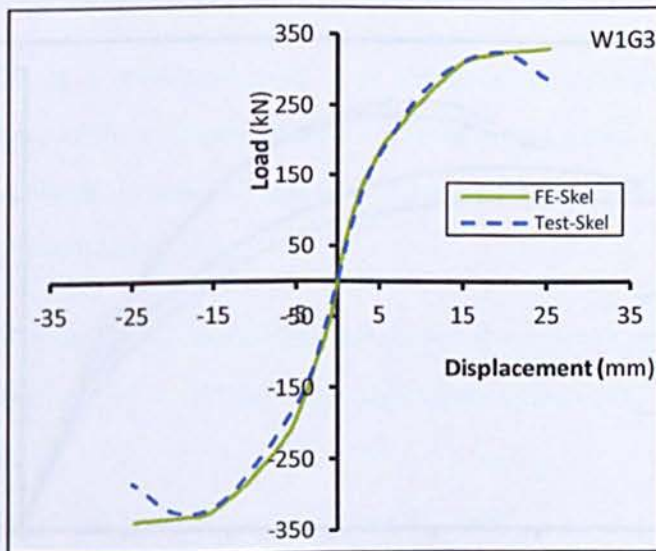


Figure 5.65: Comparison between envelop curves for hysteresis behaviour of FE and test results for W1G3 specimen

Degradation of hysteresis loops is visible for composite specimens. However diagonal tension field actions are more robust for W1G2 and W1G3 specimen. This was due to alignment of GFRP ply direction with steel plate diagonal tension fields. Formation of very strong tension fields resulted in an excellent base shear of 324.7 kN for W1G3 specimen at relatively small amplitude of displacement. Hysteresis diagrams are stable for W1G1 specimen even after delamination of GFRP plies. This is due to sufficient clamping of the fibres by main and secondary fish plates. This phenomenon is more visible during the last couple of cycles of hysteresis loops for W1G3 specimen. Figure 5.66 shows monotonic test results for W1G1, W1G and W1G3 in comparison with W1 specimen. The maximum base shears increase by 9% for W1G1 specimen and by 30% for W1G2 and W1G3 in comparison with W1 specimen. This graph indicates reduction of ductility for the W1G1, W1G2 and W1G3 specimens. However, an investigation of these two specimens reveals that termination of both tests occurred due to formation of plastic hinges at the end of boundary members.

One of the reasons for using GFRP laminates for strengthening of steel plate is the possibility of increasing the functionality of beam element against the action of diagonal tension field.

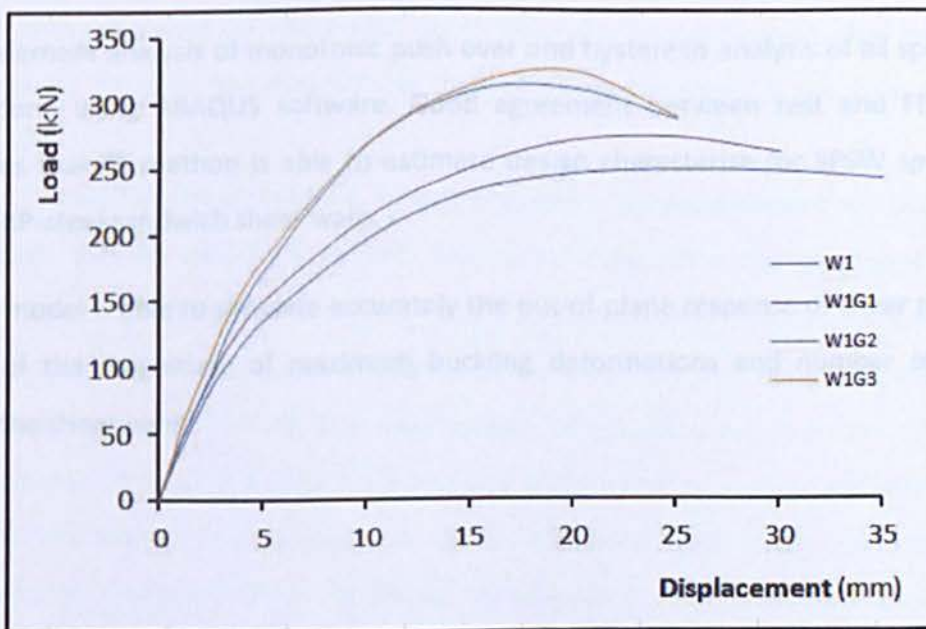


Figure 5.66: Monotonic test results for W1, W1G1, W1G2 and W1G3 specimens

5.6. Summary

The main focus of this chapter was evaluation of the quasi-static test results for frame-only specimen (specimen F), steel plate shear walls with two different thicknesses of steel plate (specimens W1 and W2) and finally GFRP-steel sandwich shear wall with different lay-up for GFRP plies (specimen W1G1, W1G2 and W1G3). Preliminary Finite element analysis was used for estimating the maximum shear load in each test. In-plane storey drift and state of stresses were monitored and recorded for all specimens during the test. Inclination angles of diagonal tension field action in the shear panels were measured at different nominal drift indices. Infrared thermal camera was used to detect delamination between GFRP plies and steel plate and also any delamination of GFRP layers from each other.

GFRP plies were laminated on both sides of steel plate using bagging techniques. No additional adhesive was used for bonding of GFRP layers. Sandwich panels were designed using different GFRP lay-up. The response of GSSW specimens during the test was dominated by number of layers and orientation of GFRP plies. Inclination angles, shear capacity and state of stresses were monitored and recorded for sandwich specimen to study the function of GFRP plies in sandwich specimens.

Finite element analysis of monotonic push over and hysteresis analysis of all specimens were done using ABAQUS software. Good agreement between test and FE results indicates that FE method is able to estimate design characterise for SPSW specimens and GFRP-steel sandwich shear walls.

The FE model is able to simulate accurately the out-of-plane response of shear panels in terms of the magnitude of maximum buckling deformations and number of waves within the shear panel.

6. SEISMIC BEHAVIOUR OF SPSW SYSTEMS WITH CUT-OUTS

EXPERIMENTAL AND NUMERICAL STUDY

6.1. Introduction

In general buildings, the doors, windows and lift entrances are sometimes located in the shear walls. In such cases by introducing large size cut-outs within the steel plate span for SPSW, the capacity of lateral load resisting system could be reduced. Using coupled wall system or stiffening of the shear panels are two alternatives for enhancing the system performance against lateral loads.

The AISC seismic provisions state that a cut-out should be strengthened at edges by steel stiffeners to neutralize disruption of tension field continuity and minimize stress concentration and edge buckling. It also allows other forms of cut-outs that can be justified by testing or analysis (AISC, 2005). Furthermore, AISC design guide 20 provides a discussion on design of perforated steel plate shear walls where steel boundary elements are analyzed and designed for inclined yielding stresses of the adjacent plate (AISC, 2007).

Chapter 5 described the test set-up, loading procedure and experimental results, as well as FE model and analysis for specimens without cut-outs within the steel plate. In this chapter the effect of cut-outs on the maximum loading capacity and the lateral stiffness of SPSW systems are investigated. A 300mm diameter cut-out was created at the centre of the steel plate type I and II. The specifications of boundary members are similar to those reported in chapter 5. The main focus of this chapter is in-plane stiffness of the system at the load level for which drift control is often a major design consideration. Two different methods were employed for restoring the perforated specimens' characters to those without cut-outs. Having in mind that laminating FRP plies is easier and faster than welding steel stiffeners especially for thinner steel plates, GFRP plies

CHAPTER 6: SEISMIC BEHAVIOUR OF SPSW SYSTEMS WITH CUT-OUTS

were used for strengthening of infill panel type I. The specimen with steel plate type II was strengthened by optimal designed steel stiffeners.

Table 6.1: Loading amplitudes used for quasi-static test of W10, W20, W10G and W20S specimens in accordance with ATC-24 protocol

Specimen	Test Cycle	Nominal Drift Index	Nominal Displacement (mm)	Number of Input Cycles
All specimens*	1,2,3	0.04%	0.4	3
All specimens	4,5,6	0.08%	0.8	3
All specimens	7,8,9	0.12%	1.2	3
All specimens	10,11,12	0.25%	2.5	3
All specimens	13,14,15	0.35%	3.5	3
All specimens	16,17,18	0.5%	5	3
All specimens	19,20,21	1%	10	3
All specimens	22,23	1.5%	15	2
All specimens	24,25	2%	20	2
All specimens	26,27	2.5%	25	2
All specimens	28,29	3%	30	2
W20, W20S	30	3%	35	1
W10	30,31	3.5%	35	2

* All specimens with cut-outs

6.2. Test results and behaviour of W10 specimen during the test

W10 specimen was constructed using steel plate type I and bolt connections between steel plate and fish plates. General view and test set up for this specimen is shown in Figure 6.1-a. The cyclic displacement loads with gradually increasing amplitudes were applied to the specimen in accordance with ATC-24 protocol. Based on preliminary load-displacement finite element analysis a maximum load of 250 kN is expected for running of this test (Figure 6.1-b).

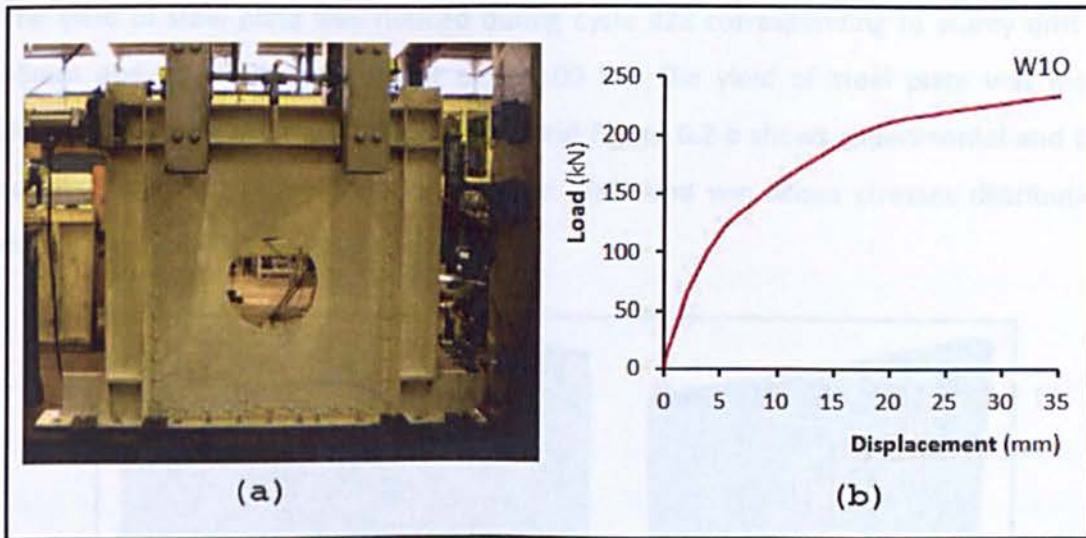


Figure 6.1: (a) Test set up and, (b) Preliminary finite element analysis results for W10 specimen

The specimen exhibited non-linear behaviour even at early stage of the loading. During first 6 cycles up to nominal drift index of 0.8% no buckling of steel plate and plate popping noises were observed. A maximum base shear of 23.89 kN was achieved during cycle #6. A very low volume plate popping noise was noted when specimen passed through its initial position during cycle #7 corresponding to storey drift of 1.2 mm. A maximum base shear of 31.76 kN reached during cycles #7 to #9. The first sign of visible buckling in the steel plate was observed during cycles #10 to #12 and the maximum base shear reached 67.57 kN corresponding to nominal drift index of 2.5%. A permanent deformation was observed within the steel plate during cycles #13 to #15 with base shear of 88.68 kN corresponding to nominal drift index of 3.5%. The occurrence of premature deformation in the steel plate was mainly due to creation of cut-out in the steel plate. Existence of cut-out precludes proper distribution of diagonal tension field during the post buckling behaviour of steel plate. During the 5 mm amplitude, the plate popping noises were noted for all three cycles #16 to #18. These events occurred once specimen passed through its -2 mm displacement history instead of its initial position. The delay of buckling sounds was mainly due to permanent deformation of steel plate. A maximum base shear of 115.62 kN was achieved during cycle #18. The white paint around the cut-out started to flack when the amplitude of displacement reached 10 mm during cycles #19 to #21. A maximum base shear reached 165.5 kN during this amplitude.

The yield of steel plate was noticed during cycle #22 corresponding to storey drift of 15mm and maximum base shear of 195.09 kN. The yield of steel plate was more developed during cycle #23. Figure 6.2-a and Figure 6.2-b shows experimental and the results from FEA for deformation of steel plate and von Mises stresses distribution during the cycle #23 for W10 specimen.

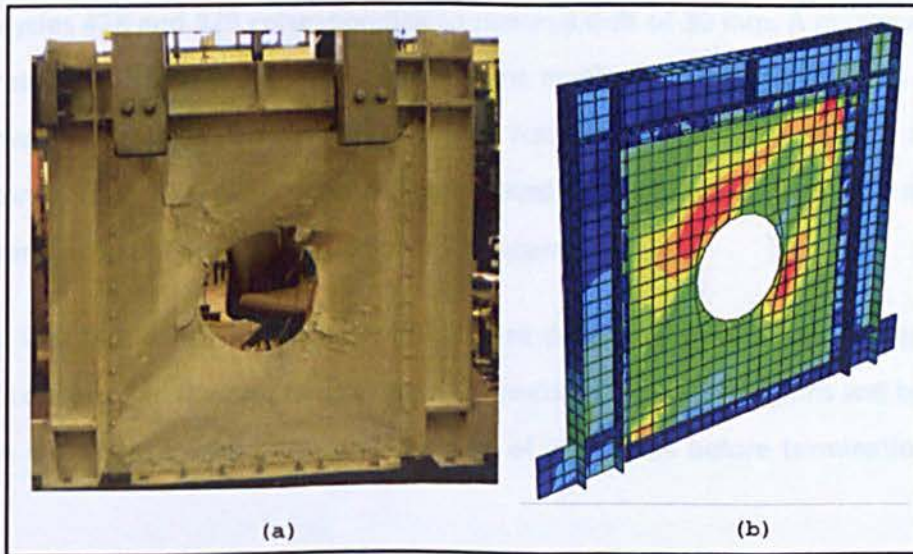


Figure 6.2: (a) Deformation of steel plate, (b) FE results for von Mises stress distribution for W10 during cycle #23

During cycles #24 and #25 local buckling at steel plate to fish plate connection area was observed at the top and bottom of the columns (Figure 6.3). A maximum base shear reached 209.91 kN corresponding to storey drift of 20 mm.



Figure 6.3: Occurrence of local buckling in the steel plate and fish plate

An investigation of all connections shows that no fracture occurred in the connections up to cycles #26 and #27 corresponding to displacement amplitude of 25 mm. However, the first sign of yielding at the bottom part of left column was noticed during cycle #27 at a maximum base shear of 219.96 kN.

Plastic hinges were developed at the bottom of right column and top ends of columns during cycles #28 and #29 corresponding to nominal drift of 30 mm. A maximum storey shear reached 225.31 kN for this displacement amplitude. During cycle #28 a strong sound was noted which was related to weld fracture between left column and base plate connection. The same fracture was noted for right column during cycle #30 corresponding to nominal drift index of 3.5% (Figure 6.4).

The test was terminated during cycle #31 due to development of plastic hinges at both ends of columns and fracture of both weld connections between columns and base plate joints. A maximum storey shear was reached of 222.67 kN before termination of this test.

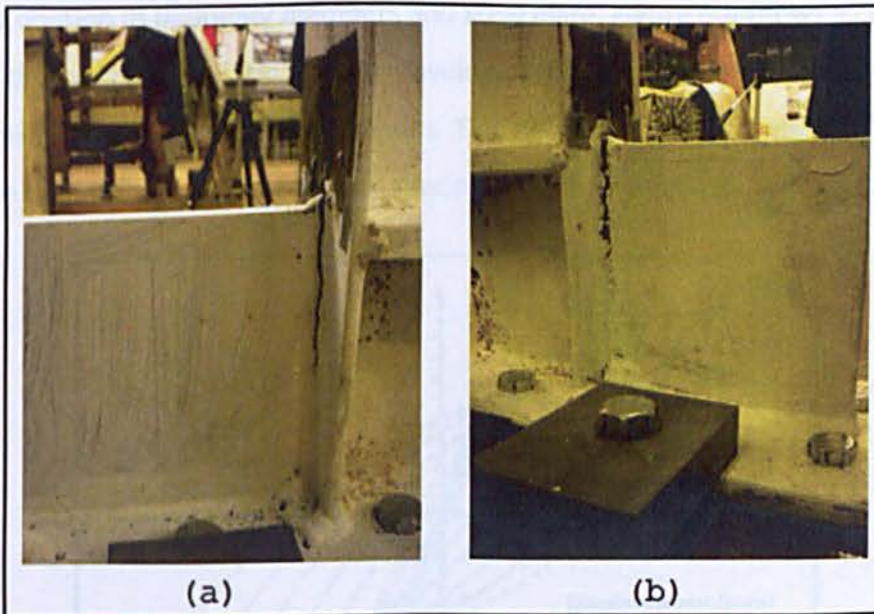


Figure 6.4: Weld fracture between column and connection plate during storey drift of (a) 30 mm for left column, (b) 35 mm for right column

The relation between storey shear and storey drift recorded during the quasi-static test for W10 specimen is shown in Figure 6.5.

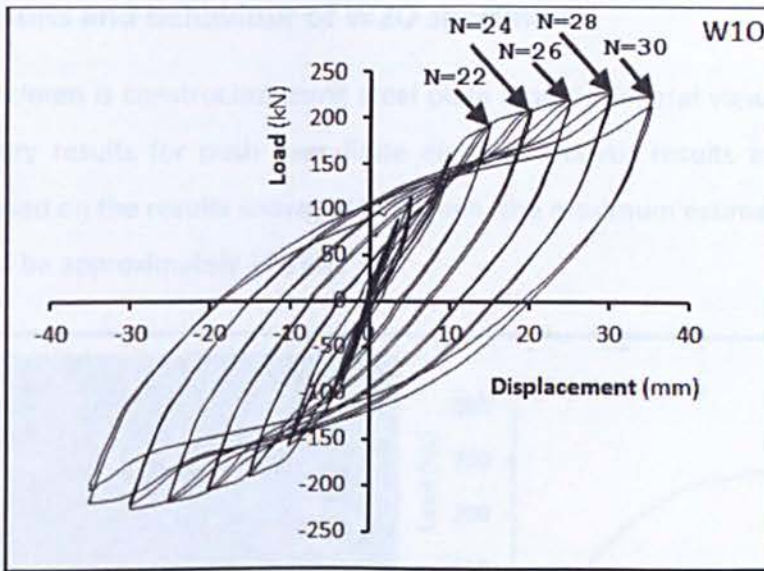


Figure 6.5: Hysteresis behaviour of W10 specimen during the quasi-static test

Finite element analysis was also conducted for W10 specimen using ABAQUS software. A good agreement was achieved between test and finite element results such as maximum shear load for different storey drifts, out-of-plane deformation of steel plate, stress distribution in boundary members and steel plate. Figure 6.6 shows a comparison between the cyclic quasi-static test and envelope of the hysteresis curves attained from cyclic explicit finite element analysis results. This figure indicates the ability of FE model to capture the ultimate load capacity of specimen during each cycle.

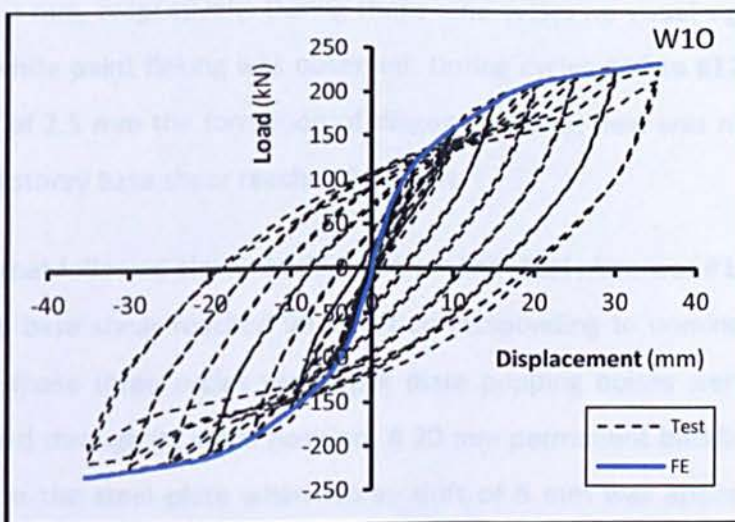


Figure 6.6: Comparison between cyclic test results and envelope of FE hysteretic analysis for W10 specimen

6.3. Test results and behaviour of W20 specimen

The W20 specimen is constructed using steel plate type II. General view of test set up and preliminary results for push over finite element analysis results are depicted in Figure 6.7. Based on the results shown in this graph, the maximum estimated shear load is predicted to be approximately 270 kN.

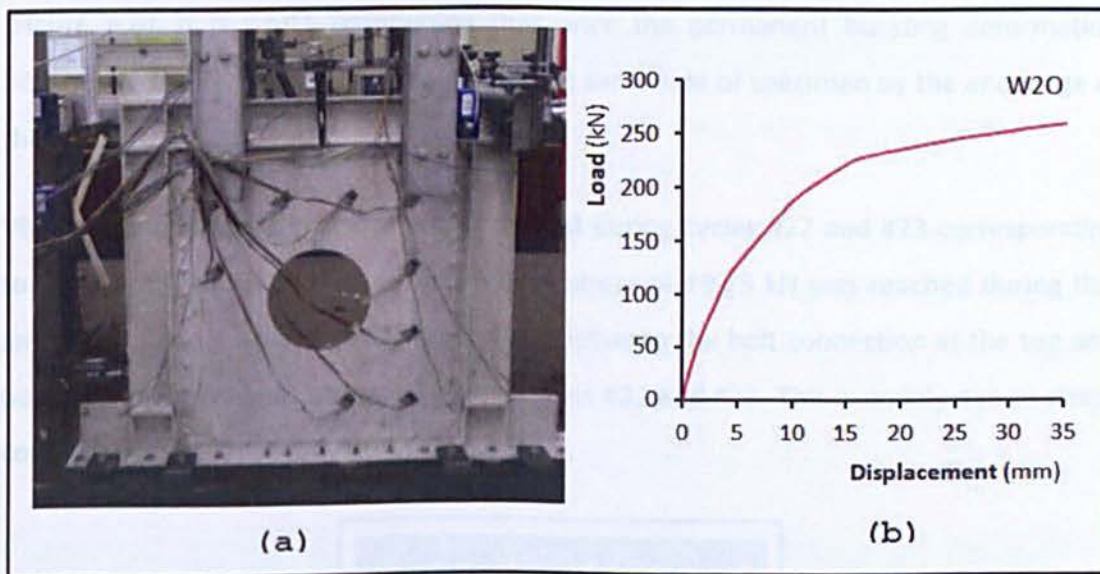


Figure 6.7: Test set up and preliminary FE analysis results for W20

The response of specimen up to nominal drift index of 0.12% was linear. A maximum base shear of 15.62kN, 30.75 kN and 45.55 kN was reached for storey drift of 0.4 mm, 0.8 mm and 1.2 mm, respectively. During these nine cycles no visual sign of steel plate buckling and white paint flecking was observed. During cycles #10 to #12 corresponding to storey drift of 2.5 mm the formation of diagonal tension field was noted within the steel plate and storey base shear reached 80.35 kN.

The first cycle that followed elastic buckling within the steel plate was #13. During cycles #13 to #15 the base shear reached 99.34 kN corresponding to nominal drift index of 0.35%. During these three cycles very weak plate popping noises were heard as the specimen passed through its initial position. A 20 mm permanent buckling deformation was recorded in the steel plate when storey drift of 5 mm was applied to specimen during cycles #16 to #18. This permanent buckling is mainly due to existence of cut-out in the steel plates which precludes proper formation and distribution of diagonal tension

field within the steel plate. In other words existence of cut-outs prevents self adjustment of the steel plate during post buckling behaviour of specimen. A maximum base shear of 121.43 kN was reached during these three cycles. The existing buckling waves in both directions of the steel plate were combined during cycles #19 to #21 corresponding to nominal drift index of 1% and base shear of 183.91 kN. However, the magnitude of permanent deformation of steel plate was increased to 26 mm during these cycles (Figure 6.8). It is worth mentioning that once the permanent buckling deformation occurred in the steel plate, it remained at the same side of specimen by the end stage of the test.

Visible stretching of steel plate was observed during cycles #22 and #23 corresponding to storey drift of 15 mm. A maximum base shear of 19.73 kN was reached during this amplitude. Local buckling of the steel plate between the bolt connection at the top and bottom of columns was observed during cycles #22 and #23. This is mainly due to stress concentration at this region of the steel plate.

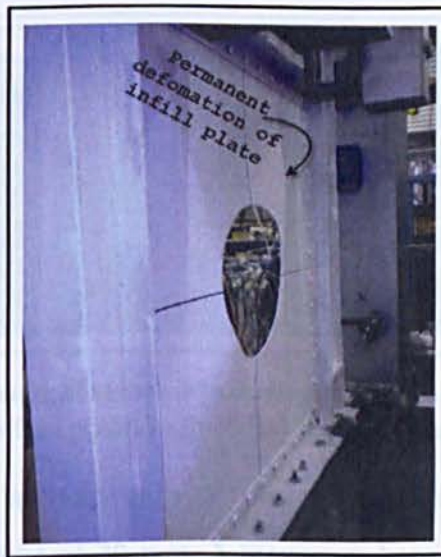


Figure 6.8: Permanent deformation of steel plate initially started at 5 mm story drift

During cycles #24 and #25 corresponding to nominal drift index of 2% considerable buckling deformation occurred in the steel plate and a maximum base shear of 237.17 kN was achieved during this amplitude. During cycle #25 a maximum out-of-plane buckling deformation of 54 mm was recorded in the steel plate. Figure 6.9 indicates measurements for out-of-plane deformation of steel plate during cycle #25.

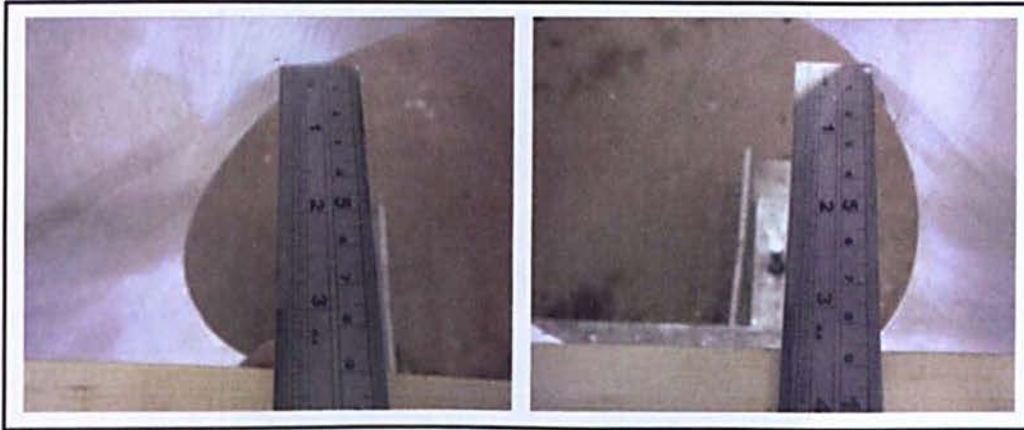


Figure 6.9: Noticeable out-of-plane buckling deformation of steel plate during cycle #25 for W20 specimen

During cycles #26 and #27 corresponding to nominal drift index of 2.5% base shear reached 247.37 kN. Local buckling and yielding of fish plates was observed at both ends of the columns. The first sign of yielding at the bottom of the left column was noticed during cycle #27. Figure 6.10 shows the buckling deformation of steel plate for cycle #25 at storey displacement of +25 mm, 0 mm and -20 mm from left to right, respectively.

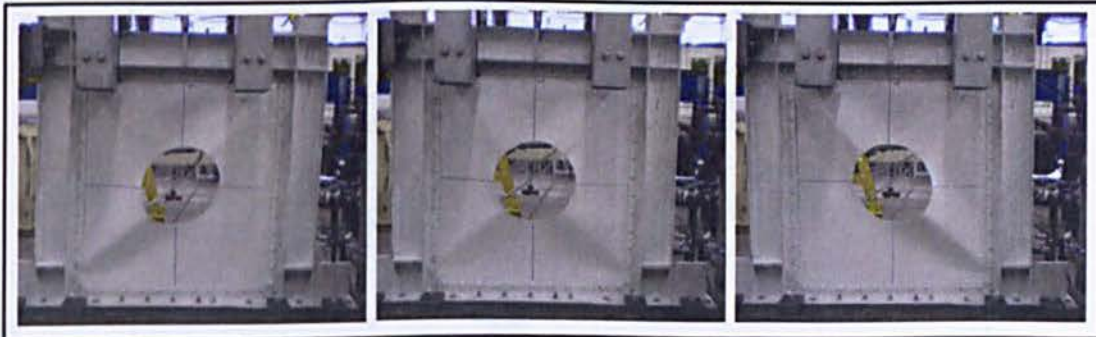


Figure 6.10: Deformed shape of steel plate during cycle #24 at storey drift of +20 mm (left), initial position (middle) and -20 mm (right)

Plastic hinges developed at both ends of the columns during cycles #28 and #29 corresponding to storey drift of 30 mm. A maximum base shear reached 254.93 kN during this amplitude. Weld fracture between column and connection plate was noticed during cycle #29. The cycle #30 corresponding to nominal drift index of 3.5% was the last cycle applied to the specimen. A maximum base shear of 253.8 kN was achieved during the cycle. Massive yield in fish plate, extending of weld fracture between column and connection plate and finally local buckling at flange at the bottom of column caused termination of test during cycle #30 (Figure 6.11).

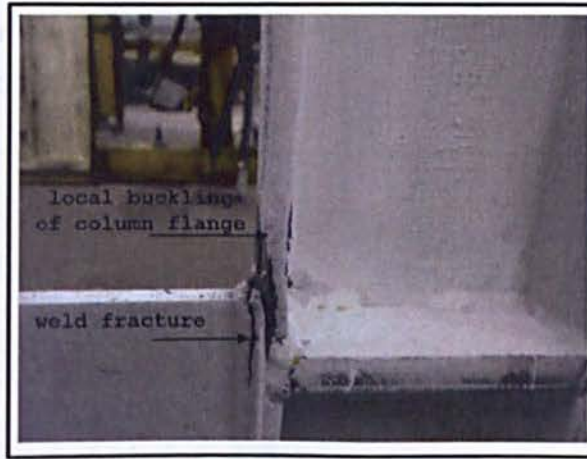


Figure 6.11: State of column at the end of the test for W20 specimen

The relation between storey shear and storey drift recorded during the quasi-static test for W20 specimen is depicted in Figure 6.12.

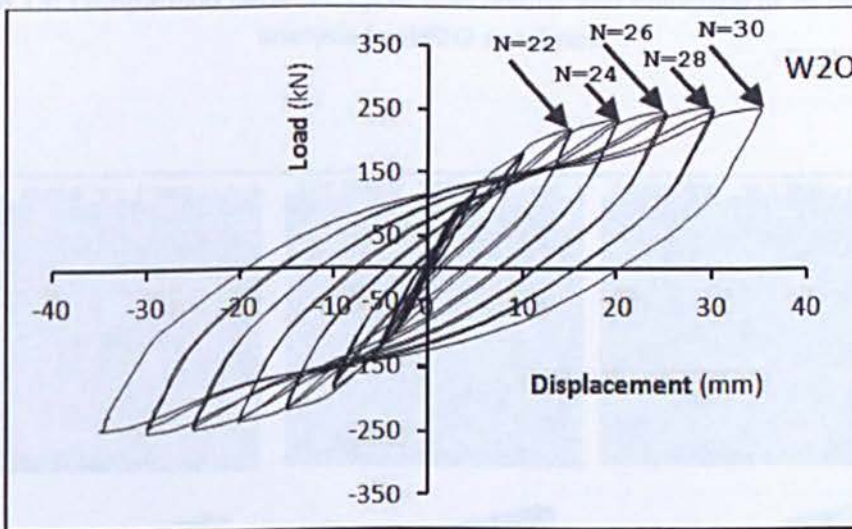


Figure 6.12: Hysteresis behaviour of W20 specimen during the quasi-static test

Finite element analysis was also conducted for W20 using ABAQUS software. A good agreement was achieved between test and finite element results such as maximum shear load capacity of specimens for different storey drifts, out-of-plane deformation of steel plate, stress distribution in boundary members and steel plate. Figure 6.13 compares the cyclic quasi-static load-displacement test results and envelope of the hysteresis curves attained from cyclic explicit finite element analysis. This figure shows the ability of FE model for capturing the ultimate load capacity of specimen during each

cycle. The capability of FE simulation for proper prediction of the steel plate buckling deformation is depicted in Figure 6.14.

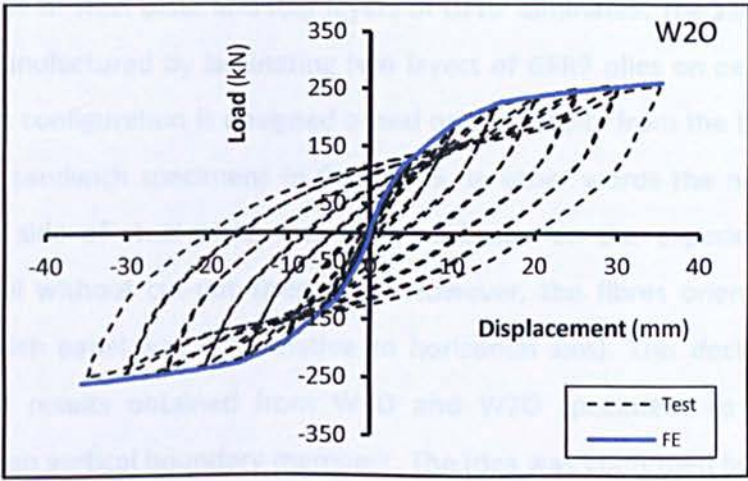


Figure 6.13: Comparison between cyclic test results and envelope of FE hysteretic analysis for W20 specimen

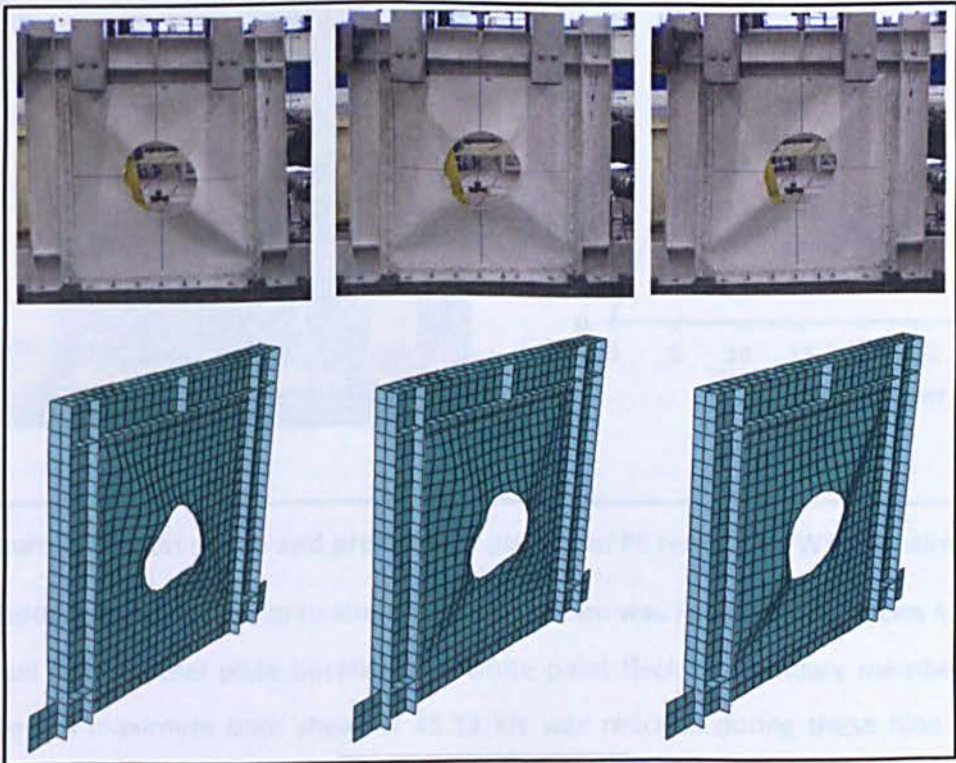


Figure 6.14: The state of W20 specimen for storey drift of 30 mm and corresponding results for finite element simulations

6.4. Test results and behaviour of W10G specimen

W10G is a sandwich specimen with 30 mm diameter cut-out in which the sandwich panel was made of steel plate and four layers of GFRP laminates. The sandwich panel of W10G was manufactured by laminating two layers of GFRP plies on each side of steel plate. This test configuration is designed based on the results from the test programme conducted on sandwich specimens in Chapter 5. In other words the number of GFRP plies on each side of steel plate was selected based on the experience gained on sandwich panel without cut-out specimens. However, the fibres orientation of GFRP plies in sandwich panel was 60° (relative to horizontal axis). This decision was made based on test results obtained from W10 and W20 specimens to prevent stress concentration on vertical boundary members. The idea was confirmed by finite element analysis of this specimen. General view of test set up and preliminary push over finite element results for W10 specimen are depicted in Figure 6.15.

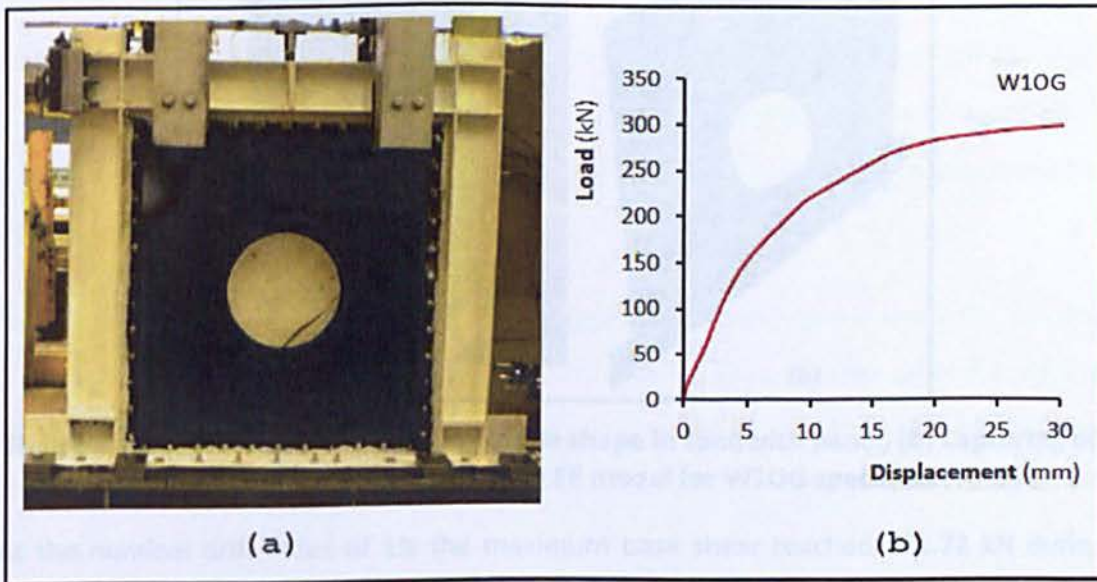


Figure 6.15: Test set up and preliminary push over FE results for W10 specimen

The response of specimen up to storey drift of 1.2 mm was linear. During cycles #1 to #9 no visual sign of steel plate buckling and white paint fleck in boundary members was observed. A maximum base shear of 45.13 kN was reached during these nine cycles. Non-linear behaviour of specimen started at storey adrift of 2.5 mm during cycles #10 to #12. A maximum base shear of 86.09 kN was reached during cycle #12.

The first cycle that followed elastic buckling in the steel plate was cycle #13. During cycles #13 to #15 the base shear reached 112.7 kN corresponding to nominal drift index of 0.35%. Considerable elastic buckling deformation was observed during cycles #16 to #18 corresponding to storey drift of 5 mm and maximum base shear of 145.23 kN. It is worth mentioning that up to cycle #18 no permanent deformation buckling was observed in sandwich panel. This result is mainly due to strengthening of the steel plate with GFRP plies. An investigation on buckling shape of sandwich panel shows that the buckling mode shape of sandwich panel was changed compared with steel plate mode shape (Figure 6.16-a). This restricted the out-of-plane deformation of the sandwich panel. The finite element analysis of this specimen captured this mode shape of buckling at storey drift of 5 mm (Figure 6.16-b).

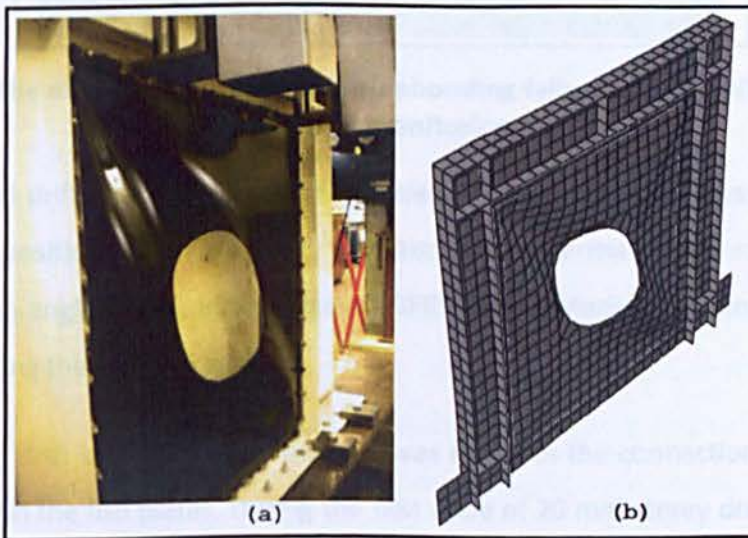


Figure 6.16: (a) Alteration of buckling mode shape in sandwich panel, (b) Capturing of changing in buckling mode by FE model for W10G specimen

At the nominal drift index of 1% the maximum base shear reached 221.72 kN during cycles #19 to #21. During cycle #21 infrared thermal camera captured an image around the cut-out that is indication for debonding of GFRP plies. This area is marked in Figure 6.17.

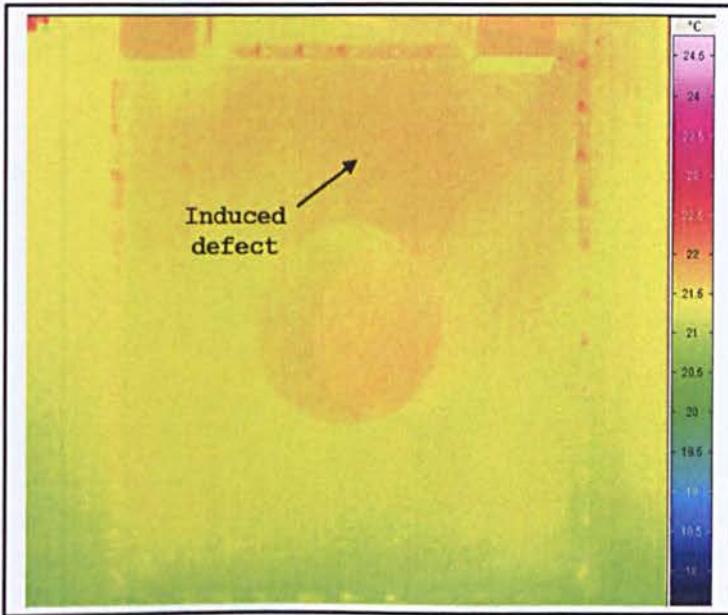


Figure 6.17: The area that is indication for debonding failure of GFRP plies as result of infrared monitoring

At the nominal drift index of 1.5% during cycles #22 and #23 crack was noted in GFRP plies at the position that had been monitored by thermal camera. These cracks appeared at an angle of 60°, in direction of GFRP fibres. Maximum base shear reached 268.19 kN during this amplitude.

Up to nominal drift index of 2% no fracture was noted in the connections. No buckling was observed in the fish plates. During the first cycle of 20 mm storey drift, the crack of GFRP laminates extended to the bottom of the cut-out (Figure 6.18) and maximum base shear reached 288.55 kN. During the second cycle of this amplitude the yield of left column was noted at the bottom end.

During cycles #26 and #27 corresponding to nominal drift index of 2.5% plastic hinges were developed at both ends of the columns. A maximum base shear reached 288.31 kN during these cycles. Separation between steel plate and GFRP laminates was observed during cycle #27. Weld fracture between columns and connection plates was also noticed during cycle #27. During this cycle sign of yield was noted at both ends of the beam element.

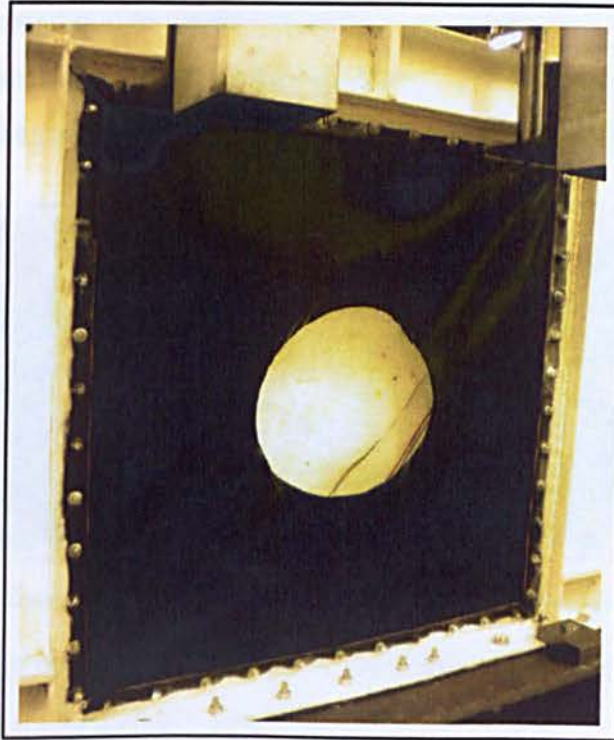


Figure 6.18: Extension of tears in GFRP laminates

During cycles #28 and #29 corresponding to nominal drift index of 3% plastic hinges formed at both ends of the beam (Figure 6.19-a). A maximum base shear reached 264.18 kN during the last two cycles of the test. Once the test terminated, inspection of fish plates and their connections to boundary members revealed that no local buckling at connection area of fish plates and steel plate had occurred (Figure 6.19-b). This is because part of shear load had transferred from columns to beam element.

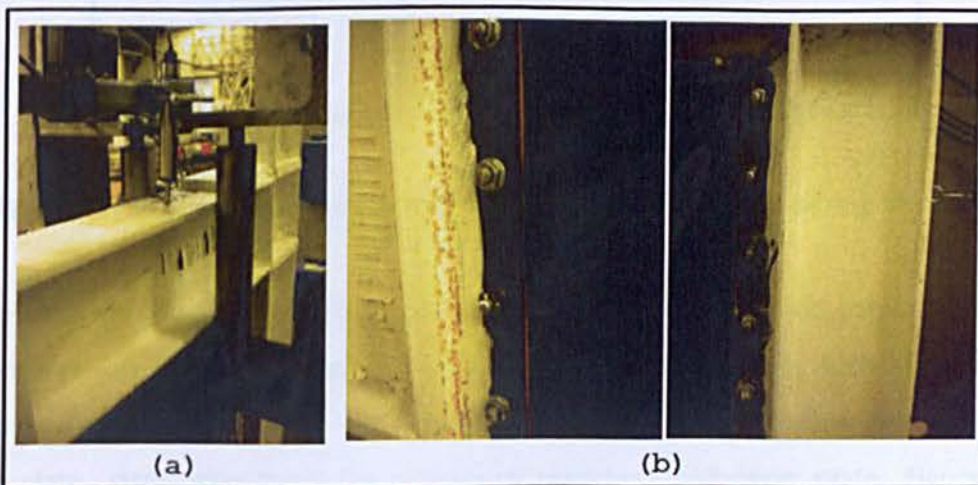


Figure 6.19: (a) Formation of plastic hinges at the end of beam, (b) No buckling was noted at fish plates during the last cycle

The test was terminated due to development of plastic hinges at both ends of boundary members and extension of weld fracture between columns and connection plates. Figure 6.20 shows the state of deformed specimen during the last cycle of the loading.

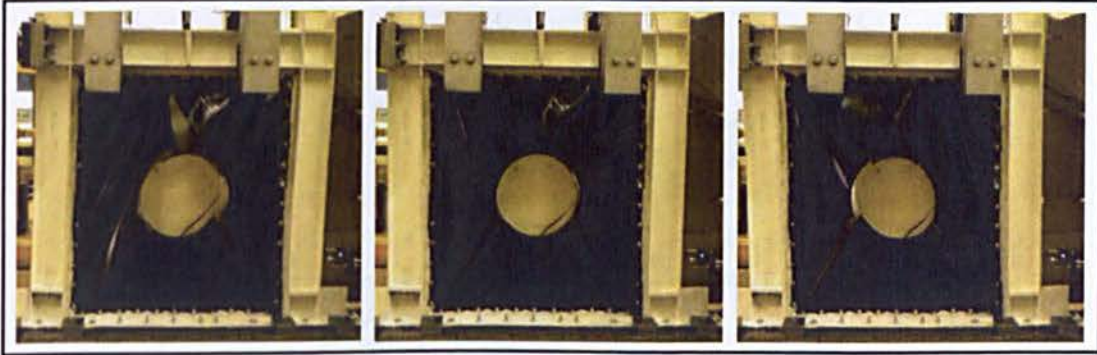


Figure 6.20: The state of W10G specimen during the last cycle of loading

The relation between storey shear and storey drift recorded during the quasi-static test for W10G specimen is depicted in Figure 6.21.

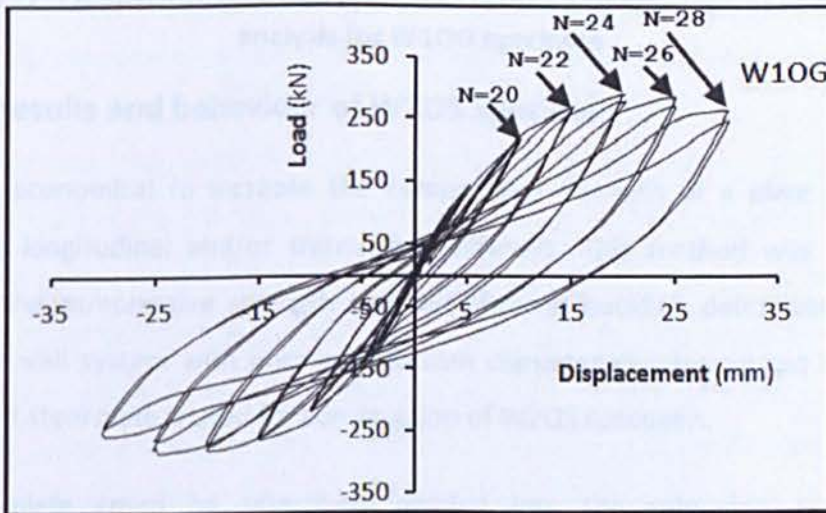


Figure 6.21: Hysteresis behaviour of W10G specimen recorded during the quasi-static test

Finite element analysis was also conducted for W10G using ABAQUS software. A good agreement was achieved between test and finite element results such as maximum shear load capacity of specimens for different storey drifts, out-of-plane deformation of steel plate, stress distribution in boundary members and steel plate. Figure 6.22 compares load-displacement during the cyclic quasi-static test and envelope of the

hysteresis curves obtained from cyclic explicit finite element analysis. This figure indicates the ability of FE model for capturing the ultimate load capacity of specimen during each cycle. There is a reasonable agreement between test and finite element results.

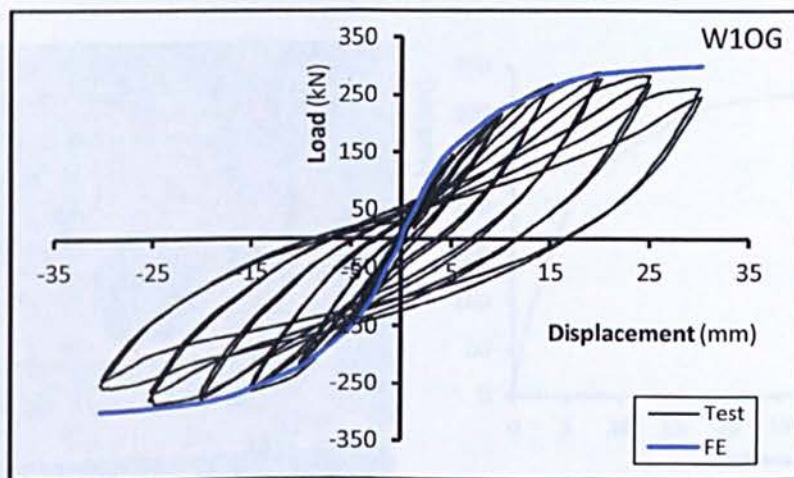


Figure 6.22: Comparison between cyclic test results and envelope of FE hysteretic analysis for W10G specimen

6.5. Test results and behaviour of W2OS Specimen

It is often economical to increase the compressive strength of a plate element by introducing longitudinal and/or transverse stiffeners. This method was applied for improving the compressive strength and out-of-plane buckling deformation of steel plate shear wall system with encased 300 mm diameter circular cut-out in the steel plate. Type II steel plate is used for construction of W2OS specimen.

The steel plate could be effectively divided into the subpanels by individual arrangements of flat stiffeners in order to develop sufficient tension fields across the shear panel. Finite element analysis using the ABAQUS software was carried out to determine the optimal dimension of stiffeners. The study was focused on assumption for one-side flat stiffeners. In order to prevent stress transmission between stiffeners and boundary members, the span of stiffeners was just short of plate edges. Utilisation of appropriate stiffeners with sufficient flexural stiffness and low torsional rigidity, the overall buckling of steel plate transferred to local buckling of sub panels. Based on aforementioned criteria, two longitudinal and two transverse stiffeners with cross

section dimensions $t_s=3$ mm and $h_s=50$ mm were selected for W2OS specimen. The general view of the specimen and preliminary push over finite element analysis results are depicted in Figure 6.23. The maximum estimated shear capacity of the specimen is about 320 kN.

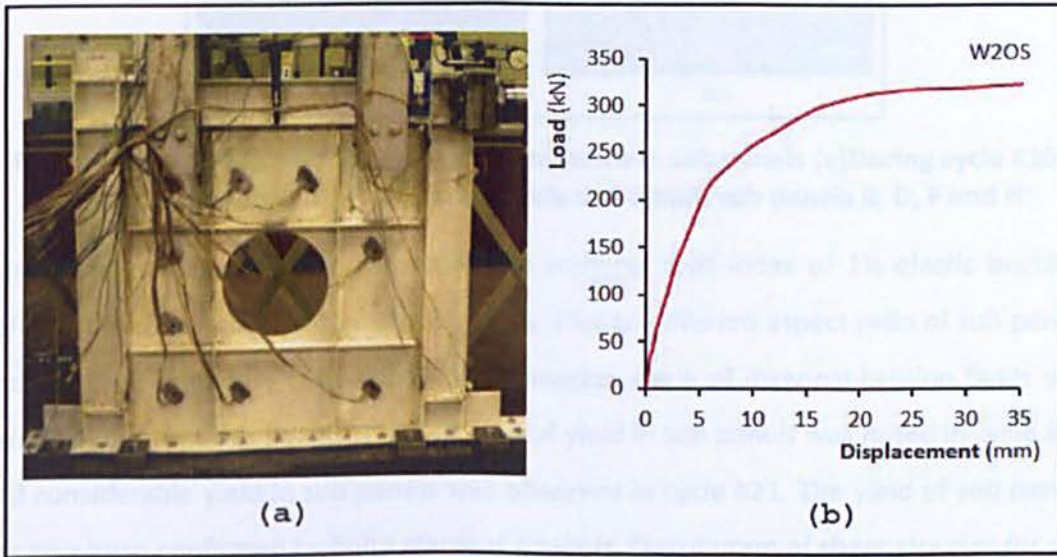


Figure 6.23: (a) General view and stiffener arrangements (b) Preliminary finite element analysis results for W2OS specimen

The specimen had a significant initial stiffness and base shear during first three cycles reached 21.78 kN at 0.4 mm storey drift. The specimen exhibited non-linear behaviour even at early stage of the loading and the base shears were recorded as 37.37 kN and 55.11 kN at storey drifts of 0.8 mm and 1.2 mm, respectively. This non-linearity could be due to complex geometry of infill panel and residual stresses introduced to the infill panel during welding of stiffeners to infill panel. During nominal drift indices of 0.25% and 0.35% corresponding to cycles #10 to #12 and #13 to #15 the storey shear reached 105.38 kN and 142.11 kN, respectively. Up to storey displacement of 3.5 mm no visual sign of infill panel and sub panel buckling was observed.

During cycles #16 to #18 formations of diagonal tension field and minor buckling was noted in some of the sub panels. Figure 6.24-a and Figure 6.24-b illustrate position and inclination angles of diagonal tension field for sub panels during cycles #16 and #18, respectively. During these cycles base shear reached 178.29 kN corresponding to storey drift of 5 mm.

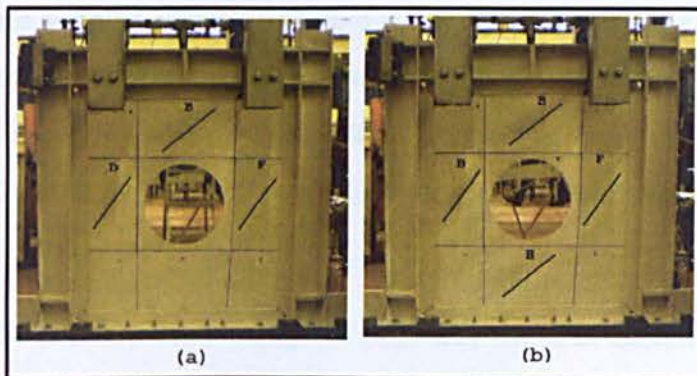


Figure 6.24: Formation of buckling deformations in sub panels (a)During cycle #16 within sub panels B, D, F, (b)During cycle #18 within sub panels B, D, F and H

During cycles #19 to #21 corresponding to nominal drift index of 1% elastic buckling deformations was observed in all sub panels. Due to different aspect ratio of sub panels and different boundary conditions, the inclination angle of diagonal tension fields was varied in different sub panels. The first sign of yield in sub panels was noted in cycle #19 and considerable yield in sub panels was observed in cycle #21. The yield of sub panels has also been confirmed by finite element analysis. Distribution of shear stresses for sub panels according to von Mises criterion and corresponding scale (MPa) is shown in Figure 6.25. A maximum base shear of 251.87 kN was achieved for storey drift of 10 mm.

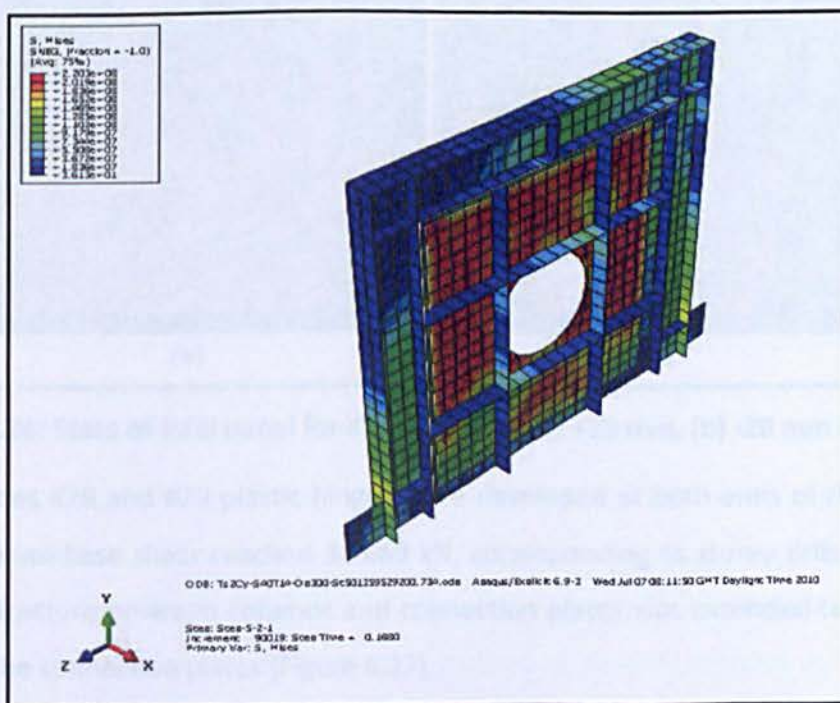


Figure 6.25: Counter plot of sub panels based on von Mises criteria at nominal drift index of 1%

A very weak plate popping noises was heard during cycles #22 and #23. This was due to buckling and post buckling behaviour in couple of sub panels. During cycle #23 a 5 mm weld crack was noted in welding of the left column and connection plate. A maximum base shear of 292.68 kN was achieved during cycles #22 and #23 corresponding to storey drift of 15 mm.

During cycles #24 and #25 the first sign of yield was noted at bottom end of the right column. A maximum base shear of 314.89 kN was reached corresponding to nominal drift index of 2%. The weld fracture between right column and connection plate was extended to 25 mm during cycles #26 and #27 and the same fracture occurred for welding between left column and connection plate during cycle #27. A maximum base shear of 313.05 kN was reached corresponding to storey drift of 25 mm. The out-of-plane buckling deformation of sub panels still was negligible. Deformation of stiffeners around the cut-out was observed during the last cycle of this amplitude. Figure 6.26 illustrates the state of infill panel during cycle #27 for the storey drift of 25 mm.

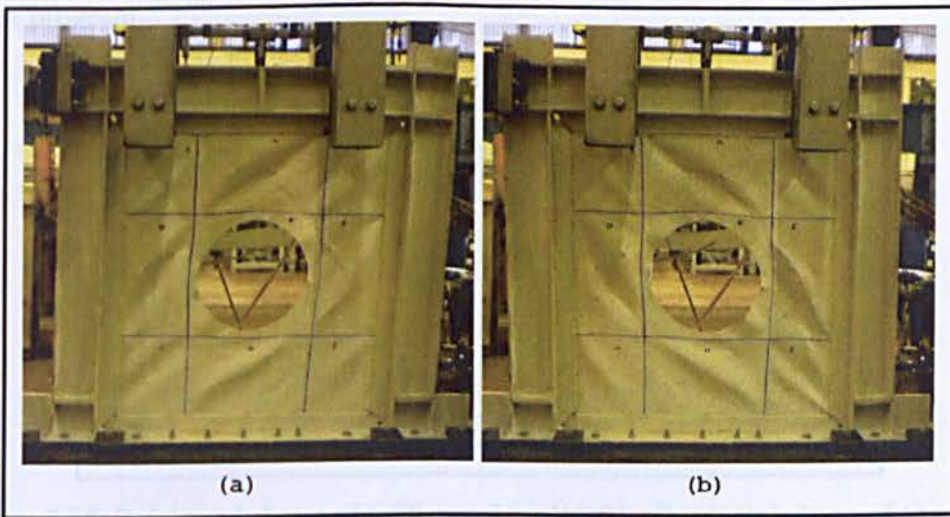


Figure 6.26: State of infill panel for storey drift of (a) +20 mm, (b) -20 mm for W20S

During cycles #28 and #29 plastic hinges were developed at both ends of the columns and maximum base shear reached 308.69 kN, corresponding to storey drift of 30 mm. The weld fracture between columns and connection plates was extended to the whole length of the connection plates (Figure 6.27).



Figure 6.27: Weld fracture and formation of plastic hinges at end of the column

During cycle #30 the decrease of shear capacity of specimen continued and maximum base shear was not exceeding 302.31 kN corresponding to nominal drift index of 3.5%. Deformation of stiffeners slightly increased during this cycle. However, none of them yielded to the end of test program. It is worth mentioning that even at final stage of test the buckling of steel plate was limited to sub panels and overall buckling of steel plate did not occurred. Figure 6.28 presents the buckling of sub panels after termination of the test program.

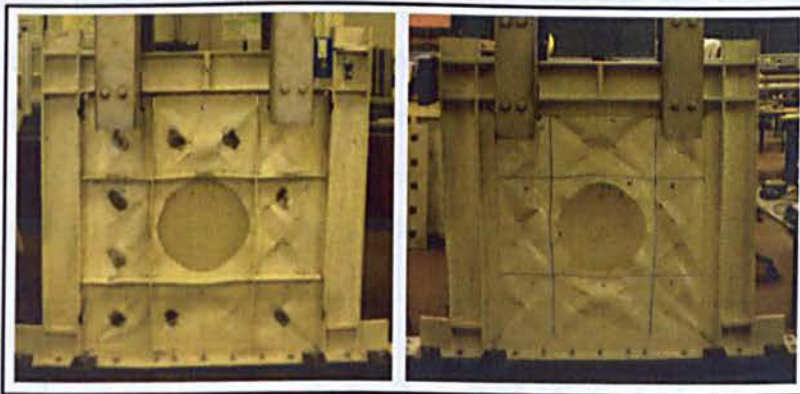


Figure 6.28: Deformed shape of infill panel for W2OS after termination of the test (overall buckling of steel plate is turned to local buckling of subpanels)

The relation between storey shear and storey drift recorded during the quasi-static test for W2OS specimen is depicted in Figure 6.29. The specimen exhibited highly ductile behaviour and the hysteresis curves were stable with significant capacity of energy dissipation. With all severe yielding in the columns and weld fracture in connection plates, the total base shear carried by the specimen was about 96% of its ultimate capacity.

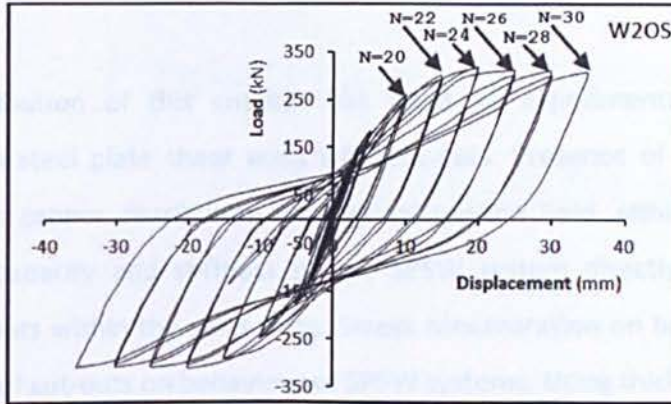


Figure 6.29: Hysteresis behaviour of W2OS recorded during the quasi-static test

Good agreement was achieved between test and finite element analysis results such as maximum shear load capacity of specimens for different storey drifts, stress distribution within the infill panel and boundary members, local buckling deformation of sub panels and inclination angle of diagonal tension field of sub panels. Figure 6.30 illustrates a comparison between the cyclic quasi-static test and envelope of the hysteresis curves attained from cyclic explicit finite element analysis results. This figure indicates the ability of FE model for obtaining the ultimate load capacity of specimen during each cycle. Gradually increasing differences were noted between the test results and FE response once drift value increased beyond 2%. This was due to development of weld fractures in the connection plates. Considering that the size of these cracks increased with loading cycles, a gradual stiffness reduction was observed in the experimental results. The FE model did not simulate this degradation of stiffness behaviour.

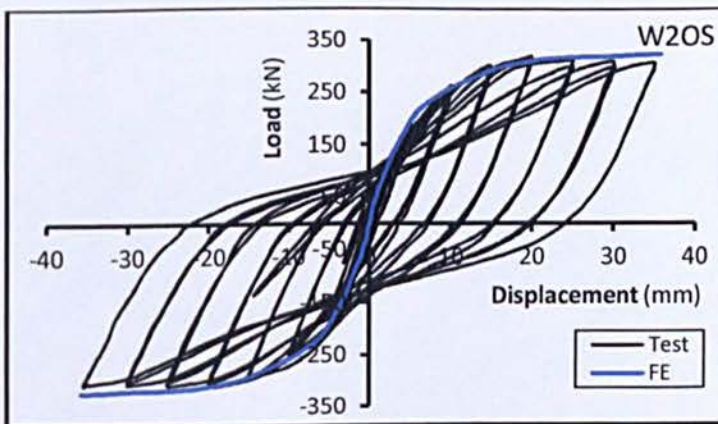


Figure 6.30: Comparison between cyclic test results and envelope of FE hysteretic analysis for W2OS specimen

6.6. Summary

The main contribution of this chapter has been an experimental and numerical investigation into steel plate shear walls with cut-outs. Presence of cut-outs in SPSW systems prevents proper distribution of diagonal tension field within the steel plate. Ultimate shear capacity and stiffness of the SPSW system directly are affected by encasing of cut-outs within the steel plate. Stress concentration on boundary elements is another effect of cut-outs on behaviour of SPSW systems. Using thicker steel plate and strengthening of shear panel are two options for improving the system's behaviour. These two methods have been investigated by experimental and numerical analysis.

The steel plate was strengthened using either uni directional GFRP laminated or flat steel stiffeners. The increase in initial stiffness, noticeable reduction in out-of-plane buckling of steel plate and significant increase in ultimate loading capacity of system are number of characteristics that have been improved during this chapter. UD-GFRP plies transferred part of diagonal tension field action to the beam element instead of the columns. As a result, the capacity of system was increased without increasing the flexural stiffness demand for columns. The well designed stiffeners changed the overall buckling of steel plate to local buckling in the sub panels. Noticeable increase in the load capacity and energy dissipation capacity was observed for this specimen.

7. DISCUSSION ON EXPERIMENTAL AND NUMERICAL RESULTS

7.1. Introduction

In Chapters 5 and 6 experimental and numerical results were presented for SPSW test specimens. A comparative study between tests and FE results revealed the capability of FE method for simulation of specimen behaviour.

7.2. Effect of steel plate thickness on the behaviour of SPSW specimens

The key performance indicator of the SPSW system is the relation between storey shear and storey displacement. Figure 7.1 illustrates the hysteresis behaviour of W1 and W2 specimens recorded during the quasi-static test. The specimens were cyclically loaded with increasing displacement in accordance with ATC-24 protocol up to the magnitude shown in Table 5.2. A maximum storey drift of 35 mm was achieved for both specimens prior to termination of the tests. Overall hysteretic behaviour was robust and stable for W1 and W2 specimens. Degradation of hysteresis loops during the last cycles was more noticeable for W1 specimen than W2 specimen.

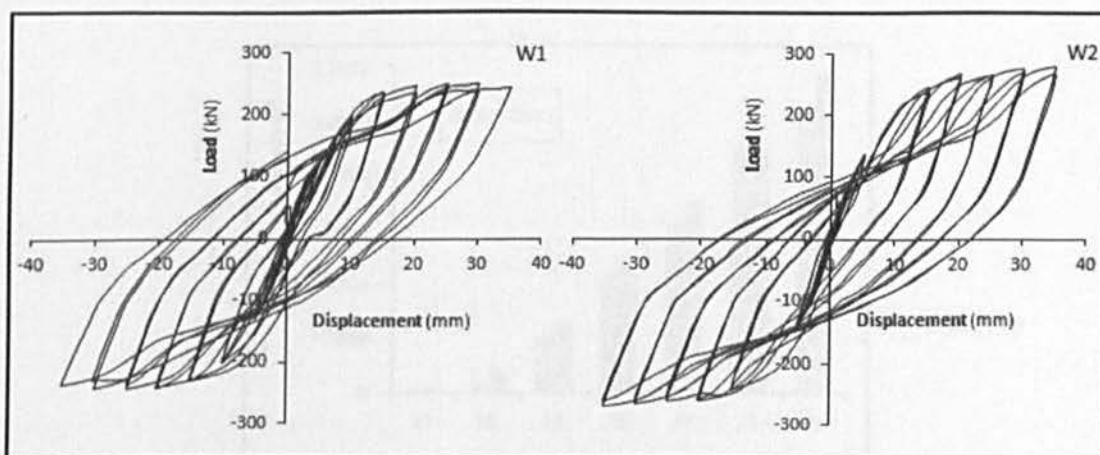


Figure 7.1: Load-displacement behaviour of W1 and W2 specimens

The W1 and W2 specimens withstood maximum load of 250.4 kN and 280.5 kN, respectively. From the load-displacement diagram the stiffness of the specimens during the pre- and post-yielding phases were 26.9 kN/mm and 9.7 kN/mm for W1 specimens, respectively and 27.6 kN/mm and 10.8 kN/mm for W2 specimen, respectively. In other words the initial stiffness of specimens is not significantly affected by thickness of the steel plate. However, the change in stiffness is more noticeable in post yield phases for both specimens (Figure 7.2).

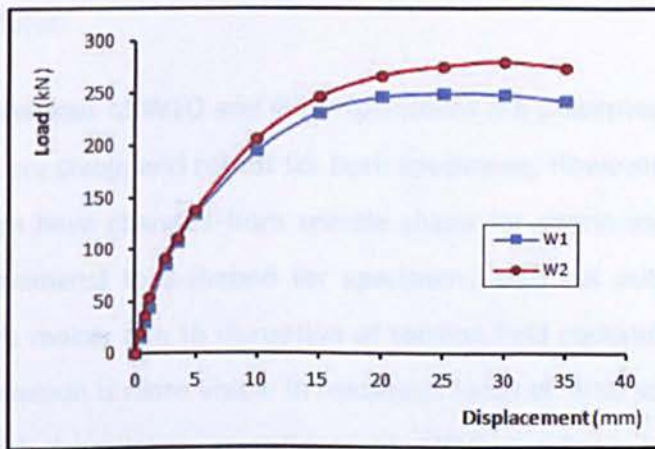


Figure 7.2: Comparison between envelopes of the cyclic quasi-static test results for W1 and W2 specimens

The area bounded by the load-displacement hysteresis loops indicates the energy dissipated by the structure through hysteretic loops. Figure 7.3 indicates hysteretic energy dissipation for W1 and W2 specimens. A comparison between cumulative energy dissipation shows that the energy dissipation capacity of W2 is 11% more than W1.

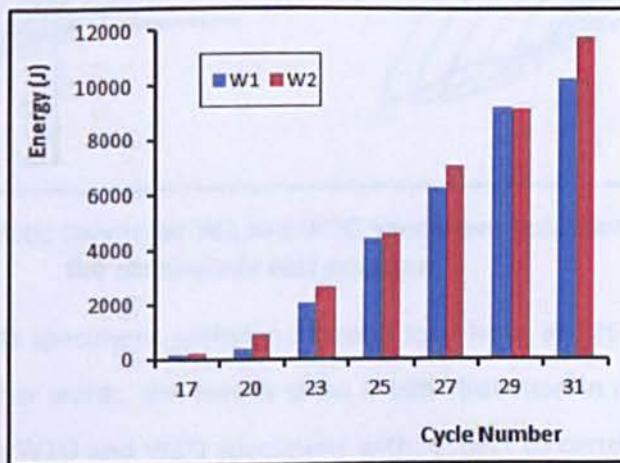


Figure 7.3: Hysteretic energy dissipation for W1 and W2 specimens

7.3. Effects of cut-outs on the behaviour of test specimens

In the present study the effects of cut-outs on seismic behaviour of SPSW systems were investigated. A 300 mm diameter cut-out was made in the steel plate of W1 and W2 specimens and labelled as W10 and W20 specimens, respectively. Due to disruption of tension field continuity within the steel plate for these specimens it was necessary to study the effects of cut-outs on the behaviour of the SPSW system. During the testing of W10 and W20 specimens, excessive out-of-plane buckling deformations were noticed within the steel plates.

The hysteresis behaviour of W10 and W20 specimens are presented in Figure 7.4. The hysteresis curves are stable and robust for both specimens. However, the overall shape of hysteresis loops have changed from spindle shape for specimens without cut outs (W1 and W2 specimens) to S-shaped for specimens with cut outs (W10 and W20 specimens). This is mainly due to disruption of tension field continuity within the steel plate. This phenomenon is more visible in hysteresis loops of W10 specimen. Figure 7.4 also indicates that degradation in stiffness for W10 specimen is more than W20 specimen.

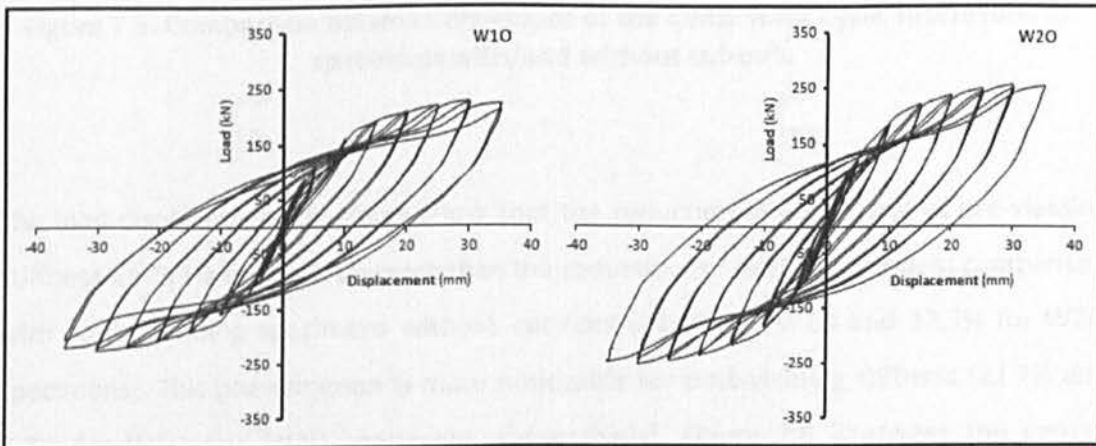


Figure 7.4: Hysteretic curves for W1 and W10 specimens recorded during the quasi-static test program

The W10 and W20 specimens withstood a total load level of 225.3 kN and 254.9 kN, respectively. In other words, the results show a 10% reduction in maximum shear load bearing capacity in W10 and W20 specimens with respect to corresponding specimens without cut-outs. Figure 7.5 compares envelope of quasi-static cyclic test results for

W10 and W20 specimens with corresponding specimens without cut-outs in the steel plate. The reduction of initial stiffness and energy dissipation capacity can be seen in this figure for "with" and "without cut-out" specimens. Based on AISC design guide 20 (AISC, 2007) frame members are required to be enough stiff to prevent the yield of boundary members prior to yield of the infill plate. This design criterion is the main reason for nonlinear relationship between thickness of the infill plate and corresponding ultimate shear load capacity of W1 and W2 specimens.

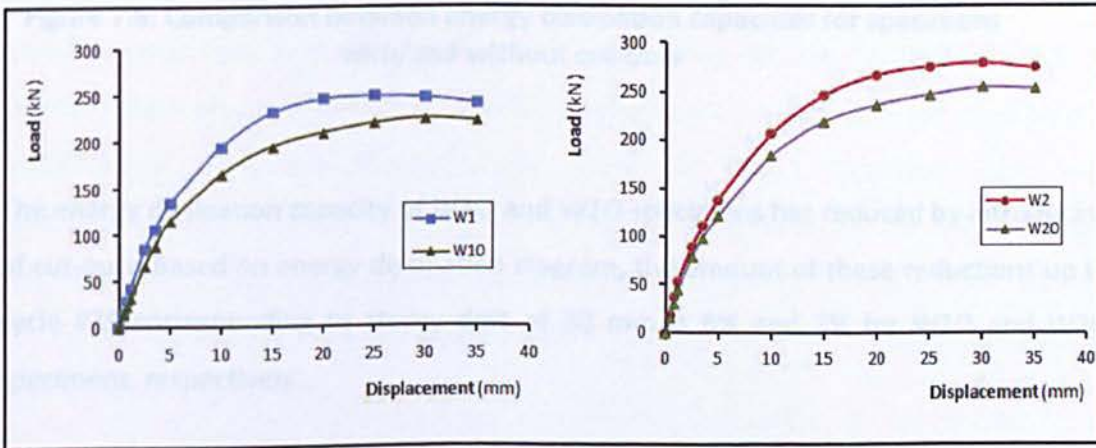


Figure 7.5: Comparison between envelopes of the quasi-static cyclic test results for specimens with/and without cut-outs

The load-displacement diagrams show that the reduction in magnitude of pre-yielding stiffness for W10 specimen is more than the reduction for W20 specimen in comparison with corresponding specimens without cut-outs (14.4% for W10 and 12.3% for W20 specimens). This phenomenon is more noticeable for post-yielding stiffness (22.7% and 9.3% for W10 and W20 specimens, respectively). Figure 7.6 illustrates the energy dissipation capacity in specimens with and without cut-outs.

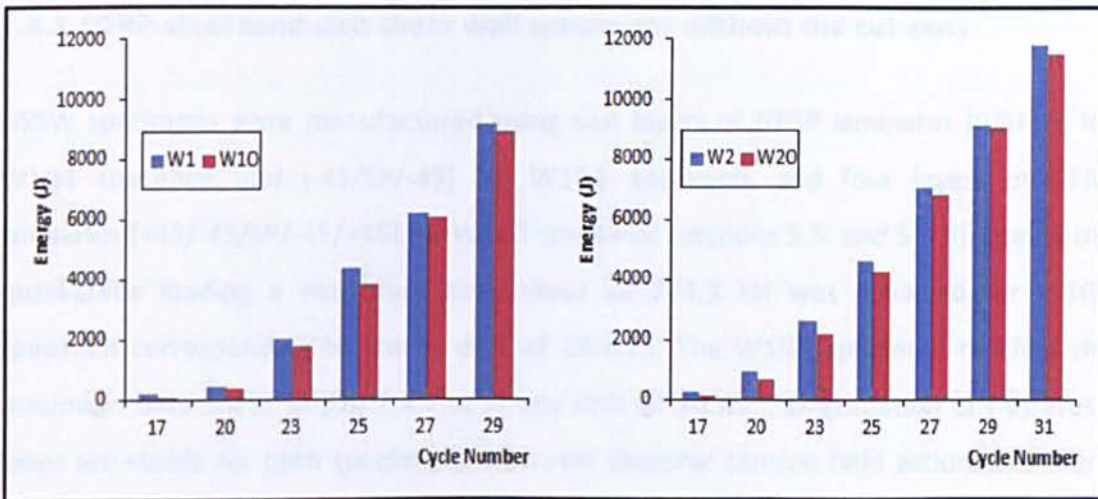


Figure 7.6: Comparison between energy dissipation capacities for specimens with/and without cut-outs

The energy dissipation capacity of W10 and W20 specimens has reduced by introducing of cut-outs. Based on energy dissipation diagram, the amount of these reductions up to cycle #29 corresponding to storey drift of 30 mm is 6% and 7% for W10 and W20 specimens, respectively.

7.4. Improving the Seismic behaviour of SPSW system using sandwich shear panels

Steel plate shear wall is inherently a dual lateral resisting system. The strength and stiffness of boundary members and distribution of diagonal tension field in the shear panel as well as the interaction between boundary members and shear panel determines the performance of SPSW system against the lateral loads. In present study the specifications of boundary members remained unchanged in all tests. The main function of steel plate is development of tension field within the steel plate. GFRP material was used for improving the seismic performance of SPSW systems. By using the sandwich panels, the-out-of plane deformation buckling of shear panel was dramatically reduced in specimens with and without cut-outs. The sandwich panel reduced the demand of flexural stiffness for columns due to effective association of the beam element for sustaining the action of diagonal tension field.

7.4.1 GFRP-steel sandwich shear wall specimens without the cut-outs

GSSW specimens were manufactured using two layers of GFRP laminates [0/SP/0] for W1G1 specimen and [-45/SP/-45] for W1G2 specimen, and four layers of GFRP laminates [+45/-45/SP/-45/+45] for W1G3 specimen (sections 5.5. and 5.5.3). During the quasi-static loading a maximum base shear of 274.8 kN was achieved for W1G1 specimen corresponding to storey drift of 25 mm. The W1G3 specimen reached the maximum base shear of 324.7 kN at storey drift of 20 mm. Degradation of hysteresis loops are visible for both specimens. However diagonal tension field actions are more robust for W1G3 specimen. This was due to alignment of GFRP ply direction with steel plate diagonal tension fields. Formation of very strong tension fields resulted in an excellent base shear of 324.7 kN for W1G3 specimen at relatively small amplitude of displacement. Hysteresis diagrams are stable for W1G1 specimen even after delamination of GFRP plies. This is due to sufficient clamping of the fibres by main and secondary fish plates. This phenomenon is more visible during the last couple of cycles of hysteresis loops for W1G3 specimen. Figure 7.7 illustrates the cyclic performance of specimens during the test.

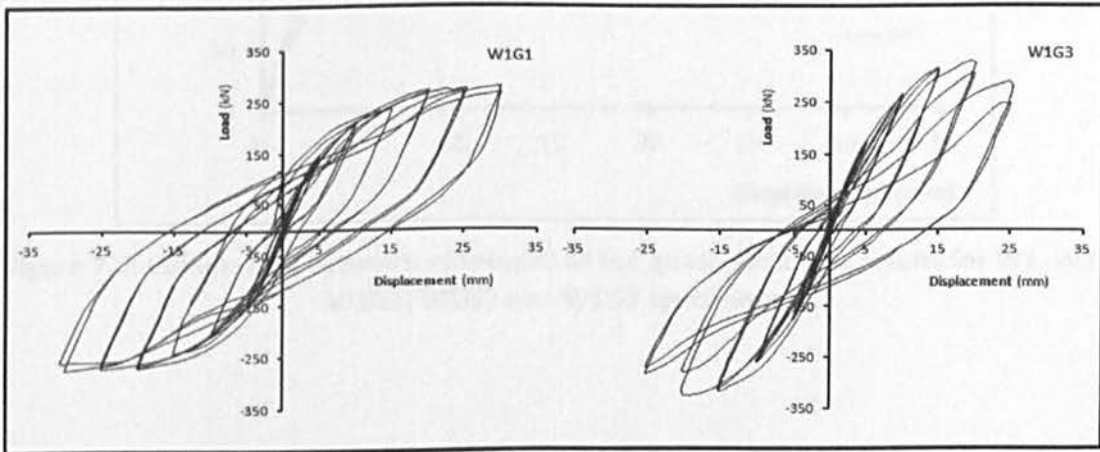


Figure 7.7: Hysteretic curves for W1G1 and W1G3 specimens recorded during the quasi-static test program

In order to investigate the effects of employing GFRP laminates on seismic characteristics of SPSW system, the envelope curves of hysteresis behaviour for W1, W2,

W1G1, W1G2 and W1G3 specimens during the quasi-static tests are compared in Figure 7.8. The maximum base shear is increased by 9% for W1G1 specimen, by 25% for W1G2 specimen and by 30% for W1G3 in comparison with W1 specimen.

The maximum base shear for W1G1 is approximately equal to maximum base shear of W2 specimen. The maximum base shear is increased by 11% and 16% for W1G2 and W1G3 specimens respectively in comparison with maximum base shear for W2 specimen. This graph indicates reduction of ductility for the W1G1 and W1G3 specimens. However, an investigation of these two specimens reveals that termination of both tests occurred due to formation of plastic hinges at the end of boundary members.

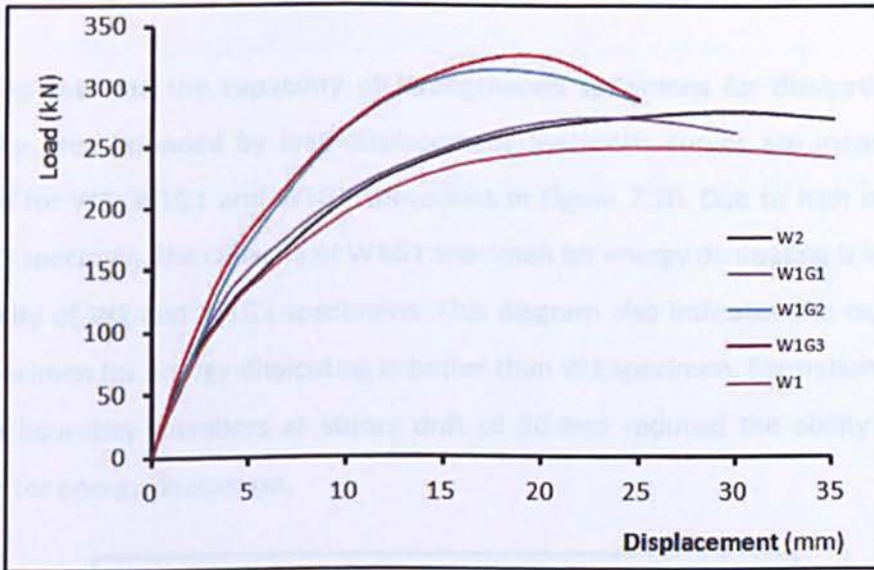


Figure 7.8: Comparison between envelopes of the quasi-static test results for W1, W2, W1G1, W1G2 and W1G3 specimens

The initial stiffness of lateral load resisting systems is the main characteristic for restricting the drift of structure during an earthquake and wind loading. Due to doubling the thickness of the infill plate, the initial stiffness magnitude for system 3.5 kN/mm has increased. However, the initial stiffness magnitudes have increased by 10 kN/mm for W1G1 and 33 kN/mm for W1G2 and 41.5 kN/mm for W1G3 in comparison with W2 specimens. Figure 7.9 compares the initial stiffness of these specimens.



Figure 7.9: The effect of GFRP laminates on initial stiffness of specimens

In order to evaluate the capability of strengthened specimens for dissipating of the energy the area bounded by load-displacement hysteresis curves are measured and compared for W1, W1G1 and W1G3 specimens in Figure 7.10. Due to high stiffness of the W1G3 specimen, the capacity of W1G1 specimen for energy dissipating is lower than the capacity of W1 and W1G1 specimens. This diagram also indicates the capability of W1G1 specimen for energy dissipating is better than W1 specimen. Formation of plastic hinges in boundary members at storey drift of 30 mm reduced the ability of W1G1 specimen for energy dissipation.

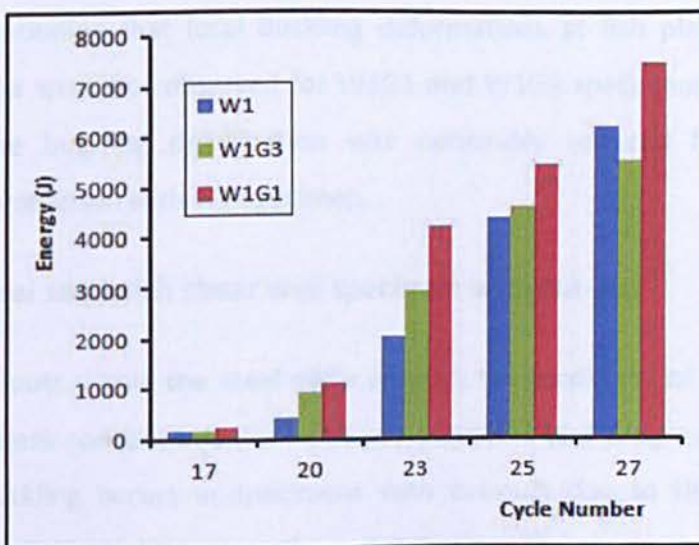


Figure 7.10: Comparative results for capability of specimens for energy dissipation

One of the reasons for employing GFRP laminates for improving the behaviour of SPSW systems is increasing the association of beam element for bearing the diagonal tension field action. Laminating the GFRP materials in the individual direction may practically implement this idea. To assess workability of this idea the vertical deflection of beam element was recorded by innovative sliding measurement system (section 4.8) during the test program (Figure 7.11).

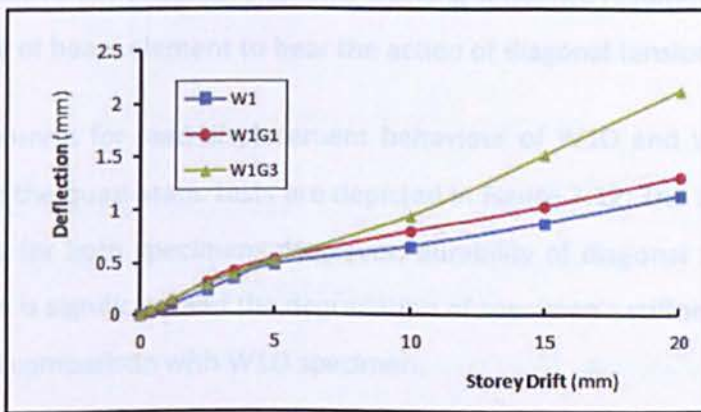


Figure 7.11: Vertical deflection measurements for mid part of the beam

The magnitude of beam deflections for W1G1 and W1G3 specimens are greater than those in W1 specimen. In other words the association of beam element for sustaining the part of tension field effect within the steel plate has reduced columns' demand for flexural stiffness and strength at the same range of shear capacity for non-strengthened specimen.

It is worth mentioning that local buckling deformations at fish plate to steel plate connections area were not observed for W1G1 and W1G3 specimens during the test. The out-of-plane buckling deformation was noticeably reduced for strengthened specimens in comparison with W1 specimen.

7.4.2 GFRP-steel sandwich shear wall specimen with cut-out

Introducing cut-outs within the steel plate disrupts the continuity of diagonal tension field actions. Stress concentration in boundary members and progressive out-of-plane deformation buckling occurs in specimens with cut-outs due to the lack of strong diagonal tension fields and its non-uniform distribution. The permanent deformation of

CHAPTER 7: DISCUSSION ON EXPERIMENTAL AND NUMERICAL RESULTS

steel plate at early stage of loading amplifies the reduction of ultimate shear capacity of the system. The effectiveness of utilising GFRP laminates for restricting the out-of-plane deformations and precluding the stress concentration in boundary members was observed for W1G1 and W1G3 specimens during the test program. All these results were considered for improving the performance of W1O specimen. However, for newly designed specimen, W1OG, two layers of plies were laid down on both sides of steel plate at $\pm 60^\circ$ relative to horizontal axis. This stacking sequence resulted in an increase in the functionality of beam element to bear the action of diagonal tension field.

The hysteresis curves for load-displacement behaviour of W1O and W1OG specimens recorded during the quasi-static tests are depicted in Figure 7.12. The stable and robust loops are visible for both specimens. However, durability of diagonal tension fields for W1OG specimen is significant and the degradation of specimen's stiffness in subsequent loops is lower in comparison with W1O specimen.

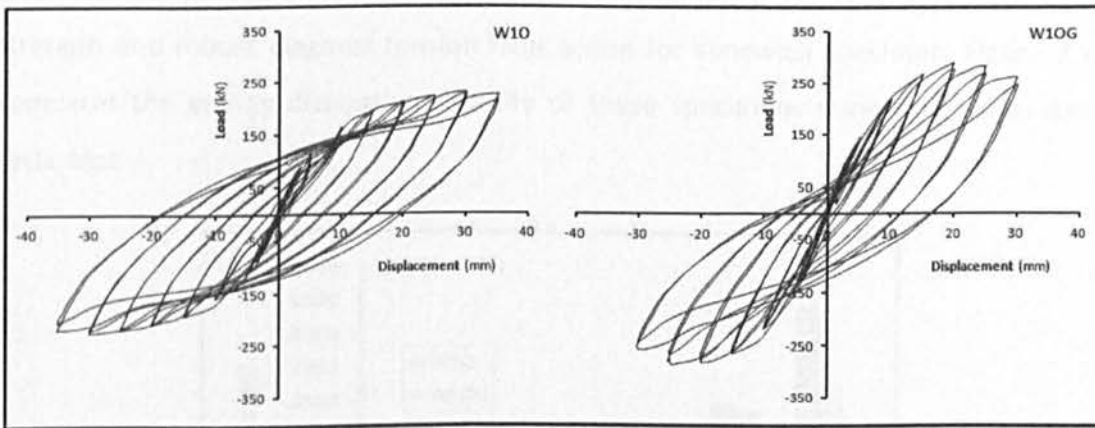


Figure 7.12: Hysteresis behaviour of W1O and W1OG specimens during the test

The ultimate shear load capacity of 225.3 kN was gained for W1O specimen at storey drift of 30mm while the W1OG specimen reached its ultimate shear capacity of 288.3 kN at storey drift of 25mm. The envelope curve for hysteresis loops of W1O and W1OG are depicted in Figure 7.13. The illustrated results indicate that the performance of W1O specimen is extremely enhanced by laminating UD-GFRP plies on the perforated steel plate. Comparing the ultimate shear capacity of W1OG specimen with W1 and W1O specimens confirms an increase of 13.3% and 21.8% in shear load capacity, respectively.

In other words the ultimate shear capacity of GFRP-SPSW specimen with cut-out, W1OG, is increased even beyond the capacity of original specimen without cut-out, W1.

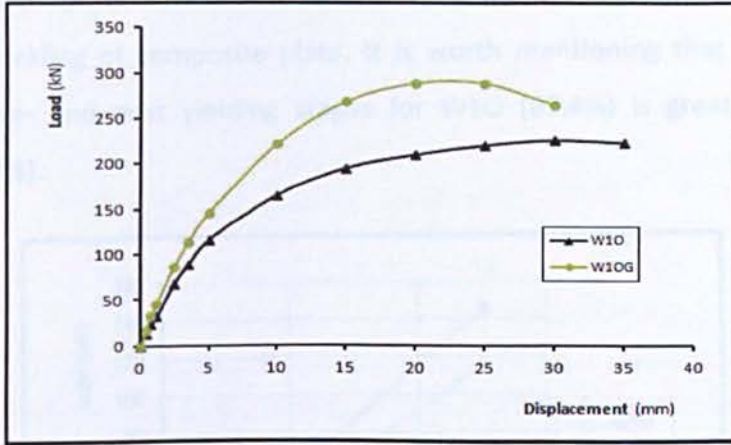


Figure 7.13: Comparison between the envelopes of quasi-static test results for W1O and W1OG specimens

The energy dissipation capacity of W1OG specimen up to its ultimate capacity is greater than the energy dissipation capacity of W1O specimen. It is because of high shear strength and robust diagonal tension field action for sandwich specimen. Figure 7.14 compares the energy dissipation capacity of these specimens during the quasi-static cyclic test.

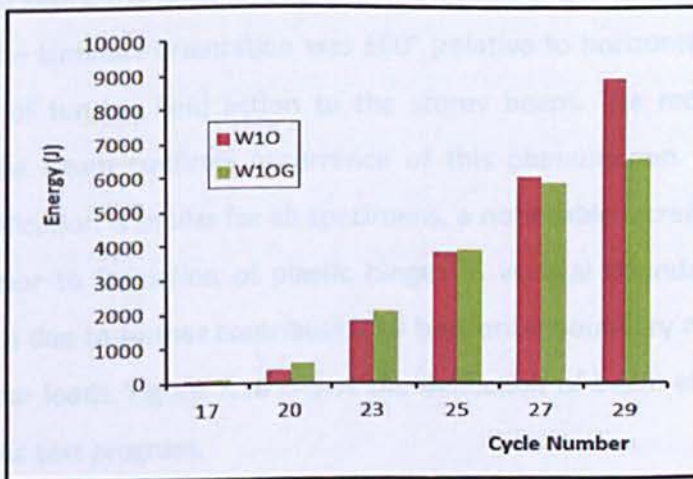


Figure 7.14: Energy dissipating capacity for W1O and W1OG specimens

Having a close look at load-displacement graph indicates initial stiffness of 23.1 kN/mm and 29.0 kN/mm for W1O and W1OG specimens, respectively (Figure 7.15). Applying GFRP laminates for strengthening of perforated steel plate has restored the initial

stiffness of specimen even above the original specimen stiffness without cut-out. This capability of specimen can effectively control the drift of structures during a lateral load event. This level of stiffness enables the specimen to restrict the out-of-plane deformation buckling of composite plate. It is worth mentioning that degradation of stiffness for pre- and post yielding stages for W1O (67.4%) is greater than W1OG specimen (57.7%).

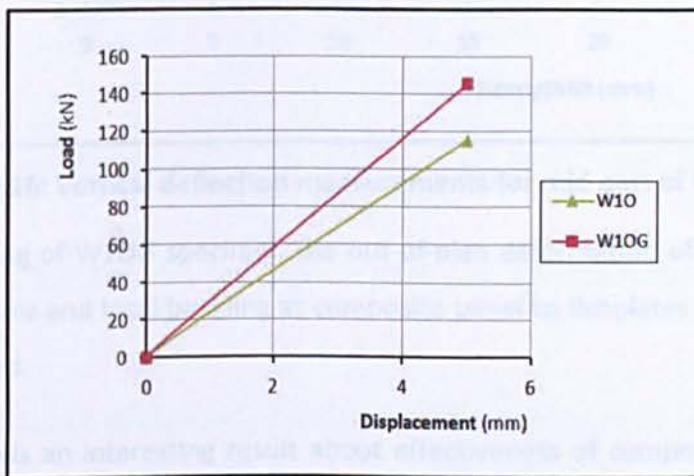


Figure 7.15: The effect of GFRP laminates on initial stiffness of specimens

One of the reasons for using GFRP laminates for strengthening of steel plate is the possibility of increasing the functionality of beam element against the action of diagonal tension field. The laminate orientation was $\pm 60^\circ$ (relative to horizontal axis) for further transformation of tension field action to the storey beam. The recorded results for deflection of the beam confirms occurrence of this phenomenon. As the boundary members' specification is similar for all specimens, a noticeable increase in the capacity of specimen prior to formation of plastic hinges in vertical boundary members was observed. This is due to further contribution of horizontal boundary member to sustain the applied shear loads. Figure 7.16 shows the deflection of beam element during the quasi-static cyclic test program.

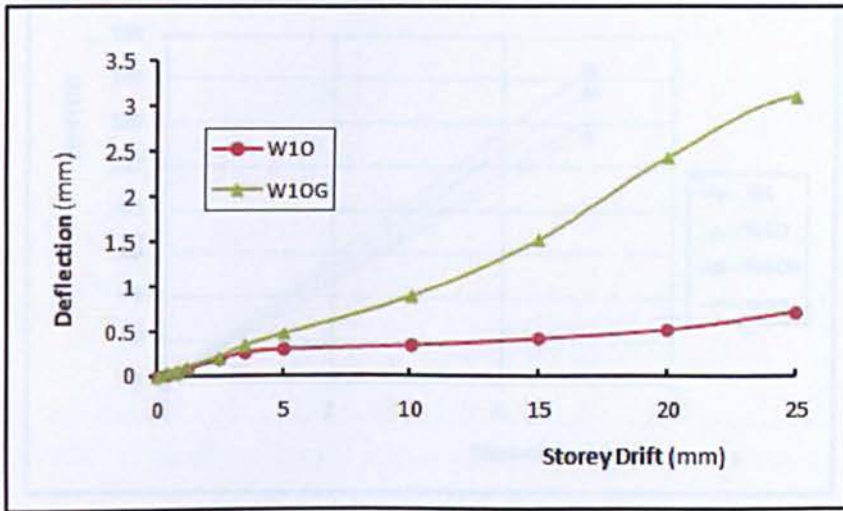


Figure 7.16: Vertical deflection measurements for mid part of the beam

During the testing of W10G specimen the out-of-plan deformation of composite panel was not noticeable and local buckling at composite panel to fishplates connection areas was not observed.

Figure 7.17 shows an interesting result about effectiveness of composite materials for enhancing the initial stiffness of perforated specimen. This figure indicates that the initial stiffness of the W10 specimen is decreased by 14.4% due to introduction of cut-out to W1 specimen. Two different methods can be used for compensating the stiffness reduction, either using a thicker plate (W20 specimen) or using composite material (W10G specimen). The results show that the initial stiffness is increased by 5% for W20 specimen and 20.3% for W10G specimen both in comparisons with W10 specimen. This means that by laminating steel plate the initial stiffness of W10 specimen has been restored to more than the initial stiffness of specimen without cut-out (W1).

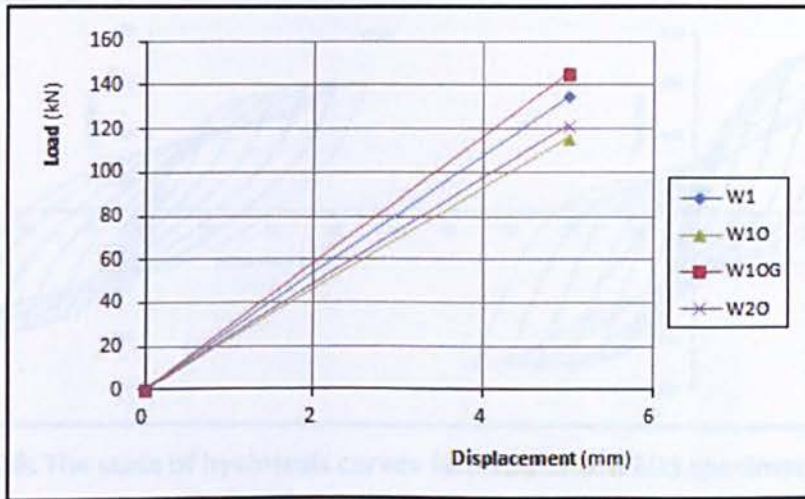


Figure 7.17: Comparative results for initial stiffness of W1, W1O, W2O and W1OG specimens

7.5. Improving the seismic behaviour of SPSW system with cut-outs using steel stiffeners

In the present research application of GFRP laminates was suggested for strengthening of very thin steel plates. However, for thicker steel plates utilising steel stiffeners is another effective option for strengthening of the steel plates. By using the stiffeners the steel plate could be effectively divided into subpanels to develop tension fields across each of them. This method is used to improve the seismic performance of the W2O specimen wherein cut-out is implemented within the steel plate type II (section 6.3). The optimal designed stiffeners provides enough in plane stiffness that prevents premature local buckling of stiffeners and also sufficient out-of-plane stiffness to preclude global buckling of steel plate prior to yielding of sub panels. Longitudinal and transverse stiffeners are welded to steel plate Type II with cut-out (section 6.5). The hysteresis behaviour of specimen with cut-out and stiffeners (W2OS) are depicted in Figure 7.18. Hysteresis curves are extremely stable and robust for W2OS specimen. Degradation of stiffness for subsequent cycles is negligible. The cumulative effects of diagonal tension fields in the sub panels for W2OS specimen is greater than the effect of diagonal tension field within the steel plate for W2O specimen.

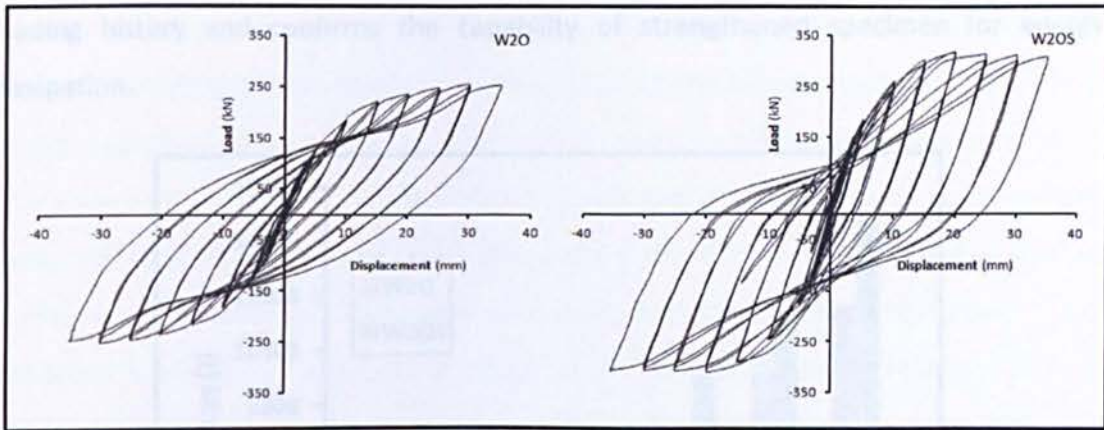


Figure 7.18: The state of hysteresis curves for W2O and W2OS specimens recorded during the quasi-static test program

The envelopes of load-displacement hysteresis curves for W2O and W2OS are presented in Figure 7.19. This figure indicates that the ultimate shear capacity of strengthened specimen (314.9 kN) has significantly increased in comparison with ultimate shear capacity of W2O specimen (254.9 kN). In other words an increase of 60 kN (19%) in ultimate shear capacity is achieved by using the stiffeners.

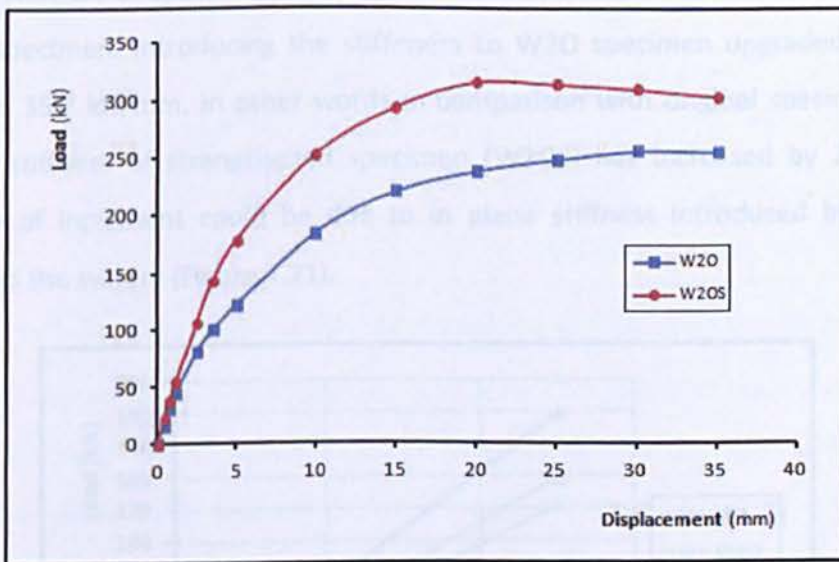


Figure 7.19: Comparison between the envelopes of quasi-static test results for W2O and W2OS specimens

By using stiffeners the S-shaped hysteresis curves for W2O specimen is changed to spindle-shaped for hysteresis loops of W2OS specimen. This shape alteration for hysteresis enables the strengthened specimen to dissipate more energy during the loading. Figure 7.20 gives the value of energy dissipating capacity for different cycles of

loading history and confirms the capability of strengthened specimen for energy dissipation.

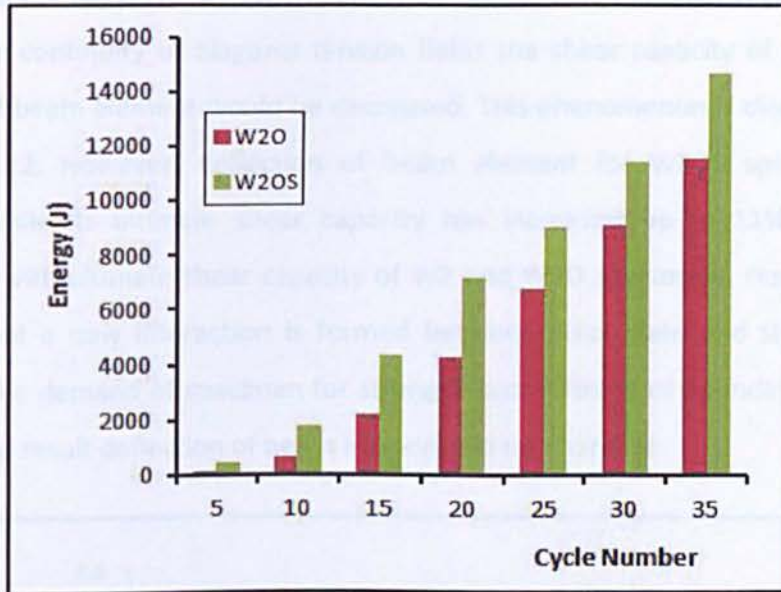


Figure 7.20: Energy dissipating capacity for W2O and W2OS specimens

The initial stiffness of specimen was reduced from 27.7 kN/mm for W2 to 24.3 kN/mm for W2O specimen. Introducing the stiffeners to W2O specimen upgraded the initial stiffness to 35.7 kN/mm. In other words in comparison with original specimen (W2O) the initial stiffness of strengthened specimen (W2OS) has increased by 22.4%. This magnitude of increment could be due to in plane stiffness introduced by the steel stiffeners to the system (Figure 7.21).

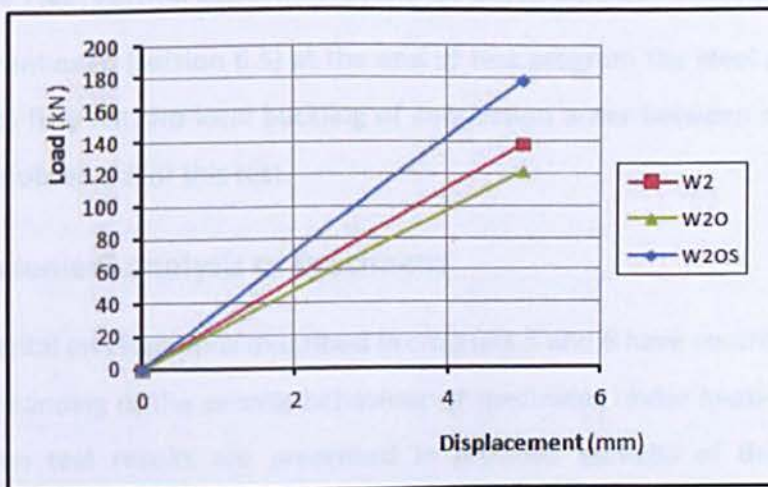


Figure 7.21: Alteration of initial stiffness for test specimen due to implementation of cut-out (W2O) and introducing the stiffeners (W2OS)

Figure 7.22 compares the results for beam element deflections recorded during the test program for W2, W2O and W2OS specimens. It is expected that introduction of cut-outs to the steel plate causes reduction in deflection of beam element. In other words due to disruption in continuity of diagonal tension fields the shear capacity of specimen and deflection of beam element would be decreased. This phenomenon is clearly presented in Figure 7.22. However, deflection of beam element for W2OS specimen is not increased while its ultimate shear capacity has increased up to 11% and 19% in comparison with ultimate shear capacity of W2 and W2O specimens, respectively. The reason is that a new interaction is formed between steel plate and steel stiffeners. Therefore, the demand of specimen for strength and stiffness of boundary members is reduced. As a result deflection of beam element did not increase.

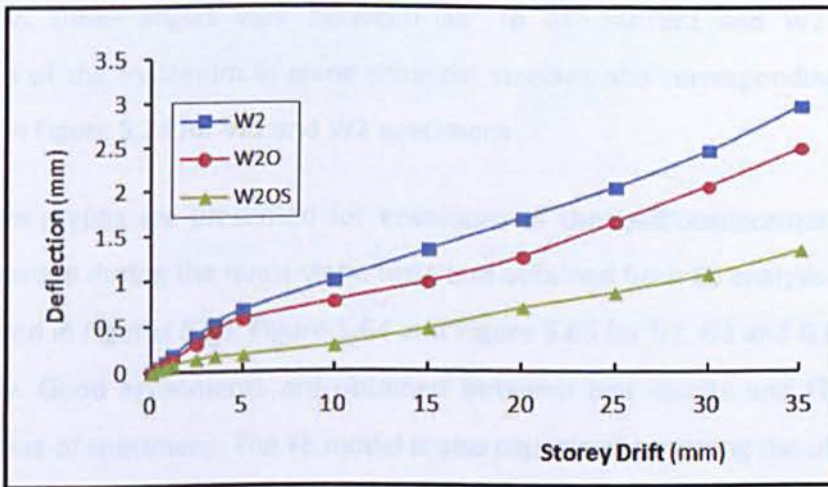


Figure 7.22: Vertical deflection results for the mid part of beam element

As already mentioned (section 6.5) at the end of test program the steel plate of W2OS specimen was fully flat. No local buckling of connection areas between steel plate and fish plate was observed for this test.

7.6. Finite element analysis of specimens

The experimental investigations described in chapters 5 and 6 have contributed towards better understanding of the seismic behaviour of specimens under quasi-static loading. Discussions on test results are presented in previous sections of this chapter. As experimental programs were restricted by the number and size of the specimens a numerical approach was developed for simulating of test specimens. The approach

CHAPTER 7: DISCUSSION ON EXPERIMENTAL AND NUMERICAL RESULTS

should enable accurate prediction of initial stiffness, post-yield stiffness and ultimate capacity of the system. Both push-over and hysteresis loading were simulated for all specimens using commercial non-linear finite element ABAQUS software. Finite element results were then validated by the experimental results. Good agreement was achieved between test results and FEA outcomes. The FE models were capable of capturing the initial stiffness, post yielding stiffness, ultimate shear load capacity, buckling mode of steel plate, inclination angle of diagonal tension field, and maximum in-plane principal stresses of steel plate.

The FEA is reasonably able to capture the inclination angles for diagonal tension of steel plates. Figure 5.27 and Figure 5.28 illustrates the magnitudes of inclination angles measured from test specimens and captured by FE models for W1 and W2 specimens respectively. These angles vary between 38° to 41° for W1 and W2 specimens. Distribution of the maximum in-plane principal stresses and corresponding angles are illustrated in Figure 5.24 for W1 and W2 specimens

Comparative graphs are presented for envelopes of the load-displacement hysteresis curves, recorded during the quasi-static tests and obtained from FE analysis. The results are illustrated in Figures 5.63, Figure 5.64 and Figure 5.65 for G1, G2 and G3 specimens, respectively. Good agreements are obtained between test results and FE results for initial stiffness of specimens. The FE model is also capable of capturing the ultimate base shear for test specimens. This ability of model is presented for W10, W20, W10G and W20S specimens in Figures 6.6, 6.13, 6.22 and Figure 6.30, respectively.

Buckling deformation of shear panels are accurately simulated by FEA models for different specimens. Figure 6.14 illustrates buckling shape of shear panel at three stages of pulling, initial position and pushing for test and FE model of W20 specimen. The model is also able to simulate the change of buckling mode for sandwich panels. This phenomenon is depicted in Figure 6.16 for W10 specimen.

The FE model is capable of capturing the effect of minor buckling in test specimens. W20S specimen experienced the first sign of buckling within the sup-panels B, D and F at storey drift of 5 mm. A contour plot of von Mises stresses shows the initiation of

these buckling deformations in sub-panels B, D and F. Figure 7.23 presents formation of minor buckling deformations and corresponding outcomes from FE model for W2OS specimen.

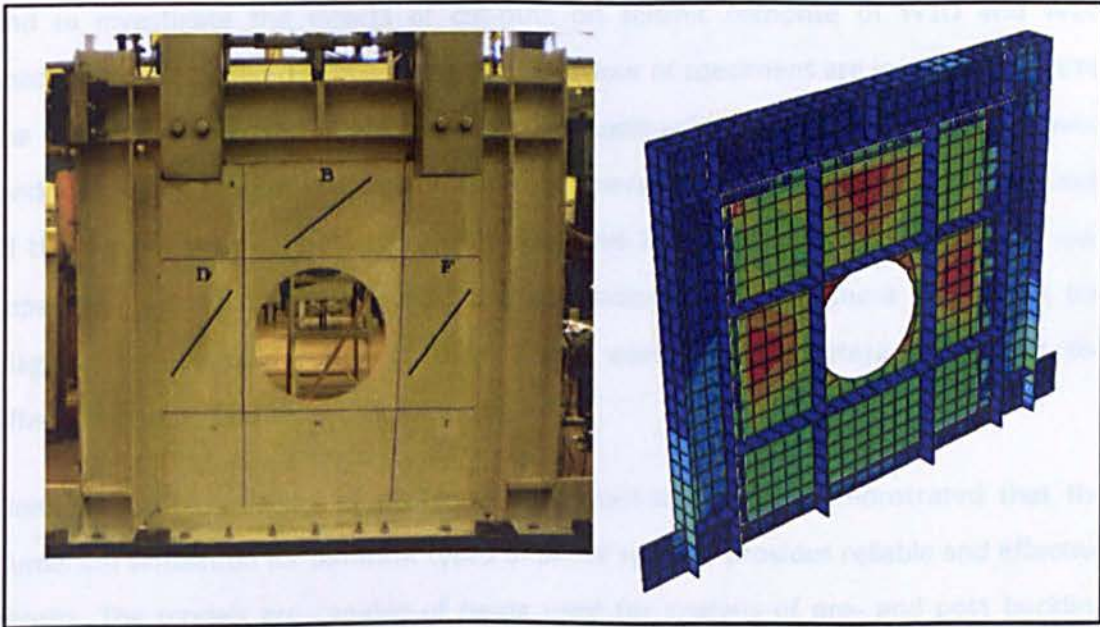


Figure 7.23: Initiation of minor buckling deformations within the sub-panels is captured by FE model for W2OS specimen.

The FEA and test results of vertical deflections of the mid part of the beam element of W2OS specimen is compared in Figure 7.24. Excellent agreement is achieved between test and FE results.

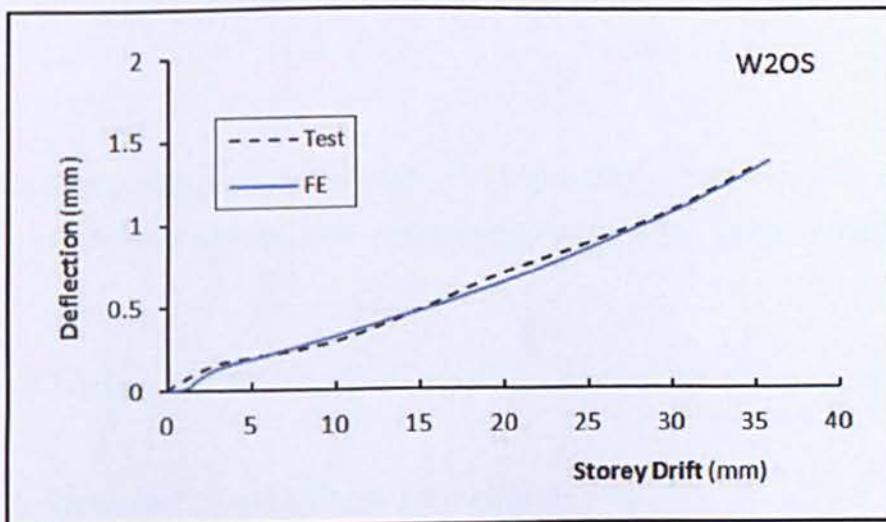


Figure 7.24: Validation of FE results for the vertical deformation of W2OS specimen at mid part of beam element

7.7. Summary

In this chapter, experimental and finite element results of various SPSW are discussed in detail. Test results were used to understand the behaviour of W1 and W2 specimens and to investigate the effects of cut-outs on seismic response of W10 and W20 specimens. It was demonstrated that the behaviour of specimens are improved by using the GFRP laminates. The effectiveness of this approach was validated by experimental evidence. Using GFRP materials and steel stiffeners for improving the seismic response of the system with cut-outs were also discussed in this chapter. Ultimate shear load capacities, initial stiffness as well as the association of beam element for bearing the diagonal tension field action of shear panel were the parameters to monitor the effectiveness of two reinforcing methods.

Finite element modelling of pushover and quasi-static tests demonstrated that the numerical simulation for different types of SPSW systems provides reliable and effective results. The models are capable of being used for analysis of pre- and post buckling behaviour of specimens, buckling deformation of shear panel, maximum in-plane principal stresses and corresponding angles, change of buckling mode and vertical deflection of beam elements. However, it is necessary to consider that the analytical results are limited in terms of modelling characteristics, since they do not consider the effect of residual stress and damage of the structure.

8. SUMMARY, CONCLUSIONS, AND RECOMMENDATIONS FOR FUTURE RESEARCH

8.1. Introduction

This chapter summarises the research work performed in the study for improving the seismic performance of SPSW systems with and without cut-outs. The research programme comprises both experimental and numerical study. The experiments investigated the behaviour of SPSW, the effect of cut-outs, the use of UD-GFRP materials to improve seismic performance of specimens with and without cut-outs. The optimal design of steel stiffeners was adapted in order to upgrade the specimen with cut-out to its original characteristics.

8.2. Summary

This thesis dealt with two main objectives. The first objective was improving the seismic performance of SPSW systems with and without cut-outs. The major concerns for this part were:

- How to increase the initial stiffness and the ultimate shear-load capacity of the system.
- How to reduce the flexural stiffness demand for columns.
- The further contribution of the beam element for taking the action of the diagonal tension field.

- To prevent local buckling of fish plates.

The second objective was the development of the FE model for reliable simulation of specimen behaviour.

An extensive test program comprising the design of specimens, the testing and the analysis of test results was conducted as part of this research. An individual configuration was considered for the edge connection of fish plates. Beam-to-column connections were moment-resisting and specifications of boundary members were consistent for all specimens. Tests designed to cover the objectives of the research were including frame-only, SPSWs with two different types of steel plate, strengthened specimens using UD-GFRP laminates with variation in the number of layers and the orientation of fibres, introducing cut-outs to two different types of steel plate and strengthening specimens by employing UD-GFRP laminates and steel stiffeners. Imaging method from infrared camera was used to capture the occurrence of possible delamination in the sandwich specimens.

A loading system was designed and constructed to apply the cyclic quasi-static load to all specimens according to ATC-24 protocol. A lateral bracing system was also designed to resist the out-of-plane buckling of specimens. Vertical deflection of the beam element was recorded by an innovative sliding measurement system that was designed and manufactured as part of this study. All parameters that were important either in interpreting the results or in controlling the tests were measured. Force, displacements and strains were monitored and recorded during the tests.

In addition to the experimental program, finite element analysis was applied to simulate the response of specimens during the test using the commercial FE analysis program ABAQUS. Finite element models based on explicit dynamic formulation were developed for the analysis of steel plate shear walls. Materials and geometrical nonlinearity and the initial imperfections of the shear panels were considered in the model. Modelling of fish plates and connection plates was included in the FE model. An initial perfect bonding was assumed between GFRP layers as well as between the steel plate and the GFRP laminate. Failure of GFRP material in FE model was considered using the Hashin failure

criteria in the ABAQUS software. Since the solution strategy in the explicit method does not involve iteration, the analysis procedure was completed without any problem of convergence. The FEA was used to simulate the monotonic and cyclic response of test specimens. The outcomes for FE models were verified by comparing the monotonic and hysteretic load versus displacement results between FEA and experiments for boundary elements including beam and columns, out-of-plane deformation of shear panels and formation of plastic hinges at the end of boundary members. The non-linear finite element modelling for pushover and quasi-static tests demonstrated that numerical simulation of SPSW system with different types of shear panels can provide reliable and meaningful results. The FE model captured all essential features of the test specimens.

8.3. Conclusions

The following conclusions can be drawn from the results of the work described in this research:

1. The change in thickness of the steel plate has negligible effect on initial stiffness of SPSW systems with and without cut-outs. Any increase in thickness of the steel plate in order to gain greater value of stiffness will increase the flexural stiffness demand for boundary members, particularly for columns. The energy dissipation capacity and ultimate load capacity of SPSW system is moderately affected by increasing the thickness of the steel plate. However, the maximum out-of-plane buckling deformation of the steel plate is noticeably dependent on the thickness of the steel plate.
2. Due to implementation of the moment-resisting connections between beam and columns as well as the proposed configuration of the edge connections of fish plates, the inner connections between beam and columns were intact and no tearing was observed at the edges of the steel plate. The set of these configurations leads to the improvement of the stability of hysteresis loops and the increase of the energy dissipating capacity of the system.
3. The initial stiffness of the SPSW system was significantly reduced by introducing cut-outs into the steel plate. The moderate reduction of the ultimate load capacity and

the energy dissipation capacity as well as the substantial increase in the maximum out-of-plane buckling deformation is the other effects of cut-outs on performance of SPSW systems. It was shown that the relation between the diameter of cut-outs and the ultimate load capacity of the SPSW system can be described by a quadratic equation (section 3.7). Disruption in the continuity of diagonal tension fields in SPSW systems with cut-outs caused a permanent buckling deformation in the steel plate at an early stage of cyclic loading. Non-uniform distribution of the diagonal tension fields is caused local buckling of the fish plates for specimens with cut-outs.

4. Due to the advantages of GFRP materials, UD-GFRP laminates were used to improve the seismic performance of SPSW systems with and without cut-outs. The design can be optimized to meet the stiffness, strength and other requirements:
 - The sandwich shear panels are required to behave in a symmetrical manner for in-plane and out-of-plane deformations. Adding the laminates to both sides of the steel plate with a symmetrical configuration can meet this requirement.
 - The panel is subjected to cyclic loading, so to prevent tearing of laminates in matrix area it is necessary for each laminate to contain at least two layers. As a result, for sufficient strengthening of shear panels at least four layers of UD-FRP laminates are employed [+L/-L/SP/-L/+L].
5. The initial stiffness and ultimate load capacity of the shear wall system are significantly increased by employing GFRP-steel sandwich panels. The magnitude of increase depends on stacking a sequence of the plies, the number of layers and the orientation of the fibres.
 - Despite the increase in ultimate load capacity and initial stiffness of the sandwich panel, the increase in flexural demand of columns was not noticeable. This is because of the further contribution of beam elements to sustain the diagonal tension field action.
 - In multi storey structures, increasing the fibre orientation angle can reduce the flexural stiffness demand of floors' columns. In order to reduce the contribution of

the roof beam for the bearing action of diagonal tension field, the fibre orientation angle needs to be reduced.

- A substantial increase in the initial stiffness of sandwich panels is an effective approach for restricting the storey drift of high-rise buildings.

Increasing the initial stiffness of the sandwich panel reduces out-of-plane buckling deformation of shear panels. This phenomenon is essential for shear panels with cut-outs, because the permanent deformation of the shear panel can be prevented.

- The use of sandwich panels prevented the local buckling of fish plates for shear panels with and without cut-outs.
 - The capacity of the sandwich panels for dissipating of the energy depends on the configuration of composite layers.
6. Installation of steel stiffeners to a steel plate divides the shear panel into a number of sub-shear panels with individual boundary members and aspect ratio. In other words sub-panels act as SPSW in multi storey buildings in which longitudinal and transverse stiffeners act as beams and columns of building. An effective arrangement of stiffeners is necessary for neutralising the effects of diagonal tension fields in adjacent sub-panels. An optimal design of stiffeners depends on dimension of stiffeners. Utilising steel stiffeners for improving the seismic performance of SPSW systems with cut-outs and optimal design leads to the following results:
- A significant increase in initial stiffness and post-yield stiffness of the system
 - A substantial increase in the energy dissipating capacity
 - A negligible out-of-plane deformation buckling of the shear panel
 - Due to the performance of sub-panels as independent shear panels, beam and columns are mainly affected by adjacent sub-panels. In other words a new interaction is formed between stiffeners and shear panel. As a result the ultimate load capacity of the system is significantly increased. However, demands for flexural stiffness of boundary members are not noticeably increased.

7. The use of infrared camera is an effective NDT technique for detection of subsurface defects such as debonding and delamination formed during initial construction or during the loading.
8. An innovative sliding-measurement system was well designed for measuring the vertical deflection of beam element and allows the study of the inclination angle effect for transferring the tension field action loads to the beam element.
9. Nonlinear finite element models with explicit dynamic formulation were able to simulate accurately the push-over and quasi-static cyclic behaviour of SPSW systems. It was therefore concluded that the finite element method is a reliable technique to simulate the response of SPSW systems, particularly the SPSW systems with dimensions bigger than the test limitations of the existing research facility.
 - Using an explicit formulation which does not involve iteration precludes the occurrence of numerical difficulties during the analysis.
 - By including the initial imperfection of the shear panel, material and geometry nonlinearity, fish plates and connection plates in FE models, reasonably accurate results were obtained.
 - The in-plane displacement of beam and columns and out-of-plane deformations of shear panels were accurately simulated by the FE model
 - The FE model is able to detect the yield of the steel plate and the formation of plastic hinges in the boundary members
 - The weld fractures and residual stresses are not simulated in the FE model. Some reasonable discrepancy therefore appears between the test and analysis results after fractures occurred in connections.
 - A perfect bond is assumed between the composite layers and the steel plate. If delamination occurs prior to the rupture of fibres the difference between test and FE results will be increased.

8.4. Recommendations for future research

Further development is required for improving the seismic behaviour of SPSW systems. GFRP plies were used for strengthening thin steel shear panels particularly in the case of cut-outs and need to be explored more. The interaction between the steel plate and the boundary members is affected by the interaction between the steel plate and the steel stiffeners. Further investigation is needed to improve these interactions. Further developments are suggested on the following areas:

- Optimal design for GFRP-Steel sandwich shear walls including the number of composite laminates and the orientation angle of fibres based on the minimum displacement demand of boundary members.
- Improving the debonding issue between the steel plate and the composite laminates by using damage models in FEA.
- Effects of initial imperfections on seismic performance of sandwich shear walls.
- Application of stiffeners with bolt connections to steel plate, in order to reduce the cost of construction and the effects of residual stresses from high temperature of welding.
- The use of pure FRP materials for shear wall applications with special attention to the strain rate of materials and connection of laminates to boundary members.
- The topological design of laminates to satisfy the design requirement.
- The method used for the testing of specimens in the present research was quasi-static. However, due to the dynamic nature of earthquake load, tests on GFRP-steel sandwich shear walls and the specimens with cut-outs under dynamic load are suggested.

REFERENCES

AASHTO-LRFD (2005) " Bridge design specifications", SI units, 3rd ed, American Association of State Highway and Transportation Officials; Interim Revisions.

Agelidis N & Mansell DS (1982) " Steel Plate Cores in Tall Buildings ". *Civil Engineering Transaction of the Institution of Engineers*, pp.11-18.

AISC AISC (2005-a) " Prequalified Connections for Special and Intermediate Steel Moment Frames for Seismic Applications ", ANSI/AISC 358-05, Chicago, IL.

AISC AISC (2005-b) " Specification for Structural Steel Buildings ", ANSI/AISC 360-05, Chicago, IL.

AISC AISC (2005-c) " Seismic Provisions for Structural Steel Buildings ", ANSI-AISC 341-05, Chicago, IL.

AISC AISC (2007) " Steel Plate Shear Walls ", Chicago, IL.

Alinia MM (2005) " A study into optimization of stiffeners in plates subjected to shear loading " *Thin Walled Structures*, 43 (845-860).

Alinia MM & Dastfan M (2006) " Behaviour of Thin Steel Plate Shear Walls Regarding Frame Members ". *Journal of Constructional Steel Research*, 62(7), pp. 730-738.

Alinia MM & Dastfan M (2007) " Cyclic behaviour, deformability and rigidity of stiffened steel shear panels ". *Journal of Constructional Steel Research*; 63(4) : 554-63.

REFERENCES

Alinia MM, Gheitasi A & Erfan S (2009-c) " Plastic shear buckling of unstiffened stocky plates ". *Journal of Constructional Steel Research*, 65(2009) 1631-1643.

Alinia MM, Habashi HR & Khorram A (2009-d) " Nonlinearity in the postbuckling behaviour of thin steel shear panels ". *Journal of Thin-Walled Structures*, 47, PP: 412-420.

Alinia MM, Jamshidi AH & Habashi HR (2009-b) " The gusset plate effect in steel plate shear wall system ". In *3rd International Conference on Integrity, Reliability and Failure*. Porto, Portugal, July 2009.

Alinia MM & Sarraf R (2009-a) " On the design of stiffeners in steel plate shear walls ". *Journal of Constructional Steel Research*; 65 : 2069-2077.

Alipour Tabrizi M & Rahai AR (2011) " perforated Steel Shear Walls With Frp Reinforcement Of Opening edges ". *Australian Journal of Basic and Applied Science*, 5(10): 672-684.

Applied-Technology-Council (1992) " Guidelines for Cyclic Seismic Testing of Components of Steel Structures ", ATC-24,. Redwood City, CA.

Arabzadeh A, Soltani M & Ayazi A (2011) " Experimental investigation of composite shear walls under shear loading ". *Thin Walled Structures* Vol. 49, pp. 842-854.

Astaneh-Asl A (2000) " Experimental and Analytical Studies of Composite (Steel-Concrete) Shear Walls ", Research project, Sponsored by National Science Foundation: Department of Civil and Environmental Engineering, University of California at Berkeley.

Astaneh-Asl A (2001) " Seismic behaviour and Design of Steel Shear Walls ". Moraga, CA: Steel Technical Information and Product Services Report, Structural Steel Educational Council.

Astaneh-Asl A (2001-a) " Experimental and Analytical Studies of Steel Shear Walls ", Research Project, Sponsored by General Service Administration and SWMB, Department of Civil and Environmental Engineering, University of California at Berkeley.

REFERENCES

Astaneh-Asl A (2001-b) " Seismic Behavior and Design of Composite Shear Walls ": Steel Tips Report, Structural Steel Educational Council, Moraga, CA.

Astaneh-Asl A (2002-b) " Seismic behaviour and Design of Composite Steel Shear Walls ". Moraga, CA: Steel Technical Information and Product Services Report, Structural Steel Educational Council.

Astaneh-Asl A & Zhao Q (2000) " Cyclic Tests of Steel Plate Shear Walls ", Research Report to Sponsor: Department of Civil and Environmental Engineering, University of California at Berkeley.

Astaneh-Asl A & Zhao Q (2002-a) " Cyclic Behavior of Steel Shear Wall Systems ". *proceedings, Annual Stability Conference, Structural Stability Research Council, April, Seattle.*

Atasoy M (2008) " Lateral stiffness of unstiffened steel plate shear walls " , Middle East Technical University, Ankara, Turkey.

Baldelli Jr (1983) " Steel Shear Walls for Existing Buildings ". *Engineering Journal, AISC, 20(2), 70-77.*

Bambach MR, Elchalakani M & Zhao XL (2009) " Composite Steel-CFRP SHS Tubes under Axial Impact ". *Journal of Composite Structures Vol. 87, pp. 282-292.*

Basler K (1961) " Strength of plate girders in shear ". *Journal of Structural Divisions, ASCE, No. 2967, ST 7, pp. 151-180, October 1961, Part I.*

Basler K & Thuerlimann (1963) " Strength in bending ". *Transaction, ASCE, Vol. 128, Part II, Paper No. 3489, 1963, pp. 655-682.*

Behbahanifard MR (2003-b) " Cyclic behaviour of unstiffened steel plate shear walls " , , University of Alberta.

Behbahanifard MR, Grondin Gy & Elwi AE (2003-a) " Experimental and numerical investigation of steel plate shear walls ", Structural Engineering Report No. 254. Edmonton: Dept. of Civil and Environmental Engineering, University of Alberta.

REFERENCES

Behbahanifard MR, Grondin Gy & elwi AE (2004) " Analysis of steel plate shear walls using explicit finite element method ". In *13th World conference on Earthquake Engineering, Vancouver, B.C., Canada, August 1-6, 2004, Paper no. 2420.*

Berman JW (2011) " Seismic behaviour of code design steel plate shear walls ". *Engineering Structures Vol. 33*, pp. 230-244.

Berman JW & Bruneau M (2003-a) " Experimental investigation of light-gauge steel plate shear walls for the seismic retrofit of buildings ", technical Report. No. MCEER-03-0001, Multidisciplinary Centre for Earthquake Engineering Research, Buffalo, N.y.

Berman JW & Bruneau M (2003-b) " Plastic Analysis and Design of Steel Plate Shear Walls ". *Journal of Structural Engineering, ASCE, Vol. 129, No. 11, November 1, 2003.*

Berman JW & Bruneau M (2004-a) " Plastic Design and Testing of Light-Gauge Steel Plate Shear Walls ". In *13th World Conference on Earthquake Engineering, Vancouver, B.C., Canada, August 1-6, 2004, Paper No. 3323.*

Berman JW & Bruneau M (2004-b) " Steel Plate shear Walls are not Plate Girders ". *AISC Engineering Journal, Third quarter, PP. 95-106.*

Berman JW & Bruneau M (2005-b) " Experimental investigation of light-gauge steel plate shear walls ". *Journal of Structural Engineering, ASCE, Vol. 131, No. 2, PP. 259-267.*

Berman JW & Bruneau M (2008-a) " Capacity Design of Vertical Boundary Elements in Steel Plate Shear Walls ". *Engineering Journal, AISC, first quarter, 57-71.*

Berman JW, Celik OC & Bruneau M (2005-a) " Comparing hysteretic behaviour of light-gauge steel plate shear walls and braced frames ". *Engineering Structures Vol. 27*, pp. 475-485.

Berman JW, Lowes LN, Okazaki T, Bruneau M, Tsai KC, Driver RG, Sabeli R & Moore WP (2008-b) " Research Needs and Future Directions for Steel Plate Shear Walls ". *ASCE Journal of Structures, 2008.*

REFERENCES

Bhowmick AK, Driver RG & Grondin Gy (2009) " Seismic analysis of steel plate shear walls considering strain rate and p-delta effects ". *Journal of Constructional Steel Research*, 65(5), pp. 1149-1159.

Bhowmick AK, Grondin Gy & Driver RG (2011a) " Estimating fundamental periods of steel plate shear walls ". *Engineering Structures*, 33, pp. 1883-1893.

Bhowmick AK, Roberts TM & Grondin Gy (2011b) " Application of Indirect Capacity Design Principles for Seismic Design of Steel Plate Shear Walls ". *ASCE, Journal of Structural Engineering* Vol. 137, PP. 521-530.

Bruneau M (2007) " Innovations in Earthquake Resistant Steel Structures " In *Ninth Canadian Conference on Earthquake Engineering*. Ottawa, Ontario, Canada, 26-29 Jun.

Bruneau M, whittaker AS & Uang CM (1998) " *Ductile design of steel structures* ": McGraw-Hill, New York.

Caccese V, Elgaaly M & Chen R (1993) " Experimental study of thin steel plate shear walls under cyclic load ". *ASCE Journal os Structural Engineering*, PP. 573-587.

Celebi M (1997a) " Response of Olive View Hospital to Northridge and Whittier Earthquakes ". *J. of Structural Engineering*, ASCE 123, 389-396.

Celebi N (1997b) " Response ogf Olive View Hospital to Northridge and Whittier Earthquakes ". *J. of Structural Engineering*, ASCE 123, 389-396.

Celik OC, Berma JW & Bruneau M (2004) " Cyclic testing of braced laterally restrained by steel studs to enhance performance during earthquake ", Technical report MCEER-04-0003, multidisciplinary centre for Earthquake Engineering research, Buffalo, NY.

Chan R, Albermani F & Kitipornchai s (2011) " Stiffness and Strength of Perforated Steel Plate Shear Walls ". *procedia Engineering*, vol 14, PP. 675-679.

Chao SH & Goel SC (2005) " Performance-based seismic design of EBF using target drift and yield mechanism as performance criteria ", Research report umcee 05-05, Ann Arbor (MI, USA): University of Michigan.

REFERENCES

Chen R (1991) " Cyclic behaviour of Unstiffened Thin Steel Plate Shear Walls ", University of Maine, Orono, ME.

Chen S-J & Jhang C (2011) " Experimental study of low-yield-point steel plate shear wall under in-plane load ". *Journal of Constructional Steel Research*.

Chen WF, GOTO Y & Liew JYR (1996) " *Stability design of Semirigid Frames* ": Wiley, New York.

Cheng Y (2010) " Shear resistance of cold-formed steel framed shear walls with 0.686 mm, 0.762 mm, and 0.838 mm steel sheet sheathing ". *Engineering Structures*, 32, pp. 1522-1529.

Choi I & Park H (2008) " Cyclic Test for Framed Steel Plate Walls With Various Steel plate Details ". In *The 14th World Conference on Earthquake Engineering, October 12-17*. Beijing, China.

Chopra AK (2001) " *Dynamics of Structures: Theory and Applications to Earthquake Engineering* ", Prentice-Hall, Inc., Englewood Cliffs, N.J.

Clough RW & Penzin J (1993) " *Dynamics of Structures* ", 2nd Edition, McGraw-Hill, Inc, New York, NY.

Computers and Structures I (1984-2011) SAP2000, Nonlinear, Computers and Structures, Inc. Berkeley, CA.

Cowper GR & Symonds PS (1957) " Strain hardening and strain rate effects in the impact loading of cantilever beams ", Brown University division of Applied Mathematics, Report No. 28, Providence, RI.

CSA CSA (1994) " Limit states Design of Steel Structures ". In *CAN/CSA 16-01, Toronto, Ontario, Canada*.

CSA CSA (2001) " Limit states Design of Steel Structures ". In *CAN/CSA 16-01, Toronto, Ontario, Canada*.

REFERENCES

Das A (2007) " Performance based design of steel plate shear wall using target drift and yield mechanism ".

Das A, Adam F & Ghosh S (2008) " Design of Steel Plate Shear Walls Considering Inelastic Drift Demand ". In *14th World Conference on Earthquake Engineering*. Beijing, China.

Dastfan M & Driver RG (2008) " Flexural stiffness limits for frame members of steel plate shear wall systems ", In *Proceedings of 2008 Annual Structural Stability Research Council Conference*, April 2-5, Nashville, TN, PP. 321-334.

De Matteis G & Mazzolani FM (2003) " Pure Aluminum Shear Panel as Passive Control System for Seismic Protection of Steel Moment resisting Frames ". *Proceedings Conference on Behaviour of Steel Structures in Seismic Areas, June, Naples, Italy*, pp. 599-608.

De Matteis G & Mistakidis ES (2003) " Seismic Retrofitting of Moment Resisting Frames using Low Yield Steel Panels as Shear Walls ". *Proceedings Conference on Behaviour of Steel Structures in Seismic Areas, June, Naples, Italy*, pp. 677-682.

Deilami A & Rowghani-Kashani J (2011) " Analysis and Design of Steel Plate Shear Walls Using Orthotropic Membrane Model ". *Procedia Engineering*, vol 14, PP. 3338-3345.

Driver RG, Kulak G, Kennedy DJL & Elwi AE (1997) " Seismic Behaviour of Steel Plate Shear Walls ", Structural Engineering Report, No. 215, Department of Civil and Environmental Engineering, University of Alberta, Edmonton, Canada.

Driver RG, Kulak G, Kennedy DJL & Elwi AE (1998-a) " Cyclic Test of a Four-Storey Steel Plate Shear Wall ". *Journal of Structural Engineering, ASCE*, Vol. 124, No. 2, PP. 112-120.

Driver RG, Kulak G, Kennedy DJL & Elwi AE (1998-b) " FE and Simplified Models of Steel Plate Shear Walls ". *Journal of Structural Engineering, ASCE*, Vol. 124, No. 2, PP. 121-130.

Elgaaly M (1998) " Thin Steel Plate Shear Walls Behaviour and Analysis ". *Thin Walled Structures*, Vol. 32, pp. 151-180.

REFERENCES

- Elgaaly M (2000) " Post-buckling behaviour of thin steel plates using computational models". *Advances in Engineering software*, Vol. 31, PP. 511-517.
- Elgaaly M & Caccese V (1990) "Steel Plate Shear Walls". *Proceeding of the AISC National Steel Construction Conference, Chicago, IL, PP.4-1, 4-28.*
- Elgaaly M, Caccese V & Du C (1993) " Post-buckling Behaviour os Steel plate Shear Walls Under Cyclic Loads". *Journal of Structural Engineering, ASCE, Vol. 119, No. 2, PP. 588-605.*
- Elgaaly M & Liu Y (1997) " Analysis of Thin-Steel Plate Shear Walls". *Journal of Structural Engineering, ASCE, Vol. 123, No. 11, PP. 1487-1496.*
- Eurocode-8 (2003) " Design of structures for earthquake resistance. Part 1: General rules, seismic action and rules for buildings ", Brussels.
- Farzad N (2001) " *The Seismic Design Handbook* ", 2nd Edition, Springer.
- Featherston CA (2000) " The use of Finite Element Analysis in the Examination of Instability in Flat Plates and Curved Panels under Compression and Shear " *International Journal of Non-Linear Mechanics*, 2000(5), pp. 515-529.
- FEMA-356 (2000) " Federal Emergency Management Agency ". In *Prestandard and Commentary for the Seismic Rehabilitation of buildings, (FEMA 356), Washington, D.C.*
- FEMA-450 (2003) " NEHRP Recommended Provisions for Seismic Regulations for New Buildings and other Structures: Part 1-Provisions 2. In *Federal Emergency Management Agency, FEMA 450, Washington, DC.*
- Fujitani H, Yamanouchi H, Okawa I, Uchida N & Matsutani T (1996) " Damage and performance of tall buildings in the 1995 Hyogoken Nanbu earthquake ". *Proceedings. The 67th Regional Conference, Council on Tall Building and Urban Habit*, 103-125.
- Garlock MM, Ricles JM & Sause R (2008) " Influence of design parameters on seismic response of post-tensioned steel MRF systems ". *Journal of EGINEERING structures*, Vol. 30, pp. 1037-1047.

REFERENCES

Gholhaki M & Sabouri-Ghomi S (2009) " Effect of Ductility Factor on Force Modification Factor of Thin Steel Plate Shear Walls ". In *The Science and Research Magazine of Structure and Steel*, pp. PP: 52-63. Iran: Iranian Society of Steel Structures (ISSS).

Ghosh S, Adam F & Das A (2009) " Design of steel plate shear walls considering inelastic drift demand ". *Journal of Constructional Steel Research*, 65: 1431-1437.

Gilmor MI (2002) " Canadian Requirements for Seismic Design of Ductile Steel Structures ". *proceedings, NASCC Annual Conference, April, Seattle*. 30.

Gioncu V (2000) " Influence of strain-rate on the behaviour of steel members ", In *behaviour of Steel Structures in Seismic Areas*, Montral, 21-24 August, Balkema, Rotterdam.

Goel R & Choopra AK (1998) " Period formulas for concrete shear wall buildings ". *ASCE Journal of Structural Engineering*, 124(4): 426-33.

Guan N (2008) " Experimental Research and Theoretical Analysis on Behaviour of Two-side Connected Steel-concrete Composite Shear Walls ".

Gupta A & Krawinkler H (2000) " Dynamic P-delta effects for flexible inelastic steel structures ". *Journal of structural Engineering, ASCE*, 126(1), 145-154.

Gupta MK, Kharmale SB & Ghosh S (2009) " Ductility-Based Seismic Design of Steel Plate Shear Walls: practical Application Using Standard Sections ". *International Journal of Advanced Structural Engineering*, Vol. 1, No. 2, pp 93-110.

Habashi HR & Alinia MM (2010) " Characteristics of the wall-frame interaction in steel plate shear walls ". *Journal of Constructional Steel Research*, 66, pp. 150-8.

Harries KA, Peack AJ & Abraham EJ (2009) " Enhancing Stability of Structural Steel Sections Using FRP ". *Journal of Thin-Walled Structures* Vol. 47, pp. 1092-1101.

Hatami F, Ghamari A & Rahai AR (2011) " Investigating the properties of steel shear walls reinforced with carbon fiber polymers (CFRP) ". *Journal of Constructional Steel Research*.

REFERENCES

Hatami F & Rahai AR (2008) " An Investigation of FRP Composite Steel Shear Walls (CSPSW) under Cyclic loading on Laboratory ". In *14th World Conference on Earthquake Engineering, China*.

Heidebrecht A & Smith B (1973) " Approximate analysis of tall wall-frame structures ". *Journal of structural Divisions, ASCE, 99(2): 199-221*.

Hibbit, Karlson & Sorensen (2007) " ABAQUS/Standard User's Manual ", Version 6.10, HKS Inc., Pawtucket, RI.

Hibbit, Karlson & Sorensen (2010) " ABAQUS/Standard User's Manual ", Version 6.10, HKS Inc., Pawtucket, RI.

Hughes OF, Ghosh B & Chen Y (2004) " Improved prediction of simultaneous local and overall buckling of stiffened panels ". *Thin Walled Structures, 42, pp. 827-856*.

Kaneko H (1997) " Influence of strain-rate on yield ratio, In Kobe earthquake damage to steel moment connections and suggested improvement, JSSC Technical Report No. 39.

Karnovsky I & Lebed O (2001) " *Formulas for structural dynamics* ", McGraw Hill.

Kharrazi M (2005) " Rational method for analysis and design of steel plate shear walls ". Doctoral Dissertation.

Kharrazi M, Ventura CE, Prion HGL & sabouri-Ghomi S (2004) " Bending and Shear Analysis and Design of Ductile Steel Plate Walls ". *13th World Conference on Earthquake Engineering*.

Krawinkler H & Popov EP (1982) " Seismic Behaviour of Moment Connections and Joints ". *ASCE Journal of the Structural Division, Vol. 108, No. ST2, PP. 373-391*.

Kuhen P, Peterso JP & Levin LR (1952) " A Summary of Diagonal Tension. Part I: Methods and Analysis ", Technical Note 2661, National Advisory Committee for Aeronautics, Washington, DC.

REFERENCES

Kulak G (1985) " Behaviour of Steel Plate Shear Walls " , . *AISC International Engineering Symposium on Structural steel, Amer. Inst. of Steel Construction.*

Kulak G (1986) " unstiffened steel plate shear walls: static and seismic behaviour ". *Steel structures recent research advances and their applications to design, edited by Pavlonic, M. N., Elsevier Applied Science publishers, pp. 561-580.*

Kulak G (1991) "unstiffened Steel Plate Shear Walls ". In *Structures Subjected to Repeated Loading-Stability and Strength*, pp. pp.237-276 [TM Narayana r and Roberts, Editors, editor]. London: Elsevier Applied science Publications.

Kulak G, Kennedy DJL & Driver RG (1994) " Discussion of Experimental study of thin Steel-Plate shear Walls Under Cyclic Load ". *ASCE Journal of Structural Engineering, Vol 120, No. 10, PP. 3072-3073.*

Kulak G, Kennedy DJL, Driver RG & Medhekar M (1999) " Behaviour and Design of Steel plate Shear Walls ", Proceedings, North American Steel Construction Conf, Toronto, Canada, pp. 11-1 to 11-20.

Kulak G, Kennedy DJL, Driver RG & Medhekar M (2001) " Steel plate Shear walls- An overview ". *American Institute of Steel Construction Engineering Journal, first quarter, pp. 50-62.*

Kulkarni SU, Li B & Yip WK (2008) " Finite element analysis of precast hybride-steel concrete connections under cyclic loading ". *Journal of Constructional Steel Research, 64, pp. 190-201.*

Lange J & Naujoks B (2006) " Behaviour of Cold-Formed Steel Shear Walls under Horizontal and Vertical Loads ". *Thin Walled Structures, 44, pp. 1214-1222.*

Lee S, Wang D, Liao Y & Mathias N (2010) " Performance Based Seismic Design of a 75-Storey Buckling Restrained Slender Steel Plate Shear Wall Tower ". *Council on Tall Buildings and Urban Habit (CTBUH) Journal.*

REFERENCES

Lee SS & Goel SC (2001) " Performance based design of steel moment frames using target drift and yield mechanism ", Research Report UMCEE 01-17, Department of Civil and Environmental Engineering, University of Michigan, Ann Arbor, MI., USA.

Leelathaviwat s, Goel S & Stojadinovic B (1998) " Towards performance based seismic design of structures ". *Earthquake Spectra*, 15(3): 435-61.

Li CH, Tsai KC, Chang JT & Lin CH (2011) " Cyclic Test of Coupled Steel Plate Shear Wall Substructure ". *procedia Engineering*, vol 14, PP 582-589.

Lin CH, Tsai KC, lin YC, Wang KJ, Hsieh WD, Weng YT, Qu BY & Bruneau M (2006) " The Sub-structural Pseudo-dynamic Tests of A Full-storey Steel Plate Shear wall ", Proceeding of the 4th International conference on earthquake Engineering. Paper No. 155, Taipei, Taiwan.

Lopez-Garci D & Bruneau M (2006) " Seismic Behaviour of Intermediate Beams in Steel Plate Shear Walls ", Proceeding of the 8th National Conference on Earthquake Engineering, April 18-22, San Francisco, California, USA.

Lubell AS (1997) " Performance of Unstiffened Steel Plate Shear Walls Under Cyclic Quasi-Static Loading ", University of British Columbia, vancouver, BC, Canada.

Lubell AS, Prinion HGL, Ventura CE & Rezai M (2000) " Unstiffened steel plate shear wall performance under cyclic loading ". *ASCE Journal of Structural Engineering*, April, PP. 453-460.

Maiorana E, Pellegrino C & Modena C (2008-a) " Elastic stability of plates with circular and rectangular holes subjected to axial compression and bending moment ". *Thin Walled Structures*,1016-25.

Maiorana E, Pellegrino C & Modena C (2008-c) " Non-linear analysis of perforated steel plates subjected to localised symmetrical load ". *Journal of Constructional Steel Research*.

REFERENCES

Manjoine MJ (1994) " Influence of rate of strain and temperature on yield stress of mild steel ". *Journal of Applied Mechanics*, 11: 211-218.

Matteis GD, Landolfo R & Mazzolani FM (2003) " seismic response of MR frames with low-yield steel shear panels ". *Engineering Structures*, 25, pp. 155-168.

McKinley B (1999) " Large deformation structural performance of double skin composite construction using British Steel's bi-steel ".

McKinley B & Boswell L (2002) " Behaviour of double skin composite construction ". *Journal of Constructional Steel Research* Vol. 58, No. 10, pp. 1347-1359.

Memarzadeh P, Azhari M & Saadatpour MM (2009) " The Effect of Out-of-Plane Flexural Stiffness of Boundary Frame on Buckling Stress Patterns of steel Plate Shear Wall ". *AMATH' 09 Proceedings of the 15th American Conference on Applied Mathematics*.

Memarzadeh P, Saadatpour MM & Azhari M (2010) " Nonlinear Dynamic Response and Ductility Requirements of A typical Steel Plate Shear Wall Subjected to El Centro Earthquake ". *Iranian Journal of Science & Technology* Vol. 34, No. B4, pp. 371-384.

Mimura H & Akiyana H (1977) " Load-Deflection Relationship of Earthquake-Resistant Steel Shear Walls with Developed Diagonal Tension Field ", pp. pp. 109-114: *Transactions of the Architectural Institute of Japan*.

Mistakidis ES, Matteis GD & Formisano A (2007) " Low yield metal shear panels as an alternative for the seismic upgrading of concrete structures ". *Advances in Engineering software*, 38, pp. 626-636.

Monnier AY & Harasimowicz A (2007) " Shear Strength ". *Modern Steel Construction, AISC, Enerro*, pp. 22-25.

Montgomery Cj & Medhekar M (2001) " Discussion of Unstiffened Steel Plate Shear Wall Performance Under Cyclic Loading by Lubell, A.S., Prion, H.G.L., Ventura, C.E., and Rezai, M ". *Journal of Structural Engineering, ASCE*, Vol. 127, No. 8, PP.973.

REFERENCES

Nakashima M (1995-a) " Strain-Hardening Behaviour of Shear panels Made of Low-Yield Steel -I: Test *Journal of Structural Engineering, ASCE, Vol. 121, No. 12, PP. 1742-1749.*

Nakashima M, Akazawa T & Tsuji B (1995-b) " Strai Hardening Behaviour of Sher Panels Made of Low-Yield Steel -II ". *Journal of Structural Engineering, ASCE, Vol. 121, No. 12, PP. 1750-1757.*

Nakashima M, Iwai S, Iwata M, Takeuchi T, konomi S, Akazawa T & Sabouri K (1994) " Energy dissipation behaviour of shear panels made of low yield steel ". *Engineering quake Engineering and Structural Dynamics, No. 13, PP. 1299-1313.*

Neagu C, Dubina D & Dinu F " Seismic performance of ductile shear wall frame system ", Proceeding of the 11th WSEAS International Conference on Sustainability in Science Engineerin.

NEHRP (2000) National Earthquake Hazards Reduction Program, Recommended Program Provisions for Seismic Regulations for New Buildings and other Structures. Building Seismic Safety Council, washington, D.C. 2 Vols., FEMA 368 and 369. .

Neuenhofer A (2006) " Lateral stiffness of shear walls with openings ". *Journal of structural Engineering, ASCE, 132(11), 1846-51.*

NRCC (1995) National Building Code of Canada, Canadian Comission on Building and Fire Codes, National Research Council of Canada, Ottawa, ON.

NRCC (2005) National Building Code of Canada, Canadian Comission on Building and Fire Codes, National Research Council of Canada, Ottawa, ON.

Paik JK (2007) " Ultimate strength of perforated steel plates under shear loading ". *thin Walled Structures, 45: 301-6.*

Park H, Kwack J, Jeon S, Kim W & Choi I (2007) " Framed steel plate wall behaviour under cyclic lateral loading ". *journal of structural Engineering, ASCE, 133(3), 378-388.*

REFERENCES

Pavlovic L, Detzel A, Kuhlmann U & Beg D (2007) " Shear resistance of longitudinally stiffened panels- Part 1: Tests and numerical analysis of imperfections 2. *Journal of constructional Steel Research*, 63: 337-50.

Popov EP (1980) " Seismic behaviour of Structural Sub-assemblages ". *ASCE Journal of Structural Division*, 106(ST7), pp. 1451-1474.

Popov EP, Amin NR, Louie JJC & Stephan RM (1986) " Cyclic behaviour of large beam-column assemblies ". *AISC Engineering Journal*, (1), PP. 9-23.

Purba RH (2006) " Design recommendations for perforated steel plate shear walls ". M.Sc Thesis, State University.

Purba RH & Bruneau M (2007) " Design recommendations for perforated steel plate shear walls ", Technical Report No. MCEER-07-0011, Multi Disiplinary Centre for Erthquake Engineering Research, State Uni. of New York at Buffalo, Buffalo, N.Y.

Purba RH & Bruneau M (2009) " Finite Element Investigation and design Recommendations for Perforated Stel Plate Sher Wall ". *ASCE Journal of Structural Engineering*, Vol. 135, No. 11, November 1, PP. 1367-1376.

Qu B & Bruneau M (2010-b) " Behaviour of Vertical Boundary Elements in Steel Plate Shear Wall ". *Engineering Journal, AISC*, PP 109 -122.

Qu BY & Bruneau M (2008) " Seismic Behaviour and Design of Boundary Frame members of Steel Plate Shear Walls ", Technical Rep. No. MCEER-08-0012, Multidisciplinary Centre for Earthquake Engineering Research, Buffalo, New York.

Qu BY & Bruneau M (2009) " Design of steel Plate Shear Walls Considering Boundary Frame Moment Resisting Action ". *AsCE Journal of Structural Engineering*, 135(12): 1511-1521.

Qu BY & Bruneau M (2010-a) " Capacity Design of Intermediate Horizontal Boundary Elements of Steel Plate Shear Walls ". *journal of structural engineering, ASCE Vol. 136, No. 6, pp. 665-675.*

REFERENCES

Rahai AR & Alipour M (2011) " Behaviour and Characteristics of Innovative Composite plate Shear Walls ". *Procedia Engineering*, vol 14, PP 3205-3212.

Rahai AR & Alipour Tabrizi M (2010) " Behaviour and Characteristics of Inovative Composite Plte Shear Walls ". In *12th East-Asian Pacific Conference on Structural Engineering. EASEC12, Hongkong.*

Rahai AR & Hatami F (2009) " Evaluation of composite shear wall behaviour under cyclic loadings ". *Journal of Constructional Steel* 65, PP: 1528-1537.

Record EN (1978) " Patent Problems, Challenge Spawn Steel Seismic Walls ", pp. 17: McGraw Hill.

Redwood RG & Channagiri VC (2006) " Earthquake-Resistant Design of Concentrically Braced Steel Frames ". *Canadian Journal of Civil engineering*, 18 (5): 839-850.

Rezai M (1999) " Seismic behavior of steel plate shear walls by shake table testing ", University of British Columbia, Vancouver, Canada.

Rezai M, H FH, Ventura CE & Prion HGL (1996) " Experimental modal analysis of a Steel Plate Shear Wall Frame ", Department of Civil Engineering, University of British Columbia, Vancouver, Canada.

Rezai M, Ventura CE & Prion HGL (2004) " Simplified and detailed finite element models of steel plate shear walls ". In *13th Worold Conference on Earthquake Engineering, Vancouver, B.C., Canada, August 1-6, Paper No. 2804.*

Rezai M, Ventura CE, Prion HGL & Lubell AS (1997a) " Dynamic properties of steel plate shear wallframe by impact testing ". " *proceeding of the International Modal Analysis Conf. (IMAC)* ", Vol 2, SEM, Bethlehem, CT, USA.

Rezai M, Ventura CE, Prion HGL & Lubell AS (1997b) " Vibration testing of an unstiffened steel plate shear wallframe ", *Second Symposiom on Applied Mechanics Structures: Seismic Eng. Vol 4.*

REFERENCES

Rezai M, Ventura CE, Prion HGL & Lubell AS (1998) " Unstiffened Steel Plate Shear Walls: Shake Table Testing ". *Proceedings, Sixth U.S. National Conf. on Earthquake En., Seattle, May 31-June 4.*

Rezai M, Ventura CE, Prion HGL & Lubell AS (2000) " Numerical Investigation of Thin Unstiffened Steel Plate Shear Walls ". *12th World Conference on Earthquake Engineering, Auckland, New Zealand.*

Roberts TM (1995) " Seismic resistance of steel plate shear walls ". *Engineering Structures Vol. 17, No. 5, PP. 344-351.*

Roberts TM & Sabouri-Ghomi S (1991) " Hysteretic characteristics of unstiffened plate shear panels ". *Thin Walled Structures Vol. 12, No.2, pp. 145-162.*

Roberts TM & Sabouri-Ghomi S (1992a) " Hysteretic Characteristics of un-stiffened perforated steel plate shear panels ". *Thin Walled Structures Vol. 14, PP. 139-151.*

Roberts TM & Sabouri-Ghomi S (1992b) " Hysteretic characteristics of unstiffened perforated steel plate shear panels ". *Thin Walled Structures Vol. 14, PP. 139-151.*

Rockey KC (1979) " the buckling and post-buckling behaviour of shear panels which have a central circular cutout ", University of Strathclyde. In *International Conference on Thin-Walled Structures, 3rd, 6th April.*

Rockey KC, Porter DM & Evans HR (1973) " Ultimate load capacity of stiffened webs subjected to shear and bending ". *Steel Box girder bridges, ICE, pp. 45-61.*

Saatciglu M & Humar J (2003) " Dynamic Analysis of Buildings for Earthquake Resistant Design ". *Canadian Journal of Civil engineering, 30:338-359.*

Sabouri-Ghomi S (1992) " Behaviour of un-stiffened steel plate shear wall under static load ". *The first International Conference on Seismology and Earthquake Engineering, May 27-29*

Vol. 3, Pp. 175-184.

REFERENCES

Sabouri-Ghomi S & Roberts TM (1991) " Nonlinear Dynamic Analysis of Steel Plate Shear Walls ". *computers & Structures* Vol. 39, No. 1/2, PP. 121-127.

Sabouri-Ghomi S & Roberts TM (1992) " Nonlinear Dynamic Analysis of Steel Plate Shear Walls Including Shear and Bending Deformations ". *Engineering Structures* Vol. 14, No. 5, PP. 309-317.

Sabouri-Ghomi S, Ventura CE & Kharrazi M (2003) " Shear analysis and design of ductile steel plate walls ". In *Fourth International Conference, STESSA 2003, Behaviour of \steel Structures in Seismic Area*. Naples, Italy.

Sabouri-Ghomi S, Ventura CE & Kharrazi M (2005) " Shear Analysis and design of Ductile steel Plate Walls ". *journal of structural engineering, ASCE, June 2005*.

Saeki E, Sugisava M, Yamaguchi T & Wada A (1998) " Mechanical properties of low-yield-point steels ". *J Mater Civil Eng, ASCE; 10(3); PP 143-52*.

Salmon C G & Johnson J E (1997) " *Steel Structures design and behaviour* ", 4 edition, Prentice Hall, New York, 1024p.

Schumacher A, Grondin Gy & Kulak G (1997) " Connection of Infill Panels in Steel Plate shear Walls ", Structural Engineering report No. 217, Dep. Civil Engineering, University of Alberta, Edmonton, Canada.

Schumacher A, Grondin Gy & Kulak G (1999) " Connection of infill panels in Steel Plate Shear Walls ". *Canadian Journal of Civil engineering, 26:549-563*.

Scibilia N & Sacco MM (2003) " Design of Steel Plate Shear Walls in High-Rise Buildings ". *Proceedings, Conference on Behaviour of Steel Structures in seismic Areas, June, Naples, Italy, pp. 197-202*

Seal CK, Hodgson MA & Ferguson WG (2007) " Cyclic Plasticity of Steel ". In *Materials Science and Technology Conference and Exhibition* September 16-20, Detroit, Michigan, U.S.A.

REFERENCES

Shishkin Jj, Driver RG & Grondin Gy (2005) " Analysis of Steel Plate Shear Walls Using the Modified Strip Model ", Structural Engineering Reprt No. 261, Department of Civil and Environmental Engineering, University of Alberta, Edmonton, AB, Canada.

Shishkin Jj, Roberts TM & Grondin Gy (2009) " Analysis of Steel Plate Shear Walls Using Modified Strip Model ". *journal of structural engineering, ASCE Vol. 135.*

Sugii K & yamada M (1996) " Steel Panel Shear Walls, with and without concrete Covering ". " *11th Worol Conference on Earthquake Engineering "*, paper No. 403, *Acapulco, Mexico.*

Takahashi Y, Takemoto Y, Takeda T & Takagi M (1973) " Experimental Study on Thin Steel Shear Walls and Particular Bracings Under Alternative Horizontal Load ", pp. pp. 185-191. Lisbon, Portugal: IABSE Symposium on Resistance and Ultimate Deformability of Structures Acted on by Well-defined Repeated Loads.

Temblay R, Cote B & Leger P (1999) " P-delta amplification factors in multi-storey steel moment resisting frames ". *Canadian Journal of Civil engineering, 26: 535-548.*

Thorburn LJ & Kulak G (1987) " Cyclic and Static Behaviour of Thin Panel Steel Plate Shear Walls ", Structural Engineering Report No. 145. Edmonton, Canada: Department of Civil Engineering, University of Alberta.

Thorburn LJ, Kulak G & and Montgomery CJ (1983) " Analysis of Steel Plate Shear Walls ": Structural Engineering report No. 107, Departemant of Civil Engineering, University of Alberta, Edmonton, Alberta, Canada

Timler PA (1998) " Design Procedure Development, Analytical Verification, and Cost Evaluation of Steel Plate Shear Wall Structures ". Vancouver, BC: University of British Columbia.

Timler PA & Kulak G (1983) " Experimental study of Steel Plate Shear Walls ": Structural Engineering Report No. 114, Department of Civil Engineering, University of Alberta, Edmonton, Alberta, Canada.

REFERENCES

- Timoshenko S & Woinowsky-krieger S (1959) "*Theory of plate and shells* ": McGraw-Hill.
- Timoshenko S & Young D (1955) "*Vibration problems in engineering* ", Third ed, New Jersey: D. Van Nostrand Company Inc.
- Torii S, Teramoto T, Kihara H & Kitamura H (1996) "The Response Control design of High-rise Building With Low Yield Steel Wall ". " *11th world Conference on Earth. Eng* ", Acapulco, Mexico, Paper No. 97.
- Tremblay R (2005) " Fundamental periods of vibration of braced steel frames for seismic design ". *Earthquake Spectra*, 21(3): 833-60.
- Tromposch EW & Kulak G (1987) " Cyclic and Static Behavior of Thin Panel Steel Plate Shear Walls ", pp. 158p: Department of Civil Engineering, University of Alberta, Edmonton, Structural Engineering Report No. 145.
- Troy RG & richard RM (1979) " Steel Plate Shear Walls Resist Lateral Load, Cut Costs ". *Civil Engineering, ASCE Vol. 49, February*, pp. 53-55.
- Troy RG & Richard RM (1998) " Steel plate Shear Wall Design ". *Structural Engineering*.
- Ugural A & Fenster S (2003) " Advanced strength and applied elasticity ", 4th ed, New Jersey: Prentice Hall. .
- Vian D (2005) " Steel plate shear walls for seismic design and retrofit of building structures ". PhD Thesis, State University, New York
- Vian D & Bruneau M (2004) " Testing of special LYS steel plate shear walls ". In " *13th World conference on EARTHQUAKE ENGINEERING* ". Vancouver, B.C; Canada, August 1-6, 2004, Paper No. 978.
- Vian D, Bruneau M & Purba RH (2009) " Specil perforated Steel Plate Shear Walls with Reduced Beam Section Anchor Beams. II: Analysis and Design Recommendations ". *journal of structural engineering, ASCE Vol.135, no. 3*, pp. 221-228.

REFERENCES

Vian D, Lin YC, Bruneau M & Tsai KC (2003) " Cyclic Performance of Low Yield Strength Steel Panel Shear Walls ". In " *The Sixteenth KKCNN Symposium on Civil Engineering* ", December 8-10, Korea.

Villaverde R (2007) " Methods to Assess the Seismic Collapse Capacity of Building Structures: State of the Art ". *journal of structural engineering, ASCE Vol. 133, No. 1, 99. 57-66.*

Wagner H (1931) " Flat Sheet Metal Girders with Very Thin Webs, Part I- General Theories and Assumptions ". Washington, DC: National Advisory Committee for Aeronautics.

Wallace BJ & Krawinkler H (1989) " Small-scale model tests of structural steel assemblies ". *Journal of structural Engineering, ASCE, 115(8), 1999-2015.*

Xue M & Lu L (1994-a) " Interaction of Steel Plate Shear Panels with Surrounding Frame Members ". " *Proceedings of the Structural Stability Research Council Annual Technical Session, Bethlehem, PA, PP. 339-354.*

Xue M & Lu L (1994-b) " Monotonic and Cyclic Behaviour of Infilled Steel Shear Panels, ". " *Proceedings of the 17th Czech and Slovak International Conference on Steel Structures and Bridges*", Bratislava, Slovakia.

yamada M & Yamakaji T (2000) " Steel Panel Shear Wall - Analysis on the Centre Core Steel Panel Shear Wall System ". *Proceedings, 3rd International Conference STESSA, Behaviour of Steel Structures in Seismic Areas, August, Montreal, Canada, pp. 541-550.*

Yamaguchi T, Nakata Y, Takeuchi T, Ikebe T, nagao T, Minami A & Suzuki T (1998) " Seismic Control Devices Using Low-Yield -Point Steel", Nippon Steel Technical Report No. 77, PP. 65-72.

Yang TY & Whittaker AS (2002) " MCEER demonstration hospitals-mathematical models and preliminary results ", Technical Report, Multidisciplinary Centre for Earthquake engineering Research, State university of New York at Buffalo, Buffalo, NY.

REFERENCES

Youssef M (2006) " Analytical prediction of the linear and nonlinear behaviour of steel beams rehabilitated using FRP sheets " *Engineering Structures*, 28, pp. 903-911.

Youssef N, Wilkerson R, Fischer K & Tunick D (2009) " Seismic Performance of a 55-storey Steel Plate Shear Wall ". *The Structural Design of Tall Buildings Vol. 19, No. 1-2*, pp. 139-165.

Zhao Q & A A-A (2007) " Seismic Behavior of Composite Shear Wall Systems and Application of Smart Structures Technology ". *Steel Structures, Vol 7*, pp. 69-75.

Zhao Q & Astaneh-Asl A (2003) " Cyclic Behavior of Composite Shear wall System ". *Journal of Structural Engineering, ASCE, February 2003*.

Zhao Q & Astaneh-Asl A (2004) " Cyclic Behavior of an innovative steel shear wall ". In *13th World Conference on Earthquake Engineering, Vancouver, B.C., Canada, August 1-6, 2004, paper No. 2576*.

Zhao XL & Zhang L (2007) " Stat-of-The-Art Review on FRP Strengthened Steel structures ". *Journal of Engineering Structures Vol. 22*, pp. 1808-1823.

APPENDIX A: USER DEFINED SUBROUTIN FOR LOADING SYSTEM AND DATA ACQUISITION

```

'JOB=JOB1
'COMPILED=2011/01/13 17:10:48
'TYPE=dt80
DT=\d
001: BEGIN"JOB1"
002: CATTN
003: 'Spans and polynomial declarations
004: S1=0,262,-42.35368,9098.7224"mm"
005: Y2=0,0.963855"uStrain"
006: Y3=0,0.94786"uStrain"
007: S4=0,262,-43.85,8841.1"mm"
008: S5=0,262,-20.4,9369"mm"
009: S6=0,26,6703,-25.5"mm"
010: S7=0,26,6720,9.9"mm"
011: S8=0,26,6720,-111.4"mm"
012: S9=0,26,6753,-77.3"mm"
013: S10=0,26,7002,68"mm"
014: S11=0,0,0,0"mm"
015: Y12=0,50.05,0.376,-.001,-.002"kn"
016: 'Thermistor declarations
017: 'Switches declarations
018: 'Parameter declarations
019: 'Global declarations
020: RS1S
021: 'schedule definition
022:
023: 'Constants
13CV("AC1Amplitude(mm)")=0.6 'mm
800CV("AC1revAmplitude(mm)")=0.6 'mm
12CV("numOfCycles")=3
650CV=5 ' Hz Frequency of the motor (inverter)
413CV("Degree Stage1 limit")=10 ' Limit of Stage1 of Quarter cycle, degree
414CV("Degree Stage2 limit")=30 ' Limit of Stage2 of Quarter cycle, degree
700CV("Degree Stage3 limit")=60 ' Limit of Stage3 of Quarter cycle, degree
701CV("Degree Stage4 limit")=80 ' Limit of Stage1 of Quarter cycle, degree
' Stage 5 ends at 90 and
270 degrees
417CV("DegreeInc1")=5 ' Quarter cycle increment 1, degree
418CV("DegreeInc2")=10 ' Quarter cycle increment 2, degree
419CV("DegreeInc3")=10 ' Quarter cycle increment 3, degree
702CV("DegreeInc4")=10 ' Quarter cycle increment 4, degree
703CV("DegreeInc5")=5 ' Quarter cycle increment 5, degree
600CV=1 ' 1=CDS_A1, 2=LDS_C20 controlled
024: 'zero CDS,LDS,LoadCell
' Variables used 5,15-21CV
1BGI(4w,S1,"AC1z",=5CV)
2BGI(4w,S4,"AC2z",=15CV)
3BGI(4w,S5,"AC3z",=16CV)
16BGI(4w,S6,"AT16z",=17CV)
1419BGI(4w,S7,"BT119z",=18CV)
1420BGI(4w,S8,"BT120z",=19CV)
1519BGI(4w,S9,"CT219z",=20CV)
1520BGI(4w,S10,"CT220z",=21CV)
4HV(Y12,"AL4z",w,=300CV,GL30V)
'max,min deflection, Cycle Completion def
IF(600CV<0.5,1.5){6CV=5CV-13CV 7CV=5CV+800CV 8CV=5CV+0.05}
IF(600CV<1.5,2.5){6CV=21CV-13CV 7CV=21CV+800CV 8CV=21CV+0.05}
14CV=12CV-0.5 'nos of cycle -0.5
710CV=12CV+0.5 'nos of cycle +0.5
10CV=1 ' load cycle stage 1=forwarding,2=reversing,

```

APPENDIX A

```

          ' 3=forwarding back to mean
11CV=0      'current loading cycle 0=first cycle
1CV=3      ' 3= stop motor, 2=reverse, 0= forward
411CV=0    'strating increment of cycle
412CV=0    'starting angle of cycle
405CV=0    'Initial delay time before stopping motor
025: 'zero STRAIN GAUGES variables 24-68CV
5BGI(3W,Y3,"AR5z",=24CV) 6BGI(3W,Y3,"AR6z",=25CV)
7BGI(3W,Y3,"AR7z",=26CV) 8BGI(3W,Y3,"AR8z",=27CV)
9BGI(3W,Y3,"AR9z",=28CV) 10BGI(3W,Y3,"AR10z",=29CV)
11BGI(3W,Y3,"AR11z",=30CV) 12BGI(3W,Y3,"AR12z",=31CV)
13BGI(3W,Y3,"AR13z",=32CV) 1401BGI(3W,Y2,"BU101z",=33CV)
1402BGI(3W,Y2,"BU102z",=34CV) 1403BGI(3W,Y2,"BU103z",=35CV)
1404BGI(3W,Y2,"BU104z",=36CV) 1405BGI(3W,Y2,"BU105z",=37CV)
1406BGI(3W,Y2,"BU106z",=38CV) 1407BGI(3W,Y2,"BU107z",=39CV)
1408BGI(3W,Y2,"BU108z",=40CV) 1409BGI(3W,Y2,"BU109z",=41CV)
1410BGI(3W,Y2,"BU110z",=42CV) 1411BGI(3W,Y2,"BU111z",=43CV)
1412BGI(3W,Y2,"BU112z",=44CV) 1413BGI(3W,Y2,"BU113z",=45CV)
1414BGI(3W,Y2,"BU114z",=46CV) 1415BGI(3W,Y2,"BU115z",=47CV)
1416BGI(3W,Y2,"BU116z",=48CV) 1417BGI(3W,Y2,"BU117z",=49CV)
1418BGI(3W,Y2,"BU118z",=50CV) 1501BGI(3W,Y3,"CR201z",=51CV)
1502BGI(3W,Y3,"CR202z",=52CV) 1503BGI(3W,Y3,"CR203z",=53CV)
1504BGI(3W,Y3,"CR204z",=54CV) 1505BGI(3W,Y3,"CR205z",=55CV)
1506BGI(3W,Y3,"CR206z",=56CV) 1507BGI(3W,Y3,"CR207z",=57CV)
1508BGI(3W,Y3,"CR208z",=58CV) 1509BGI(3W,Y3,"CR209z",=59CV)
1510BGI(3W,Y3,"CR210z",=60CV) 1511BGI(3W,Y3,"CR211z",=61CV)
1512BGI(3W,Y3,"CR212z",=62CV) 1513BGI(3W,Y3,"CR213z",=63CV)
1514BGI(3W,Y3,"CR214z",=64CV) 1515BGI(3W,Y3,"CR215z",=65CV)
1516BGI(3W,Y3,"CR216z",=66CV) 1517BGI(3W,Y3,"CR217z",=67CV)
1518BGI(3W,Y3,"CR218z",=68CV)
026: 'New Zeros From First Amplitudes
027: 'schedule definition
028: RA"CtrMotor"("B:",ALARMS:OV:100KB,DATA:OV:10MB) LOGONA GA
029: HB
030: 1DNO=1CV
031: DELAY=405CV
032: 1DNO=3
033: 706CV=405CV
IF(405CV>4000){706CV=4000}
DELAY=1000+706CV
034: 1BGI(4W,S1,"CDS1")
035: GB
036: 'schedule definition
037: RB"LogData"("B:",ALARMS:OV:100KB,DATA:OV:50MB) LOGONB GB
038: ' Displacement Sensors Variables 4,22,23,159-163CV
1BGI(4W,S1,"AC1live",w,=4CV)
2BGI(4W,S4,"AC2live",w,=22CV)
3BGI(4W,S5,"AC3live",w,=23CV)
16BGI(4W,S6,"AT16live",w,=159CV)
1419BGI(4W,S7,"BT119live",w,=160CV)
1420BGI(4W,S8,"BT120live",w,=161CV)
1519BGI(4W,S9,"CT219live",w,=162CV)
1520BGI(4W,S10,"CT220live",w,=163CV)
' Displacement sensors Normalized readings variables 164-171CV
164CV("AC1")=5CV-4CV 'CDS1
165CV("AC2")=15CV-22CV 'CDS2
166CV("AC3")=16CV-23CV 'CDS3
167CV("AT16")=17CV-159CV 'LDS1
168CV("BT119")=18CV-160CV 'LDS2
169CV("BT120")=19CV-161CV 'LDS3
170CV("CT219")=20CV-162CV 'LDS4
171CV("CT220")=21CV-163CV 'LDS5

039: IF(600CV><0.5,1.5){601CV=164CV 602CV=4CV}
IF(600CV><1.5,2.5){601CV=171CV 602CV=163CV}
410CV(w)=ABS(601CV/13CV)
415CV(w)=SIN(D2R(413CV)) 416CV(w)=SIN(D2R(414CV))
704CV(w)=SIN(D2R(700CV)) 705CV(w)=SIN(D2R(701CV))
IF(410CV><0,415CV){411CV=417CV}
IF(410CV><415CV,416CV){411CV=418CV}
IF(410CV><416CV,704CV){411CV=419CV}
IF(410CV><704CV,705CV){411CV=702CV}
IF(410CV>705CV){411CV=703CV}
412CV(w)=412CV+411CV
IF(412CV>360){412CV=412CV-360}
040: IF(600CV><0.5,1.5){6CV=5CV-13CV 7CV=5CV+800CV 8CV=5CV+0.05}
IF(600CV><1.5,2.5){6CV=21CV-13CV 7CV=21CV+800CV 8CV=21CV+0.05}

```

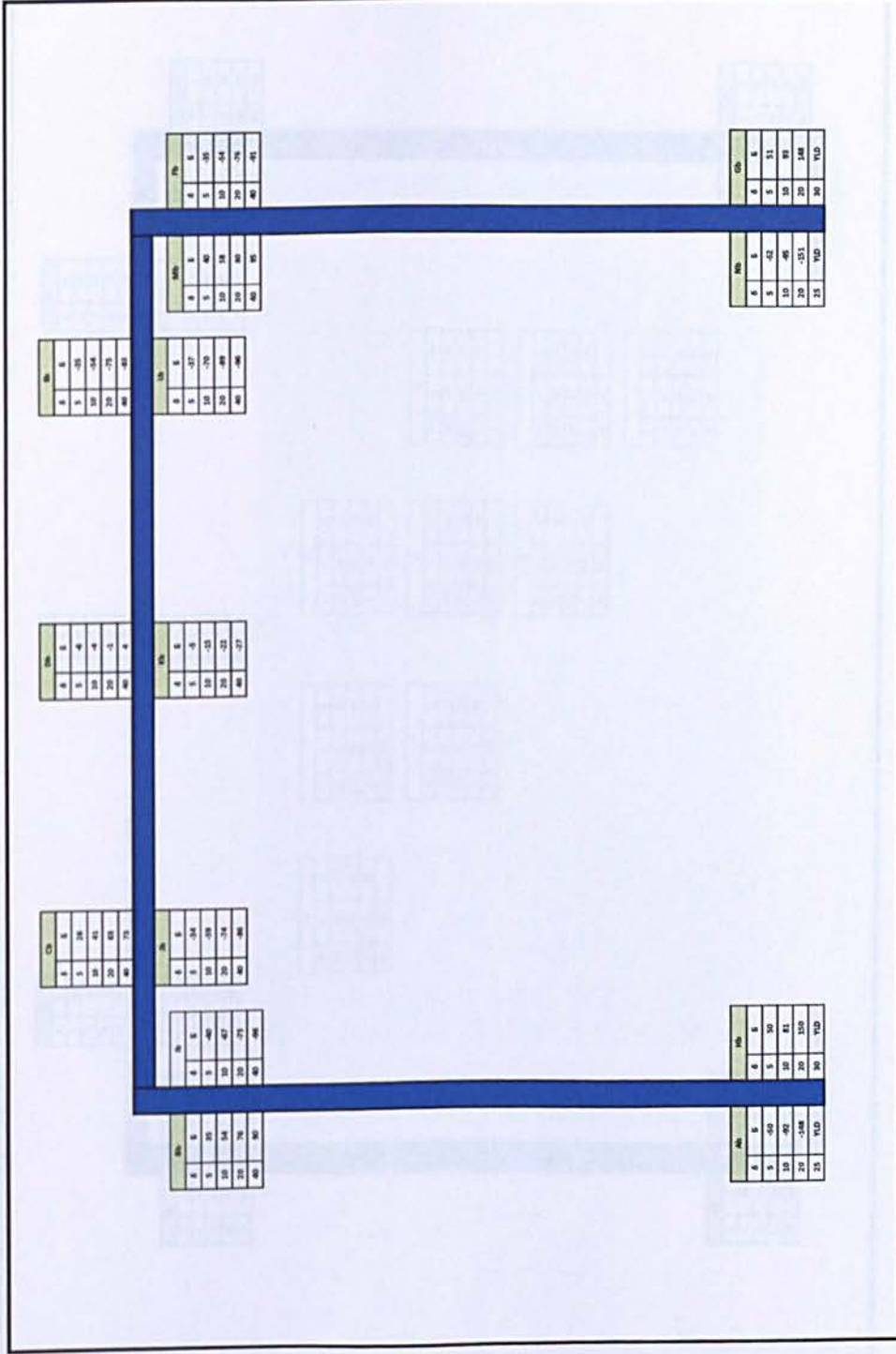
APPENDIX A

```

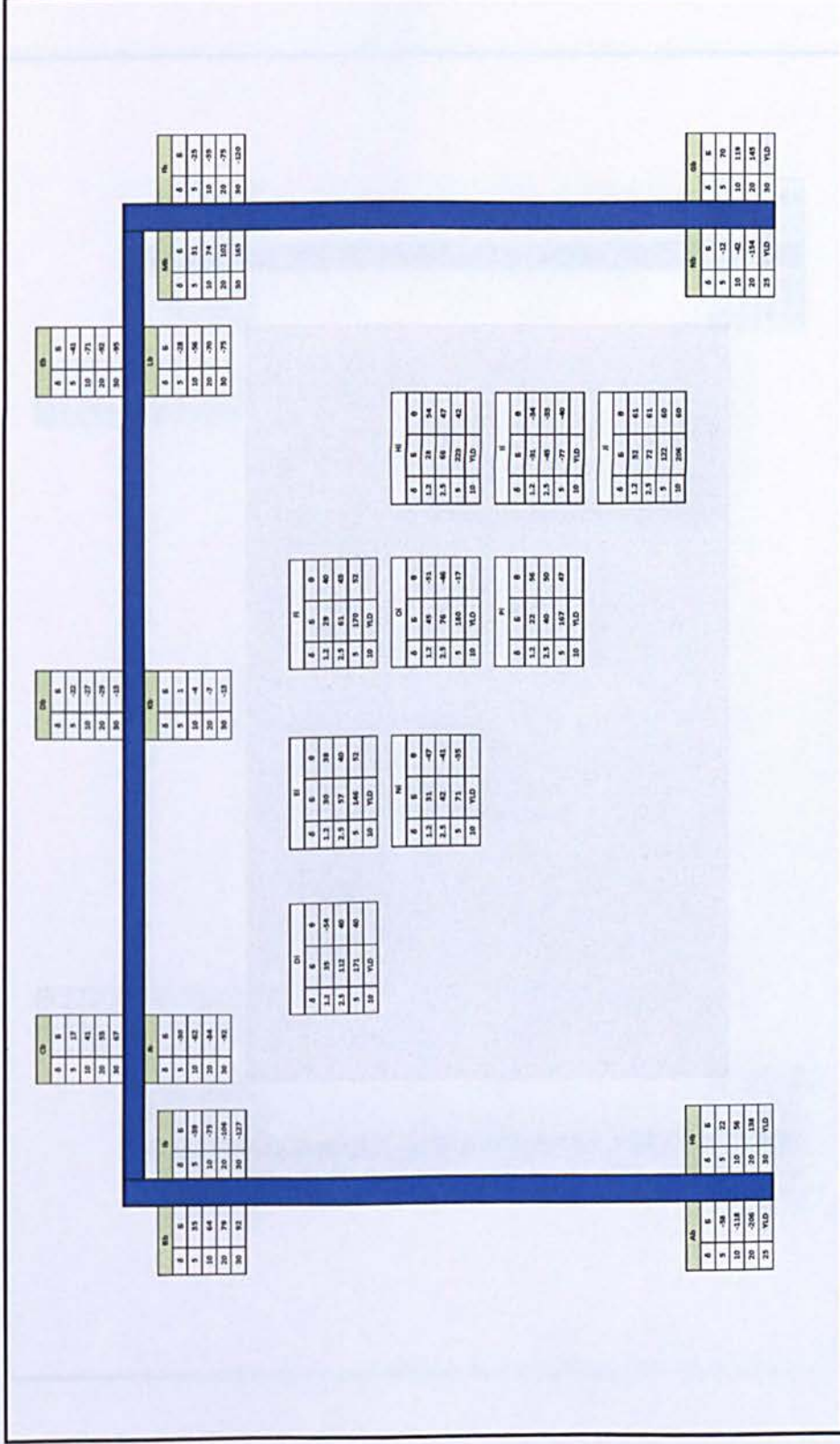
651CV=0.001904*650CV*650CV
403CV(W)=ABS(ABS(SIN(D2R(412CV)))*13CV-ABS(601CV))
IF(403CV<651CV){405CV=6.48*SQRT(403CV/2)*1000}
IF(403CV>651CV){405CV=(650CV/5+(403CV-651CV)*105/650CV)*1000}
ALARM(10CV><0.5,1.5)AND
ALARM(602CV>6CV)"FORWARD"{1CV=0}
ALARM(10CV><0.5,1.5)AND
ALARM(602CV<6CV)"REVERSE"{10CV=2}
ALARM(10CV><1.5,2.5)AND
ALARM(602CV<7CV)"REVERSE Started"{1CV=2}
ALARM(10CV><1.5,2.5)AND
ALARM(602CV>7CV)"Last Forward"{10CV=3}
ALARM(10CV><2.5,3.5)AND
ALARM(602CV>7CV)"FORWARD to mean"{1CV=0}
ALARM(10CV><2.5,3.5)AND
ALARM(602CV<8CV)"Cycle COMPLETE"{10CV=1 11CV=11CV+1 1CV=3}
ALARM(11CV><14CV,710CV)"STOPED"{10CV=0 1CV=3 H}
041: 'Log STRAIN GAUGES & LoadCell
4HV(Y12,"AL4",w,=301CV,GL30V) 302CV("AL4")=301CV 'zero removed -300CV
' direct reading variables 69-113CV
' final corrected variables 114-158CV
5BGI(3W,Y3,w,=69CV) 114CV("AR5")=69CV-24CV 6BGI(3W,Y3,w,=70CV)
115CV("AR6")=70CV-25CV 116CV("AR7")=71CV-26CV 8BGI(3W,Y3,w,=72CV)
7BGI(3W,Y3,w,=71CV) 118CV("AR9")=73CV-28CV 10BGI(3W,Y3,w,=74CV)
117CV("AR8")=72CV-27CV 120CV("AR11")=75CV-30CV 12BGI(3W,Y3,w,=76CV)
9BGI(3W,Y3,w,=73CV) 122CV("AR13")=77CV-32CV 1401BGI(3W,Y2,w,=78CV)
119CV("AR10")=74CV-29CV 124CV("BU102")=79CV-34CV 1403BGI(3W,Y2,w,=80CV)
118BGI(3W,Y3,w,=75CV) 126CV("BU104")=81CV-36CV 1405BGI(3W,Y2,w,=82CV)
121CV("AR12")=76CV-31CV 128CV("BU106")=83CV-38CV 1407BGI(3W,Y2,w,=84CV)
13BGI(3W,Y3,w,=77CV) 130CV("BU108")=85CV-40CV 1409BGI(3W,Y2,w,=86CV)
123CV("BU101")=78CV-33CV 132CV("BU110")=87CV-42CV 1411BGI(3W,Y2,w,=88CV)
1402BGI(3W,Y2,w,=79CV) 134CV("BU112")=89CV-44CV 1413BGI(3W,Y2,w,=90CV)
125CV("BU103")=80CV-35CV 136CV("BU114")=91CV-46CV 1415BGI(3W,Y2,w,=92CV)
1404BGI(3W,Y2,w,=81CV) 138CV("BU116")=93CV-48CV 1417BGI(3W,Y2,w,=94CV)
127CV("BU105")=82CV-37CV 140CV("BU118")=95CV-50CV 1501BGI(3W,Y3,w,=96CV)
1406BGI(3W,Y2,w,=83CV) 142CV("CR202")=97CV-52CV 1503BGI(3W,Y3,w,=98CV)
129CV("BU107")=84CV-39CV 144CV("CR204")=99CV-54CV 1505BGI(3W,Y3,w,=100CV)
1408BGI(3W,Y2,w,=85CV) 146CV("CR206")=101CV-56CV 1507BGI(3W,Y3,w,=102CV)
131CV("BU109")=86CV-41CV 148CV("CR208")=103CV-58CV 1509BGI(3W,Y3,w,=104CV)
133CV("BU111")=88CV-43CV 150CV("CR210")=105CV-60CV 1511BGI(3W,Y3,w,=106CV)
1412BGI(3W,Y2,w,=89CV) 152CV("CR212")=107CV-62CV 1513BGI(3W,Y3,w,=108CV)
135CV("BU113")=90CV-45CV 154CV("CR214")=109CV-64CV 1515BGI(3W,Y3,w,=110CV)
1414BGI(3W,Y2,w,=91CV) 156CV("CR216")=111CV-66CV 1517BGI(3W,Y3,w,=112CV)
137CV("BU115")=92CV-47CV
1416BGI(3W,Y2,w,=93CV)
139CV("BU117")=94CV-49CV
1418BGI(3W,Y2,w,=95CV)
141CV("CR201")=96CV-51CV
1502BGI(3W,Y3,w,=97CV)
143CV("CR203")=98CV-53CV
1504BGI(3W,Y3,w,=99CV)
145CV("CR205")=100CV-55CV
1506BGI(3W,Y3,w,=101CV)
147CV("CR207")=102CV-57CV
1508BGI(3W,Y3,w,=103CV)
149CV("CR209")=104CV-59CV
1510BGI(3W,Y3,w,=105CV)
151CV("CR211")=106CV-61CV
1512BGI(3W,Y3,w,=107CV)
153CV("CR213")=108CV-63CV
1514BGI(3W,Y3,w,=109CV)
155CV("CR215")=110CV-65CV
1516BGI(3W,Y3,w,=111CV)
157CV("CR217")=112CV-67CV
1518BGI(3W,Y3,w,=113CV) 158CV("CR218")=113CV-68CV
042: 'schedule definition
043: RC"Zeros"("B:",ALARMS:OV:100KB,DATA:OV:1MB)1M LOGONC GC
044: 'zero CDS,LDS,LoadCell=300CV
' variables used 5,15-21CV
5CV
15..21CV
300CV
045: 'zero STRAIN GAUGES variables 24-68CV
24..68CV
046: END
'end of program file

```

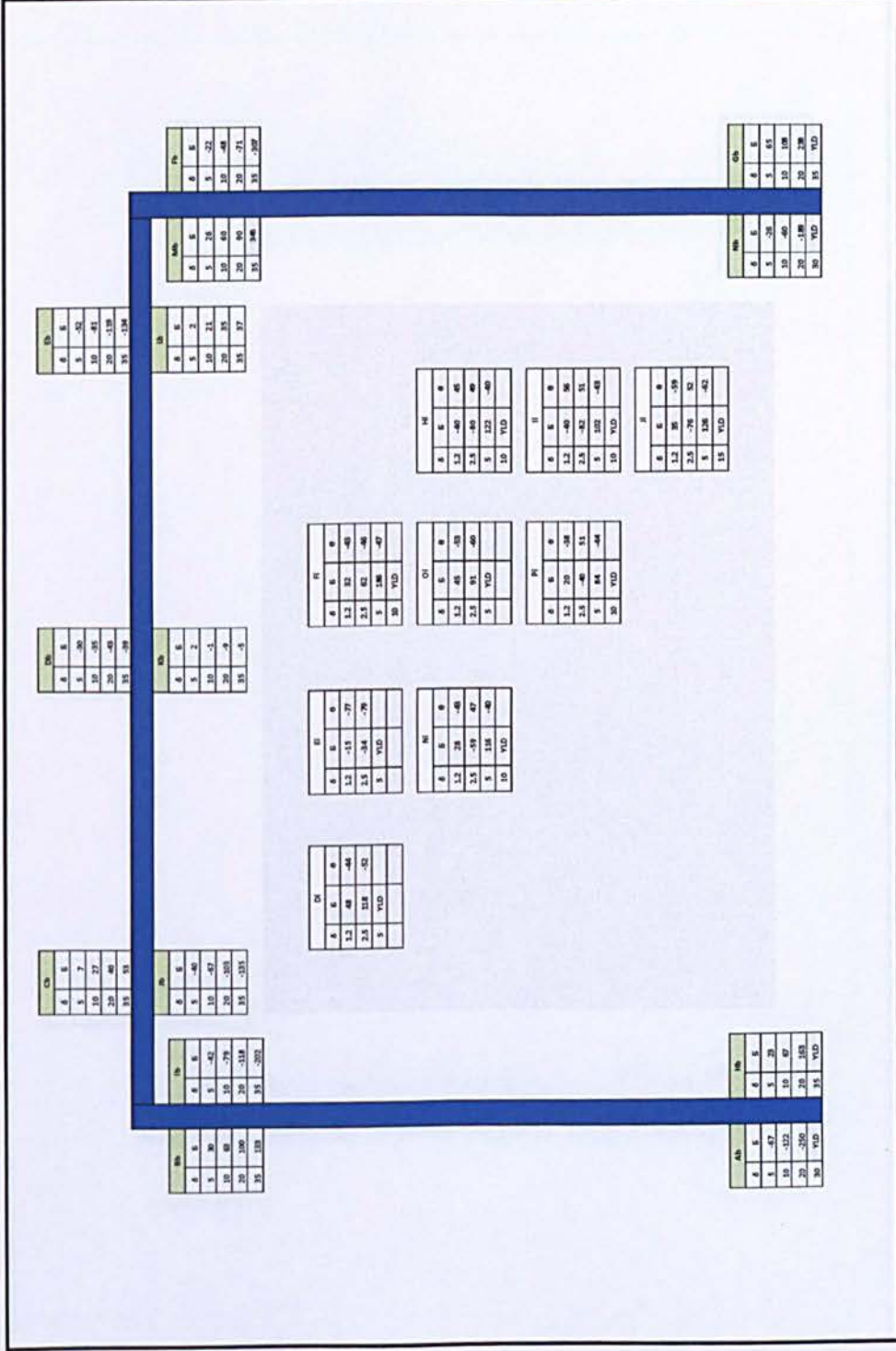
APPENDIX B: THE STATE OF MAXIMUM PRINCIPLE STRESSES IN TEST SPECIMENS

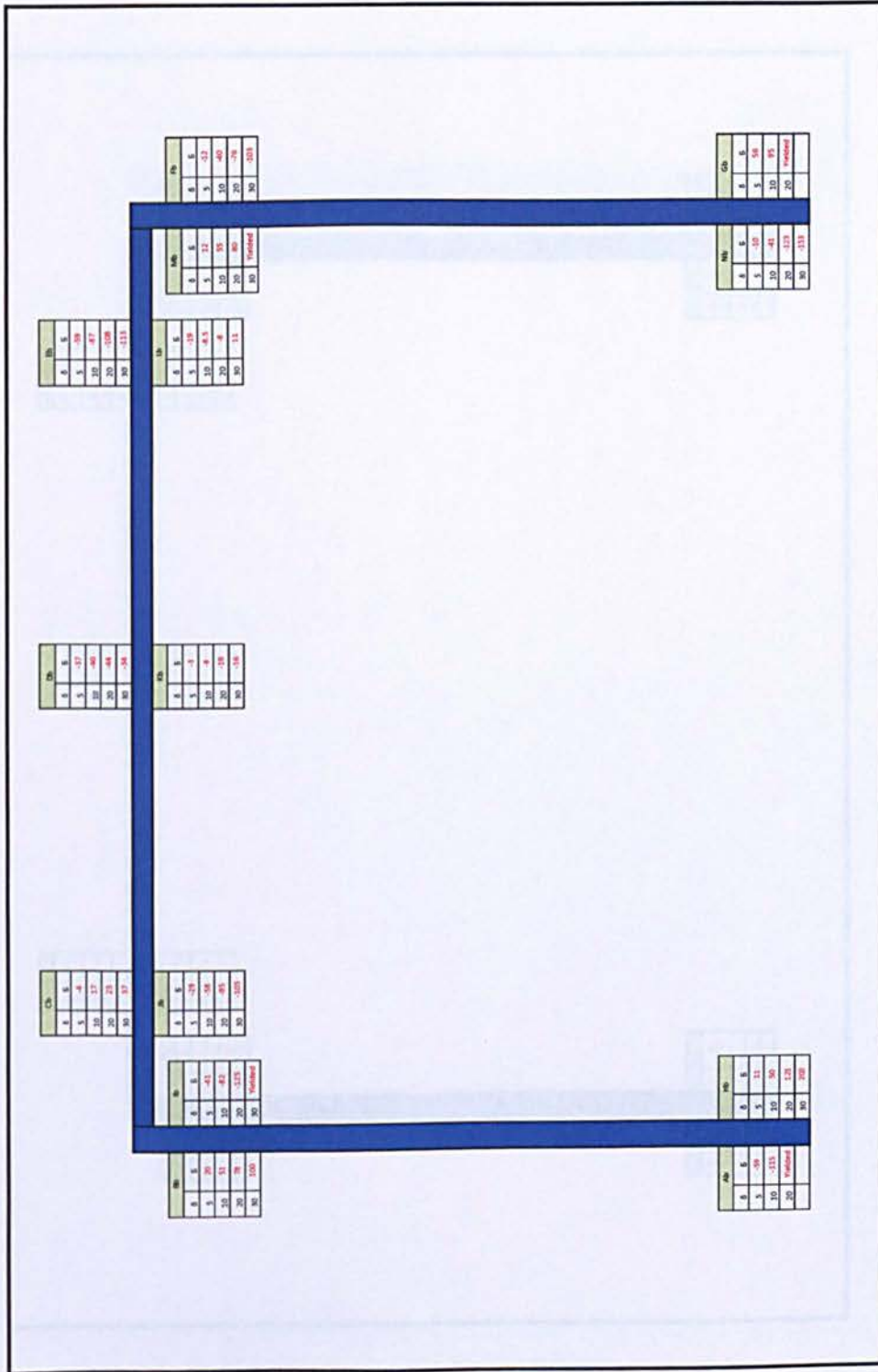


Frame-only specimen

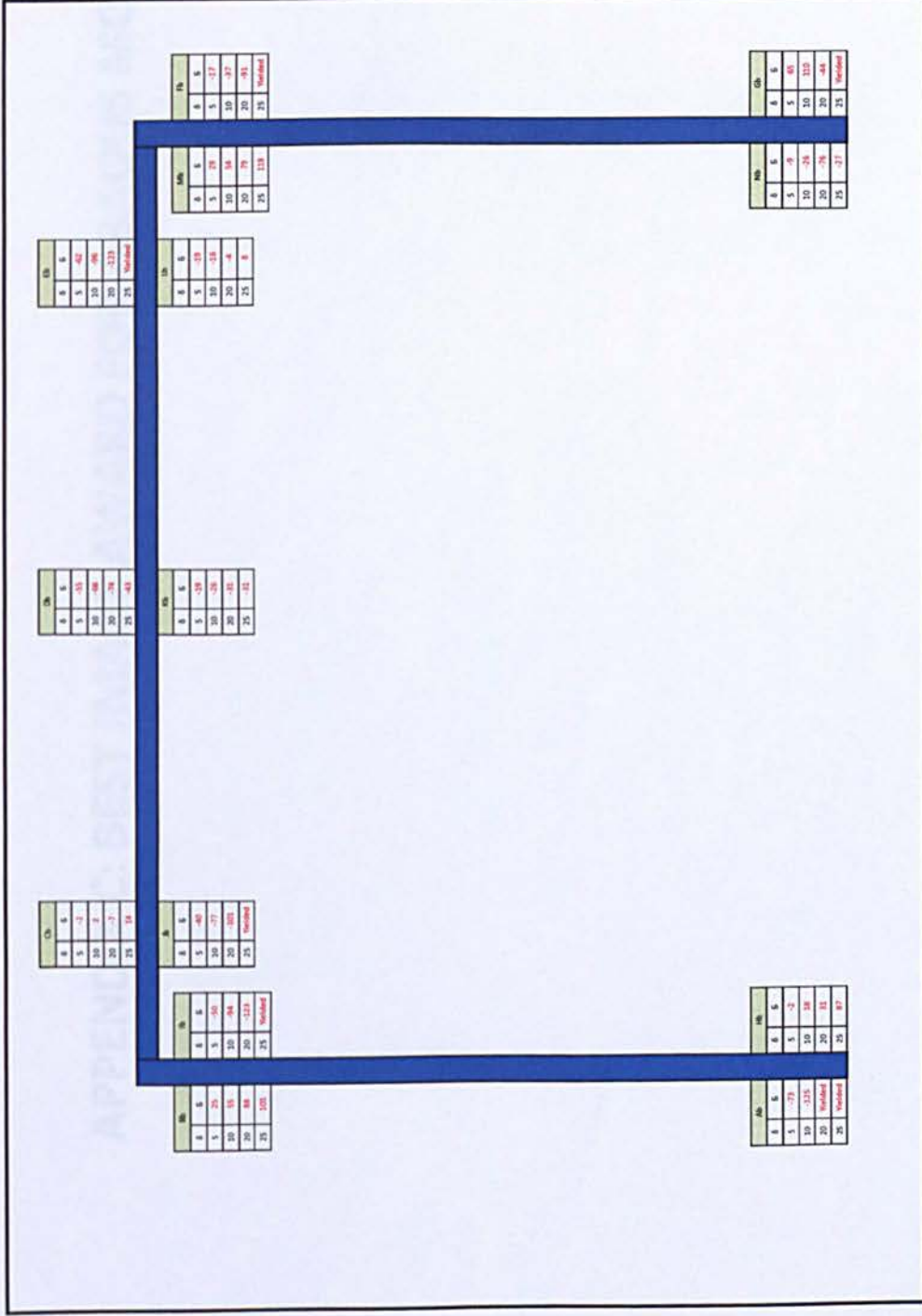


W1 specimen





W1G1 specimen




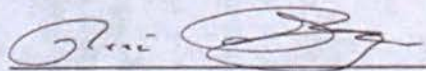
W1G3 specimen

APPENDIX C: BEST IMAGE AWARD FOR ABAQUS MODELLING

DASSAULT SYSTÈMES SIMULIA CORP.

Best Image Award

Ahmad Maleki
Kingston University

 
Rene Sprunger
BDM, SIMULIA

APPENDIX D: PUBLISHED PAPERS

1. Maleki, A., Donchev, T., Hadavinia, H., Cheah, A. Behaviour of steel shear wall Systems with cut-outs and stiffeners. Proc. *International conference in Structures and Architecture*, Guimaraes, Portugal, 2010.
2. Maleki, A., Donchev, T., Hadavinia, H., Limbachiya, M. Numerical modelling and experimental investigation of GFRP-steel sandwich shear walls. *International conference on Thin Walled Structures. ICTWS2011, 5-7 Sept 2011, Timisoara, Romania*
3. Maleki, A., Donchev, T., Hadavinia, H., Limbachiya, M. Improving the seismic resistance of structures using FRP/steel shear walls. Proc. *The 6th International Conference on FRP composites in Civil Engineering CICE 2012*, Rome, Italy, 13-15 June 2012.